www.NRL.NAVY.mil

2001 NRL REVIEW

THE NAVY'S CORPORATE LABORATORY

NAVAL RESEARCH LABORATORY
WASHINGTON, DC 20375-5320

REPORT DOCUMENTATION PAGE

Form Approved OMB No. 0704-0188

1. REPORT DATE (DD-MM-YYYY)	2. REPORT TYPE	3. DATES COVERED (FROM - TO)
01-01-2001		xx-xx-2001 to xx-xx-2001

4. TITLE AND SUBTITLE
2001 NRL Review
Unclassified

5a. CONTRACT NUMBER
5b. GRANT NUMBER
5c. PROGRAM ELEMENT NUMBER

6. AUTHOR(S)

5d. PROJECT NUMBER
5e. TASK NUMBER
5f. WORK UNIT NUMBER

7. PERFORMING ORGANIZATION NAME AND ADDRESS
Naval Research Laboratory
Washington, DC20375-5320

8. PERFORMING ORGANIZATION REPORT NUMBER

9. SPONSORING/MONITORING AGENCY NAME AND ADDRESS
,

10. SPONSOR/MONITOR'S ACRONYM(S)
11. SPONSOR/MONITOR'S REPORT NUMBER(S)

12. DISTRIBUTION/AVAILABILITY STATEMENT
APUBLIC RELEASE
,

13. SUPPLEMENTARY NOTES

14. ABSTRACT

Today, when government and science seem inextricably linked, when virtually no one questions the dependence of national defense on the excellence of national technical capabilities, it is noteworthy that in-house defense research is relatively new in our Nation?s history. The Naval Research Laboratory (NRL), the first modern research institution created within the United States Navy, began operations in 1923.

15. SUBJECT TERMS

16. SECURITY CLASSIFICATION OF:			17. LIMITATION OF ABSTRACT	18. NUMBER OF PAGES	19. NAME OF RESPONSIBLE PERSON
a. REPORT	b. ABSTRACT	c. THIS PAGE	Public Release	253	Fenster, Lynn lfenster@dtic.mil
Unclassified	Unclassified	Unclassified			19b. TELEPHONE NUMBER International Area Code Area Code Telephone Number 703767-9007 DSN 427-9007

NRL REVIEW STAFF

Senior Science Editor

Dr. John D. Bultman

TID Coordinator

Jonna Atkinson

TID Consultant

Kathleen Parrish

Head, TID

James Lucas (Acting)

Computerized Composition and Design

Jonna Atkinson, Donna Gloystein, and Jan Morrow

Editorial Assistance

Maureen Long

Graphic Support

Jonna Atkinson, Donna Gloystein, and Jan Morrow

Historical Update

Dr. David van Keuren

Photographic Production

Gayle Fullerton and Michael Savell

Production Assistance

Rosie Bankert, Diltricia Montgomery, and Paul Sweeney

Distribution

Rosie Bankert

Cover photos:

- Virtual Reality Room (top)
- Test preparation in the Nike Laser Target Facility (center)
- Optical Sciences laser experiment (bottom)

CONTENTS

THE NAVAL RESEARCH LABORATORY

FEATURED RESEARCH

ACOUSTICS

ATMOSPHERIC SCIENCE AND TECHNOLOGY

CHEMICAL/BIOCHEMICAL RESEARCH

ELECTRONICS AND ELECTROMAGNETICS

ENERGETIC PARTICLES, PLASMAS, AND BEAMS

INFORMATION TECHNOLOGY AND COMMUNICATIONS

MATERIALS SCIENCE AND TECHNOLOGY

OCEAN SCIENCE AND TECHNOLOGY

OPTICAL SCIENCES

REMOTE SENSING

SIMULATION, COMPUTING, AND MODELING

SPACE RESEARCH AND SATELLITE TECHNOLOGY

SPECIAL AWARDS AND RECOGNITION

PROGRAMS FOR PROFESSIONAL DEVELOPMENT

GENERAL INFORMATION

View from the Top

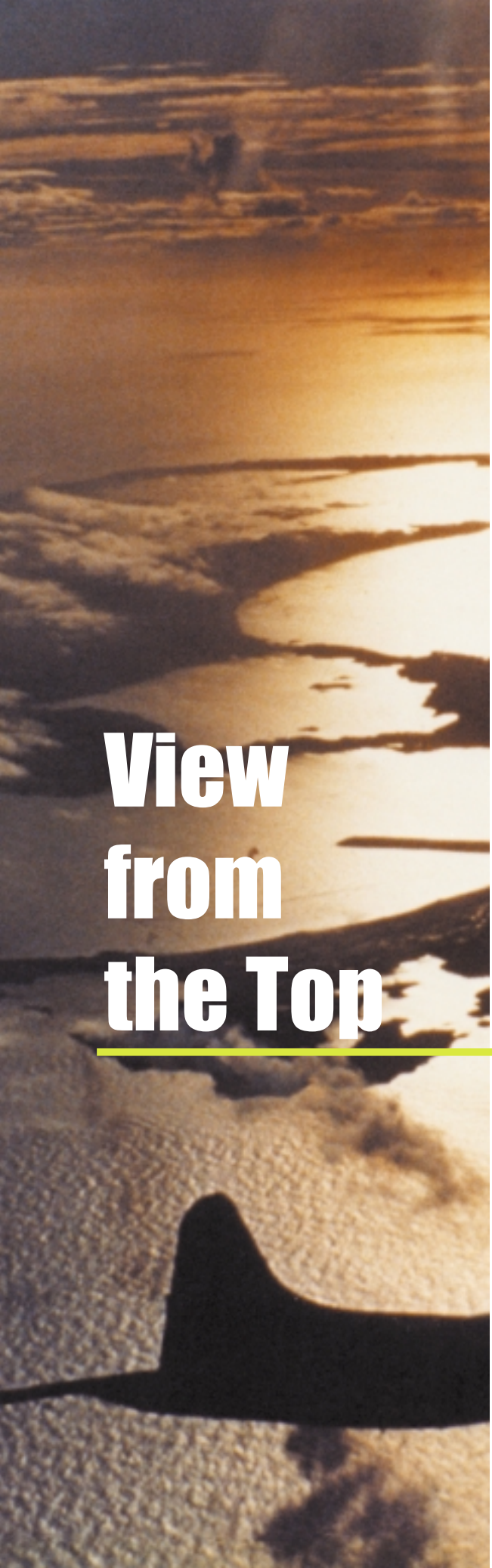

View from the Top

CAPT Douglas H. Rau, USN
Commanding Officer

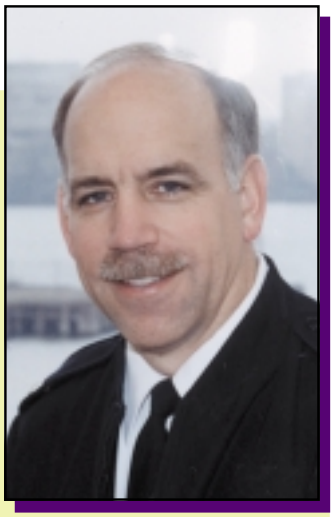

The past year has been a remarkable time for NRL and our Navy. We have seen renewed interest in future military capabilities and a heightened awareness of the vulnerabilities of our people and our platforms. Leading into the new year, we have a new Chief of Naval Operations, a new Chief of Naval Research, and a new President … all who have expressed their commitment to keeping our Military the best in the world.

Before we forget the past leaders of our Navy and nation, I would like to reflect on the parting words of the outgoing Secretary of the Navy, the Honorable Richard Danzig. As SECNAV he was a fan of NRL and we were honored to host him for a day of briefings and have him present the Captain Robert Dexter Conrad award to Dr Coffey. I was also fortunate enough to brief him on some special projects NRL is working in direct support of the Sailors and Marines deployed.

Reflecting on his goals and hopes for the future, the Secretary stated very succinctly, that we must do the following:

***Honor Sailors and Marines**: People are our greatest asset and we must give them every tool necessary to succeed. We must improve their quality of life and quality of work, so they are empowered and encouraged to "be all they can be."*

***Embrace Technology**: We understand and have demonstrated the value of transitioning new science and technology to the Fleet. We must continue to work with the sponsors and program managers to facilitate this transition and enhance our fighting capabilities.*

***Deliver Value**: I have certainly felt that Value has been a corner stone of NRL's legacy. Understanding the requirements and understanding the realm of the possible is an NRL trademark!*

NRL is the Great Research Laboratory that Thomas Edison envisioned in 1915. We will continue to hold that position of esteem, provided we Honor our People, Embrace Technology, and Deliver Value in everything we do!

Thank you for proudly serving NRL, our Navy and our Nation!

from the Commanding Officer and the Director of Research

Dr. Timothy Coffey
Director of Research

As we enter the new millennium and as I approach my 20th year as Director of Research, it is useful to reflect on the Lab's history and my own experiences regarding enduring themes that have emerged over the years. These reflections might act as guideposts for the future.

I believe that the single most important decision that NRL makes is its choice of people. This is especially important at this time as one generation prepares to move out of the Laboratory to be replaced by the next generation. Another decision of comparable importance relates to the choice of research areas that the Laboratory undertakes.

The historical productivity of the Lab suggests that NRL has generally done a good job on both of these matters. I continue to believe these will remain the most important decisions that we make.

Clearly, many of NRL's great contributions have involved teamwork, often among the different disciplines represented at the Lab. This will be even more important in the future.

Another attribute that has distinguished NRL as a scientific establishment has been its devotion to science and engineering in support of the naval forces. This was a key factor in Edison's vision of the role of NRL and will remain as key to the future of NRL as it was 77 years ago. Experience suggests that NRL must be prepared to preserve areas of long-term importance that are perhaps not currently in vogue. The Lab must be fully familiar with the role of science and technology in modern warfare. It also must understand that, in spite of rhetoric to the contrary, it actually takes years to prepare a technology for viable insertion into warfighting.

It is my perception that the coexistence of a strong basic research program and a substantial applied research program has been key to the Lab's ability to deal with these issues and will remain key to future success. Because of its unique placement under the Chief of Naval Research and its synergistic role with the Office of Naval Research, NRL is one of the few organizations that is well positioned to deal with the likely revolution in military technologies in the 21st Century. If past is prologue, NRL will account for itself very well in this regard. The content of this *NRL Review* clearly supports this conclusion.

THE NAVAL RESEARCH LABORATORY

MISSION

To conduct a broadly based multidisciplinary program of scientific research and advanced technological development directed toward maritime applications of new and improved materials, techniques, equipment, systems, and ocean, atmospheric, and space sciences and related technologies.

The Naval Research Laboratory provides

- primary in-house research for the physical, engineering, space, and environmental sciences;
- broadly based exploratory and advanced development programs in response to identified and anticipated Navy needs;
- broad multidisciplinary support to the Naval Warfare Centers; and
- space and space systems technology development and support.

NRL – OUR HERITAGE

Today, when government and science seem inextricably linked, when virtually no one questions the dependence of national defense on the excellence of national technical capabilities, it is noteworthy that in-house defense research is relatively new in our Nation's history. The Naval Research Laboratory (NRL), the first modern research institution created within the United States Navy, began operations in 1923.

Thomas Edison's Vision: The first step came in May 1915, a time when Americans were deeply worried about the great European war. Thomas Edison, when asked by a *New York Times* correspondent to comment on the conflict, argued that the Nation should look to science. "The Government," he proposed in a published interview, "should maintain a great research laboratory....In this could be developed...all the technique of military and naval progression without any vast expense." Secretary of the Navy Josephus Daniels seized the opportunity created by Edison's public comments to enlist Edison's support. He agreed to serve as the head of a new body of civilian experts—the Naval Consulting Board—to advise the Navy on science and technology. The Board's most ambitious plan was the creation of a modern research facility for the Navy. Congress allocated $1.5 million for the institution in 1916, but wartime delays and disagreements within the Naval Consulting Board postponed construction until 1920.

The Laboratory's two original divisions—Radio and Sound—pioneered in the fields of high-frequency radio and underwater sound propagation. They produced communications equipment, direction-finding devices, sonar sets, and perhaps most significant of all, the first practical radar equipment built in this country. They also performed basic research, participating, for example, in the discovery and early exploration of the ionosphere. Moreover, the Laboratory was able to work gradually toward its goal of becoming a broadly based research facility. By the beginning of World War II, five new divisions had been added: Physical Optics, Chemistry, Metallurgy, Mechanics and Electricity, and Internal Communications.

The War Years and Growth: Total employment at the Laboratory jumped from 396 in 1941 to 4400 in 1946, expenditures from $1.7 million to $13.7 million, the number of buildings from 23 to 67, and the number of projects from 200 to about 900. During WWII, scientific activities necessarily were concentrated almost entirely on applied research. New electronics equipment—radio, radar, sonar—was developed. Countermeasures were devised. New lubricants were produced, as were antifouling paints, luminous identification tapes, and a sea marker to help save survivors of disasters at sea. A thermal diffusion process was conceived and used to supply some of the ^{235}U isotope needed for one of the first atomic bombs. Also, many new devices that developed from booming wartime industry were type tested and then certified as reliable for the Fleet.

NRL Reorganizes for Peace: Because of the major scientific accomplishments of the war years, the United States emerged into the postwar era determined to consolidate its wartime gains in science and technology and to preserve the working relationship between its armed forces and the scientific community. While the Navy was establishing its Office of Naval Research (ONR) as a liaison with and supporter of basic and applied scientific research, it was also encouraging NRL to broaden its scope and become, in effect, its corporate research laboratory. There was a transfer of NRL to the administrative oversight of ONR and a parallel shift of the Laboratory's research emphasis to one of long-range basic and applied investigation in a broad range of the physical sciences.

However, rapid expansion during the war had left NRL improperly structured to address long-term Navy requirements. One major task—neither easily nor rapidly accomplished—was that of reshaping and coordinating research. This was achieved by transforming a group of largely autonomous scientific divisions into a unified institution with a clear mission and a fully coordinated research program. The first attempt at reorganization vested power in an executive committee composed of all the division superintendents. This committee was impracticably large, so in 1949, a civilian director of research was

named and given full authority over the program. Positions for associate directors were added in 1954.

The Breadth of NRL: During the years since the war, the areas of study at the Laboratory have included basic research concerning the Navy's environments of Earth, sea, sky, and space. Investigations have ranged widely—from monitoring the Sun's behavior to analyzing marine atmospheric conditions to measuring parameters of the deep oceans. Detection and communication capabilities have benefitted by research that has exploited new portions of the electromagnetic spectrum, extended ranges to outer space, and provided a means of transferring information reliably and securely, even through massive jamming. Submarine habitability, lubricants, shipbuilding materials, fire fighting, and the study of sound in the sea have remained steadfast concerns, to which have been added recent explorations within the fields of virtual reality, superconductivity, and biomolecular science and engineering.

The Laboratory has pioneered naval research into space from atmospheric probes with captured V-2 rockets through direction of the *Vanguard* project—America's first satellite program—to inventing and developing the first satellite prototypes of the Global Positioning System. Today NRL is the Navy's lead laboratory in space systems research, fire research, tactical electronic warfare, microelectronic devices, and artificial intelligence.

The consolidation in 1992 of NRL and the Naval Oceanographic and Atmospheric Research Laboratory, with centers at Bay St. Louis, Mississippi, and Monterey, California, added critical new strengths to the Laboratory. NRL now is additionally the lead Navy center for research in ocean and atmospheric sciences, with special strengths in physical oceanography, marine geosciences, ocean acoustics, marine meteorology, and remote oceanic and atmospheric sensing. The expanded Laboratory is focusing its research efforts on new Navy strategic interests and needs in the post-Cold War world. Although not abandoning its interests in blue-water operations and research, the Navy is also focusing on defending American interests in the world's littoral regions. NRL scientists and engineers are working to give the Navy the special knowledge and capabilities it needs to operate in these waters.

2000 IN REVIEW

During 2000, NRL scientists initiated new research thrusts while contributing to areas of continuing Laboratory expertise. In the ocean sciences, NRL marine geophysicists, led by Dr. Peter Vogt, hosted a conference in Bay St. Louis, Mississippi, to explore the possibility of initiating a systematic international effort to map the entire ocean floor to at least 100-meter spatial resolution. Despite the advances in mapping the Moon, outer moons, and the near planets of our solar system, only a few percent of the ocean floor has been mapped to 100-meter resolution. Resolution at such a spatial scale reveals a wealth of hitherto unknown features and seafloor processes. The intent of the NRL-sponsored GOMaP workshop (Global Ocean-floor Mapping Project) was to explore the possibilities of using state-of-the-art surface ship technologies, and possibly also autonomous undersea vehicles, for systematic mapping. The Juan de Fuca tectonic plate and the Gulf of Mexico were proposed as pilot areas for initiating GOMaP. An international conference/meeting is planned to further consider the idea, informally dubbed "Wet *Clementine*" at NRL.

In space science, NRL scientists reported obtaining the first ever far-ultraviolet image of a meteor. The image was taken by the Global Imaging Monitor of the Ionosphere (GIMI) onboard the DoD Space Test Program's Advanced Research and Global Observation Satellite (ARGOS). The image of the meteor should provide a unique tool for understanding the composition and structure of meteors, which pose a constant threat to satellite operations. GIMI is one of nine primary experiments on the ARGOS mission, which was launched into polar orbit on February 23, 1999, to study space weather. GIMI's objective is to obtain simultaneous wide-field far ultraviolet/extreme ultraviolet images of ionospheric and upper atmospheric emissions. GIMI images will be used to determine chemical densities on a global basis and to detect disturbances in the ionosphere that are caused by auroral activity, gravity waves, and foreign materials from meteors, suspected "ice comets," rocket exhausts, and chemical releases. In between atmospheric observations, the detector is gathering data for an all-sky survey of stars and data on celestial diffuse sources at far-ultraviolet wavelengths.

A three-dimensional numerical model of the evolving magnetic fields in a flaring region of the Sun was developed by scientists at NRL to help explain the nature and origin of solar eruptions. The NRL-

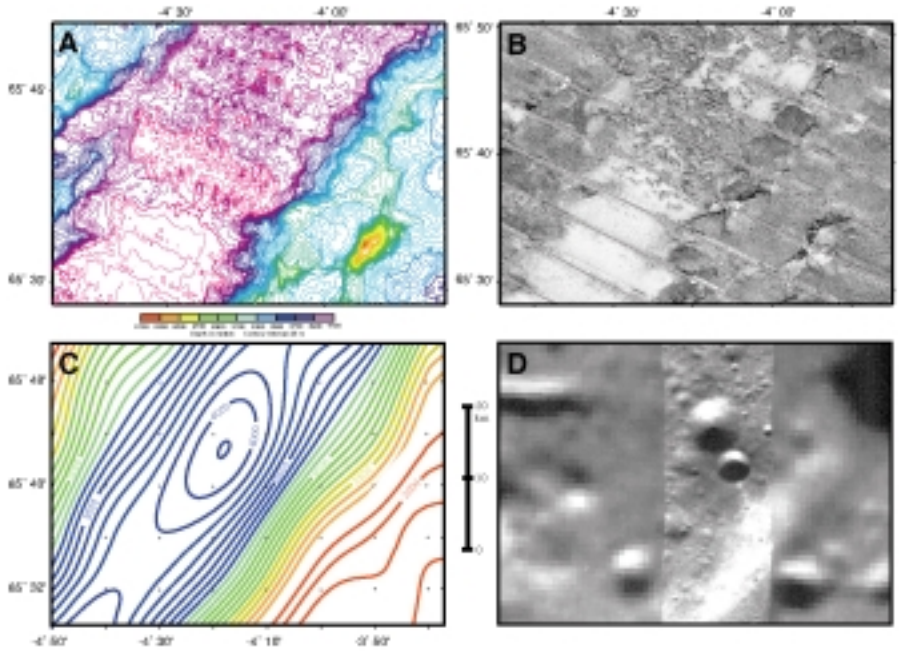

A small ocean floor area in the Norwegian Sea (ca. 3000 km^2, somewhat less than 0.001% of the global seafloor) illustrates the resolution of multibeam bathymetry (A, 25-meter depth contour interval) and sidescan sonar imagery (B, with darker indicating stronger backscatter) that GOMaP would return. By contrast, most of the ocean floor has only been "mapped" homogeneously by satellite altimetry, with geoid undulations used to "predict" bathymetry at ca. 20 km resolution (C). A comparably sized area of the Moon (D) shows 20 to 40-m pixel resolution *Clementine* imagery (central swath), comparable to what GOMaP would do in ca. 1-km water depths, while the adjacent lunar area corresponds to what GOMaP would return in the deepest ocean (7 to 10-km).

developed model, nicknamed the "pressure cooker model," has closely matched actual observations, making the model a viable tool for understanding how energetic solar eruptions occur and also, possibly, for predicting them in advance. The key strength of the NRL model is its novel description of the conditions allowing the release of energy, leading to eruptive flares that result in coronal mass ejections. The NRL model differs from competitors in that it assumes the magnetic field to have a more complicated geometry, with a null point located high in the solar atmosphere. Other solar models have never been compared with actual observations as precisely as has the "pressure cooker."

In other space science work, NRL scientists and engineers have been selected to develop critical components for the next-generation Gamma-ray telescope. The Laboratory is a member of an international consortium chosen by NASA to develop the primary instrument for the Gamma Ray Large Area Space Telescope (GLAST), planned for launch in 2005. The GLAST will be the successor to the Energetic Gamma-Ray Experiment Telescope on NASA's Compton Gamma Ray Observatory, which recently concluded its scientific mission. Researchers within NRL's Cosmic Ray Astrophysics Branch will be responsible for the design, development, and test of the massive GLAST calorimeter, which will measure the energy of incoming gamma rays. The Laboratory's X-ray Astronomy Branch will be responsible for building the computers to discriminate the gamma rays from the background cosmic rays in the events seen by GLAST.

In other research, scientists from NRL's Materials Science and Technology Division, in collaboration with researchers at Carnegie Mellon University, have conceived and demonstrated a revolutionary new type of digital storage memory. Called Vertical Giant Magnetoresistance Random Access Memory (VRAM), the new technology has the potential to replace all mechanically driven storage media, including computer hard drives and compact discs. The goal is a technology that will produce a 100 to 1,000-fold increase in storage capacity over semiconducting memory. VRAM dramatically reduces the need for transistors, leading to lower cost, and it retains information without continual refreshing, thereby reducing the power requirement. It is also estimated that VRAM technology will increase memory access speed by a factor of ten. The high-density, nonvolatility, radiation-harness, and low-power attributes of VRAM make it well suited to space, avionics, and shipboard applications.

Laboratory researchers have fabricated new glass materials for use in the development of a new class of extremely compact and efficient opto-electronic devices. These photonic bandgap nanochannel materials will have widespread use in both military and commercial applications. Photonic bandgap structures embedded with nonlinear optical materials show promise in the development of optical switches and limiters having improved performance. Such optical limiters can be used to protect the human eye against accidental or hostile damage from lasers. It is hoped that the payoffs from the NRL research will include the fabrication of next-generation optical sensors and

Under a CRADA, NRL and the University of Texas at Houston have developed a system for two-way communication of emergency medical information between an ambulance in the field and a hospital trauma center. A standard ambulance (left) has been retrofitted with the jointly developed hardware and software for use by emergency medical personnel (above).

miniaturized optical systems; high-speed opto-electronic components for high-bandwidth communication; low noise, high gain optical amplifiers; thresholdless/low-threshold lasers; identification systems based on engineered optical properties; and efficient directional antennas for RF/microwave devices.

In other research, NRL scientists within the Optical Sciences Division, in cooperation with Sarnoff Corporation and Sensors Unlimited, demonstrated the first room-temperature operation of an interband III-V laser diode that emits at a wavelength greater than three microns. This work brings the GaSb-based technology closer to achieving truly practicable and portable mid-IR laser systems. Such a laser would need to operate continuously at room temperature if it were to find widespread commercial and military application. The NRL work is an important step in that direction.

NRL researchers have recently made progress in the application of Nuclear Quadrupole Resonance (NQR) to the detection of landmines. NQR is a leading candidate to succeed the still-current World War II metal detection technology. Many mines, especially antipersonnel mines, are now built of plastic and are thus not amenable to metal-based detection systems. In the recent NRL work, researchers have made progress in increasing the signal-to-noise ratio by use of efficient pulse sequence and by improved design of the detector coil. Additionally, researchers have pioneered the use of low power RF for NQR use. Both advances make the application of NQR to mine detection a more viable technology. The NRL technology has been licensed to Quantum Magnetics of San Diego, California. In related matters, NRL has received a patent (US 6,054,856) for a specialized detection coil used in its NQR system. The NRL research on NQR technology has been funded jointly by the Federal Aviation Administration and the Department of Defense.

In other counter-terrorism R&D, researchers at NRL, in cooperation with Research International of Woodinville, Washington, have developed two portable instruments for the detection of bioterrorism agents. The first device, the Smart Air Sampler (SASS) is a lightweight, low-power, portable air sampler capable of concentrating airborne particles by several hundred thousand times into a small amount of water. The resulting SASS samples can then be tested in a versatile, portable biosensor, the RAPTOR, that can detect the presence of minute concentrations of viruses, bacteria, and toxins in liquid samples. The RAPTOR is a completely self-contained instrument that integrates optics, fluidics, electronics, and software into one compact system for laboratory and field assays. It runs highly specific antibody-based assays in a disposable cartridge the size of a credit card. Both the SASS and RAPTOR were used and evaluated by the Seattle Fire Department during the December 1999 World Trade Organization meeting.

Technology Transfer: During FY 00, NRL's Technology Transfer Office continued to facilitate the implementation of NRL technology for commercial use to benefit the civilian community. The two principal mechanisms for transfer of NRL technology and expertise are Cooperative Research and Development Agreements (CRADAs) and licenses to NRL patents. NRL signed CRADAs in FY 00 on topics ranging from fundamental investigations with potential benefits to both military and commercial customers to projects that involved

the implementation of mature technology developed for defense use into commercial systems.

The growing interest in using sensors for a wide range of commercial applications has led to several collaborations. For example, under the scope of a CRADA, NRL and Solex Robotics, Inc., are evaluating NRL's technology for the remote inspection of storage tanks and comparing the NRL technology to alternative technology developed by Solex. The goal is to develop a system that will identify flaws in the storage tanks before they fail and cause environmental contamination. Under another CRADA, NRL and Veriteq, Inc., are developing a data logging system to integrate with NRL's apparatus for the detection and monitoring of corrosion in ship ballast tanks.

NRL's fiber optic sensors are being evaluated for use in the oil and gas exploration industry. Halliburton Energy Services, Inc., has entered into a CRADA directed at implementing NRL's fiber optic sensors for monitoring pressure and temperature in oil wells. Schlumberger Technology Corporation and NRL are working together under a CRADA to develop borehole sensors that can operate at elevated temperatures.

An example of a CRADA that will benefit commercial and military users equally is the one between NRL and Sigma Coatings for the development of environmentally benign, metal-free marine antifouling coatings. Similarly, the CRADA between NRL and MBI International to develop a new microbial-based, heavy metal biosorbent has application in environmental remediation efforts of both military and commercial sites.

In FY 00, NRL signed licenses with industry for phthalonitrile resin compositions for use in composite structures in the aerospace, marine, and transportation industries. The NRL resins are lightweight and flame-resistant. NRL has licensed its side-pumped fiber amplifier, also known as the V-groove amplifier. This amplifier offers advantages over other designs in the fields of optical communications, test and measurement instrumentation, and lasers. NRL also signed a license for its TORA™ algorithms. The TORA™ algorithms allow efficient message routing to a defined subset of wireless communications transceivers. NRL's licensee will include TORA™ as an option on its spread spectrum radio transceiver for customers requiring a mobile wireless network for data transmission, particularly in congested areas.

NRL TODAY

ORGANIZATION AND ADMINISTRATION

The Naval Research Laboratory is a field command under the Chief of Naval Research, who reports to the Secretary of the Navy via the Assistant Secretary of the Navy for Research, Development and Acquisition.

Heading the Laboratory with joint responsibilities are CAPT Douglas H. Rau, USN, Commanding Officer, and Dr. Timothy Coffey, Director of Research. Line authority passes from the Commanding Officer and the Director of Research to three Associate Directors of Research, a Director of the Naval Center for Space Technology, and an Associate Director for Business Operations. Research divisions are organized under the following functional directorates:

- Systems
- Materials Science and Component Technology
- Ocean and Atmospheric Science and Technology
- Naval Center for Space Technology.

NRL operates as a Navy Working Capital Fund (NWCF). All costs, including overhead, are charged to various research projects. Funding in FY 00 came from the Chief of Naval Research, the Naval Systems Commands, and other Navy sources; government agencies, such as the U.S. Air Force, the Defense Advanced Research Projects Agency, the Department of Energy, and the National Aeronautics and Space Administration; and several nongovernment activities.

PERSONNEL DEVELOPMENT

At the end of FY 00, NRL employed 3134 persons—45 officers, 129 enlisted, and 2960 civilians. In the research staff, there are 842 employees with doctorate degrees, 376 with masters degrees, and 493 with bachelors degrees. The support staff assists the research staff by providing administrative, computer-aided design, machining, fabrication, electronic construction, publication, personnel development, information retrieval, large mainframe computer support, and contracting and supply management services.

NRL main site, located off Interstate 295 in S.W. Washington, D.C., as viewed from the Potomac River.

Opportunities for higher education and other professional training for NRL employees are available through several programs offered by the Employee Development Branch. These programs provide for graduate work leading to advanced degrees, advanced training, college course work, short courses, continuing education, and career counseling. Graduate students, in certain cases, may use their NRL research for thesis material.

For non-NRL employees, several postdoctoral research programs exist. There are also agreements with several universities for student opportunities under the Student Career Experience Program (formerly known as Cooperative Education), as well as summer and part-time employment programs. Summer and interchange programs for college faculty members, professional consultants, and employees of other government agencies are also available.

NRL has active chapters of Women in Science and Engineering, Sigma Xi, Toastmasters International, Federally Employed Women, and the Federal Executive and Professional Association. Three computer clubs meet regularly—NRL Microcomputer User's Group, NeXT, and Sun NRL Users Group. An amateur radio club, a drama group (the Showboaters), and several sports clubs are also active. NRL has a Recreation Club that provides basketball and softball leagues and swim, sauna, whirlpool bath, gymnasium, and weight-room facilities. The Recreation Club also offers classes in martial arts, aerobics, swimming, and water walking.

The Community Outreach Program traditionally has used its extensive resources to foster programs that provide benefits to students and other community citizens. Volunteer employees assist with and judge science fairs, give lectures, and serve as tutors, mentors, coaches, and classroom resource teachers. The program also sponsors African American History Month art and essay contests for local schools, student tours of NRL, a student Toastmasters Youth Leadership Program, an annual holiday party for neighborhood children in December, and a book donation program for both students and teachers. Through the Community Outreach Program, NRL has active partnerships with four District of Columbia, three Aberdeen, Maryland, and three Calvert County, Maryland, public schools.

NRL has an active, growing Credit Union. Since its creation in 1946, NRL Federal Credit Union (NRL FCU) has grown to over $200 million in assets and serves about 22,000 NRL employees, contractors, select employee groups, and their families. NRL FCU is a leader in providing innovative financial services such as a dynamic home page and Online Access (Internet home banking) with bill payer. Focusing on the credit union philosophy of *People Helping People*, NRL FCU offers a wide array of no-fee services plus financial education and assistance. NRL FCU is a full service financial institution providing various mortgage programs and creative lending services. For information about membership or any financial service, call (301) 839-8400 or click www.nrlfcu.org.

Public transportation to NRL is provided by Metrobus. Metrorail service is three miles away.

For more information, see the *NRL Review* chapter, "Programs for Professional Development."

SCIENTIFIC FACILITIES

In addition to its Washington, D.C., campus of about 130 acres and 102 main buildings, NRL maintains 11 other research sites, including a vessel for fire research and a Flight Support Detachment. The many diverse scientific and technological research and support facilities are described in the following paragraphs.

RESEARCH FACILITIES

Radar

NRL has gained worldwide renown as the "birthplace of radar" and, for a half-century, has maintained its reputation as a leading center for radar-related research and development. A number of facilities managed by NRL's Radar Division continue to contribute to this reputation.

A widely used major facility is the Compact Antenna Range (operated jointly with the Space Systems Development Department) for antenna design and development, as well as radar cross section measurements. The range is capable of simulating farfield conditions from 1 to 110 GHz with a quiet zone of approximately 7 ft in diameter and 8 ft in length. Instrumentation covers from 1 to 95 GHz. Another strong division capability is in the Computational Electromagnetics (CEM) Facility, which has capabilities for complex electromagnetic modeling, including radar target and antenna structures. The Radar Signature Calculation Facility within this group produces detailed computations of radar cross sections of various targets, primarily ships. The CEM facility includes multiple-cpu supercomputers that are also used to design phased array radar antennas. There is tremendous synergism between the CEM group and the Compact Range Facility. This provides the ability to design in the CEM environment, test in the compact, and have immediate feedback between the theoretical and experimental aspects to shorten the development cycle for new designs.

In connection with airborne radar, the division operates a supercomputer-based Radar Imaging Facility, and an inverse synthetic aperture radar (ISAR) deployed either in the air, on the ground, or aboard ship for radar-imaging data collection. A P-3 aircraft equipped with the AN/APS-145 radar and cooperative engagement capability is also available for mounting experiments.

In connection with ship-based radar, the division operates a Radar Test Bed Facility at the Chesapeake Bay Detachment (CBD), Randle Cliffs, Maryland. Represented are radars for long-range air search, point defense, and surface search functions. The point defense radar, with its large (4 ft × 8 ft) X-band phased array antenna, and the ANSPQ-9B ADM systems are designed to be mobile so that testing is not limited to this specific environment.

Other installations operated by the division include an Electromagnetic Compatibility (EMC) Facility supported by a mode-stirred chamber, and a Com-

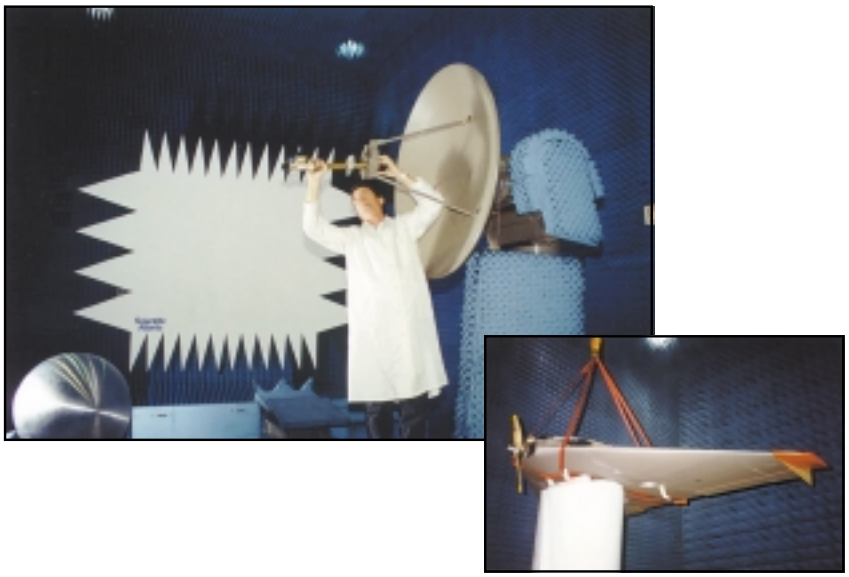

A view of the interior of the compact range, with the primary reflector in the background. In the foreground, an antenna assembly is being readied for testing on the range positioner, while the inset photo shows a small unmanned aerial vehicle as it undergoes radar cross section measurements.

puter-aided Engineering (CAE) Facility. The microwave microscope, a high-resolution (2-cm) capability for investigating backscatter from both surface and volumetric clutter is now operational, and a millimeter-wave radar system operating in the 94 GHz region is currently being developed. The division provides direct technical support and has direct access to data from the AN/TPS-71, the Navy's relocatable over-the-horizon radars. Concepts and engineering developments in connection with target identification are explored by using an experimental Cooperative Aircraft Identification system.

Information Technology

The Information Technology Division (ITD) is at the forefront of DoD research and development in artificial intelligence, telecommunications, computer networking, human-computer interaction, information security, parallel computation, and computer science.

The division maintains local area computer networks to support its research and hosts testbeds for advanced high-performance fiber-optic network research. These networks make available hundreds of high-performance computers to local and remote users. The ITD research networks connect to NRL's internal network via high-speed links ranging from DS-3 (45 Mbps) links on NASA Science Internet (NSI); to OC-03c on DREN/S-DREN; to OC-48c (2.4 Gbps) on ATDnet. The ATDnet is a metropolitan ATM network that supports advanced network research at OC-48c speeds and higher; other major partners include the National Aeronautics and Space Administration, the National Security Agency, the Defense Information Systems Agency, the Defense Advanced Research Projects Agency, and the Defense Intelligence Security Agency. Research on ATDnet includes introduction and testing of new networking protocols; wave division multiplexing to greatly increase network capacity; and the evolution to all-optical networks, with switching at the optical layer. Research on the high-end computational assets and networks result in close association with applications that demand these leading-edge capabilities and have allowed ITD to achieve significant results in a number of areas. These include current efforts in pushing the state of the art in motion imagery with progressive scan in high-definition TV (HDTV) where 1.5 Gbps data streams are needed to handle the raw output. A new Motion Imagery Laboratory (MIL) introduced last year provides the environment for experiments in the convergence of the progressive video, high-performance computing, very large data sets at hundreds of gigabytes, and high-speed networking that allows the user to be enveloped in the data presentation with a capability for real-time manipulation. The Defense Research and Engineering Network (DREN) is a high-speed continental United States network that connects the four Major Shared Resource Centers (MSRCs) and nineteen Distributed Centers (DCs) of DDR&E's High Performance Computing Modernization Program (HPCMP) as well as a number of user organizations that use the HPCMP resources.

As a Distributed Center in the HPCMP, ITD's Center for Computational Science supports a range of shared resources including massively parallel computer systems and high-performance networks. Current systems include an SGI Origin2000 with 128 processors and 128 Gbytes of memory; an experi-

The 128-processor Silicon Graphics Origin2000 system, currently with 128 Mbytes of RAM. The next-generation Origin3000 in the background transitions from beta to experimental use in FY 01. The NRL Center for Computational Science, as a Distributed Center of the DoD High Performance Computing Modernization Program, provides such systems (at no cost) for anyone approved by the Program Office.

mental 64-processor SGI Origin3000; and a Sun HPC Ultra with 148 distributed processors and 30 Gbytes of memory. The CCS also has more than 12.5 Tbytes of on-line shared rotating disk and robotic storage systems for fileserving and archiving that hold 300 Tbytes of multimedia data but are scalable to over a Petabyte. The Scientific Visualization Laboratory in CCS provides general support across NRL to assist scientists and engineers in producing visual renderings of their work. The Center manages the NRL local area network, NICEnet, which is transitioning from the older FDDI and shared Ethernet local area networks to a fully switched environment based on ATM backbones and both high-speed Ethernet and ATM to the users's desktops. The evolutionary goal is to provide digital transparency of resources with security across the information infrastructure—from globally available archives, to the computational engines, to the networks that bring it all together at 10 Gbps directly to the desktops of the most demanding users—in 2002. NICEnet provides external connections to other networks and to the Internet.

The division facilities also include an Information Security Engineering Laboratory, a Robotics Laboratory, a high-data-rate multimedia satellite transmission facility, and an experimental facility with special displays, eye and gesture trackers, and speech I/O devices for research in human/computer interaction. Laboratories for the development and testing of communication and network protocols both for Internet Protocols (IP) and ATM research are also included. These network testbeds are routinely interfaced to the DoD wide-area research networks for collaboration with other government laboratories. A wireless networking testbed is being used to develop Mobile Ad Hoc Networking (MANET) standards that can meet a wide range of military and commercial needs.

The Virtual Reality (VR) Laboratory provides the facilities and expertise to allow NRL scientists to use virtual reality in a variety of scientific investigations. Research areas include shipboard firefighting, simulation-based design, command, and control, and scientific visualization. A number of high-speed graphics workstations, including Onyx Reality Engine 2 and Infinite Reality computers, and a variety of VR peripherals comprise the VR Lab computer equipment inventory.

Current VR technologies available include desktop VR systems, head-mounted displays (HMDs), the Responsive Workbench, and the surround-screen Immersive Room. The Responsive Workbench is an interactive 3-D tabletop environment that displays computer-generated, stereographic images on the workbench surface for use in battlespace situation awareness, simulation-based design, and other applications. The surround-screen Immersive Room is a multiuser, high-resolution 3-D visual and audio environment that projects computer-generated images onto three walls and the floor to create an immersive, large-scale, shared virtual environment. It uses an SGI Onyx RE2 so scientists can interact and control their supercomputing calculations in real time.

The NEWAVE facility has been developed as a multiscreen distributed simulation laboratory and viewport. Powered by SGI and Pentium workstations and linked to the NRL parallel computing facilities with ATM/SONET networking, the facility is capable of handling high-performance computing, graphics, and distributed simulation.

Optical Sciences

The Optical Sciences Division has a broad program of basic and applied research in optics and electro-optics. Areas of concentration include fiber optics, integrated optical devices, signal processing, optical information processing, fiber-optic and infrared (IR) sensors, laser development, surveillance, and reconnaissance.

The division occupies some of the most modern optical facilities in the country. This includes an Ultralow-loss, Fiber-Optic Waveguide Facility using high-temperature infrared glass technology. There is also a Focal-Plane Evaluation Facility to measure the optical and electrical characteristics of infrared focal-plane arrays being developed for advanced Navy sensors. The IR Missile-Seeker Evaluation Facility performs open-loop measurements of the susceptibilities of IR tracking sensors to optical countermeasures. The Large-Optic, High-Precision Tracker system is used for atmospheric transmission and target signature measurements. The Infrared Test Chamber is an ultradry test chamber used to measure the IR signatures of new surface treatments, scale models, and components used for observable control on ships, aircraft, and missiles.

There are several fiber-optic sensor facilities with fiber splicers, an acoustic test cell, a three-axis magnetic sensor test cell, equipment for evaluating optical fiber coatings, and various computers for concept analysis. The Digital Processing Facility is used to collect, process, analyze, and manipulate infrared data and imagery from several sources. The Emittance Measurements Facility performs measurements of directional hemispherical reflectance. Extensive laboratories exist to develop and test new laser and nonlinear frequency conversion concepts and to evaluate nondestructive test and evaluation techniques.

The newest facilities are a scanning probe facility equipped with both an atomic force microscope and a magnetic force microscope and an ultra-high vacuum, surface analysis chamber with both X-ray and ultraviolet photoemission spectroscopy for determination of energy levels in metals, semiconductors, and organic materials.

Electronic Warfare

The scope of the Tactical Electronic Warfare (TEW) Division's program for electronic warfare (EW) research and development covers the entire electromagnetic spectrum. The program includes basic technology research and advanced developments and their applicability to producing EW products. The range of ongoing activities includes components, techniques, and subsystems development as well as system conceptualization, design, and effectiveness evaluation. The focus of the research activities extends across the entire breadth of the battlespace. These activities emphasize providing the methods and means to counter enemy hostile actions—from the beginning, when enemy forces are being mobilized for an attack, through to the final stages of the engagement. In conducting this program, the TEW Division has an extensive array of special research and development laboratories, anechoic chambers, and modern computer systems for modeling and simulation work. Dedicated field sites and an NP-3D EW flying laboratory allow for the conduct of field experiments and operational trials. This assembly of scientists, engineers, and specialized facilities also supports the innovative use of all fleet defensive and offensive EW resources now available to operational forces through the Naval Science Assistance Program.

Laboratory for Structure of Matter

This laboratory investigates the atomic arrangements in materials to improve them or facilitate the development of new substances. Various diffraction methodologies are used to make these investigations. Subjects of interest include the structural and functional aspects of energy conversion, ion transport, device materials, and physiologically active substances such as drugs, antibiotics, and antiviral agents. Theoretical chemistry calculations are used to complement the structural research. A real-time graphics system aids in modeling and molecular dynamics studies. The facilities include three x-ray diffraction units, one being a state-of-the-art facility, and an atomic force microscope.

Chemistry

NRL has been a major center for chemical research in support of naval operational requirements since the late 1920s. The Chemistry Division continues this tradition with a broad spectrum of basic and applied research programs focusing on controlled energy release (fuels, fire, combustion, countermeasure decoys, explosives), surface chemistry (corrosion, adhesion, tribology, adsorbents, film growth/etch), advanced materials (high-strength/low-weight structures, drag reduction, damping, polymers, thin films), and advanced detection techniques (environment, chemical/biological, surveillance). Facilities for research include:

Chemical analysis facilities, including a wide range of modern photon/electronic, magnetic- and ion-based spectroscopic/microscope techniques for bulk and surface analysis;

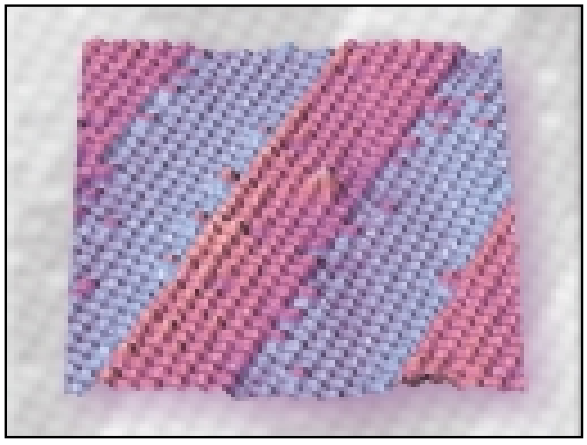

Color-enhanced scanning tunneling microscopy image of a cross-section showing the atomic-scale structure at the interfaces between GaSb and InAs superlattice layers. This work, incorporating sample preparation by scientists in the Electronics Sciences and Technology Division, STM measurement and interpretation by Chemistry Division staff, and modeling by theorists in the Materials Science and Technology Division, illustrates the multidisciplinary character of NRL research.

Synchrotron Radiation Facility, with intense, monochromatic X-ray photon beams tunable from 10 eV to 12 KeV available from two beam lines developed by NRL at the National Synchrotron Light Source at the Brookhaven National Laboratory. Environmental target chambers span a pressure range from 10^{-12} to 10^{5} atm and temperatures from 10 to 1500 K;

Nanometer measurement facility, which includes fabrication and characterization capability based on scanning tunneling microscopy/spectroscopy, atomic force microscopy, and related techniques;

Materials synthesis/property measurement facility, with special emphasis on polymers and surface/film processing;

Fire research facilities, ranging from laboratory combustion chemistry, to a 10^{4} ft^{3} fire-research chamber (Fire I) and the 475-ft ex-USS *Shadwell* (LSD-15) advanced fire research ship; and

Marine Corrosion Test Facility, located on Fleming Key at Key West, Florida, offers an ocean-air environment and clean, unpolluted, flowing seawater for studies of environmental effects on materials. Equipment is available for experiments involving weathering, general corrosion, fouling, and electrochemical phenomena as well as coatings, cathodic protection devices, and other means to combat environmental degradation.

Materials Science and Technology

NRL has capabilities for X-ray and electron-diffraction analyses and for electron and Auger spectroscopy. Scanning, transmission, and combined scanning-transmission electron microscopes are used to study surface and/or internal microstructures. The division has a secondary ion mass spectrometer for surface analysis that significantly extends the diagnostic capability of the technique. A high-resolution, reverse-geometry mass spectrometer is used to probe reactions between ions and molecules. The Laboratory has a fully equipped fatigue and fracture laboratory and hot isostatic press facilities. The Laboratory's cryogenic facilities include dilution refrigerators and superconducting magnetic sensors for measuring ultrasmall magnetic fields. Also available are two molecular beam epitaxy devices for growing thin films. In addition, division facilities include:

High-Power Microwave (HPM) Facility: The large anechoic chamber (4.9 m × 4.9 m × 9.8 m) can be used at frequencies ranging from 0.5 to 94 GHz. Effects, susceptibility, and survivability of systems are the major research areas of interest.

Trace Element Accelerator Mass Spectrometry (TEAMS) – 3 MV Tandem Pelletron Accelerator Facility: Used for standard materials analysis such as Rutherford backscattering, for MeV-energy ion implantation, and for accelerator mass spectrometry (AMS). AMS measures trace elements in parallel with 3-D imaging at 10-μm lateral resolution (0.01 μm in depth) to 10-ppt sensitivity, and isotopes for sample dating and forensics.

Laser Facilities: Pulses of up to several joules are available from one system, while time resolutions down to 30 femtoseconds are produced by another. Synchronized Q-switched oscillators are configured for pump-probe experiments.

Thin-Film Preparation Facilities: The division has several major capabilities for preparation of thin films of advanced materials, such as high-temperature superconductors and active dielectrics. These include ion-assisted evaporation (which produces dense, adherent films), various dc plasma sources (which can etch as well as deposit films), and pulsed laser deposition (for production of chemically complex films).

Ion Implantation Facility: The facility consists of a 200-keV ion implanter with specialized ultra-high vacuum chambers and associated in situ specimen analysis instrumentation.

Laboratory for Computational Physics and Fluid Dynamics

The Laboratory for Computational Physics and Fluid Dynamics (LCP & FD) is in round-the-clock production for computational studies in the fields of compressible and incompressible fluid dynamics, reactive flows, fluid-structure interaction (including submarine, ship, and aerospace applications), plasma physics, atmospheric and solar magnetoplasma dynamics, application of parallel processing to large-scale problems such as unstructured grid generation for complex flows, and other disciplines of continuum and quantum computational physics. The facility is used to develop and maintain state-of-the-art analytical and computational capabilities in fluid dynamics and related fields of physics, to establish in-house expertise in parallel processing and on-line graphical rendering for large-scale scientific computing, to perform analyses and computational experiments on specific relevant problems, and to transfer this technology to new and ongoing projects through cooperative programs.

LCP&FD maintains a very powerful collection of computer systems. There is currently a total of 136 parallel SGI processors, 80 parallel HP processors, 36 clustered Alpha processors, and several other

support systems. In addition, there are more than 50 Macintosh computers, most of which are capable of large calculations both independently and in parallel ad hoc clusters.

The individual systems are composed of a 64 R12K processor SGI Origin2000, two parallel processing systems in classified environments, an eight R12K processor Origin, an 18 R10K processor Power Challenge, and a six R8K processor PowerOnyx. The HP Exemplar systems consist of a 64-processor X-class SPP system and a 16-processor S-class SPP system. The Alpha cluster is a collection of 21264 processor Linux systems well coupled with Myrinet high-speed switched interconnect. A 16-processor SGI 3000 will arrive by the end of the year. Additional processors are expected to be added to this system next year.

Each system has on the order of 200 Gigabytes of disk for storage during a simulation, and at least 256 Megabytes of memory per processor. All unclassified systems share a common disk space for home directories as well as almost 250 Gigabytes of AFS space that can be used from any AFS capable system throughout the allowed internet.

The AFS capability also allows access to other storage systems including NRL's multiresident AFS (MRAFS) system that automatically handles archival to a multi-terabyte tape archival system.

Plasma Physics

The Plasma Physics Division is the major center for in-house Navy and DoD plasma physics research. The division conducts a broad experimental and theoretical program in basic and applied research in plasma physics, which includes laboratory and space plasmas, pulsed-power sources, plasma discharges, intense electron and ion beams and photon sources, atomic physics, laser physics, advanced spectral diagnostics, plasma processing, nonlinear dynamics and chaos, and numerical simulations. The facilities include an extremely high-power laser—Pharos III—for the laboratory simulation of space plasmas and nuclear weapons effects studies and a short pulse, high-intensity Table-Top Terawatt (T^3) laser to study intense laser-plasma, laser-electron beam, and laser-matter interactions. The division also has an 11 m^3 space chamber capable of reproducing the near-Earth space plasma environment and a Large Area Plasma Processing System (LAPPS) facility to study material modification such as surface polymerization or ion implantation. The division has developed a variety of pulsed-power sources to generate intense electron and ion beams, powerful discharges, and various types of radiation. The largest of these pulsers—GAMBLE II—is used to study the production of megampere electron and ion beams and to produce very hot, high-density plasmas. Other generators are used to produce particle beams that are injected into magnetic fields and/or cavities to generate intense microwave pulses. A large array of high-frequency microwave sources (2.45, 35, and 83 GHz) are available to conduct research on microwave processing of advanced ceramic materials. In particular, the division added a 15-kW, continuous wave, 83 GHz gyrotron to its facility for research on high-frequency microwave processing of materials. The Russian-made gyrotron produces a focused, high-intensity millimeter-wave beam (10^3-10^5 W/cm^2) that has unique capabilities for rapid, selective heating of a wide range of nonmetallic materials. The new gyrotron-based system will be used to investigate the application of such beams to important areas of material processing, including coating of materials, soldering and brazing, and treatment of ceramics, semiconductors, and polymers.

A major 3 kJ KrF laser facility (Nike) opened in June 1995. This facility is made up of 56 laser beams and is single pulsed (4 nanosecond pulse). This facility provides intense radiation for studying inertial confinement fusion (ICF) target heating at short wavelengths (0.25 microns) and high-pressure physics.

Electronics Science and Technology

In addition to specific equipment and facilities to support individual science and technology programs, NRL operates the Nanoelectronics Processing Facility (NPF), the Penthouse Processing Facility (PPF), the Laboratory for Advanced Material Synthesis (LAMS), the EPICENTER, the Laser Facilities (LF), and the Space Solar Cell Characterization Facility (SSCCF). The NPF's mission is to provide service to both NRL and external organizations requiring micro- and nanofabrication processing support. Lithography is a particular strength of the NPF, with definition of feature sizes down to 150 angstroms possible with an e-beam nanowriter. The NPF can supply items ranging from individual discrete structures and devices to circuits with very-large-scale integration complexity. The PPF is dedicated to processing III-V semiconductor devices and circuits in addition to serving the hands-on fabrication needs of individual NRL scientists. The PPF uses a single-pass air-ventilation system to minimize human risk from potentially hazardous III-V semiconductor processes and associated chemicals, thereby further meeting existing safety standards. The LAMS uses organometallic vapor phase epitaxy to synthesize a wide range of thin films such as InSb, InGaP, InP, and GaN. The EPICENTER (a joint activity of the Electronics Science and

Source chamber of the Large Area Plasma Processing System (LAPPS) processing reactor. The coils generate 100-200 Gauss magnetic fields inside the stainless steel high vacuum chamber. A low current electron beam is produced in the chamber that generates large area plasma sheets. These sheets are then used for processing materials such as etching silicone or coating plastics.

Technology, Materials Science and Technology, Optical Science, and Chemistry Divisions) is dedicated to the production of multilayer microstructures using in situ surface analytical techniques in one of several ultrahigh vacuum, molecular-beam-epitaxy growth and processing chambers—one for growth of conventional III-V semiconductors, one for vacuum processing, one for growth of III-V semiconductor ferromagnetic materials, one for growth of 6.1 angstrom III-V semiconductors and another for growth of magnetic materials and II-VI semiconductors. The Laser Facilities consist of an Ultrafast Laser Laboratory (ULL) that is optimized for the characterization of photophysical and photochemical processes in materials on a timescale of tens of femtoseconds and a Laser Single-Event Effects Facility (LSEF) that uses a synchronously pumped dye laser system for simulating the effects of charge deposited in semiconductors characteristic of space radiation. The SSCCF studies the effect of particle irradiation on new and emerging solar cell technologies for space applications.

Bio/Molecular Science and Engineering

The Center for Bio/Molecular Science and Engineering conducts research and development using biotechnological approaches to solve problems for the Navy, DoD, and the nation at large. Problems currently being addressed include advanced material development (for electronic, biomedical, and structural applications), environmental quality (including pollution cleanup and control), and biological warfare defense. The approach to these problems involves long-term research focused on the study of complex materials systems, coupled with integrated exploratory and advanced development programs. The staff of the Center is an interdisciplinary team that performs basic and applied research and development in areas that require expertise in bio- and surface chemistry, biophysics, genetic engineering, cell biology, advanced organic synthesis, solid-state and theoretical physics, and electronics and materials engineering. In addition, the Center has many collaborations throughout the Laboratory, at universities, and in industry to ensure that a broad base of the required expertise and critical evaluations are part of the research and development programs. Highlights of the program include the manipulation of biologically derived structures on the nanometer scale, the development of ferroelectric liquid crystal systems with microsecond response times, discovery of an advanced resist system for high-speed, high-density integrated circuits, the patterning of neuronal cells to form neural networks, and the development of biosensors for environmental monitoring.

The Center occupies renovated laboratories and offices in Building 30. These modern facilities, designed to be used well into this century, include general laboratories for research in chemistry, biochem-

istry, molecular biology, and physics. Specialized areas include a 600-ft^2 Class 1000 clean room; an advanced Electron Microscope facility; and a Scanning Probe Microscope laboratory. Instrument rooms provide access to a variety of spectrophotometers (IR, GC-MS, NMR, and UV-Vis) and other equipment used in biochemical or physical analyses of biomaterials. Additional laboratories accommodate an X-ray diffraction instrument, a liquid crystal fabrication facility, and equipment for advanced electronics and biosensor programs.

Acoustics

The Acoustics Division has three integrated structural acoustic facilities—two pools (including one with a sandy bottom) and a large in-air, semi-anechoic laboratory—that support research in submarine target characteristics for antisubmarine warfare, submarine acoustic design and quieting, sensors for hull-mounted sonars, mine detection and identification, torpedo quieting, and noise control in the interior of air and submarine structures. Scaled submarine targets, real mines, sensors mounted on hull simulators, underwater buried objects, actual torpedoes, small aircraft fuselages, and satellite payload launch fairings can all be examined with advanced nearfield holographic and scanning 3-D laser vibrometer systems to measure and visualize the sound fields near a structure, the vibrations of the structure itself, the resulting farfield and interior sound fields, and the physics of the sound-structure-fluid interactions.

The division operates several sound sources for the generation and reception of sound in at-sea experiments. Sound sources include three XF-4 units, one ITC 2077 source that can be operated while being towed by a ship, and two battery-operated organ-pipe sources that can project single tones from offboard moorings. In addition, the division has several battery-operated rubidium-clock controlled, programmable sound source moorings that can transmit sounds having arbitrary waveforms.

The division has a number of acoustic receiving arrays for at-sea experiments. Receive systems include a moored 32-channel array that RF telemeters data to a recording site at a rate up to 50 kHz/channel, a 16-channel midfrequency array, and a 128-channel autonomously recording receiving system with 2.2 terabyte capacity. These systems acquire data with rubidium-clock sampling accuracy. The division also has unique, self-recording digital acquisition buoy systems (DABS) that are used to obtain multichannel (up to 128) acoustic data in the 10 Hz to 5 kHz regime. These systems provide up to 250 Gbytes of data on a single 15-inch reel of 1-inch tape.

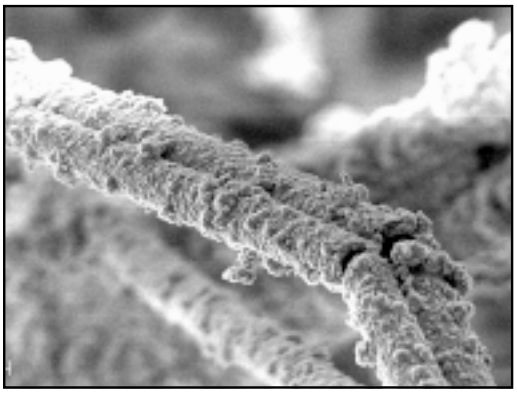

Bio-derived lipid tubules can be metallized and mixed into a polymer matrix to make lightweight dielectric composites for antenna isolation.

The Acoustics Division has a satellite-linked buoy system with underwater receive arrays designed to collect acoustic and oceanic data, unattended, for periods of up to one month. The system currently can handle 64 channels of acoustic data (distributed on one or two arrays), and can implement onboard signal processing prior to data transmission. Two-way satellite communication is supported, providing a high-speed data link (up to 1.5 Mbps) for data transfer from the buoy to shore, and a low-speed command and control link to remotely control buoy functions. The system also contains high-speed (up to Mbps) line-of-sight communications using a GPS-linked directional antenna.

The division conducts underwater acoustic communciations research using digital, acoustic modems capable of receiving and processing signal from eight channels at various carrier frequencies and with various bit rates. An Acoustic Communication Laboratory provides environment simulation, pre-experiment testing and preparation, and post-experiment data analysis.

The division operates high-frequency (up to 600 kHz) acoustic measurement systems to obtain scattering, target strength, and propagation data using bottom-moored instrumentation towers and a high-speed, remotely operated vehicle. These data are used to simulate the performance of weapons and mine countermeasure sonars.

The Tactical Oceanography Simulation Laboratory (TOSL) is a modeling and simulation architecture consisting of a set of tools for processing climatology and real-time environmental data and applying energy propagation models to those data. TOSL features a high-performance computational capability to provide calculations in support of training, war games, operations rehearsal, and other distributed simulation functions. TOSL is coupled via Ethernet

NRL's satellite-linked buoy system during a recent ocean deployment. Data from one or two arrays of hydrophones are collected and stored within the buoy, and simultaneously transmitted to ships in the vicinity and to shore using RF and satellite communications.

and SIPRNET with the Tactical Oceanography Wide Area Network (TOWAN) repository of environmental data, which allows full participation in a distributed simulation environment.

Remote Sensing

The Remote Sensing Division conducts a program of basic research, science, and applications to develop new concepts for sensors and imaging systems for objects and targets on Earth, in the near-Earth environment, and in deep space. The research, both theoretical and experimental, leads to discovering and understanding of the basic physical principles and mechanisms that give rise to background environmental emissions and targets of interest and to absorption and emission mechanisms of the intervening medium. Accomplishing this research requires the development of sensor systems' technology. The developmental effort includes active and passive sensor systems used for study and analysis of the physical characteristics of phenomena that evolve from naturally occurring background radiation, such as that caused by the Earth's atmosphere and oceans and man-made or induced phenomena, such as ship/submarine hydrodynamic effects. The research includes theory, laboratory, and field experiments leading to ground-based, airborne, or space systems for use in remote sensing, astrometry, astrophysics, surveillance, nonacoustic ASW, meteorological/oceanographic support systems for the operational Navy, and the environmental/global climate change initiatives. Special emphasis is given to developing space-based platforms and exploiting existing space systems.

The Remote Sensing Division conducts airborne hyperspectral data collections for characterization of the environment. Hyperspectral data are series of pictures, taken simultaneously, of a scene at many different wavelengths (colors). The sensors are built and calibrated in-house, although they rely heavily on commercial off-the-shelf elements. The most recent sensor was specifically designed for use over ocean areas. It covers the 400 to 1000 nanometer wavelength range with 128 different wavelengths (channels). The sensor consists of a standard video camera lens, a grating spectrograph, and a 1024 × 1024 pixel charge-coupled device (CCD). The spectrograph and CCD are specially designed to achieve high sensitivity in the blue end of the spectrum to optimize water-penetrating measurements. This makes possible measurements such as the determination of the ocean bottom type (coral, sea grass, sand, rock, etc.) to water depths of as much as 20 meters (in clear water), and the identification of material in the water column (phytoplankton, sediments, colored dissolved organic matter, etc.). The sensor is very compact and can be flown at heights of 8000 to 10,000 feet, simply "looking" out of a hole in the bottom of the airplane. At ground speeds of 90 knots, the data can still be collected digitally and stored on computer. It is then processed in a ground system operating on a standard personal computer.

Proper interpretation of the hyperspectral data requires calibration of the sensor. This means both radiometric calibration and spectral calibration. The latter plays a critical role in the successful correction of the data for atmospheric effects. The Remote Sensing Division operates an Optical Calibration Facility to perform these calibrations. NIST radiometric standards are transferred to a large integrating sphere. The integrating sphere has 10 precisely controlled quartz-halogen lamps to enable linearity measurements. A set of gas emission standards provides wavelength calibration. As a result, the complete process of data collection through data analysis can be handled in-house.

The Navy Prototype Optical Interferometer (NPOI), a major facility of the Remote Sensing Division, is actually two collocated instruments for making high-angular-resolution optical measurements of stars. Light from widely separated individual siderostats is combined simultaneously to synthesize the angular resolution of a telescope tens to hundreds of meters in diameter. Four siderostats are

placed in an array with extremely accurate metrology to enable very-high-precision measurements of stellar positions (wide-angle astrometry). These measurements are used by the U.S. Naval Observatory to refine the celestial reference frame, determine Earth rotation parameters, and thus satisfy Navy requirements for precise time and navigation data. They also provide determinations of basic astrophysical parameters, such as stellar masses and diameters. Additional relocatable siderostats can be placed out to distances of 250 m from the array center and used to construct very-high-resolution images of stars. These images provide fundamental astrophysical information on stellar structure and activity. When complete, the NPOI will be the most advanced high-resolution imaging optical interferometer in the world.

To validate numerical and theoretical efforts ongoing within the Remote Sensing Division, extensive hierarchical-coupled experiments are carried out in the Free-Surface Hydrodynamics Laboratory. This laboratory is used to study free-surface turbulence interactions, wave-generation phenomena, jet-flow phenomena, vorticity dynamics, and free-surface/surfactant interactions. Emphasis is placed on those processes that determine the fluxes of heat, mass, and momentum across the air-sea interface. State-of-the-art diagnostic tools are available, such as Langmuir film balance to measure the properties of surface films, hot-wire and laser-Doppler anemometry, and the new quantitative flow techniques of laser speckle, particle tracking, and particle image velocimetry. The laboratory is also equipped with an IR camera with a 20×10^{-3} K resolution. These experimental diagnostic techniques use high-powered lasers, high-tolerance optical lenses, and extensive ultra-high-resolution video-imaging hardware and PC-based computerized systems. Further computational assets consist of powerful graphical computer work stations, the NRL Connection Machine, and other off-site Cray supercomputer systems.

Oceanography

The Oceanography Division is the major center for in-house Navy research and development in oceanography. It is known nationally and internationally for its unique combination of theoretical, numerical, experimental, and remote sensing approaches to oceanographic problems. The division numerically models the ocean and coastal areas of the world. This modeling is conducted on the Navy's and DoD's most powerful vector and parallel-processing machines. To study the results of this intense modeling effort, the division operates a number of highly sophisticated graphic systems to visualize ocean and coastal dynamic processes. The seagoing experimental programs of the division range worldwide. Unique measurement systems include towed sensor and advanced microstructure profiler systems for studying micro- and fine-scale ocean structures; a wave measurement system to acquire in situ spatial properties of water waves; a salinity mapper that acquires images of spatial and temporal sea surface salinity variabilities in littoral regions; an integrated absorption cavity, optical profiler system, and towed optical hyperspectral array for studying ocean optical characteristics; and self-contained bottom-mounted upward-looking acoustic Doppler current profilers for measuring ocean variability. In the laboratory, the division operates an environmental scanning electron microscope for detailed studies of biocorrosion in naval materials. The division's remote sensing capabilities include the ability to analyze and process multi/hyper-spectral, IR, SAR, and other satellite data sources. The division is a national leader in the development and analysis of Sea WiFS data for oceanographic processes and naval applications in littoral areas.

Marine Geosciences

The Marine Geosciences Division is the major Navy in-house center for research and development in marine geology, geophysics, geodesy, geoacoustics, geotechnology, and geospatial information and systems. The division has unique suites of instrumentation and facilities to support laboratory and field experimental programs.

The instrumentation used in the field experiments is deployable from ships, remotely operated and unmanned vehicles, and airborne platforms and by divers. Seafloor and subseafloor measurements use the Deep-Towed Acoustic Geophysical System (DTAGS—250 to 650 Hz); high-resolution sidescan sonars (100 and 500 kHz); the Acoustic Seafloor Characterization System (ASCS-15, 30, and 50 kHz); ocean bottom seismometers and magnetometer; the In Situ Sediment Acoustic Measurement System (ISSAMS); underwater stereo photography; and nearshore video imaging systems. ISSAMS has specialized probes that measure acoustic compressional and shearwave velocities and attenuation, pore water pressure, and electrical conductivity in surficial marine sediments. The Remote Mine Hunting System, Oceanographic (RMSO), an unmanned, diesel-powered, radio-controlled, 8-m semisubmersible, is used to develop improved hydrographic survey techniques, sensor systems, and navigation capabilities.

Laboratory facilities include sediment physical,

geotechnical, and geoacoustic properties and sediment core laboratories. The Electron Microscopy Facility is the focal point for research in microscale biological, chemical, and geological processes. The key instrumentation includes a 300 kVa transmission electron microscope with environmental cell. The environmental cell allows hydrated and gaseous experiments. The Moving Map Composer Facility is used to design and write mission-specific map coverages for F/A-18 and AV-8B tactical aircraft onto militarized optical disks. The National Imagery and Mapping Agency also uses this state-of-the-art computer facility to update the compressed aeronautical chart library on CD for distribution. The Geospatial Information Data Base (GIDB) capability provides Internet access to the Digital Nautical Chart data, mapping data, imagery, and other data types such as video and pictures. This development tool can be used for planning, training, and operations. The division also operates the NRL Magnetic Observatory at Stennis Space Center, Mississippi. This magnetically clean area consists of an array of magnetometers that measure Earth's ambient magnetic field. The observatory is part of a worldwide observing system.

Marine Meteorology

The Marine Meteorology Division is located in Monterey, California. NRL-Monterey (NRL-MRY) is the only Navy facility with a mission to serve the Navy's needs for basic research in atmospheric sciences and its need for the development of meteorological analysis and prediction products to support global and tactical operations. The division is dedicated to advancing fundamental scientific understanding of the atmosphere, to applying scientific discoveries in the development of innovative objective weather prediction systems, and to developing ways to provide atmospheric data input to the tactical decision maker.

NRL-MRY is collocated with Fleet Numerical Meteorology and Oceanography Center (FNMOC), the Navy's operational center of expertise in numerical weather prediction. This provides NRL-MRY efficient access to a variety of classified and unclassified computer resources, databases, and numerical prediction systems. Large supercomputer mainframes and databases at FNMOC are used along with DoD High Performance Computing Modernization Program resources and local NRL-MRY resources to develop and transition operational analysis and prediction systems, and to provide on-site and remote access to the model output data for continued research purposes. In addition, interfaces to the Defense Research and Engineering Network have also been established.

Locally, to support research and development needs, NRL-MRY has established the Bergen Data Center. This Center includes a 24TB capacity data center with a hierarchical storage management capability to provide archival and easy retrieval of research data sets. The John B. Hovermale Visualization Laboratory provides state-of-the-art capability for data visualization, which aids the interpretation of both observational and modeled data and the development of weather briefing tools. High-performance graphics workstations, network file-servers, and tactical applications systems are used to conduct numerical weather prediction experiments, process and analyze satellite data, perform simulation studies, and provide demonstrations of tactical weather products. State-of-the-art satellite receiving and processing systems allow local collection of real-time geostationary data globally, from four different satellites, for applications research in support of the Navy and Joint Typhoon Warning Center operations. This capability has allowed NRL-MRY to take the lead in developing meteorological applications of satellite data for the NSDS-E (Navy Satellite Display System-Enhanced), which is currently being installed at the Navy's regional meteorological/oceanographic (METOC) centers.

Space Science

The Space Science Division conducts and supports a number of space experiments in the areas of upper atmospheric, solar, and astronomical research aboard NASA, DoD, and other government-agency space platforms. Division scientists are involved in major research thrusts that include remote sensing of the upper and middle atmospheres, studies of the solar atmosphere, and astronomical radiation ranging from the ultraviolet through gamma rays and high-energy particles. In support of this work, the division maintains facilities to design, construct, assemble, and calibrate space experiments. A network of computers, workstations, image-processing hardware, and special processors is used to analyze and interpret space data. The division's space science data acquisition and analysis efforts include: data analyses of the Oriented Scintillation Spectrometer Experiment (OSSE) for NASA's Compton Observatory; observation of the Sun's interaction with the Earth's upper atmosphere through the Solar Ultraviolet Spectral Irradiance Monitor (SUSIM) experiment in support of NASA's Upper Atmosphere Research Satellite (UARS); observation and analysis of solar flares using the Bragg Crystal Spectrometer (BCS) on the Japanese Yohkoh space mission; and observation and

analysis of the evolution and structure of the solar corona from the disk to 0.14 AU. This latter effort involves acquiring and analyzing data from the Large-Angle Spectrometric Coronagraph (LASCO) and Extreme Ultraviolet Imaging Telescope (EIT) on the Solar Heliospheric Observatory satellite. In each of these missions, NRL maintains a complete database of spacecraft observations and control over acquisition of data from new observations. These data are available to qualified investigators at DoD and civilian agencies. In addition, the division has a sounding rocket program that affords the possibility of obtaining specific data of high interest and of testing new instrument concepts. These include the general area of high-resolution solar and stellar spectroscopy, extreme ultraviolet imagery of the Sun, and high-resolution, ultraviolet spectral-imaging of the Sun.

In addition, selected celestial and atmospheric targets in the ultraviolet and X-ray bands are observed by three Advanced Research and Global Observation Satellite (ARGOS) experiments—Global Imaging of the Ionosphere (GIMI), High-Resolution Airglow and Auroral Spectroscopy (HIRAAS), and Unconventional Stellar Aspect (USA). ARGOS was successfully launched on February 23, 1999. As part of this program, NRL is establishing collaborative programs to make use of ARGOS data to validate various upper atmosphere models and to study time phenomena in X-ray sources.

Optical calibration facilities, including clean rooms, are maintained to support these activities. These calibration facilities are routinely used by outside groups to support their own calibration requirements.

Space Technology

In its role as a center of excellence for space systems research, the Naval Center for Space Technology (NCST) designs, builds, analyzes, tests, and operates spacecraft as well as identifies and conducts promising research to improve spacecraft and their support systems. NCST facilities that support this work include large and small anechoic radio frequency chambers, clean rooms, shock and vibration facilities, an acoustic reverberation chamber, large and small thermal/vacuum test chambers, a spacecraft robotics engineering and control system interaction laboratory, satellite command and control ground stations, a fuels test facility, and modal analysis test facilities. Also, the Center maintains and operates a number of electrical and electronic development laboratories and fabrication facilities for radio frequency equipment, spacecraft power systems, telemetry, and command and control systems, and includes an electromagnetic interference-electromagnetic compatibility test chamber. NCST has a facility for long-term testing of satellite clock time/frequency standards under thermal/vacuum conditions linked to the Naval Observatory; a 5-m optical bench laser laboratory; and an electro-optical communication research laboratory to conduct research in support of the development of space systems.

RESEARCH SUPPORT FACILITIES

Technical Information Services

The Ruth H. Hooker Research Library offers a full range of traditional library services to support the research program of the Naval Research Laboratory. In addition, it is actively engaged in developing a "digital library" that is available 24-hours-a-day, 7-days-a-week. The single-point-of-access to this digital library is the InfoWeb Information System and Gateway (http://infoweb.nrl.navy.mil), which provides desktop access to important scientific databases, such as Science Citation Index Expanded and INSPEC, as well as to reference tools and electronic publications, including more than 1,200 research journals. A key InfoWeb service is TORPEDO *Ultra*, released in January 2000, which hosts several hundred licensed journals and thousands of NRL publications, such as technical reports, journal articles, conference proceedings, and press releases. TORPEDO *Ultra* is the only known system to permit integrated searching, browsing, display, and printing of scientific journals from multiple publishers along with agency publications. The Library's Web-based catalog, locally mounted Science Citation Index Expanded, and an e-mail alerting service called Contents-to-Go, have been enhanced to display the full content of publications that reside in TORPEDO *Ultra*. Links to licensed publications available from Web sites have also been implemented. New license agreements with Academic Press, the IEEE, the Institute of Physics, Kluwer, and other publishers will expand the number of journals available through TORPEDO *Ultra*.

The Technical Information Services Branch combines publications, graphics, and photographic services into an integrated organization. Publication services include writing, editing, composition, publications consultation and production, and printing management. Quick turnaround black and white as well as color copying services are provided. The primary focus is on using computer-assisted publishing technology to produce scientific and technical information containing complex artwork, equations, and tabular material.

TID Publications design specialists review proofs for the 2000 NRL Review.

Graphic and photographic support includes technical and scientific illustrations, computer graphics, design services, photographic composites, display panels, sign making, and framing. Photographic services include still-camera coverage for data documentation both at NRL and in the field. Photographic images can also be captured with state-of-the-art digital cameras. Photofinishing services provide custom processing and printing of black and white and color films. Quick-service color prints are also available. Video services include producing video reports of scientific and technical programs. A video studio and editing facility with high-quality Beta Cam and digital video editing equipment are available to support video production. The NRL Exhibits Program develops and produces displays, audiovisual material, and multimedia programs for presentation at technical meetings, conferences, and symposia. The Multimedia Center has the capability of authoring/producing multimedia programs. The Center uses two complete multimedia systems with Macromedia Director and Adobe Photoshop and a digital video editing system, the AVID Media Composer 1000. The Imaging Center offers high-quality output from computer-generated files in EPS, Postscript, PICT, TIFF, Photoshop, and PowerPoint. Photographic-quality color prints and viewgraphs are available from Kodak dye-sublimation printers. High-resolution scanning to a Macintosh or PC disk is available. The NovaJet Pro 600c printer offers exceptional color print quality up to 600 dpi. It produces large-format posters and signs up to 60 inches wide.

The Administrative Services Branch is responsible for collecting and preserving the documents that comprise NRL's corporate memory. Archival documents include personal papers and correspondence, laboratory notebooks, and work project files—documents that are appraised for their historical or informational value and considered to be permanently valuable. The branch provides records management services, training, and support for the maintenance of active records, including electronic records and e-mail, as an important information resource. The Administrative Services Branch is also responsible for NRL's postal mail services, NRL's Forms and Reports management programs (including electronic forms), and scheduling of NRL auditoriums. The Administrative Services Branch also compiles and publishes the NRL Code Directory and Organizational Index and provides NRL Locator service.

Center for Computational Science

The Center for Computational Science (CCS) conducts research and development to further the advancement of computing and communications systems to solve Navy problems. Promising technologies are transitioned to production systems. The CCS develops and maintains a leading-edge information infrastructure that provides support for NRL, Navy, and DoD research. The CCS participates as a Distributed Center in the DoD High Performance Computing Modernization Program with three massively parallel High Performance Computing (HPC) systems: a 128-processor SGI Origin2000 with 128 Gbyte of memory, a 64-processor experimental Origin3000 with 128 Gbyte memory, and a 148-processor Sun HPC Cluster with 30 Gbytes of memory. File services and archival storage are provided by robotic storage systems running the Multiresident Andrew File System (MRAFS) for both NRL and HPC applications.

The CCS pioneered and maintains the Washington area ATDnet experimental ATM network and is a partner in the MONET research effort. MONET is a leading-edge, all-optical, transparent network being deployed within ATDnet as a part of the DARPA/HPCC Next Generation Internet initiative.

The CCS collaborates with industry and DoD in the development of leading-edge progressive motion imagery for broadcast and network dissemination of all-digital HDTV signals at 720-p and 1080-p.

Additional CCS computational facilities are provided for general NRL use. These include the Scientific Visualization Laboratory (Viz Lab), which functions as an information center, a video production unit, and a training center for the latest tools in scientific visualization and visual supercomputing. Researchers have direct or networked access to computational and high-end graphics workstations. The Viz Lab staff also assists researchers in porting their scientific applications to the Virtual Reality Lab's GROTTO for 3-D, interactive, stereo viewing. In addition, the Viz Lab has recently installed a completely digital, broadcast-video editing suite. Alone or assisted, a researcher can quickly produce a professional-quality video, including titles and special effects, from a montage of computer-generated video, stills, graphs, overheads, or even raw data.

The CCS manages the NRL local area network, NICEnet, which provides access to NRL campus-wide and remote assets, including DoD unclassified and classified networks and the Internet. NICEnet has FDDI backbones and Ethernet, Fast Ethernet, ATM, and FDDI to the desktops. NICEnet provides dial-in services, including SLIP/PPP and ISDN, and has a laboratory-wide cable television network.

The CCS provides site license and support contracts for most workstations and desktop computers and manages acquisition contracts, on-line software distribution, consulting and e-mail support, and training services. The CCS staffs a help desk and facilitates software demonstrations to assist NRL researchers.

FIELD STATIONS

NRL has acquired or made arrangements over the years to use a number of major sites and facilities for research. The largest facility is located at the Stennis Space Center (NRL-SSC), in Bay St. Louis, Mississippi. Others include a facility at the Naval Postgraduate School in Monterey, California (NRL-MRY), and the Chesapeake Bay Detachment (CBD) in Maryland. Additional sites are located in Maryland, Virginia, Alabama, and Florida.

Flight Support Detachment (NRL FSD)

Located at the Naval Air Station Patuxent River, Lexington Park, Maryland, the Flight Support Detachment (NRL FSD) is manned by approximately 9 officers, 80 enlisted, four civilians, and 20 contract maintenance technicians. NRL FSD is currently responsible for the maintenance and security of six, uniquely configured, P-3 Orion turboprop research aircraft. The FSD conducts numerous single-aircraft deployments around the world in support of a wide range of scientific research projects.

In FY 00, NRL FSD provided flight support for diverse research programs including: Advanced Radar Periscope Detection and Discrimination (ARPDD), an advanced variant of the APS-137 ISAR radar used for detecting submarine periscopes; Cooperative Engagement Capability (CEC), an airborne suite to test USN Aegis Cruiser systems; Remote Ultra-low Light Imager (RULLI); Airborne Geographical Sensor Suite (AGSS), involving data and gravimeter testing to detect variations in the ocean floor; Real Aperture Radar (RAR); Integrated Electronic Warfare System (IEWS), a system that simulates radar of various surface and airborne platforms; Navy Tactical Aircraft Directional Infrared Countermeasures/Advance Technology Demonstration (TADIRCM), in-flight detection, threat determination and tracking technology testing; and NAVOCEANO Oceanographic Surveillance (OS).

The Flight Support Detachment continues to improve both capabilities and diversity among its aircraft platforms. Researcher 442 has completed its

NRL's uniquely configured P-3, taking off from NAS Patuxent River, will enable command and control (C2), electronic warfare (EW), and electro-optics (EO) research and development well into the 21st century.

scheduled rework to install an E-2C "Hawkeye" rotodome antenna and is currently supporting the Navy's Theater Air Defense programs. The FSD also completed its 38th year of mishap-free flying, accumulating more than 59,000 flight hours.

Chesapeake Bay Detachment (CBD)

CBD occupies a 168-acre site near Chesapeake Beach, Maryland, and provides facilities and support services for research in radar, electronic warfare, optical devices, materials, communications, and fire research. A ship-motion simulator (SMS) is used to test and evaluate radar, satellite communications, and line-of-sight RF communications systems under dynamic conditions (various sea states). The SMS can handle up to 12,000 pounds of electronic systems. A roll motion of up to 30 degrees (15 degrees to port and 15 degrees to starboard) can be applied to this axis. The pitch axis has a fixed motion of 10 degrees (5 degrees to stern and 5 degrees to bow). Periods along both axes, pitch and roll, are variable—from a slow 32-s to a brisk 4-s rate. Variable azimuth motion can also be added to the pitch and roll action. Synchronized positioning information (×1 and ×36) is available for each of the three axes of the SMS.

Because of its location high above the western shore of the Chesapeake Bay, unique experiments can be performed in conjunction with the Tilghman Island site, 16 km across the bay from CBD. Some of these experiments include low clutter and generally low-background radar measurements. By using CBD's support vessels, experiments are performed that involve dispensing chaff over water and radar target characterizations of aircraft and ships. Basic research is also conducted in radar antenna properties, testing of radar remote-sensing concepts, use of radar to sense ocean waves, and laser propagation. CBD also hosts facilities of the Navy Technology Center for Safety and Survivability, which conducts fire research on simulated carrier, surface, and submarine platforms.

Stennis Space Center (NRL-SSC)

NRL-SSC, a tenant activity at NASA's John C. Stennis Space Center, is located in the southwest corner of Mississippi, about 50 miles northeast of New Orleans, Louisiana, and 20 miles from the Mississippi Gulf Coast. Other Navy tenants at SSC include the Commander, Naval Meteorology and Oceanography Command and the Naval Oceanographic Office, who are major operational users of the oceanographic and atmospheric research and development

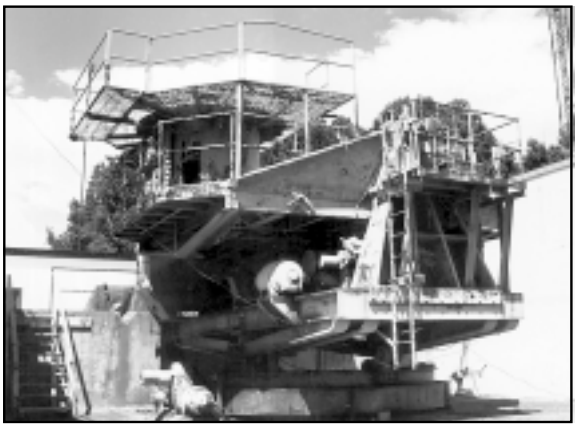

The ship-motion simulator, located on the shoreline of the Chesapeake Bay at NRL's Chesapeake Bay Detachment, allows radar, satellite communications, and line-of-sight RF communications systems to be tested before shipboard installation or in lieu of actual at-sea testing.

performed by NRL. The Naval Oceanographic Office provides access for NRL researchers to one of the Navy's largest supercomputers. This unique concentration of operational and research oceanographers makes SSC the center of naval oceanography and the largest such grouping in the Western world. Additional Navy tenants at SSC include Special Boat Unit 22, and the Human Resources Service Center, South East.

NRL-SSC provides administrative and business operations for entities of the Acoustics, Marine Geosciences, and Oceanography Divisions. NRL-SSC occupies more than 175,000 square feet of research, computation, laboratory, administrative, and warehouse space. Facilities include the new microscopy center, a visualization laboratory, numerous large antennas to receive available oceanographic and meteorological satellite data, the Magnetic Observatory—part of a worldwide observing system, the Pattern Analysis Laboratory, a Map Data Formatting Facility, and numerous laboratories for acoustic and oceanographic computation, instrumentation, analysis, and testing. Special areas are available for constructing, staging, refurbishing, and storing sea-going equipment.

Marine Meteorology Division (NRL-MRY)

NRL's Marine Meteorology Division (NRL-MRY) is located in Monterey, California, on the grounds of the Naval Postgraduate School (NPS) Annex, which is about a mile from the NPS main campus. As a tenant activity of the Naval Support Activity, Monterey Bay, the NRL facility is collocated with the Navy's operational Fleet Numerical Meteorology and Ocean-

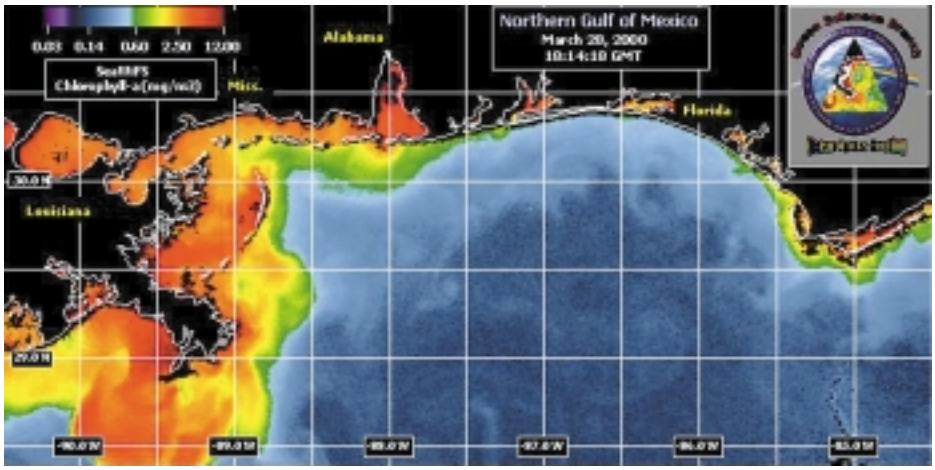

Ocean color imagery from Sea Wide Field-of-View satellite provides understanding of the bio-optical properties along coastal regions.

ography Center (FNMOC) and with a NOAA National Weather Service Forecast Office (NWSFO). The NPS Annex campus, which covers approximately five acres, comprises four primary buildings—one occupied exclusively by NOAA, one that houses the FNMOC supercomputer/operational facility, and two large buildings containing office space, computer laboratories, and conference facilities that are shared by FNMOC and NRL-MRY personnel. The site also provides warehouse space and recreational facilities. NRL-MRY occupies approximately 30,000 square feet in shared buildings. This includes not only office space, but also a small library, the John B. Hovermale Visualization Laboratory, the Bergen Data Center, the Geostationary Satellite Processing Facility, and space for the hardware supporting the Tactical Environmental Support System (TESS), the Tactical Atmospheric Modeling System/Real-Time (TAMS/RT), and the Master Environmental Laboratory.

NRL-MRY is dedicated to advancing fundamental scientific understanding of the atmosphere, including the air-sea interface, and to applying those scientific discoveries in the development of innovative objective weather prediction systems. FNMOC is the Navy's central site facility for the production and distribution of numerical weather prediction products in support of Navy operations around the globe, as well as to other defense-related activities. Fleet Numerical, and the Navy's regional METOC Centers, are the primary customer for the numerical weather prediction systems that are developed by NRL-MRY. This collocation of the scientific developer with the operational customer offers advantages for the successful implementation of new systems and system upgrades, and for the rapid infusion of new research results from the community at large. NRL-MRY has efficient access to FNMOC's large classified vector supercomputer and other systems. This allows advanced development to take place using the real-time on-site global atmospheric and oceanographic databases. Collocation also offers the opportunity for FNMOC scientists to team with NRL-MRY scientists during the transition and implementation process, and NRL-MRY scientists remain readily available for consultation on any future problems that arise.

NRL-MRY benefits from the opportunities provided by NPS for continuing education and for performing collaborative research with the Department of Meteorology and Oceanography.

Midway Research Center

The Midway Research Center (MRC) is located on a 158-acre site in Stafford County, Virginia. Located adjacent to the Quantico Marine Corps' Combat Development Command, the MRC has 10,000 square feet of operations and administration area and three precision 18.5-m-diameter parabolic antennas housed in 100-ft radomes. The MRC, under the auspices of the Naval Center for Space Technology, provides NRL with state-of-the-art facilities dedicated solely to space-related applications in naval communications, navigation, and basic research.

Other Sites

Some field sites have been chosen primarily because they provide favorable conditions to operate specific antennas and electronic subsystems and are close to NRL's main site. Pomonkey, Maryland, a field site south of NRL, has a free-space antenna range

to develop and test a variety of antennas. The antenna model measurement range in Brandywine, Maryland, has a 4.6-m diameter turntable in the center of a 305-m-diameter ground plane for conducting measurements on scale-model shipboard and other antenna designs. A site on the cliffs overlooking the Chesapeake Bay provides an over-the-water range of approximately 10 miles to Tilghman Island.

Research Platforms

Mobile research platforms contribute greatly to NRL's research. These include six P-3 Orion turboprop aircraft and one ship, the ex-USS *Shadwell* (LSD-15), berthed in Mobile Bay, Alabama. The ex-*Shadwell* is used for research on fire-suppression techniques on-board ship.

LOOKING AHEAD

To provide preeminent research for tomorrow's Navy, NRL must maintain and upgrade its scientific and technological equipment to keep it at the forefront of modern research facilities. The physical plant to house this equipment must also be state of the art. NRL has embarked on a Corporate Facilities Plan to accomplish these goals. This plan and future facility plans are described below.

THE CORPORATE FACILITIES INVESTMENT PLAN (CFIP)

The CFIP is a capital investment plan that uses both Congressionally approved military construction (MILCON) and Laboratory overhead funds to provide modern, up-to-date laboratory facilities for NRL. Past MILCON projects have included the Electro-Optics Building at NRL-DC and a new Ocean Acoustics Research Laboratory at NRL-SSC. Future MILCON projects include an already approved Nano-Science Research Laboratory in FY 01 and a proposed Autonomous Vehicles Research Building in the FY 03 time frame.

To complement these efforts, overhead funds have been used to renovate and upgrade laboratory and support areas in several existing buildings. Modern laboratory facilities have recently been provided for the Center for Bio/Molecular Science and Engineering, the Materials Science and Technology Division, the Remote Sensing Division, the Acoustics Division, the Information Technology Division, and the Radar Division.

In parallel with efforts to upgrade laboratory buildings to the most modern standards, those buildings that were built during World War II and do not lend themselves to renovation are being demolished. This will provide space for the construction of future MILCON buildings, and it will also reduce the Laboratory's overhead costs.

Information Technology

The Information Technology Division's Center for Computational Science (CCS) operates three scalable, massively parallel Global Shared Memory (GSM) computer systems. A 128-processor SGI Origin2000 and an experimental 64-processor SGI Origin3000 have cache-coherent Non-Uniform Memory Access (ccNUMA) architectures. A 148-processor Sun HPC Cluster distributed system has 96 processors that operate symmetrically in a Cache-Only Memory Access (COMA) architecture. Plans for FY 01 include the addition of an experimental multi-threaded architecture (MTA) high-performance computer with 32 or more processors. These systems comprise the Distributed Center (DC) at NRL whose hardware is funded by the DoD High Performance Computing Modernization Program (HPCMP). The systems are used in the innovative exploration and evaluation of MPP technology for the solution of significant militarily relevant problems relating to computational and information science. The systems allow for leading-edge research in support of heterogeneous parallel processing applications by the Navy and DoD science and technology communities.

Chemistry

The revolutionary opportunities available in nanoscience/nanotechnology have led to a National Nanotechnology Initiative. NRL has been a major contributor to progress to date, but has been hampered by inadequate infrastructure. The manipulation and measurement of materials with nanometer dimensions is very difficult. One must be able to reliably and precisely locate structures with nanometer dimensions in much larger areas. Furthermore, the measurement of nanostructure properties is difficult simply because there are not many atoms/molecules present. A building designed for nanoscience must

be carefully constructed to minimize potential sources of "noise." Vibrations, thermal drift, and humidity drift can cause major problems in positioning a tool. Good signal-to-noise ratio requires electromagnetic and acoustic interference-free environments. Airborne contamination can readily cover over a nanostructure. NRL has a commitment of FY 01 MILCON funds to design and build a special nanoscience laboratory that will minimize these "noise" sources. Construction will begin in calendar year 2001 with completion scheduled by 2003.

Plasma Physics

The Plasma Physics Division has set up a Large Area Plasma Processing System (LAPPS) facility to investigate a new technique to produce plasmas for plasma processing. Applications include production of large-area flat-screen displays or elements for phased arrays or materials modification such as surface polymerization or ion implantation. The system is based on low-energy electron beam ionization of a background gas to produce the desired plasma. The system may have advantages over existing techniques for production of large-area (square meter) plasmas, efficiency of plasma production, and control of reactive species.

Electronics Science and Technology

Important division emphasis is focussed on the continual upgrading of the Nanoprocessing Facility (NPF) and the Penthouse Processing Facility (PPF) and expanding activities in the nanoelectronics, heterostructures, and vacuum electronics science and technology programs. The NPF has added a second JEOL nanowriter to give this facility superior capability in defining nanoscale patterns and lines. The Laboratory for Advanced Material Synthesis facility will continue to upgrade its organometallic vapor-phase epitaxy equipment for thin-film semiconductors and provide safer and more environmentally benign processing and waste-disposal techniques. The EPICENTER (a joint activity of the Electronics Science and Technology, Materials Science and Technology, Optical Science, and Chemistry Divisions) will continue to expand into new materials areas to provide new insight into epitaxial semiconductor growth processes that will form the basis for use in the electronic devices of tomorrow. These facilities are enhanced by the new Joint Laboratory for Proximal Probe Nanofabrication that serves as a resource for characterization patterning and process definition necessary for advanced nanodevice fabrication.

Ocean Research Laboratory

NRL's Ocean Research Laboratory is a 52,000 square-foot building that houses the Oceanography Division of the Ocean and Atmospheric Science and Technology Directorate. The building contains office space, oceanographic laboratories, staging areas, a small machine shop, electronic and secure laboratories, and computing facilities for research and development in ocean science and remote sensing.

Acoustics

NRL's Salt Water Tank Facility is designed to provide a controlled environment for studying complex bubble-related processes found in the ocean. It is an experimental pool facility for studies of underwater acoustics, fluid dynamics, and air-sea interface environmental topics under saline conditions. This facility is currently being used to study the acoustics of bubbly media, including bubble entrainment and ambient noise generation, scattering from bubbly structures, and propagation through bubbly media. Future studies include the interaction of bubbles with turbulent flows, bubble coalescence and dissolution, effects of surfactants and contaminants, and bubble-related gas exchange across the air-sea interface.

Remote Sensing

The Remote Sensing Division has developed and installed 74 MHz receivers on the National Radio Astronomy Observatory's Very Large Array (VLA), thereby producing the world's highest angular resolution and most sensitive astronomical interferometric array operating below 150 MHz. In contrast to the VLA's maximum baseline of 35 km, all previous astronomical interferometers operating below 150 MHz had baselines less than 5 km because ionospheric structure had been thought to impose phase variations that would corrupt the interferometric imaging. Work in the Remote Sensing Division has shown that radio astronomical techniques can now remove the ionospheric phase variations and extend interferometer baselines to arbitrary lengths. In its first year of operation, the NRL/NRAO 74 MHz system has been used for a variety of innovative observations with encouraging initial results in solar system, Galactic, and extragalactic astrophysics. The success of the NRL/NRAO 74 MHz system indicates that it is possible to open a new high-resolution, high-sensitivity astronomical window by going to an even larger, more sensitive system. The Remote Sensing Division, in collaboration with the Netherlands Foun-

dation for Research in Astronomy, is currently designing a follow-on instrument, the Low Frequency Array (LOFAR). LOFAR will be a fully electronic, broadband array operating in the 15 to 150 MHz range, with a collecting area of 1 square km at 15 MHz and a maximum baseline of 500 km resolution and sensitivity over the state of the art.

The Remote Sensing Division is also developing other new facilities-class sensors including the Navy Ultrawideband Synthetic Aperture Radar (NUSAR). NUSAR is a fully capable high-resolution (less than 1 meter impulse response) synthetic aperture radar system made to be operated from light aircraft. It is fully polarimetric and can operate as an along-track interferometer. Its frequency range will be expandable, and ultimately it will operate from VHF to X-band.

Marine Geosciences

The Marine Geosciences Division has greatly enhanced the capabilities and quality of seafloor sediment fabric analyses through completion of installation and staff training for its 300-kV transmission electron microscope (TEM) and accompanying environmental cell (EC). The TEM-EC is housed in a specially built facility imparting a null effect on the functioning of the TEM-EC electronics. The new facility will improve transition of developed capabilities and sediment fabric understanding to applied issues of acoustic and shock-wave propagation, mine burial, and mine countermeasures.

Vacuum Ultraviolet Space Instrument Test Facility

The Space Science Division facilities include an ultraclean solar instrument test facility in Building A-13 on the main NRL campus. The new facility is designed to satisfy the rigorous contamination requirements of state-of-the-art solar spaceflight instruments. The facility has a 400-ft^2 Class 10 clean room and a large Solar Coronagraph Optical Test Chamber (SCOTCH). This completely dry-pumped, 550-ft^3 vacuum chamber is maintained at synchrotron levels of cleanliness. Solar instrumentation up to 1 m in diameter and 5 m in length can be physically accommodated in the chamber. The instrument's optical performance is probed and calibrated with a variety of visible and XUV sources mounted on the chamber's 11-m beamline. The optical testing and characterization of the Large-Angle Spectrometric Coronagraph (LASCO) instrument for the European Space Agency's Solar Heliospheric Observatory satellite were conducted in this chamber. Coronagraph stray-light characterization was carried out by mounting a set of baffles in the main beamline, illuminating the instrument with a simulated solar beam, and measuring the residual radiation. A stray light background measurement of 10^{-12} was successfully measured in the LASCO C3 channel. Coronagraph calibration was carried out by installing back-illuminated calibrated opals in front of the instrument entrance aperture. Instrument polarization properties were analyzed by using a variety of polarizers installed in a wheel located between the opal and the instrument. The wheel was remotely controlled from outside the chamber. Instrument Mueller matrices were verified with a 12-in. diameter, two-plate partial polarizer. Calibration and focus of XUV solar instrumentation are accomplished by exposing the instrument to an XUV windowless collimator at the end of the tank. The facility also has a small thermal bake/vacuum test chamber used for vacuum conditioning and thermal testing of spaceflight components and subassemblies. Both the SCOTCH and the small test chamber are instrumented with temperature-controlled quartz-crystal monitors and residual gas analyzers for real-time, quantitative measurements of volatile contamination.

REHABILITATION OF SCIENTIFIC FACILITIES

Specialized facilities are being installed or upgraded in several of the research and support divisions.

Flight Support Detachment

NRL's Flight Support Detachment (FSD) has continued to improve both capabilities and diversity among its aircraft platforms. Aircraft 153442 has undergone extensive modifications with Lockheed Martin to install a "rotodome" antenna and full AEW radar system. The aircraft is currently supporting the Navy's Theater Air Defense programs and providing a testbed for advanced EW radar research. Additionally, all aircraft have completed extensive bomb-bay design improvements that will allow the aircraft to carry more diverse scientific payloads. Aircraft 158227's communications capabilities were significantly upgraded with a state-of-the-art satellite telephone; aircraft 154589 is next in line to receive this INMARSAT system. These upgrades and modifications will ensure that NRL will have the finest airborne research capabilities well into this century.

Radar

About 75% of the Radar Division moved into the newly renovated Building 60 quarters in January 2000. The remainder of the division will occupy the adjacent Building 42 when the renovation is complete in about 2002. The "High Bay" facility in Building 48 is scheduled to be replaced by a newer facility to be built in Building 71.

Information Technology

The Information Technology Division continues to transition stable technology from high-performance network testbed activities into the NRL local area network. This effort includes deployment of ATM technology at stream rates of 622 Mbps (OC12c) and 2.5 Gbps (OC48) across the enterprise. The current computing architectures, the SGI Origin2000, the SGI Origin3000, and the Sun Ultra, are continuously undergoing upgrade and evaluation of both hardware and software. The NRL CCS works closely with the DoD HPC community and the HPC vendors to provide insight, balance, and value-added capabilities within the MPP testbed infrastructure.

Materials Science and Technology

Renovation of Building 3 has been completed. The building is composed of two of the original five buildings at NRL and contains modern laboratories for studies of thin-film deposition and characterization, superconducting materials, magnetic materials, and other materials science projects. The new space features the most modern molecular beam epitaxy and other materials synthesis and processing equipment, an up-to-date fatigue and fracture laboratory, and state-of-the-art diagnostic equipment, including electron microscopes, spectrometers, and electron and X-ray diffraction equipment. The newly renovated building also contains office and laboratory space for approximately 70 technical personnel.

Plasma Physics

A state-of-the-art short-pulse (0.4 ps), high-intensity Table-Top Terawatt (T^3) laser currently operates at 2.5 TW and 5×10^{18} W/cm^2 for a variety of physics studies. The T^3 laser will be upgraded to boost its power to 25 TW and intensities to $>10^{19}$ W/cm^2. This will provide a facility to do fundamental physics experiments in intense laser-plasma interactions, intense laser-electron beam interactions, and intense laser-matter interactions.

The division is building a repetitively pulsed (5 pps) krypton fluoride (KrF) laser called Electra. Electra will develop the technologies needed for inertial fusion energy (IFE). A laser for a power plant would have to fire five times per second, run for several years, and meet stringent cost and efficiency requirements. Electra will develop the technologies that can meet these requirements. It will have a laser output of around 400 to 700 Joules. The size of Electra was chosen to be large enough to be scalable to a power plant size, but small enough to be flexible.

Electronics Science and Technology

The Electronics Science and Technology Division continues to upgrade and expand its capability in nanofabrication science. Facilities will be enhanced with two new laboratories and an expanded EPICENTER that includes a new vacuum processing chamber and two new epitaxial growth chambers. The additional epitaxial growth chambers will allow new classes of ferromagnetic III-V semiconductors to be grown. These semiconductors allow the realization of new device structures based on spin-polarized transport and the creation of lasers, detectors, and high-speed electronics important to DoD. The newest laboratories that are adding equipment are the Laboratory for Proximal Probe Nanofabrication (LPPN), which will explore the limits of nanolithography with proximal probes, and the Laboratory for Advanced Materials Processing (LAMP), which will explore the chemistry and physics of processes used routinely in the formation of modern devices and extend these processes into the nanoscale fabrication range.

OUR PEOPLE are making a DIFFERENCE

The preceding pages dramatically illustrate the range of research capabilities that have been and are being developed to provide the Naval Research Laboratory with the world-class facilities for which we are known. However, these inanimate objects, however expensive and complex, are of no value without the highly motivated people who work here. It is these people who make the Laboratory the great institution that it is, who provide the ideas and sustained efforts to make these great research capabilities "come to life." In this section, we highlight some of these special people.

Dr. Anthony Dandridge is Head of the Optical Techniques Branch in the Optical Sciences Division. He has worked at NRL since 1980, specializing in the area of fiber optic sensors. Although his primary job is running his branch, he can still be found processing data in the laboratory or participating in various field tests. "My enthusiasm for working at NRL results from the variety and challenge of the work provided by the NRL environment. On one hand one can be investigating fundamental noise properties of light in fibers, while the next day one can be wrestling with problems associated with collecting data from a system on an operational submarine. The combination of this variety, the resources NRL has to offer, as well as the flexibility to follow one's own line of research makes NRL a truly unique work environment. I feel privileged to have worked with so many dedicated and talented individuals, who have come together to often work long hours to provide deliverable hardware for numerous field tests. I have experienced both the excitement associated with obtaining "good data" in physically challenging environments and the pleasure in processing that data to find how well (or in some rare cases, how badly) systems perform in real-world environments. NRL is one of the few places today that both builds technology and works to understand how that technology performs in the real world. I feel fortunate in having had the opportunity to have performed experiments on a number of test platforms both large and small, including submarines, an aircraft carrier, and a number of research vessels."

CDR Albert M. Churilla is Program Manager for Biotechnology and Environment in the Chemistry Division; he is also a member of the Navy's Strategic Environmental Research and Development Program (SERDP) panel. The Chemistry Division conducts a broad spectrum of environmental studies ranging from site evaluation and remediation, to the development of biosensors for detection of contaminates, to aerobiology studies. The Department of the Navy places great emphasis on addressing environmental issues because of their potential Navy mission impact. These concerns are approached at NRL from a multidisciplinary view, involving scientists from NRL and other, outside commands, in a number of disciplines. "NRL represents a wide breadth of scientific and engineering disciplines, with most areas having considerable depth in expertise. The ability to focus scientists from disparate but key professional backgrounds on a given problem is unique to a handful of organizations around the world. NRL's gifted scientists and technicians have made significant contributions in the development of militarily important technology in environmental and microbiological sciences."

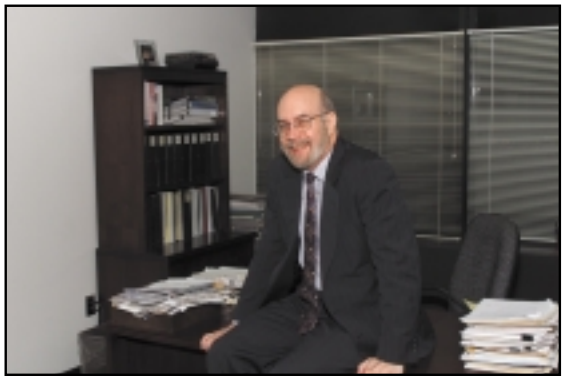

Mr. Joseph C. Ely is a senior contract specialist and has been the head of the Contracting Division since coming to NRL in 1990. His division is responsible for acquisition of supplies and services needed by NRL. During his tenure, the Procurement Information Processing System (PIPS) has been implemented at NRL and the Contracting Division has become a cost center. Also during this time, his division has undergone several reorganizations, including the addition of a section at Stennis Space Center. "A constant goal has been to make the cumbersome Federal procurement process as efficient as possible for our technical customers. Developments in information technology are having a profound effect on how we do business, and the legislative and regulatory environment seems to be changing more rapidly than ever. While my job can be challenging, I am fortunate to have the resources — especially the human resources — to meet these challenges. I am very proud to be part of NRL."

our People

Ms. Patricia Phoebus is the Associate Superintendent of the Marine Meteorology Division in Monterey, California. In addition to her management role, Ms. Phoebus remains an active research scientist in the area of data assimilation for coupled atmosphere/ocean models. "The Marine Meteorology Division joined NRL in 1992 and since that time, I've been a part of a growing enterprise as our mission and customer base have expanded. I've worked with other Division managers and scientists to establish a cohesive program that integrates a solid basic research component with our Division's strong record of achievement in developing and transitioning environmental products in support of DoD operations. By defining focus areas around several core systems — our global and mesoscale forecast models, our data assimilation scheme, our remote sensing products, and our on-scene prediction and decision aids — we've created a framework that encourages teamwork across organizational lines and builds on the camaraderie that I think has always been one of this group's greatest assets. I am honored to have the opportunity to help this Division define and achieve our research goals and continue our fine tradition of service to our operational Navy and Marine Corps customers."

Dr. Gary A. Prinz is a senior scientist in the Materials Science and Technology Division. He is a physicist specializing in thin film magnetism. "I have worked at NRL for over 33 years. I know that I could not have had as successful a career at any other institution. Access to first-rate facilities, and the courage of the NRL management to support "risky" research, has made this laboratory unique in the field of magnetism and magnetic materials. I hope that three decades from now, one of our recent hires will be able to provide a similar tribute, and I'll be around to read it in the *NRL Review*."

are making a *Difference*

These are some of the highly motivated people who make the Laboratory the great institution that it is.

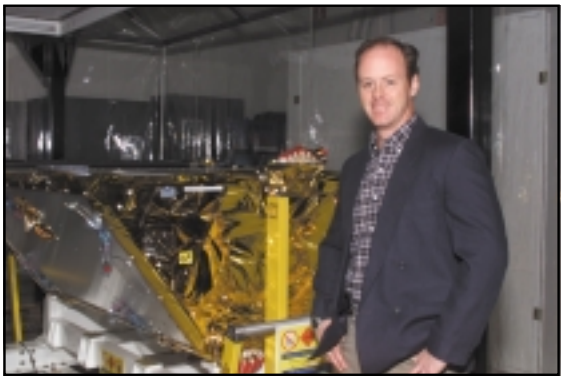

Mr. William C. Raynor joined NRL in 1991 as an environmental test engineer. He is the head of the Naval Center for Space Technology's (NCST) Processing and Test Section and the Program Manager of the Special Sensor Ultraviolet Limb Imager (SSULI). His section provides mechanical fabrication, assembly, integration, testing, and launch processing support of NCST and NRL space flight programs. Mr. Raynor represents NRL as a member of the Aerospace Testing Seminar advisory board and the International Standards Organization Working Group for Space System Interfaces, Integration, and Test. "I feel very fortunate in having the opportunity to work with an organization with such a prestigious legacy in the development of spacecraft technology. It is truly an honor to be teamed with the dedicated engineers, scientists, and support staff of NCST and NRL. I believe that it is the people of NRL that make it so great, the vision of our directors and researchers, the competitive spirit of the project teams to continually push the envelope of technology, and the inner drive of each individual to tackle the "hard" problem. NRL provides the ultimate environment for innovation. I firmly believe that patriotism is the motivating essence, the back beat perhaps, within the NRL community – not just in the support of our primary mission to support the warfighter, but in the knowledge that the research performed at NRL ultimately provides positive impact to the quality of life for all citizens of the United States and the world."

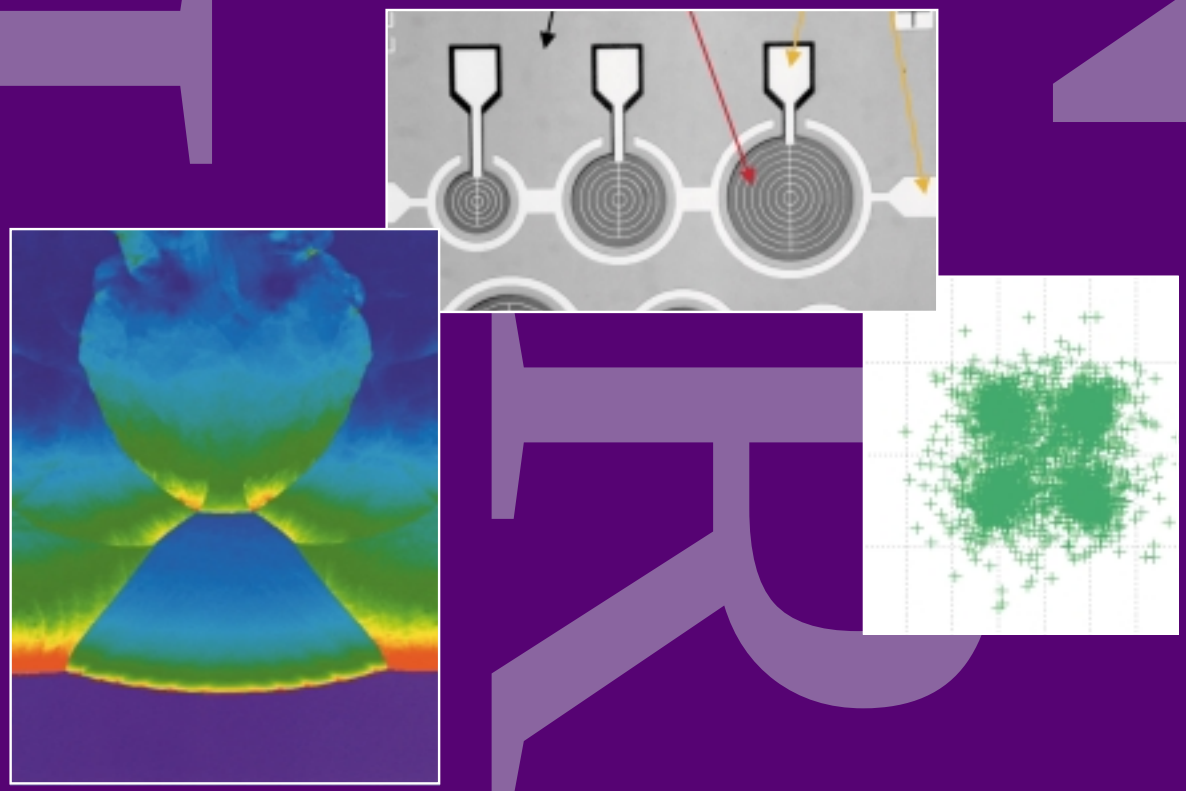

Featured Research

Efficient Electrical Spin Injection and Realization of a spin-LED

B.T. Jonker, Y.D. Park*
Materials Science and Technology Division

B.R. Bennett
Electronics Science and Technology Division

H.-D. Cheong, G. Kioseoglou, and A. Petrou
State University of New York at Buffalo

Electrical spin injection into a semiconductor is a prerequisite for realizing the potential of semiconductor-based spintronic devices. This has been an elusive goal, however, and only modest effects (≤1%) have been obtained. We report highly efficient electrical spin injection from a magnetic contact into a GaAs-based light-emitting diode (LED) heterostructure — a spin-LED — in which the spin injection efficiency exceeds 50%. The samples are grown by molecular beam epitaxy. The semimagnetic semiconductor ZnMnSe serves as a source of spin-polarized electrons that are injected via an applied bias voltage into a GaAs quantum well. Radiative recombination of spin-polarized carriers results in the emission of circularly polarized light. The quantum selection rules relate the optical polarization to the carrier spin polarization, enabling a quantitative measure of spin injection efficiency. The measured circular polarization of the electroluminescence (EL) exceeds 50%, demonstrating that highly efficient spin transport occurs across the ZnMnSe/AlGaAs interface despite the large 0.5% lattice mismatch.

INTRODUCTION

Spin injection and transport in semiconductor heterostructures is a promising avenue to add new spin-dependent functionality to the many attractive properties of semiconductor devices.[1] The seminal proposal by Datta and Das[2] of a spin-polarized field effect transistor, with magnetic source and drain contacts for spin injection and detection, has stimulated a great deal of effort to better understand the behavior of spin-polarized carriers in semiconductor hosts under conditions of dynamic transport. Optical pumping has routinely been used to create spin-polarized carrier populations in semiconductor heterostructures, and has provided tremendous insight into their behavior.[3] Very recently, extraordinarily long spin lifetimes and diffusion lengths have been observed in optically pumped systems.[4,5] Spin diffusion lengths of many microns have been reported in GaAs,[4] for example, illustrating that a spin-polarized mode of operation is certainly feasible for every modern transport device.

It is very desirable to electrically inject spin-polarized carriers via a magnetic contact to increase the potential for practical applications, as originally proposed. This would provide a very simple and direct implementation of spin injection in which the contact area defines the spin source. It would also significantly broaden application horizons. Electrical spin injection has been an elusive goal, however. Several attempts using magnetic metal contacts to Si[6] or InAs-based two-dimensional electron gas structures[7,8] have resulted in very similar and modest spin-injection effects measured at or below the 1% level. Substantially larger injection efficiencies and related effects are clearly desirable to successfully implement new device concepts. Spin scattering at the interface between the magnetic contact and semiconductor host

*National Research Council Postdoctoral Associate at NRL

appears to be the limiting factor, but very little is known about such interfacial contributions. The small measured effects reported to date also make it difficult to unambiguously identify the factors that affect spin injection.

THE spin-LED

Principle of Operation

We report here the robust and efficient *electrical injection* of spin-polarized carriers from a magnetic contact into a semiconductor heterostructure. This is demonstrated by the fabrication of a spin-polarized light-emitting diode (spin-LED) structure. In a normal LED, electrons and holes recombine in the vicinity of a *p-n* junction or quantum well to produce light when a current flows under forward bias conditions. This light is unpolarized, because all carrier spin states are equally populated, permitting all dipole-allowed radiative transitions to occur with equal probability. In the work reported here, an epilayer of the II-VI semimagnetic semiconductor $Zn_{1-x}Mn_xSe$ is used as the spin-injecting contact to a III-V semiconductor-based LED structure, which consists of a GaAs quantum well flanked by $Al_yGa_{1-y}As$ barrier layers. Figure 1 shows a cross-section of the layered structure. Spin-polarized electrons are electrically injected across the II-VI/III-V heterointerface and into the GaAs quantum well, where they radiatively recombine. Radiative recombination of spin-polarized carriers results in the emission of right (σ-) or left (σ+) circularly polarized light.[3] Polarization analysis of the electroluminescence from such a structure effectively interrogates the spin population of the GaAs quantum well. Thus the existence of circularly polarized electroluminescence demonstrates successful electrical spin injection. A simple analysis of the circular polarization using these selection rules provides a quantitative assessment of injection efficiency. The spin polarization of these electrons deduced from the optical polarization is at least 50%, demonstrating highly efficient spin injection across a heterointerface.

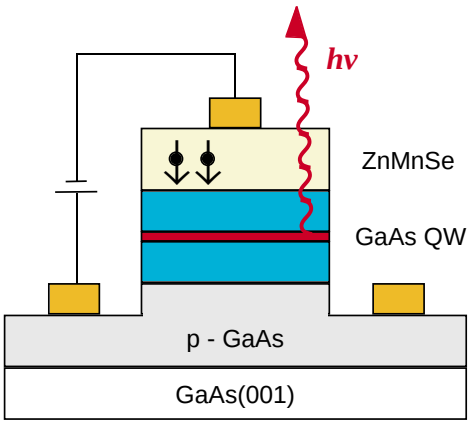

FIGURE 1
Schematic cross section of the samples illustrating the layered structure, contact metallization and voltage biasing during measurement. The layer thicknesses are not to scale.

Semimagnetic semiconductors such as $Zn_{1-x}Mn_xSe$ are well studied, and are noted for the very large band edge spin splitting they exhibit in an applied magnetic field (giant effective Zeeman effect).[9] For modest fields, the spin splitting significantly exceeds *k*T at low temperature. In particular, the splitting of the spin-up ($m_j = +1/2$) and spin-down ($m_j = -1/2$) electron states in $Zn_{0.94}Mn_{0.06}Se$ is approximately 10 meV at 3 Tesla, so that the conduction band effectively forms a completely polarized source of spin-down electrons. This same effect has been used in the past to create a spin superlattice, in which carriers of opposite spin occupy alternating layers of a multilayer structure.[10] Under appropriate electrical bias, these carriers are injected across the ZnMnSe/AlGaAs heterointerface and into the GaAs quantum well. Here, they radiatively recombine with an unpolarized hole population provided by *p*-type doping and emit circularly polarized light.

Device Fabrication

The samples studied were grown on semi-insulating GaAs(001) substrates by molecular beam epitaxy (MBE) in NRL's Epi-Center Facility (Code 6000), a multichamber system for MBE growth, surface analysis, and processing. The growth sequence (Fig. 1) consisted of a 1 µm *p*-type GaAs buffer layer, a 2000 Å *p*-doped AlGaAs barrier, an undoped 150 Å GaAs quantum well, and an *n*(Si)-doped 500 Å AlGaAs barrier. Dopant setbacks of 250 Å were used on either side of the well, and $p(\text{Be}) = 10^{18}$ cm^{-3}. The sample was then transferred to a second MBE chamber connected to the first, where a 2000 Å epilayer of *n*(Cl)-doped $Zn_{0.94}Mn_{0.06}Se$ was grown. This growth was initiated by exposing the (2×4)-As reconstructed surface of the AlGaAs to the Zn flux for 60 s at the growth temperature of 300°C to minimize the formation of defects near the interface.[11] For these growth conditions, the ZnSe/GaAs conduction band (CB) offset is 100 meV,[12] with the ZnSe band edge at higher energy. The band gap of $Zn_{0.94}Mn_{0.06}Se$ is nearly equal to that of ZnSe (2.8 eV at 4.2K) due to bandgap bowing, while that of AlGaAs increases with Al concentration. An Al concentration of 0.1 was chosen for the barrier to minimize the ZnMnSe/

AlGaAs CB offset, which is calculated to be less than 10 meV. The depth of the GaAs CB quantum well is ~100 meV. A doping level of $n = 10^{17}$ cm^{-3} was used for both the AlGaAs and the ZnMnSe. Figure 2 shows a simplified flat band diagram.

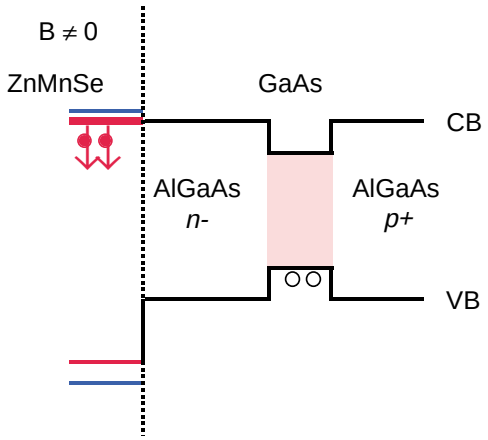

FIGURE 2
Flat band diagram illustrating the conduction and valence band (CB, VB) offsets in the spin-LED structure. The CB of the $Zn_{0.94}Mn_{0.06}Se$ splits with applied field, so that the spin down states are occupied. The holes in the GaAs quantum well are unpolarized. The band offsets are exaggerated for clarity.

The samples were processed into surface-emitting LED mesa structures 200-400 µm in diameter using standard photolithographic techniques. Mesa isolation was achieved by chemically etching to the p-GaAs buffer, and electrical contacts were made to the ZnMnSe and p-GaAs base via Ti/Au liftoff. The top metal contact consists of concentric rings, leaving most of the mesa surface optically transparent. Figure 3 shows the final processed structures.

Demonstration of Electrical Spin Injection

Electrical leads were attached, and the samples were placed in a magnetic cryostat with optical access along the field direction (Faraday geometry). The LED structures were electrically biased to inject electrons from the ZnMnSe into the GaAs quantum well at current densities of ~ 0.01 A/cm^2. The surface-emitted electroluminescence was measured with a spectrometer using a combination of a quarter wave plate and linear polarizer for polarization analysis.

Figure 4 shows representative spectra of the light emitted from the spin-injected LED for selected values of the applied field. The spectra are normalized and aligned to the zero field spectrum to facilitate comparison. At zero field, no optical polarization is observed, as expected, since $Zn_{0.94}Mn_{0.06}Se$ is a Brillouin paramagnet, which acquires a net magnetization only in a magnetic field. The emission peaks near 1.524 eV, which is attributed to recombination with heavy holes. This confirms that radiative recombination occurs in the GaAs quantum well. The polarization rapidly increases with applied field as the spin-polarized electron population is created in the ZnMnSe and injected into the LED structure. The corresponding spectra reveal a significant difference in intensity between the σ+ and σ– components of the electroluminescence, even at 0.5T. Other effects that might contribute to the optical polarization were carefully considered and were either eliminated or included in the error bars. For example, the Faraday rotation resulting from transmission through the ZnMnSe is negligible due to the very short path length (2000 Å), and because the GaAs emission wavelength is far from that corresponding to the band gap of $Zn_{0.94}Mn_{0.06}Se$. Photoluminescence data from the GaAs well show little polarization.

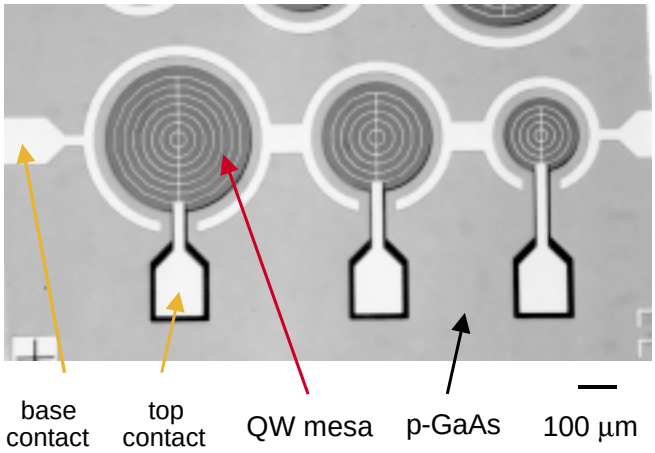

FIGURE 3
The processed surface-emitting LEDs. The top contact bond pad is insulated from the p-GaAs by a layer of SiN.

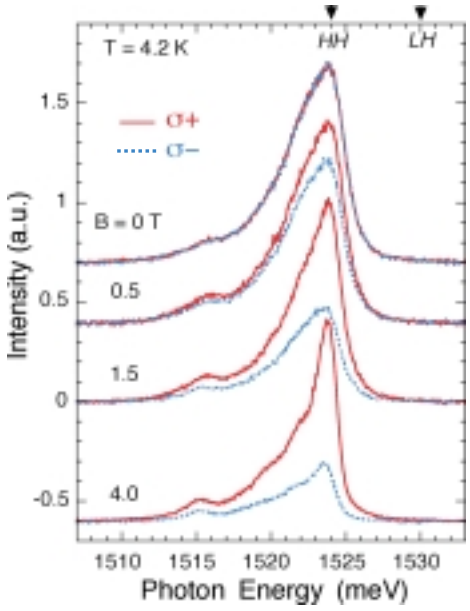

FIGURE 4
Electroluminescence spectra from one of the spin-LED samples for selected values of applied magnetic field, analyzed for left (σ+) and right (σ-) circular polarization. The peaks are normalized and shifted to lower energies by the following amounts to align with the zero field spectrum: 0.5 T (0.11 meV), 1.5T (0.61 meV), 4T (2.15 meV). The relative positions of the heavy and light hole features (*HH*, *LH*) obtained from photoreflectivity (B = 0) are indicated.

At B = 4T, two distinct features are visible at ~ 2 meV and 4 meV to the low energy side of the heavy hole peak. These are consistent with contributions from donor- and acceptor-bound excitons, respectively. These features are more distinct at 8T and are discussed elsewhere. The feature near 1.515 eV is attributed to recombination in bulk GaAs and also exhibits a strong polarization, indicating that some portion of the spin-polarized electrons retain their spin until they recombine in the *p*-GaAs buffer layer. It should be noted that the observation of polarization in such a simple dc measurement clearly demonstrates that the electron spin lifetime is much longer than the radiative recombination time.[4,5]

The degree of circular polarization is obtained from the integrated intensity as P_{circ} = [I(σ+) - I(σ-)]/ [I(σ+) + I(σ-)] and is summarized in Fig. 5 as a function of applied field. P_{circ} saturates around 4T at a value of 50% and decreases slightly at the highest fields. This decrease is not well understood at present but is attributed in part to the Zeeman effect in GaAs, whose spin-splitting is much smaller but opposite in sign to that of $Zn_{0.94}Mn_{0.06}Se$. In a Brillouin paramagnet such as $Zn_{1-x}Mn_xSe$, the dependence of the magnetization (and spin splitting) on applied field and temperature is well described by a Brillouin function.[9,13] The solid line in Fig. 5 shows the spin splitting of $Zn_{0.94}Mn_{0.06}Se$ calculated from a standard Brillouin function analysis and scaled by a multiplicative factor to fit the polarization data. The excellent agreement with the field dependence of the circular polarization for B < 5T confirms that the polarization of the electroluminescence results from spin-polarized electrons that are electrically injected from the $Zn_{0.94}Mn_{0.06}Se$ conduction band and into the GaAs quantum well.

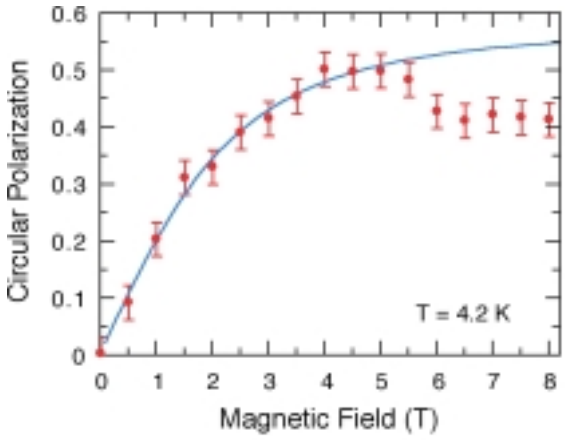

FIGURE 5
Magnetic field dependence of the optical polarization P_{circ}. The solid line is a simple Brillouin function fit to the data.

Quantitative Analysis of Spin Injection Efficiency

Figure 6 illustrates the selection rules that govern the radiative recombination of spin polarized carriers in cubic semiconductors in the Faraday geometry.[3,14] They permit a simple analysis of the data that provides a quantitative measure of the spin polarization of the carriers involved, and hence of spin injection efficiency across the ZnMnSe/AlGaAs interface and into the quantum well. In bulk zincblende semiconductors such as GaAs, the conduction band is two-fold degenerate at the center of the Brillouin zone, corresponding to spin-up and spin-down electrons ($m_j = \pm 1/2$). The valence band is four-fold degenerate, and consists of heavy hole (*HH*) and light hole (*LH*) bands with large and small effective mass, respectively, which are each two-fold spin degenerate ($m_j = \pm 3/2, \pm 1/2$). Radiative electron-hole recombination is allowed for interband transitions that obey the selection rule $\Delta m_j = \pm 1$.[3,14] The probability of a given transition is weighted by the matrix ele-

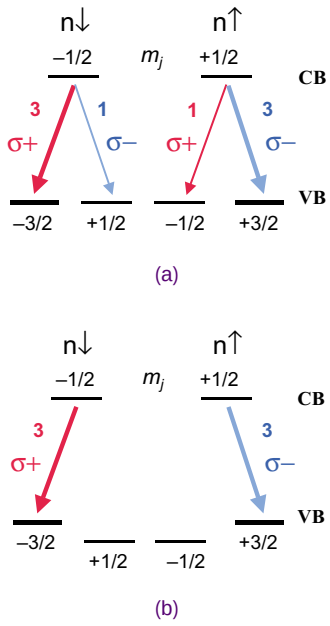

FIGURE 6
Radiative interband transitions allowed by the selection rules for the case of (a) degen-erate, and (b) nondegenerate *HH* and *LH* bands.

ment connecting the levels involved, so that transitions to *HH* states are three times more likely than those to *LH* states.

The net circular polarization of the light emitted can readily be calculated for a given occupation of the quantum well carrier states. Assuming an unpolarized spin-degenerate hole population, a general expression for the degree of circular polarization in the Faraday geometry follows directly from Fig. 6(a) and can be written in terms of the relative populations of the electron spin states n↑ (m_j = + 1/2) and n↓ (m_j = – 1/2), where 0 ≤ n ≤ 1, and n↑ + n↓ = 1:

$$P_{circ} = [I(\sigma+) - I(\sigma-)]/[I(\sigma+) + I(\sigma-)] = 0.5\ (n\downarrow - n\uparrow)/(n\downarrow + n\uparrow). \quad (1)$$

The optical polarization is directly related to the electron spin polarization (n↓ – n↑) / (n↓ + n↑) in the quantum well and has a maximum value of 0.5 due to the degeneracy of the *HH* and *LH* bands. The experimentally measured value P_{circ} = 0.5 suggests spin injection with an efficiency of 100%.

However, the *HH* and *LH* bands are separated in energy by quantum confinement, which modifies Eq. (1) and significantly impacts the analysis. The *HH*/*LH* band splitting is typically several meV, even in shallow quantum wells, and is much larger than the thermal energy at low temperature (~0.36 meV at 4.2 K), so that the *LH* states are at higher energy and are not occupied. For the structures studied here, a calculation that includes corrections for exciton binding energies yields a value of 5 meV for the *HH*/*LH* splitting. This is slightly smaller than the value of 6 meV obtained from photoreflectivity measurements (these positions are indicated in Fig. 4). In this case, only the *HH* levels participate in the radiative recombination process, as shown in Fig. 6(b), and P_{circ} is calculated as before:

$$P_{circ} = (n\downarrow - n\uparrow) / (n\downarrow + n\uparrow). \quad (2)$$

P_{circ} is equal to the electron spin polarization in the well and can be as high as 1.0. Assuming that only spin-down electrons are injected from the ZnMnSe for B > 4T, the experimentally measured value of 0.5 indicates robust electrical spin injection with an efficiency of 50%, i.e., half of the spin-down electrons injected from the ZnMnSe reach the GaAs quantum well without experiencing a scattering event that flips their spin. It should be noted that P_{circ} decreases rapidly for higher current densities, indicating that local heating at the ZnMnSe contact metallization is reducing the initial spin polarization, as expected from the strong temperature dependence of a Brillouin paramagnet. Therefore, the value of 50% should be regarded as a lower bound to the spin injection efficiency.

SUMMARY AND PROSPECTS

In summary, we have demonstrated highly efficient electrical injection of spin-polarized electrons across a II-VI/III-V semiconductor heterointerface and subsequent transport into a quantum well LED structure. Radiative recombination of the carriers results in the emission of circularly polarized light with P_{circ} = 0.5, indicating that at least 50% of the electrons retain their spin state in the process and that the probability of spin-flip scattering is low. An efficient spin-LED[15] effectively couples carrier spin with optical polarization, and may enable the transmission of polarization-encoded information or quantum information processing and transfer. Fabrication of practical devices will benefit from the use of improved contacts and stronger ferromagnets as the spin injector, perhaps including new ferromagnetic semiconductors such as $Ga_{1-x}Mn_xAs$.[16] Future systematic studies of such structures in which the character of the interface or semiconductor layers are modified in a controlled fashion promise to elucidate the mechanisms that contribute to spin scattering and provide a better understanding of spin transport in device structures. This will enable the design of

magnetoelectronic devices[1,2] that use carrier spin as a new degree of freedom to provide new functionality.

ACKNOWLEDGMENTS

This work was supported by the Office of Naval Research, in part under Research Project 02101, and the DARPA SpinS program. Y.D. Park acknowledges support from ONR as a National Research Council Postdoctoral Associate at the Naval Research Laboratory. The authors gratefully acknowledge helpful discussions with B.V. Shanabrook.

[Sponsored by ONR]

REFERENCES

[1] G.A. Prinz, "Magnetoelectronics," *Science* **282**, 1660 (1998).
[2] S. Datta and B. Das, "The Electronic Analog of the Electro Optic Modulator," *Appl. Phys. Lett.* **56**, 665 (1990).
[3] F. Meier and B.P. Zachachrenya, *Optical Orientation, Modern Problems in Condensed Matter Science* (North-Holland, Amsterdam, 1984), Vol. 8.
[4] D. Hagele, M. Oestreich, W.W. Ruhle, N. Nestle, and K. Eberl, "Spin Transport in GaAs," *Appl. Phys. Lett.* **73**, 1580 (1998).
[5] J.M. Kikkawa and D.D. Awschalom, "Resonant Spin Amplification in n-type GaAs," *Phys. Rev. Lett.* **80**, 4313 (1998); *Nature* **397**, 139 (1999).
[6] Y.Q. Jia, R.C. Shi, and S.Y. Chou, "Spin-Valve Effects in Nickel Silicon/Nickel Junctions," *IEEE Trans. Magn.* **32**, 4707 (1996).
[7] P. Hammer, B.R. Bennett, M.J. Yang, and M. Johnson, "Observation of Spin Injection at a Ferromagnet-semiconductor Interface," *Phys. Rev. Lett.* **83**, 203 (1999).
[8] S. Gardelis, C.G. Smith, C.H.W. Barnes, E.H. Linfield, and D.A. Ritchie, "Spin-valve Effects in a Semiconductor Field-effect Transistor: A Spintronic Device," *Phys. Rev.* **B 60**, 7764 (1999).
[9] J.K. Furdyna and J. Kossut, *Diluted Magnetic Semiconductors*, Vol. 25 of *Semiconductors and Semimetals* (Academic Press, New York, 1988).
[10] W.C. Chou, A. Petrou, J. Warnock, and B.T. Jonker, "Spin Superlattice Behavior in ZnSe / $Zn_{0.99}Fe_{0.01}Se$ Quantum Wells," *Phys. Rev. Lett. 67*, 3820 (1991).
[11] L. H. Kuo, L. Salamanca-Riba, B. J. Wu, G. Hoffler, J. M. DePuydt, and H. Cheng, "Dependence of the Density and Type of Stacking Faults on the Surface Treatment of the Substrate and Growth Mode in ZnS_xSe_{1-x}/ZnSe Buffer Layer/GaAs Heterostructures," *Appl. Phys. Lett.* **67**, 3298 (1995); *J. Vac. Sci. Technol.* **13**, 1694 (1995).
[12] R. Nicolini, L. Vanzetti, G. Mula, G. Bratina, L. Sorba, A. Franciosi, M. Peressi, S. Baroni, R. Resta, A. Baldereschi, J.E. Angelo, and W.W. Gerberich, "Local Interface Composition and Band Discontinuities in Heterovalent Heterostructures," *Phys. Rev. Lett.* **72**, 294 (1994).
[13] J.A. Gaj, "Magnetooptical Properties of Large-gap Diluted Magnetic Semiconductors," in Ref. 9, p. 286.
[14] C. Weisbuch and B. Vinter, *Quantum Semiconductor Structures* (Academic Press, New York, 1991), Chap. 11. [These selection rules may not be rigorously obeyed in real systems due to imperfections or distortion, but provide an analysis good to first-order.]
[15] B.T. Jonker, "Polarized Optical Emission Due to Decay or Recombination of Spin-polarized Injected Carriers," U.S. patent 5,874,749 (February 23, 1999, assignee: U.S. Navy).
[16] H. Ohno, "Making Nonmagnetic Semiconductors Ferromagnetic," *Science* **281**, 951 (1998).

THE AUTHORS

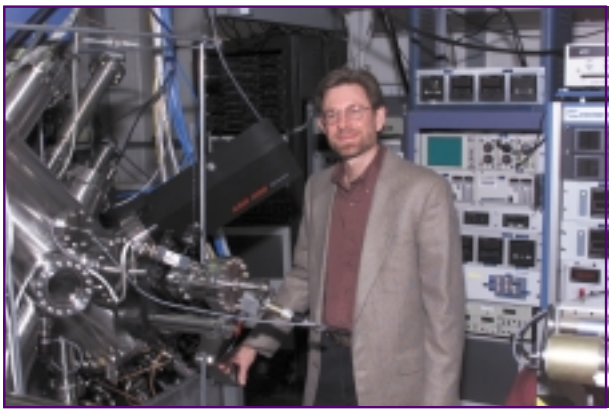

BEREND T. JONKER received a B.A. (Honors) degree in physics from Calvin College in 1977, and an M.S. and Ph.D. degrees in physics from the University of Maryland in 1981 and 1983, respectively. He came to NRL as a National Research Council Postdoctoral Fellow in 1984 and became an NRL staff member in 1986. His research has focused on spin-dependent carrier localization in semiconductor superlattices, electrical spin injection and transport in semiconductor heterostructures, and the fabrication of prototype magnetoelectronic devices. His most recent work addresses the MBE growth and study of III-V magnetic semiconductors. Dr. Jonker has authored 135 scientific publications, holds three U.S. patents with two additional pending, and is a Fellow of the American Vacuum Society.

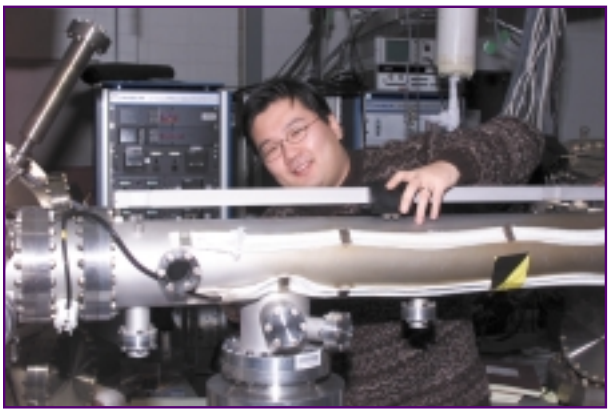

YUN D. PARK graduated with a B.S. in electrical engineering from Cornell University in 1994, and received his M.S. (1997) and Ph.D. (1998) in materials science and engineering from the University of Florida. Dr. Park's thesis explored the effects of processing and dimensionality of nanometer-sized magnetic structures, from which he authored or co-authored more than twenty scientific journal articles. Soon after graduation, Dr. Park was awarded a National Research Council Post-doctoral Fellowship at the Naval Research Laboratory, where he is currently working with Dr. B.T. Jonker in the Materials Physics Branch in the areas of magnetoelectronic devices, molecular beam epitaxy, thin-film growth, and characterization of magnetic semiconductors.

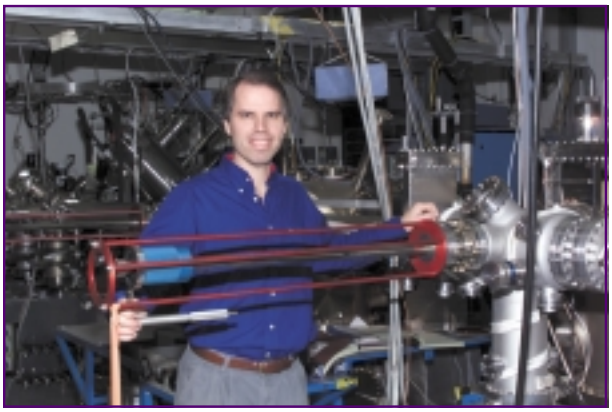

BRIAN R. BENNETT received the B.S. and M.S. degrees in 1984 and 1985, respectively, from the Massachusetts Institute of Technology. In 1992, he received the Ph.D. degree in materials science and engineering from M.I.T. Since 1992, Dr. Bennett has been at the Naval Research Laboratory. His research focuses on the growth and applications of arsenide, antimonide, and nitride semiconductor heterostructures, including studies of interfacial control, self-assembled quantum dots, field-effect transistors, resonant tunneling diodes, and infrared detectors. Dr. Bennett has published more than 100 technical papers in refereed journals. He also serves as an advisor to postdoctoral associates at NRL.

HAI-DU CHEONG received B.A. and M.S. degrees in physics from Kyungpook National University at Taegu, Korea in 1986 and 1988, respectively, and a Ph.D. in physics from State University of New York at Buffalo in 2000. He is presently a post-doctoral researcher in the Department of Materials Science and Engineering of Pohang University of Science and Technology, Korea. His research is focused on ZnO thin film growth using Laser-MBE and MOCVD techniques, optical characterization of III-V (GaAs-based) and II-VI (Zn-based) semiconductors, and time-resolved photoluminescence spectroscopy. Dr. Cheong has authored six scientific publications.

GEORGE KIOSEOGLOU received B.S and M.S degrees in physics from the Aristoteleio University, Thessaloniki, Greece, in 1987 and 1991, respectively, and a Ph.D from the State University of New York (SUNY) at Buffalo in 1999. He is currently a postdoctoral associate at SUNY Buffalo. His research involves the study of the magneto-optical properties of semiconductors and heterostructures based on them. His recent work is on electrical spin injection in GaAs-based LEDs and X-ray studies of interface quality and intermixing in semiconductor heterostructures. Dr. Kioseoglou is co-author on more than 20 publications in scientific journals.

ATHOS PETROU received a B.S. degree in physics from the University of Athens, Greece, in 1976 and M.S. and Ph.D. degrees from Purdue University in 1979 and 1983, respectively. Between 1983 and 1985 he was a research associate at Northeastern University. He joined the physics faculty at the State University of New York Buffalo in 1985. His research involves the study of the magneto-optical properties of semiconductors and heterostructures based on them. His most recent work is on electrical spin injection in GaAs-based LEDs. Dr. Petrou is a co-author of 87 publications in scientific journals and is a Fellow of the American Physical Society.

Numerical Simulations of Pulsed Detonation Engines

K. Kailasanath, C. Li, and G. Patnaik
Laboratory for Computational Physics and Fluid Dynamics

Detonations are an extremely efficient means of burning a fuel-air mixture and converting its chemical energy content into mechanical energy. Air-breathing and rocket engines based on pulsed detonations have the potential to provide the Navy with increased range and speed while reducing fuel consumption and system costs. Over the past two years, we have conducted extensive computational studies of the pulsed detonation engine concept. The results of these numerical simulations have been invaluable in developing a basic understanding of these engines. New methods for enhancing the performance of these engines have also been identified using the simulations.

INTRODUCTION

In the quest for propulsion systems with reduced acquisition costs, better efficiency, increased range, and reduced fuel consumption, pulsed detonation engines (PDEs) are a potentially revolutionary concept. The mechanical simplicity of the system will translate into reduced production and maintenance costs. Detonations are an extremely efficient means of converting a fuel into products and releasing the fuel's chemical energy content. This intrinsic advantage of detonations results in better thermodynamic efficiency. Therefore, air-breathing and rocket engines based on pulsed detonations have the potential to provide the Navy and DoD with increased range and speed while reducing fuel consumption and system costs. However, detonations have been explored for propulsion only recently.[1] The problems involved in rapidly mixing the fuel and air at high flight speeds and initiating and sustaining a detonation in a controlled manner in fuel-air mixtures have made this difficult. By focusing on pulsed systems rather than continuous systems, additional time is available between the pulses for fuel-air mixing. Several basic research issues need to be addressed in order to mature the PDE technology base. Recent advances in combustion diagnostics and computational combustion will aid in the development of a better understanding of PDEs. This article is an overview of our computational studies of pulsed detonation engines.

WHY DETONATIONS?

Very rapid material and energy conversion is a key feature of detonations. This rapid "burning" or material conversion rate, typically tens of thousands of times faster than in a flame, can lead to several advantages for propulsion, such as more compact and efficient systems. Because of the rapidity of the process, there is not enough time for pressure equilibration, and the overall process is thermodynamically closer to a constant volume process (like an explosion in a closed container) than the constant pressure process typical of conventional jet propulsion systems. To illustrate this point, three idealized thermodynamic cycles are compared in Fig. 1.

For comparison, the only process that is different in the three cycles is the mode of energy conversion or heat addition. For the three cases, heat is added at constant pressure, constant volume, or in a detonation. Hence, the three cycles have been referred to as "constant pressure," "constant volume," and "detonation" cycle, respectively. The amount of heat added is kept the same for the three cycles. In all cases, the fuel-air mixture is initially compressed "adiabatically" (without any heat loss) from 1 to 3 atm. before heat addition. After heat addition, the products of combustion are expanded adiabatically to 1 atm. Finally the system is returned to its initial state. The thermodynamic efficiency is calculated as the ratio of work output to the heat input. Since the

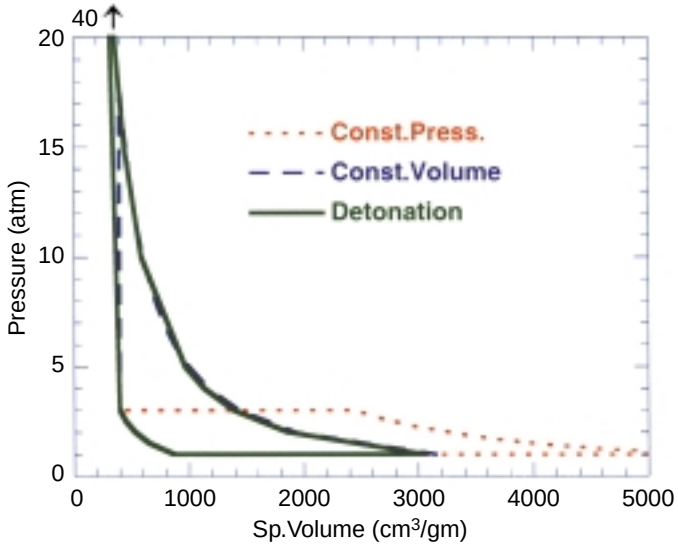

FIGURE 1
Comparison of thermodynamic cycles for constant pressure, constant volume, and detonation modes of combustion.

heat addition was maintained the same for the three processes, the differences in the work done give the relative thermodynamic efficiency of the three combustion processes. The thermodynamic efficiencies for the three cycles are calculated to be 27% for constant pressure, 47% for constant volume, and 49% for detonation. From the above numbers we see that the thermodynamic efficiency of the detonation cycle is significantly better than that of the constant pressure cycle (usually called the Brayton cycle) that is typical of combustion in various forms of jet propulsion. The detonation cycle is closer to a constant volume cycle (usually called a Humphrey cycle) except for a reduction in specific volume and increase in peak pressures. A major challenge in the development of the pulsed detonation engine is attaining this higher potential efficiency in a practical device.

PROCESSES IN A PULSED DETONATION ENGINE

The basic concept behind a pulsed detonation engine is fairly simple and is illustrated in Fig. 2 using a pipe or a tube closed at one end and open at the other. The various colors in the figure correspond to different levels of pressure, with red being the highest (30 atm.) and the violet (or purple) being the lowest (1 atm.). The tube is initially filled with a fuel-air mixture at 1 atm. A shock wave is initiated at the closed end. Chemical reactions in the shock-heated mixture generate pressure waves that couple with the shock wave to form a detonation. After a brief transition period, the detonation travels toward the open end of the tube at a nearly constant velocity called the Chapman-Jouguet (CJ) velocity. This CJ velocity and the corresponding pressure behind the detonation wave (CJ pressure) are characteristics of the fuel-air mixture. The detonation initiation process also generates expansion waves that travel toward the closed end (called head-end) of the tube. As the detonation leaves the tube, additional expansion waves form at the open end and travel toward the closed end. These expansion waves are important because they help evacuate the tube. Once the tube is evacuated, fresh fuel and air are injected into the tube. When the injection and mixing is completed, a detonation is initiated again at the closed end and the whole process is repeated. The cyclical nature of the entire process is what gives rise to the term "pulsed detonation engine (PDE)."

The propulsive thrust and other measures of the performance of such an idealized "engine" can be determined either from the momentum of the gases flowing out of the tube or the pressure at the closed end of the tube. The pressure distributions used in Fig. 2 for illustration purposes were actually values obtained from numerical simulations of an engine operating on a hydrogen-air mixture. Let us briefly look at the computational tools needed to conduct such studies.

COMPUTATIONAL TOOLS

Computational tools are being developed to analyze various problems related to PDEs such as fuel-air mixing, detonation initiation and transmission, and multiphase flow effects. The geometric complexity of the system being simulated as well as the details included in the chemical and physical models vary from problem to problem. For example, in our three-dimensional simulations of fuel-air mixing and initiation of detonations, either no chemistry model or

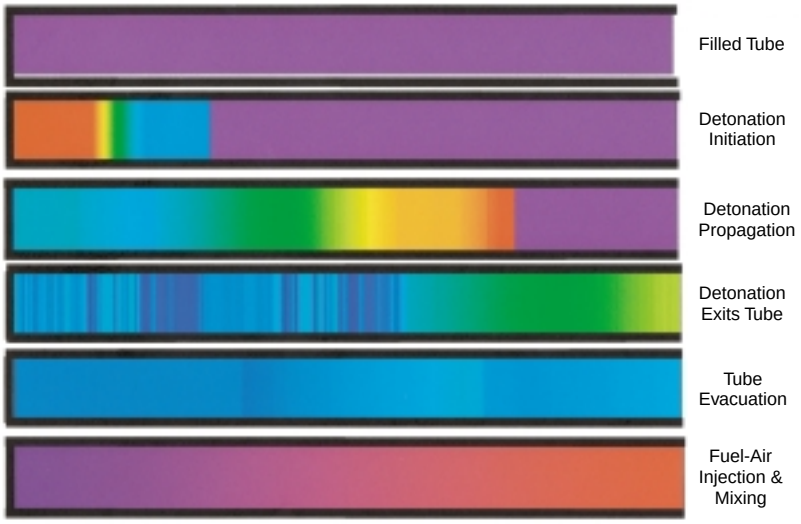

FIGURE 2
Processes in a pulsed detonation engine cycle.

simple models are included, but the details of the geometrical complexity representative of experimental configurations are included. At the other extreme, detailed multi-step chemistry and thermodynamics is included in simulations of geometrically simple systems. We also plan to include simplified chemical kinetic mechanisms of hydrocarbon combustion in some of these simulations. Next we briefly discuss the model and solution approach used in our basic study of the gas-phase reactive flow in a simple PDE.

The time-dependent, compressible, reactive flow equations for the conservation of mass, momentum and energy are solved. The terms in the conservation equations representing the different physical and chemical processes are solved separately and coupled using timestep splitting techniques. This procedure allows the individual processes to be integrated by appropriate and efficient techniques and also permits the easy substitution and elimination of different submodels for the individual processes, as needed for specific applications.

The code can compute the three-dimensional multi-species reactive flow in a simple geometry and allows for the inclusion of species diffusion, thermal conduction, and radiative heat loss. For the short duration, single-cycle simulations discussed here, the diffusive and thermal processes will have a negligible effect and hence only the convective flow with detailed chemistry is considered. For simulations such as those used in Fig. 2, the code is used to compute the one-dimensional flow, neglecting the variations in the other two directions.

For the high-speed reactive flows that are typical of detonations, an explicit algorithm such as the Flux-Corrected Transport (FCT) is very efficient and accurate for integrating the fluid convection. FCT is a conservative, monotonic algorithm with fourth-order phase accuracy. With various initial and boundary conditions, this algorithm has been used previously to solve a wide variety of problems involving detonations.

A comprehensive model for hydrogen combustion with 8 species and 48 reactions or a simplified two-step model for ethylene combustion is used for the results discussed here. Because of the complexity of the reaction scheme and the large number of computational cells in a multidimensional calculation, the solution of the chemical rate equations can take a large fraction of the total computational time. Hence, the code has been developed directly for massively-parallel computers.

PERFORMANCE OF A PDE

As discussed before, a fundamental reason for investigating PDEs is the higher thermodynamic efficiency of a detonation cycle when compared to the constant pressure and the constant volume cycles. The higher efficiency is primarily due to the higher pressures and temperatures attained during the detonation cycle. Pressure profiles and histories at various locations within a PDE have been analyzed to better understand the various factors that may control the performance. The results from one-dimensional numerical simulations have been used to generate a "typical" profile of the head-end (closed-end) pressure shown in Fig. 3. Measures of the propulsive performance such as thrust can be calculated from such information. In Fig.3, the abscissa is normalized using the detonation transit time (tube length/CJ detonation velocity) and the ordinate is normalized using the CJ detonation pressure.

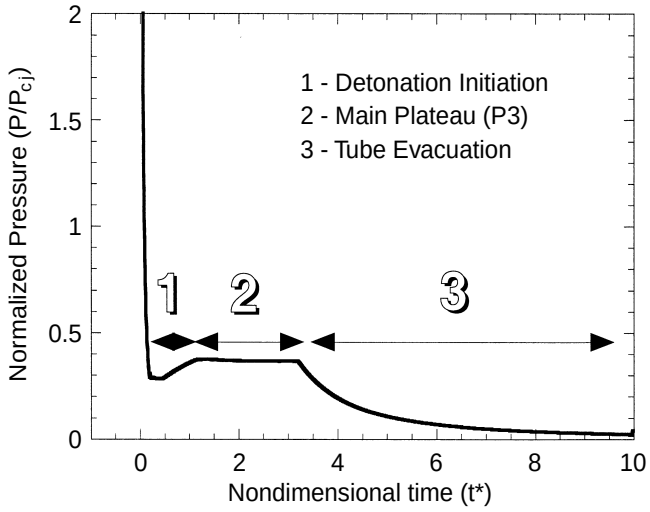

FIGURE 3
Different stages in the time evolution of the pressure at the closed end of a PDE tube.

In Fig. 3, we have divided the time history into three distinct stages or regimes: initiation, plateau, and relaxation. Different factors control the different stages. The first stage is dominated by the method used to initiate the detonations and to some extent the details of the transition process. Attention is usually focused on the second, the plateau region or stage, because the value of the plateau pressure can be related to the CJ detonation pressure and hence is a property of the fuel-air mixture. The third stage describes the relaxation of the plateau pressure to the ambient value. Until recently, this stage has not been studied in detail.

ROLE OF PRESSURE RELAXATION

We have conducted numerical simulations to investigate the role of the rate of pressure relaxation to the ambient conditions. Numerically, for the idealized straight tube PDE, this can be varied by the specification of the boundary conditions at the open end of the tube. Several choices for the open boundary condition have been tried and their effect on the flow field and performance evaluated. For the cases discussed here, a boundary condition implementation based on the method of characteristics is used. This ensures that no constraints are imposed on the flow quantities when the outflow is supersonic and enforces the required constraints when the flow becomes subsonic. Even in this formulation, there remains a free parameter in the subsonic case that needs to be specified. Various choices for this parameter result in different rates of relaxation for the pressure at the open boundary.

The results for three choices of the relaxation parameter (slow, intermediate and fast) are shown in Fig. 4. Clearly, the area enclosed by the curves, which is a measure of the thrust of the engine, is different for the three cases. The time integral of the thrust gives the impulse. The impulse per unit mass defines a quantity called "specific impulse" (I_{sp}), which is usually taken as a standard measure of the propulsive performance of an engine. It has the same unit, seconds, in the various systems of units. The numerical simulations show that the peak I_{sp} is 60% larger for a slow relaxation process than for a fast one. In practice, different relaxation rates may be attained by suitably tailoring the shape of the exhaust nozzle.

EFFECTS OF BYPASS AIR

In another series of simulations, a 50-cm long tube was filled with an ethylene-air mixture to various lengths and the rest of the tube was filled with air. Detonations were initiated at the closed end, as described earlier. Figure 5 shows the time history of the impulse for various cases. An interesting observation is that the impulse is not proportional to the amount of fuel fill. When the degree of fill is decreased from 100% to 20%, the peak impulse decreases from 604 to 381 N-s/m^2. That is a decrease of only 37%. Detailed analysis of these multidimensional simulations[2] shows that this result is due to the presence of two different sets of expansion waves, one from the fuel-air interface and the other from the exit-end of the tube. When these different sets of expansion waves reach the thrust wall, the pressure decays at

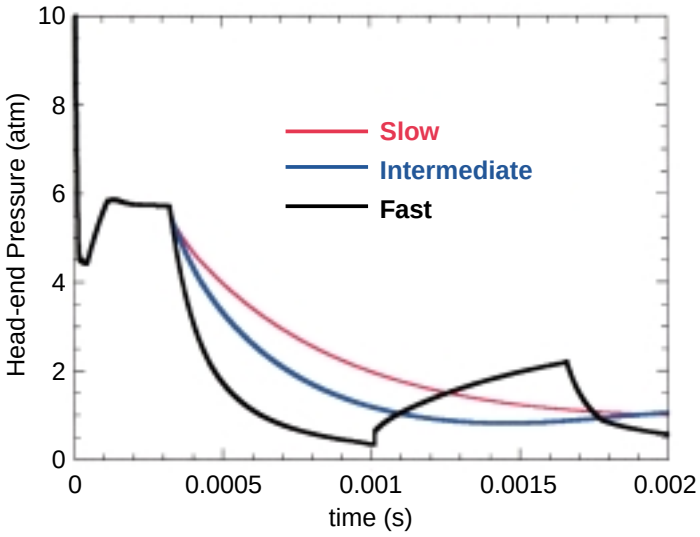

FIGURE 4
Effect of different pressure relaxation conditions at the open end on the pressure evolution at the closed end of a PDE tube.

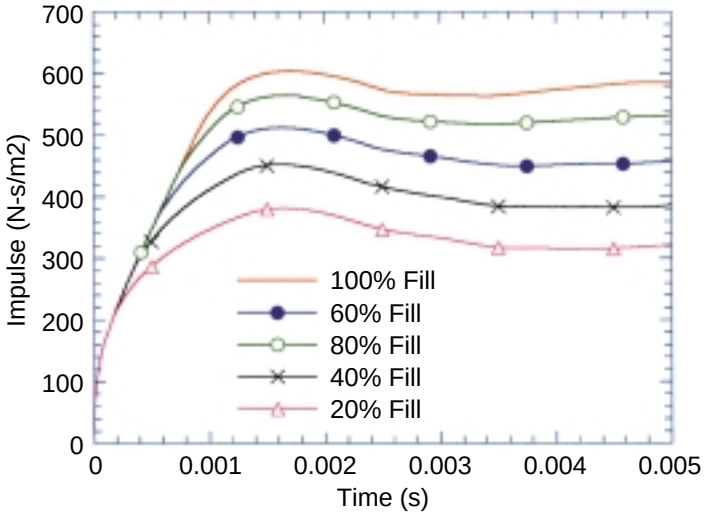

FIGURE 5
Effects of partial filling of the PDE tube with fuel-air mixture on the impulse generated.

different rates because the strength of these expansion waves is different.

This result has several implications. It provides a means of controlling the thrust by controlling the amount of fuel-air fill in the detonation chamber. Furthermore, it suggests that a significant performance drop may not occur if, during multi-cycle operations, the tube is not filled completely. There is also the intriguing possibility of enhancing the performance by using bypass air (the air that would otherwise go around the engine) during flight. This is similar to an idea that is currently used in conventional jet engines, where a major improvement in performance is achieved by effectively using some of the air that would normally bypass (flow around) the engine.

DETONATION DIFFRACTION SIMULATIONS

The large amount of energy required to directly initiate detonations in large tubes or chambers is considered to be one of the potential limitations of the PDE concept. Several techniques have been looked at to circumvent this problem. In one approach, detonation is initiated in a small tube (which requires less

energy) and then allowed to diffract (travel through an area change) into the larger tube or chamber. Preliminary experimental studies at the Naval Postgraduate School (NPS) in Monterey, California, showed that even with this technique, it was difficult to initiate a detonation if both tubes were filled with the same fuel-air mixture such as ethylene and air. However, if the smaller tube had an ethylene-oxygen mixture, it was possible to initiate detonations in the larger tube, even when it contained an ethylene-air mixture. We conducted multidimensional numerical simulations to understand and explain these observations.[3]

The front of any propagating detonation is not a straight line but has a complex shape (referred to as "detonation structure") with "triple points," where three different shock waves meet. The detonation structure in the smaller tube as well as the structures in the larger tube at a series of times are shown in Fig.6 using pressure distribution plots. As seen in the figure, when both tubes are filled with the same ethylene-oxygen mixture, a detonation successfully transmits from the smaller tube into the larger tube. There are eight pairs of triple points in the smaller tube shown in Fig. 6. As the detonation diffracts into the larger tube, expansion waves from the area change weaken the detonation structure causing some decoupling between the reaction fronts and the leading shock waves. Some of the triple points are seen to disappear by 130 microseconds after initiation in the smaller channel. However, new triple points are generated in time and the detonation is seen to recover from the effects of the area change by 165 microseconds. Note that the detonation wave has not yet reached the walls at this time. Some changes in the front are observed as the detonation front reflects from the walls but by now, a self-sustained propagating detonation has been created in the larger tube.

The picture is quite different when both tubes are filled with the same ethylene-air mixture. In this case, the detonation does not survive the diffraction into the larger tube, as seen in Fig. 7, where the pressure distribution in the larger tube is shown at a particular time (200 microseconds after initiation in the smaller channel). The front is devoid of the wave structures that are characteristic of propagating detonations.

The marked difference in the two cases can be traced to the differences in the number of triple points in the two mixtures. Our simulations of detonation structures in these ethylene-oxygen and ethylene-air mixtures showed that a key difference between the two detonations was the wider spacing between triple points for the air diluted mixtures. That is, a tube of a given size can have only fewer triple points in the air mixture than in the oxygen mixture. When a detonation in an ethylene-air mixture in the small tube (with few triple points) travels into the larger tube, it does not appear to be able to retain enough triple points to initiate a propagating detonation in the larger chamber. We can increase the number of triple points in the smaller channel by filling it with an oxygen-enriched mixture. Indeed, if we use the ethylene-oxygen mixture in the smaller tube, the detonation successfully makes the transition into the ethylene-air mixture in the larger tube as shown in Fig. 8.

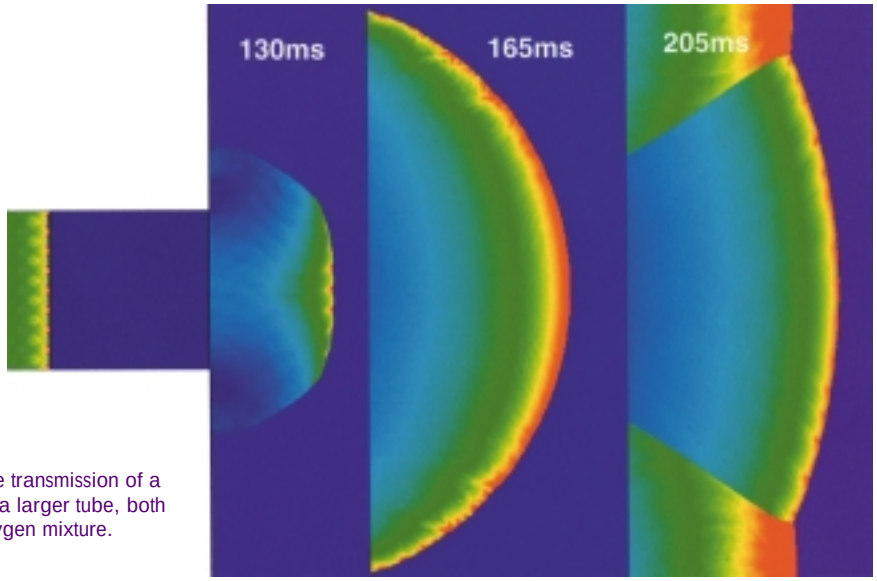

FIGURE 6
Pressure distribution showing the transmission of a detonation from a small tube to a larger tube, both filled with the same ethylene-oxygen mixture.

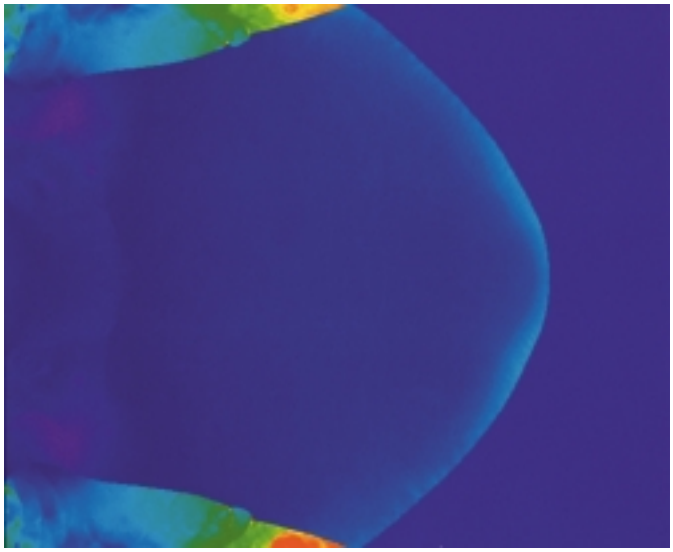

FIGURE 7
Pressure distribution in a large tube after unsuccessful transmission of a detonation from a smaller tube. Both tubes were filled with the same ethylene-air mixture.

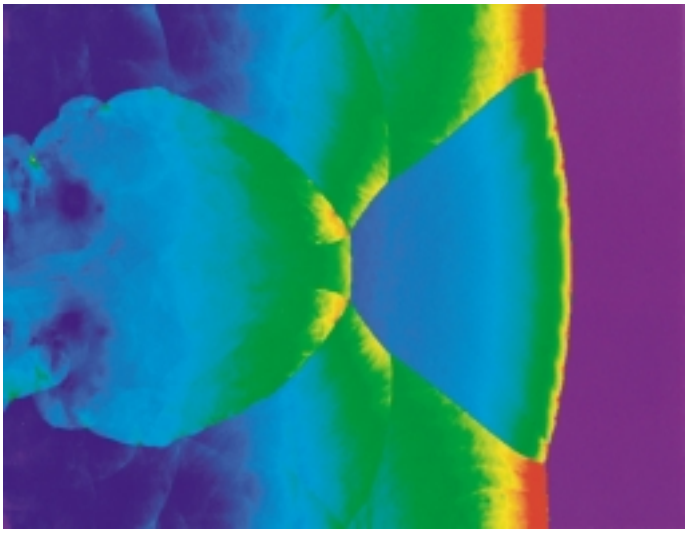

FIGURE 8
Pressure distribution showing the detonation structure in a large tube filled with an ethylene-air mixture. The detonation was initiated using a smaller tube filled with an ethylene-oxygen mixture

SUMMARY

In this article, the impact of numerical simulations on the research of the pulsed detonation engine concept has been highlighted using several examples. A fundamental understanding of various factors that control the performance of PDEs has been attained from the computational studies. This basic understanding has been used to explore means of enhancing the performance. Partially filling the tube with air is found to be one such option. The performance can also be increased by slowing the rate of pressure relaxation at the exhaust nozzle of the engine. The role of initiators is explored using multidimensional simulations. The experimental difficulties found in initiating detonations in ethylene-air mixtures has been traced to the low number of triple points in "typical" initiator tubes. The ease of initiation with fuel-oxygen mixtures has been demonstrated. The major emphasis of our current and future work will be on liquid-fueled pulsed detonation engines, because it is more advantageous to use liquid fuels in many volume-limited Naval applications. Specific issues that are being considered include the effects of droplet size, atomization, vaporization and multiphase mixing on the detonation initiation, propagation, structure and failure.

ACKNOWLEDGMENTS

This work is sponsored by the Mechanics and Energy Conversion S&T Division of the Office of Naval Research.

REFERENCES

[1] Kailasanath, K., "Review of Propulsion Applications of Detonation Waves," AIAA Journal, Vol. 38, No.9, pp. 1698-1708 (2000).

[2] Li, C., Kailasanath, K., and Patnaik, G., "A Numerical Study of Flow Field Evolution in a Pulse Detonation Engine," AIAA Paper 2000-0314, American Institute of Aeronautics and Astronautics, Reston, VA, January 2000.

[3] Li, C., and Kailasanath, K., "Detonation Diffraction in Pulse Detonation Engines," AIAA Paper 2000-3470, American Institute of Aeronautics and Astronautics, Reston, VA, July 2000.

THE AUTHORS

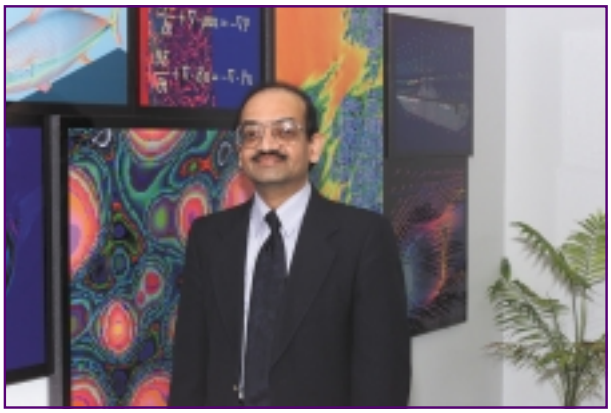

KAZHIKATHRA KAILASANATH is the Head of the Center for Reactive Flow and Dynamical Systems in the Laboratory for Computational Physics and Fluid Dynamics. He received his B.Tech degree (1976) from the Indian Institute of Technology, Madras, and M.S.A.E. (1979), and PH.D. (1980) degrees from the Georgia Institute of Technology. He has been at NRL since 1980 and became Head of the Center in 1988. His research interests include the structure, stability and dynamics of flames and detonations; combustion instabilities, multiphase flows; and the simulation of advanced propulsion system concepts. He is a Fellow of the Institute of Physics, an Associate Fellow of the AIAA, and a member of The Combustion Institute and the American Physical Society.

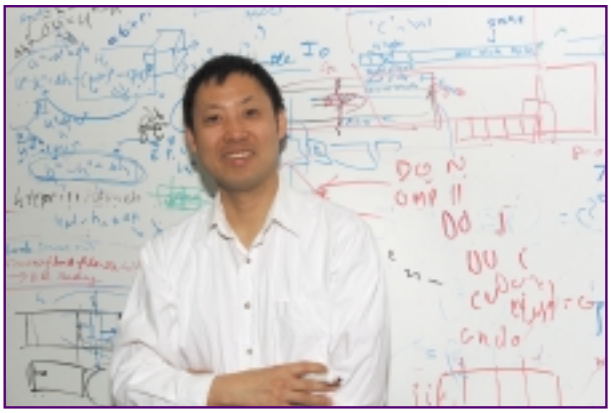

CHIPING LI graduated from the University of California, San Diego, with a Ph.D. degree in engineering sciences in 1987. He has worked at the Laboratory for Computational Physics and Fluid Dynamics in the Naval Research Laboratory as a research scientist since 1989. His areas of research include numerical simulation of reactive flows, basic combustion processes, and algorithms for parallel computation. His recent research activities focus on numerically studying combustion processes such as in supersonic flows including detonation and other types of shock-induced combustion. Dr. Li's work in this area is closely related to propulsion applications such as the ram accelerator and the pulse detonation engine.

GOPAL PATNAIK received his B.E. (Honors) in mechanical engineering in 1980 from the Birla Institute of Technology and Science, India, and his M.S. (1981) and Ph.D (1986) in mechanical engineering from Carnegie-Mellon University. Since 1982, Dr. Patnaik has been involved in the development and application of state-of-the-art computational techniques for low-speed reactive flows. Since 1997, as a member of the Laboratory for Computational Physics and Fluid Dynamics, he has used parallel computing techniques to study complex three-dimensional flames. Dr. Patnaik has published several papers and made numerous presentations on the subject. He is a member of the Combustion Institute and a senior member of AIAA.

Phase-Coherent Underwater Acoustic Communications: Building a High-Data-Rate Wireless Communication Network in the Ocean

T.C. Yang
Acoustics Division

Oceanographic and underwater acoustic research today is limited by the expense of data telemetry using cables. Naval operations are requiring that increasingly large amounts of data be transferred between submerged platforms, surveillance sensor nodes, and surface ships. This demands high-data-rate underwater acoustic communications that, until recently, have not been possible because of the time space variable nature of the underwater acoustic channel—a fading channel with severe time and frequency spread. A joint adaptive decision feedback equalizer with a phase-locked loop has recently been developed that is capable of adapting to channel variation, thereby enabling high-data-rate phase-shifted-keying communications (ACOMMS) in high signal-to-noise (SNR) propagation conditions. Real-time implementation of these algorithms has been demonstrated using high-speed digital signal processing chips. In support of Office of Naval Research ACOMMS efforts, NRL has coupled random media acoustic propagation physics simulators with ACCOM algorithms to develop realistic acoustic communications performance prediction models and improve the efficiency and adaptability of the ACCOMS processing algorithms. The studies have been supported with at-sea acoustic and environmental experiments. Our efforts to understand the impact of random media acoustic propagation on acoustic communications processing algorithms have resulted in significant breakthroughs. These breakthroughs include the development of new signal processing approaches that reduce bit error rates in low SNR propagation conditions. This article discusses the difficulties of using the underwater acoustic channel, the recent advances in communication technology, and the future of the wireless underwater communications for network-centric warfare and ocean exploration.

INTRODUCTION

The ocean is a frontier where accelerated scientific and commercial exploration can be expected in the 21st century. Acoustical oceanography uses acoustics as a means for ocean study. Weather forecasting requires sensor data, not just from the ocean surface but also from within the ocean water column. Acoustic surveillance of the ocean for hostile submarines requires real-time in situ environmental acoustic data to localize the source and maximize the detection range of Navy systems. Environmental acoustic data collected with today's technology are too sparsely sampled to meet future needs. The bottleneck lies predominantly in the undersea telemetry link; current systems use cables that are expensive and immobile. The future, however, looks promising with the advent of wireless undersea acoustic communications (ACOMMS). The availability of inexpensive acoustic sensors and fast digital processing chips can make an undersea wireless communication network a reality. Using the analogy of traffic reporting around the Beltway, where previously information came primarily from aerial surveillance by a few helicopters, real-time traffic updates today come from drivers at the scene using mobile cellular phones. This makes the use of an expensive helicopter less necessary.

The Navy has long recognized the need for high-data-rate underwater acoustic communications. A critical need is a high-data-rate undersea communication link between submarines and surface ships at a distance. Currently, the Navy uses an underwater telephone whose data rate is limited by the multipath propagation conditions commonly experienced in the ocean. Communications suffer from a long series of echoes to the extent that messages sometimes be-

come unintelligible. Under the sponsorship of the Office of Naval Research (ONR) and the Defense Advanced Research Projects Agency (DARPA), a digital high-data-rate, band-efficient, phase-coherent acoustic communication technology has recently been demonstrated by the Woods Hole Oceanographic Institution and Northeastern University. To achieve high-data rate for quadrature phase-shifted keying (QPSK) signals, the investigators implemented a jointly adaptive decision feedback equalizer (DFE) with a phased-locked loop (PLL) to adapt to the time- and space-varying underwater acoustic channel (see discussions below). Recent sea tests (e.g., ACCOMMS ATD, see below) have demonstrated data transmission at voice rate (2 kbits/s) at long ranges (> 30 km) using a midfrequency (2-5 kHz) band signal and transmission at video rate (20 kbits/s) at close ranges (2-5 km) using a high-frequency (10-30 kHz) band signal. The processing algorithms are computationally intensive. Real-time implementation of these algorithms requires the use of high-speed signal signal processing (DSP) chips. Although some technical problems remain to be solved, the feasibility of real-time high-data-rate undersea communications has opened the doors to new approaches to undersea and mine countermeasure warfare, to oceanographic studies, and to marine industrial applications.

Tactical Oceanography

Currently, information about the ocean is obtained from ships, satellites, floats, and moorings. Sensors such as thermistor chains and acoustic Doppler current profilers, either deployed from ships or moored on the ocean bottom, provide quasi-synoptic data across a two-dimensional (2D) (depth/range or depth/time) section through the evolving fields. Satellites provide a 2D measurement of ocean surface properties. With only limited data from a small number of platforms and satellites, extrapolation of the data to a 3D field or to a higher resolution grid introduces temporal/spatial aliasing. The technology push is toward a high-resolution sampling of the ocean: High-resolution data are required to understand various oceanographic processes. These processes include front dynamics, where cross-front circulation must be resolved, and surface layer dynamics, where the mechanism of mixing must be resolved.

High-resolution sampling of the ocean requires linking many sensors together. The ONR project, Autonomous Oceanographic Sampling Network (AOSN), attempts to localize oceanographic processes by using a tomographic approach and conducts detailed sampling using autonomous undersea vehicles (AUVs). Wireless undersea acoustic communications are used for command and control of AUVs and for data telemetry between the AUVs and other acoustic sensor nodes.

In the future, ocean sampling could be accomplished with a network of inexpensive sensors. Without the need to lay cable, the cost of data transmission would be significantly reduced. Significant number of sensors could be deployed and used to build an underwater network analogous to the computer Internet system.

Undersea Surveillance

In the past, undersea surveillance used permanently deployed systems (such as SOSUS). These systems are expensive and require long lead times for laying and burying cable. For protection of battle groups in hostile shallow-water areas, the emphasis is on readily deployable array systems (RDS) that can last several months. In forward areas, clandestine deployment and covert operation are required to avoid compromising the sensor system and the supported activity. Systems that have a surface expression risk easy detection, and systems that use cables risk damage by incidental trawling and anchoring. Both systems can be defeated by low-technology dragging or grappling. Wireless undersea communication systems eliminate the vulnerable telemetry hardware and avoid conspicuous emplacement.

The establishment of an acoustic local area network using wireless undersea acoustic communications could transform undersea surveillance in the future. Using a local area acoustic network, all undersea sensors could be linked together. Undersea connectivity could be a critical part of the future net-centric warfare system that extends from undersea to above sea. Target detection and localization information from undersea surveillance systems could be transmitted to friendly submarines operating in the area to achieve critical tactical advantages. An undersea network of sensors could be used as a barrier system for protecting harbors and critical choke points. Asynchronous parallel access to the network and the ability to communicate either covertly or with a low probability of interception are two research areas of great interest.

UUVs, Mine Countermeasures, and Tactical Operations

High-data-rate underwater acoustic communications provide the critical undersea data link between unmanned underwater vehicles (UUVs), submarines, and surface ships. The ability to acoustically communicate between a submarine and a surface ship is critical for coordination of tactical operations for battle

group defense. The ability to remotely command and control (downlink) and retrieve (uplink) data from UUVs using a wireless acoustic link will significantly enhance the capability of mine countermeasures (MCM) and covert operations. Transferring such duties from a remotely operated (tethered) vehicle to a UUV eliminates the risk of exposure to the mother ship and allows multiple vehicles to operate. In forward areas, in areas not accessible by conventional platforms, and in denied areas that present undue risks to manned systems, UUVs offer unique capabilities in reconnaissance and intelligence gathering due to their autonomy, low observability, deployability, and environmental adaptability. For command and control of UUVs from surface ships or submarines, a tactical midfrequency band (2-5 kHz) is used that extends horizontal telemetry ranges to 10-30 km and beyond. For high-data-rate communications between UUVs and a mother ship, a high-frequency band (10-30 kHz) will be used over short (2-5 km) ranges. The ability to acoustically communicate between Navy platforms (using phase-coherent technology) has recently been demonstrated by the Tactical Acoustic Communications Advanced Technology Demonstration (ATD) project sponsored by the Submarine Warfare Division in the Office of the Chief of Naval Operations. The use of high-data-rate acoustic communications for UUVs in future MCM missions has received great interest recently from the Navy.

Outline

We first overview the basic challenges of underwater acoustic communications and the recent advances made at NRL. We then address both the design of signal processing algorithms and the impact of environmental variability on the algorithm performance. The NRL approach to the ACOMMS problem is based on the physics of random media propagation and the resultant impact on the complex acoustic signal properties most likely to impact ACOMMS performance. Signal processing algorithms are next developed to mitigate the signal variability. Recent accomplishments and advances that are unique to this approach are described. Future research efforts and future technology development (toward a high-data-rate acoustic local area network) are addressed.

ENVIRONMENTAL INFLUENCES

The ocean poses a unique temporal and spatial variable propagation environment that is very different from the radio-frequency (RF) propagation environment experienced by the cellular phone network. Wireless communications in the ocean must be done acoustically since RF signals travel only tens of meters in seawater. High-frequency sound travels shorter distances than low-frequency sound because of sound absorption by seawater. Consequently, the carrier frequency and the available bandwidth for wireless acoustic communications will be range-dependent. To increase the data rate, band-efficient communications using modulation schemes such as phase-shifted-keying are preferred to the phase-incoherent schemes using frequency-shifted-keying. However, the performance of phase-coherent schemes is often environment-dependent. For less favorable environments (such as the so-called overspread channel), it may be necessary to consider phase-incoherent schemes for robustness.

When will phase-coherent acoustic communications work? We briefly summarize the technical challenges of underwater acoustic communications and discuss the environmental acoustic parameters that impact the algorithm performance.

Underwater Acoustic Communication Channel

The underwater acoustic communication channel is different from the RF channel in three respects: (1) the long multipath delay due to sound refraction and long duration of reverberation from the ocean boundary; (2) the severe signal fading due to time-variable transmission loss; and (3) the high Doppler spread/shift, i.e., the variability and offset of receiver frequency and phase relative to the transmitter resulting from the media and/or platform motion.

Multipath delays in underwater acoustic channels can last tens to hundreds of milliseconds, causing inter-symbol interference to extend over tens to hundreds of symbols depending on the carrier frequency and symbol rate. Inter-symbol interference in RF channels is orders of magnitude less and thus easier to deal with. Doppler shift of carrier frequency in underwater acoustic channels is several orders of magnitude larger than that of the RF channel since the sound speed is many orders lower than the speed of light. Hence, carrier frequency identification and symbol synchronization are critical for underwater systems. In addition, Doppler spread is non-negligible in the underwater communication channel as sound propagates through a random ocean medium and scatters from moving surfaces.

In a random medium, signal phase and amplitude fluctuations resulting from propagation through random environments are range, source, and receiver depth- and frequency-dependent. The temporal scale of fluctuations dictates the rate of adaptation for a coherent processor. The magnitude of the fluctua-

tions determines how well the adaptation will work. Since successful communications require a sufficient input signal-to-noise ratio (SNR), appropriate placement of the source and receiver is necessary to avoid the "shadow" zones (areas where transmission loss is high). Random media increase the probability of signal fading; signal fading occurs when multipath arrivals interfere destructively. One strategy to ameliorate signal fading is to use multiple receivers (spatial diversity). The other is to use array beamforming to improve the SNR.

Phase-Coherent Processor

The phase-coherent processor uses an adaptive channel equalizer to remove the inter-symbol interference and a phase-locked loop (PLL) to compensate for the fast phase fluctuations. The equalizer involves a feed-forward loop and a decision feedback loop (Fig. 1). The equalizer and the PLL are jointly updated to adapt for the fluctuation of the channel. An initial sequence of training data (symbols known exactly by the receiver) is used to train the processor. After training, a decision is made for each symbol by the smallest error between the estimated symbol and the true symbols (e.g., four symbols for QPSK). Symbol synchronization is done by timing from an initial pulse code, such as a Barker code, which can also be used as a wake-up signal for the processor.

The performance of the processor bears on the tap coefficients of the feed-forward and feedback loops. The processor must determine how many coefficients will be used and how fast they will be updated. Currently, user input may be required to achieve optimum performance. For an operational Naval system, it is imperative that user-input "tuning" not be required. This is considered an automation problem. To illustrate the problem, note that the tap coefficients are closely related to the multipath arrivals since their function is to remove/compensate for multipath echo arrivals. Because multipath arrivals are discrete in time (measured in terms of symbols), assigning taps where no multipath arrivals are expected will increase computational error. Also, using unnecessary taps significantly increases processing time, leaving less central processing unit (CPU) power for computation.

On the other hand, too few taps decreases the processor's ability to remove the multipath inter-symbol interference and, consequently, increases the bit error rate (BER). A significant advance in recent years is the development of a multichannel sparse equalizer algorithm that assigns taps where multipath arrivals are expected. Multipath arrivals are determined by estimating the channel impulse response function using the initial pulse (e.g., Barker code) for each channel. In many cases, spatial diversity may be necessary to minimize the BER, hence the need of the multichannel decision feedback equalizer (DFE). Note that channel impulse estimation requires high SNR for each channel. The rate of channel update should be based on some statistical inference measures. The parameters are currently set by experience.

Noting that the channel response and its rate of fluctuation vary from ocean to ocean, it is not readily apparent how the acoustic environmental condition affects the performance of the DFE and PLL; this requires an analysis of the impacting channel physics. Underwater signal fluctuations, unfortunately, do not follow simple statistical distributions; an empirical model will be inadequate. In many cases, there is no clear correlation of the BER with observable envi-

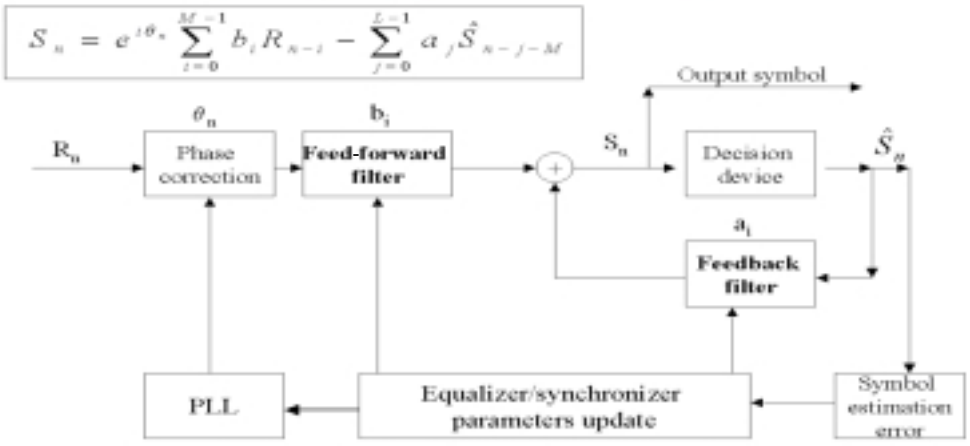

FIGURE 1
Schematic diagram of decision feedback equalizer and phase-locked loop.

ronmental acoustic variables. In environments that produce many diffused multipath arrivals, the equalizer may have to work harder (requiring longer training data) or may fail (producing high BER). But the equalizer may also fail in simple multipath environments when other conditions have changed.

The NRL ACOMMS project was created to investigate how the acoustic environment affects the performance of phase-coherent underwater acoustic communications. The long-term objective of this project is to quantitatively determine how and under what conditions the random processes in the ocean and the ambient background noise field affect the data transmission rate and bit error rate of phase-coherent acoustic communication systems. Such results could be used for predicting underwater acoustic modem performance in operational areas of interest. The short-term objectives are to relate (or correlate) the characteristics of signal propagation with the BER performance of the phase-coherent algorithm and to develop new algorithms to improve the BER. At-sea experiments are an integral part of the project because data are a prerequisite for identifying the issues affecting the processor performance and for validating new algorithms.

PERFORMANCE SIMULATIONS AND PREDICTIONS

Random fluctuations in the ocean originate from complex dynamic oceanographic processes that are not always independent of each other. These processes cause sound speed variation as a function of range, depth, and time. Since oceanographic measurements are undersampled in space and time, sorting out the sound speed variations according to the processes is not possible in practice. For this reason, a simulation model is useful for determining which oceanographic process has the most effect on acoustic communications. Only a handful of processes are expected to play a dominant role; the particular processes that need consideration depend on the acoustic frequency. For midfrequencies (2-5 kHz), surface waves, internal waves, and turbulences are important processes to consider. At high frequencies (10-30 kHz), surfaces waves, bottom roughness, turbulence, and other fine-structure inhomogeneities in the water column dominate acoustic propagation. All these processes have a wide spectrum in wavelength that overlaps the wavelengths of the ACOMMS signals. For ACOMMS analysis, the critical parameters are the temporal scales of the fluctuations; for many processes, the temporal scale can be determined from their wavenumber-frequency dispersion relations. One finds that small surface waves and turbulence cause rapid fluctuations in the phase and amplitude of the ACOMMS signals. Internal waves have a much slower fluctuation rate but can cause severe amplitude fading. Although bottom roughness is stationary, it affects the signal by the fact that each pulse hits a different part of the bottom due to surface and media fluctuation and platform motion. As a result, large surface waves also play a role.

For quantifying ACOMM performance, a simulation model consisting of three parts was created: (1) A physics-based random media model simulates sound speed variations caused by various oceanographic processes. This model generates realizations of sound speed variations as a function of range, depth, and time. (2) A full-field acoustic model propagates broadband impulse response functions through the time-varying, range-dependent sound speed fields. The time-varying impulse response functions are convolved with the transmitted signals to produce the received signals at the receiver array. (3) An ACOMMS performance analysis model evaluates the BER through the time-evolving channel.

The random media model uses parameter values based on previous experimental measurements as much as possible. Although internal waves and turbulence are modeled with different analytic expressions in the literature, we used an "approximate" spectrum that can fit both internal waves and turbulence with a change of parameter values. It is realized that the model may not be perfect, but it captures the basic physics and is expected to yield a first-order understanding of the environmental impact on the ACOMMS performance.

The simulation analysis is focused on two areas: the temporal coherence and phase fluctuation. The effect of medium fluctuation on the acoustic channel can be characterized by the temporal coherence of the impulse response function, which is defined as the normalized value of the correlation of the impulse response function, with the response function at an initial time. Its magnitude lies between 0 and 1. The temporal coherence gives an indication of how much (the coherence value) and how fast (the coherence time) the channel has changed in time. The higher the coherence loss, the harder the equalizer must update. The shorter the coherence time, the faster the equalizer needs to update. Since the equalizer is a numerical algorithm based on the minimal mean-square error criterion, there is a limit in its performance, depending on the algorithm. Using the coherence value as a measure, we find that the recursive least-square (RLS) error algorithm breaks down whenever the coherence value drops below 0.5. This conclusion is based on numerous simulations using both the conventional and sparse equalizer. We found

that the equalizer typically requires a minimum length of time (20 to 30 symbols) to adapt to a changing environment. If the channel changes in less than this minimum time required to update (coherence time < update time), the equalizer may never catch up with the channel.

For phase-modulated signals, fluctuation of the signal phase is a key variable that will impact the algorithm performance. This is because the phase of the signal changes faster than the amplitude. The PLL is implemented to remove the fast phase change that the equalizer is not able to track. The phase change of the signal can be measured by the phase spectrum, which is the Fourier transform of the phase change with respect to time. The impact of the phase change depends on the spectrum value. We found, not surprisingly, that the algorithm can tolerate slow phase changes more easily than fast phase changes. The amount of phase change tolerable by the PLL (used in conjunction with the equalizer) is thus a function of the frequency at which the phase changes. The maximum tolerable phase change is evaluated in the simulation study for a channel with a fixed multipath arrival structure. The result is plotted in Fig. 2 as a threshold curve. A high BER is expected when the channel phase fluctuation spectral values exceed the threshold curve.

Other signal properties must be included to simulate the ACOMMS performance. These include the statistical distribution of the amplitude, the spatial coherence of the signal, and the change of transmission loss caused by the random media. We used values estimated from data wherever applicable.

RECENT ADVANCES IN PHASE-COHERENT COMMUNICATIONS

The state-of-the-art multichannel sparse decision-feedback equalizer has been tested in the ACOMMS ATD program at both mid and high frequencies. The results showed that a substantial percentage of the packets were error-free with error encoding over a wide range of distances. For QPSK signals, bit-error-free packets require ≥ 12 dB SNR at the input level; multiple channels (3-4) are required for the equalizer to work; and the performance is occasionally poor due to poor channel properties and poor ability to estimate the channel impulse response. These results are common to other tests as well. Many tests have shown that BER can often be improved in post analysis by playing with the number of taps and update parameters; BER is usually high when using only one channel; and a 5-s limit on the communication packet length was used in practice at midfrequency, with duty cycle less than 50%. This means that the average data rate is less than half of the burst data rate.

NRL has developed several new algorithms to improve the performance of the multichannel DFE at midfrequencies. The new algorithms extended phase-coherent acoustic communications to low SNR (~ 1-2 dB) input cases, extended the communication packet length from 5 seconds to 10-20 seconds, and

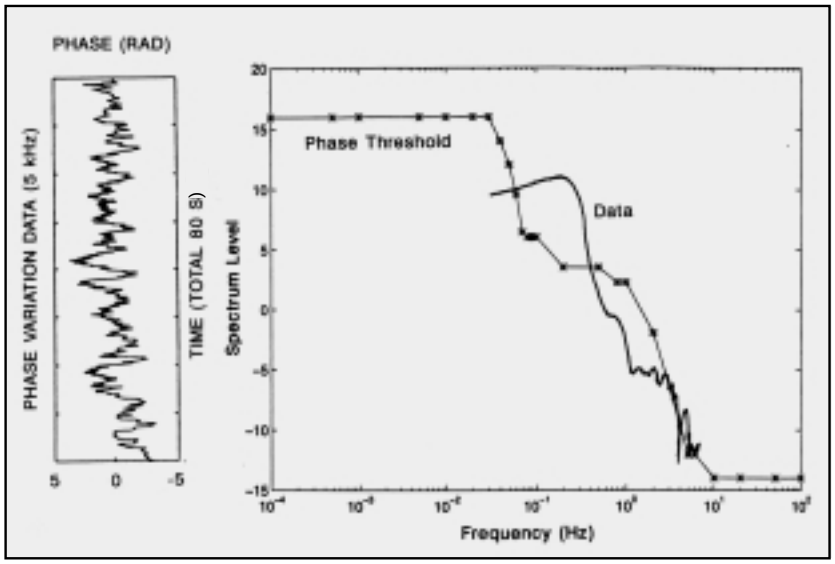

FIGURE 2
Example of phase variation time series (left) and its spectrum (right). The phase threshold (right) indicates the maximum spectral level of phase fluctuations that can be tolerated by the phase-locking loop.

reduced the number of channels from 4 to 1-2. The improved performance has been demonstrated with at-sea data as discussed below; more at-sea tests are being planned. The new algorithms have also been demonstrated to work with one set of parameters for several different environmental conditions. These accomplishments pave the way for: potential covert communications, which is a high priority for Navy operations; more energy efficient modems due to the use of longer packet length and less computational load (less number of channels); and modem algorithms capable of working autonomously in different oceans.

The improved algorithms are based on inferences drawn from physical analysis of the temporal and spatial coherence, as discussed above. Temporal fluctuation, particularly the phase fluctuation, determines the BER performance and the length of the packet. It was observed that large phase errors resulting from incorrect Doppler shift estimation could exceed the threshold values for the PLL. The error in the carrier frequency estimation could ruin symbol synchronization for a long communication packet. During the RDS2 experiment, communication packets of 10-s length were transmitted using a towed source to a drifting vertical array. QPSK signals with a 3.5 kHz carrier frequency and 500 Hz bandwidth were used. Four channels were required to process the packet using the existing algorithm, and the results were good only for the first ~5 seconds (Fig. 3). A continuous-wave (CW) tone was transmitted before the QPSK packet. Using the CW signal to estimate the correct carrier frequency and then correct the synchronization error, it was demonstrated that the entire 10-s packet was successfully equalized using only one channel (Fig. 4). This result was consistently obtained for all the 10-s packets that were transmitted during the 2-hour run in the RDS2 experiment. We note that by removing the phase due to Doppler, the residual phase is apparently small enough to fall below the phase threshold curve. The actual phase spectrum is not easily deducible from the data.

Another improvement comes from the study and use of spatial coherence to make the equalizer work with low-input (~1-2 dB) SNR. This was demon-

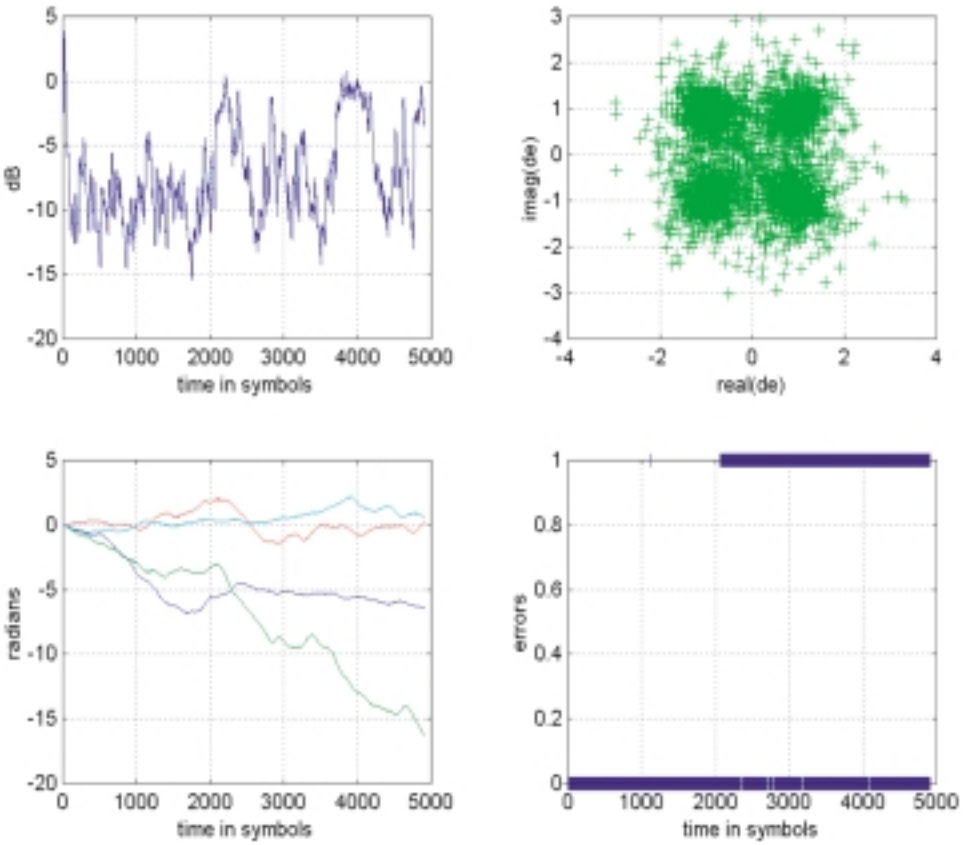

FIGURE 3
Plots of mean-squared-error (upper left), symbol constellation (upper right), phase compensation (lower left), and bit-error (lower right) versus the symbol number for a 10-s long QPSK signal. The curves in the lower left figure correspond to different channels.

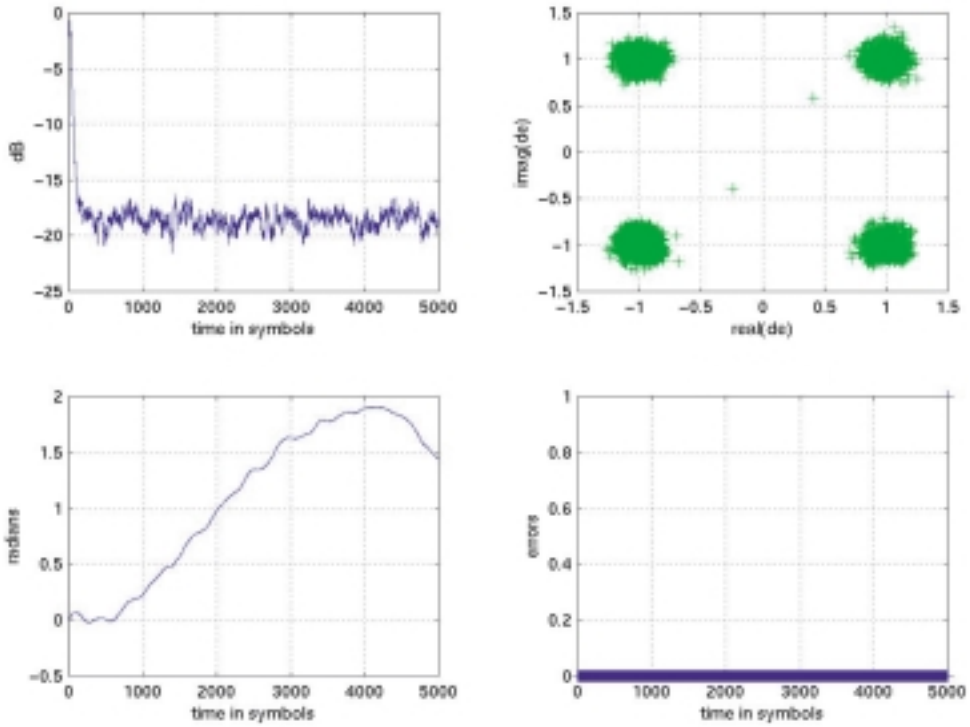

FIGURE 4
Same as Fig. 3, processed using the correct Doppler shift.

strated using the ACOMMS data collected during the ADVENT 99 experiment and concerns the use of multichannel DFE. Note that multichannel receivers (spatial diversity) were originally used to combat signal fading. In this scenario, the multichannel signals must be uncorrelated (spatially) so that they do not fade at the same time. Multichannel DFE determines the relative phase and weighting of the channel feedforward coefficients based on the minimum square error criterion. It requires high (~ 10-15 dB) SNR. Likewise, estimation of the channel impulse response requires high SNR data. For the multichannel DFE to work with low SNR data, additional processing gain and/or array gain will be required to enhance the SNR before applying the multichannel DFE. Processing gain can be achieved by spreading the signal in time using, for example, a code division spread spectrum (CDSS) scheme. Array gain can be achieved by beamforming an array of receivers. However, we note that beamforming requires the signal to be coherent over the receivers; this requirement is opposite to that of spatial diversity.

The solution is to use a combination of beamforming with spatial diversity. Subarrays of closely spaced phones are used to provide required array gain. To use multichannel DFE, the centers of the subarrays are widely spaced so that the beamformed array outputs are spatially uncorrelated. This requires a selection of phones based on the spatial coherence. We did such a study using the ADVENT 99 data. The ADVENT 99 experiment was conducted in the Adventure Bank, Sicily, in 1999 with the support of the NATO SACLANT Undersea Research Center. A fixed source and receiver array were used so that Doppler shift would not be an issue. QPSK signals with a 1.2 kHz carrier frequency and 500 Hz bandwidth was transmitted to a range of 10 km. The source was mounted at 2-3 m above the seafloor. An array of ~20 phones was used to investigate the performance of multichannel DFE (spatial diversity) versus the phone separation and number of phones. An array of 10 phones spaced 2 m apart was used to compare the performance of the combined beamforming/spatial diversity method with that using only the multichannel DFE. Figure 5 shows the BER of these two methods. The multichannel DFE used 4 phones separated by 6 meters so that the signals were not correlated. (The correlation length was ~ 4 m, as determined from the data.) For the combined beamforming/spatial diversity method, we used three overlapping subarrays, each containing five phones. The 4-channel DFE worked when the SNR was above ~ 8-10 dB but failed (BER >80%) for SNR < 8-10 dB. The NRL method worked well, even when the SNR at the phone level was as low as 1-2 dB. Figure 6(a) shows the channel impulse esti-

mated from the Barker code for the ~2 dB SNR case for which many (unnecessary) tap coefficients will be selected based on a threshold. Figure 6(b) shows the impulse response estimated after beamforming for which the tap assignment will be much less ambiguous. Comparing Fig. 6(a) with Fig. 6(b) one finds an array gain of ~ 6-7 dB as a result of beamforming. We have modified the tap assignment program to eliminate the taps that represent low-level multipath arrivals or noise fluctuations.

The performance prediction for the temporal coherence was tested during the Littoral Warfare Advanced Development (LWAD) 98-1 experiment in the Gulf of Mexico area. Time diversity was used to process data collected on a sonobuoy. The data have SNR > 10dB, so SNR is not a likely cause for BER. It was found that large BER were associated with data with signal coherence < 0.5. This result supports the performance predictions based on temporal coherence discussed in the previous section.

SUMMARY AND FUTURE WORK

Underwater connectivity is critical for many Naval operations and is an integral part of future net-centric warfare activity. Underwater connectivity requires a high-data-rate wireless acoustic communications link between surveillance sensors, UUVs, submarines, and surface ships for command, control, and data telemetry. Recent advances in phase-coherent communications technology make possible high-data-rate communications at long ranges. Real-time operating high-data-rate modems are being developed that could work reliably under diverse ocean conditions and locations. Continued ONR/NRL research can be expected to resolve environmental influences on the modem performance

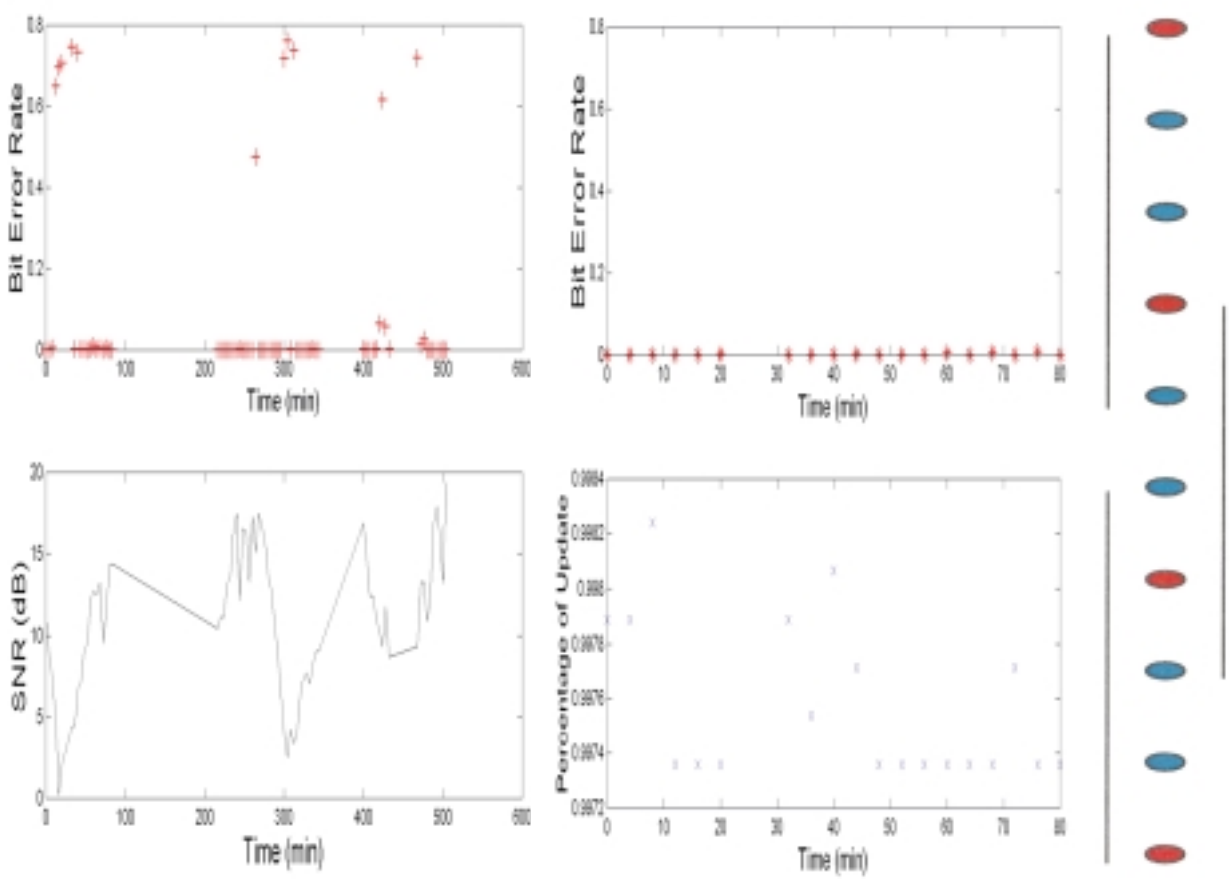

FIGURE 5
BER using 4-channel DFE (upper left) and the corresponding input SNR (lower left) for a period of ~ 9 hours. The upper right figure shows the BER using the combination of beamforming with spatial diversity for the first 80 min of the data. The BER was minimal, even when the SNR was as low as ~1-2 dB. The lower right figure shows the rate of update of the equalizer. The far right figure shows the array configurations. The red dots indicates the phones used in the multi-channel DFE. The arrows indicates the subarrays used for beamforming as discussed in the text.

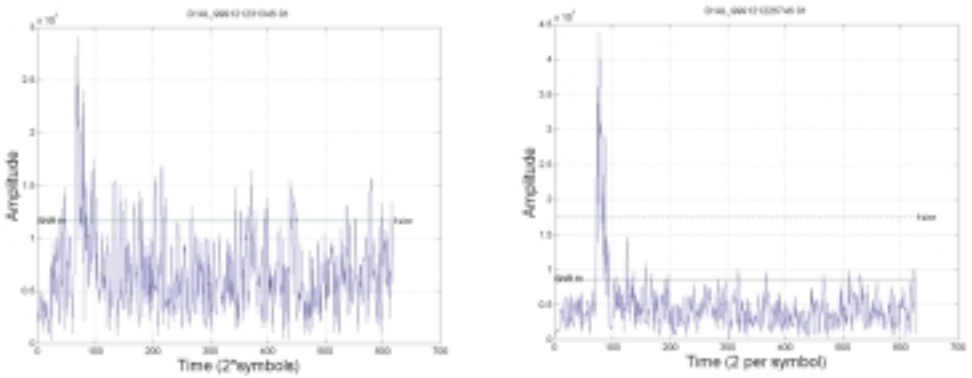

(a) (b)

FIGURE 6
Left figure shows the impulse response for a single channel with low SNR; right figure shows the same after beamforming using five sensors.

and develop improved algorithms for covert communications, multi-access networking, etc.

The NRL ACOMMS projects followed a physics-based approach that focused on identifying critical signal properties that have the most impact on the BER. Three initial performance predictions were made based on the temporal coherence length, value, and phase fluctuation spectrum. This analysis laid the framework for an improved algorithm that allows longer communication packets (10-20 s at mid frequencies) and requires fewer channels in the decision equalizer. The study of spatial coherence led to a method for combining beamforming with spatial diversity. The new method has been demonstrated to work with some data having ~1-2 dB input SNR; further tests of this new method are being planned. The low SNR requirement will extend the communication range and make covert communications possible.

Assuming the success of a local area underwater acoustic network with multi-user access, distributed networks of autonomous sensor nodes with acoustic modems could be set up in many parts of the ocean. The autonomous sensor nodes could be affordably mass-produced. Independent nodes offer the important benefit of architectural flexibility, permitting sensor-field aperture and spacing to be optimized for the intended mission. These networks could serve the dual purpose of civilian weather and oceanographic research on one hand, and acoustic ocean surveillance for the Navy on the other. To the user, the acoustic local area network will not be any different than the standard network; it will use modem handshaking protocols already developed in the RF and Internet world. As such, it is expected that the creation of an "oceanet" could greatly expand the capability for weather nowcasting and forecasting, marine mammal and fishing migration, and many other areas of undersea research. Developing an asynchronous multiple-user acoustic communications network, therefore, will be an important research topic for the future.

ACKNOWLEDGMENTS

The NRL ACOMMS experiments were the results of a collaborative effort of many people including particularly, A. Al-Kurd, E. Carey, P. Gendron, M. McCord, and J. Schindall. The support of LWAD, TTCP RDS program, and NATO SACLANT Center for Undersea Research were greatly appreciated; without this, most of the ACOMMS experiments could not have been possible. J. Schindall has developed most of the software for at-sea data transmission/collection and initial data reduction. A. Al-Kurd has conducted extensive acoustic simulations and processed data from several experiments. K. Yoo has carried out acoustic signal propagation modeling in random media to support ACOMMS data analysis and interpretations. The support, encouragement, and leadership provided by our branch head, M. Orr, are indispensable to the ACOMMS project. Comments on the manuscripts by P. Gendron, P. Mignerey, and M. Orr are greatly appreciated.

[Sponsored by ONR]

REFERENCES

There are too many references to be cited here. For recent NRL accomplishments, see the following references.

[1] T.C. Yang and A. Al-Kurd, "Performance Limitations of Joint Adaptive Channel Equalizer and Phase Locking Loop in Random Oceans: Initial Test with Data," *Proceeding of OCEANS '00*, Vol. 2, 803-808, 2000.

[2] T.C. Yang and M. Siderius, "Phase Coherent Communications at Low Frequencies During the Advent 99 Experiment in the Sicily Strait," *Proceeding of OCEANS '00*, Vol. 2, 1005-1010, 2000.

THE AUTHOR

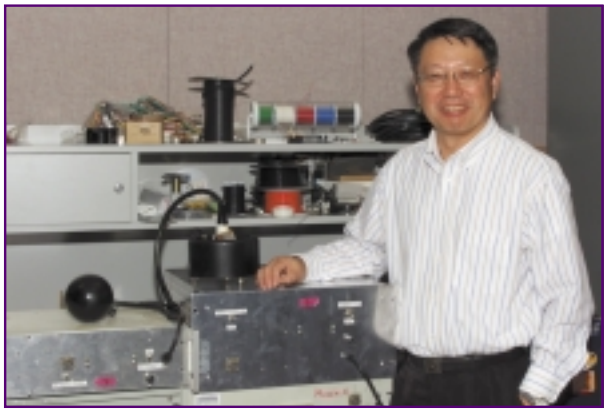

TSIH C. YANG came to NRL in 1979 and worked on Arctic acoustics until 1993. He discovered ice edge noise hot spots, published many new findings on under-ice reflectivity, low-frequency sound transmission loss, scattering and reverberation, ambient noise coherence and directionality, ice floe vibrations, and geophone array response. He was responsible for the array wet end design for the Navy Ice Mounted Surveillance System. Since 1993, he has worked on geo-acoustic inversion of ocean bottom properties, sonar array processing, and underwater acoustic communications. He pioneered matched mode processing for a vertical line array and recently developed matched-beam processing for Navy horizontal line array systems. He formerly was the head of the Arctic Section and now heads the Dispersive Wave Guide Effects Group. He received three patents and one Alan Berman Research Publication Award. Dr. Yang is a fellow of the Acoustical Society of America.

Acoustics

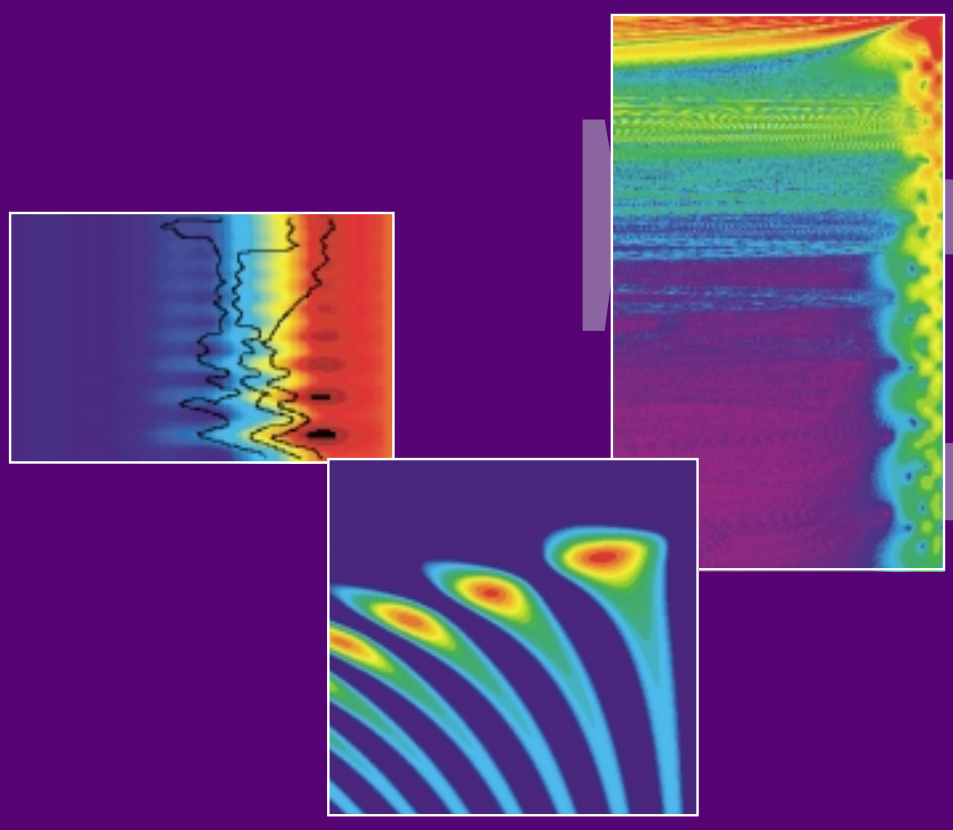

Acoustic Modeling of the Northwest Providence Channel on 15 March 2000

D.M. Fromm and G.V. Norton
Acoustics Division

J.F. McEachern
ONR Code 321SS

Introduction: On 15 and 16 March 2000, a number of marine mammals were found stranded on islands surrounding the Northwest Providence Channel in the Bahamas. U.S. Navy surface ships transited through the channel on 15 March 2000, operating their hull-mounted tactical sonars in the midfrequency (1 to 10 kHz) band. Responding to this incident, the Office of Naval Research tasked the Naval Research Laboratory to determine the best estimates of the sound pressure levels generated by these sonars as a function of range, depth, and azimuth in the channel. State-of-the-art numerical models were to be used. Inputs to modeling were to include ship and sonar operating parameters supplied by the Fleet and actual environmental data for the date and time of the event, supplemented with historical data.

Environmental Description: The Northwest Providence Channel is approximately 200 km long. It begins where the Great Bahama Canyon meets the Atlantic Ocean and transverses through the islands and banks of the Bahamas to the Florida Straits. Its width ranges from 40 to 100 km, and its depth gradually decreases from 4500 m deep at the Atlantic to 500 m deep where it exits at the straits.

In contrast to the variability of the bathymetry, the structure of the sound speed field was fairly uniform throughout the channel. Figure 1(a) presents in situ sound speed vs depth data measured during the Navy transit merged with an historic deep profile. Figure 2(a) details the in situ data; the sound speed is seen to increase very slightly with depth down to approximately 150 m, at which point the sound speed begins to decrease rapidly with depth. The change in slope of the sound speed at 150 m marks the bottom of what is referred to as a surface duct. Three independent sound speed field models predicted that this surface duct persisted throughout the New Providence Channel on 15 March 2000. This is a significant structure with respect to how sound travels in the ocean.

Another key factor was the 6.6-m/s (13-kt) winds with 0.6 to 0.9-m (2–3-ft) seas and a lack of whitecaps. Due to the low wind speed, the ocean surface was not very rough and thus did not scatter the sound significantly. The lack of whitecaps meant there was no source of bubbles for entrainment in the upper part of the water column. Consequently, some key mechanisms for scatter and absorption of sound were not present.

Acoustic Field Results: The acoustic propagation model used was RAM.[1] This model is based on the parabolic equation and is widely accepted within the research community as a validated state-of-the-art model. Figure 1(b) shows the typical structure of the sound field in the channel for a Navy 2.6

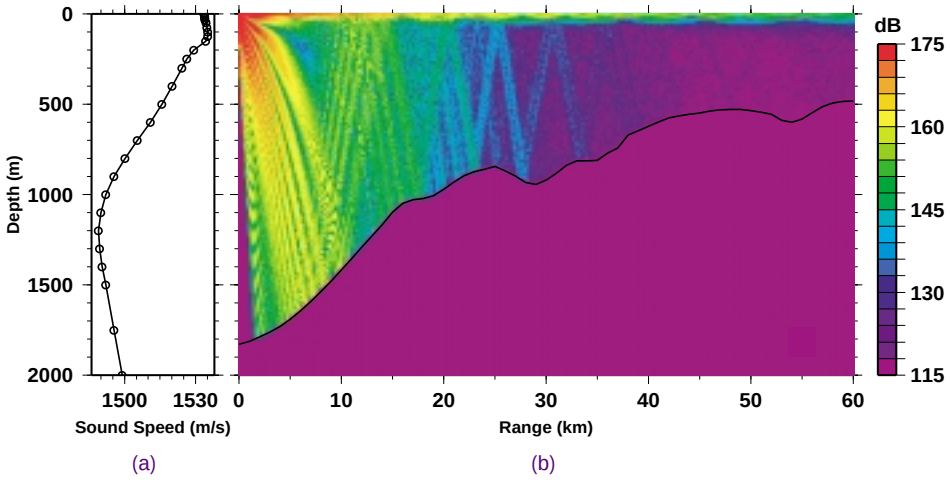

FIGURE 1
For the full water column: (a) the in situ sound speed vs depth merged with the historic deep-water profile; (b) the simulated acoustic sound pressure level in dB re 1 μPa for a frequency of 2.6 kHz.

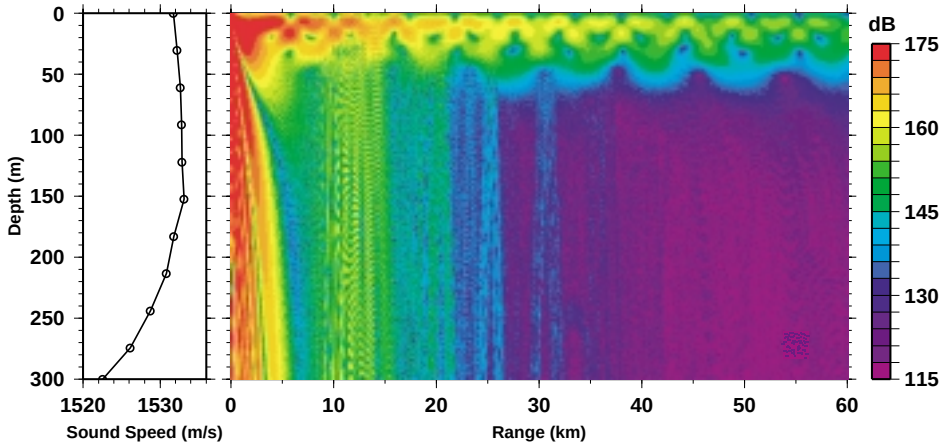

(a) (b)

FIGURE 2
For the top 300 m of the water column: (a) the in situ sound speed vs depth; (b) the simulated acoustic sound pressure level in dB re 1 μPa for a frequency of 2.6 kHz.

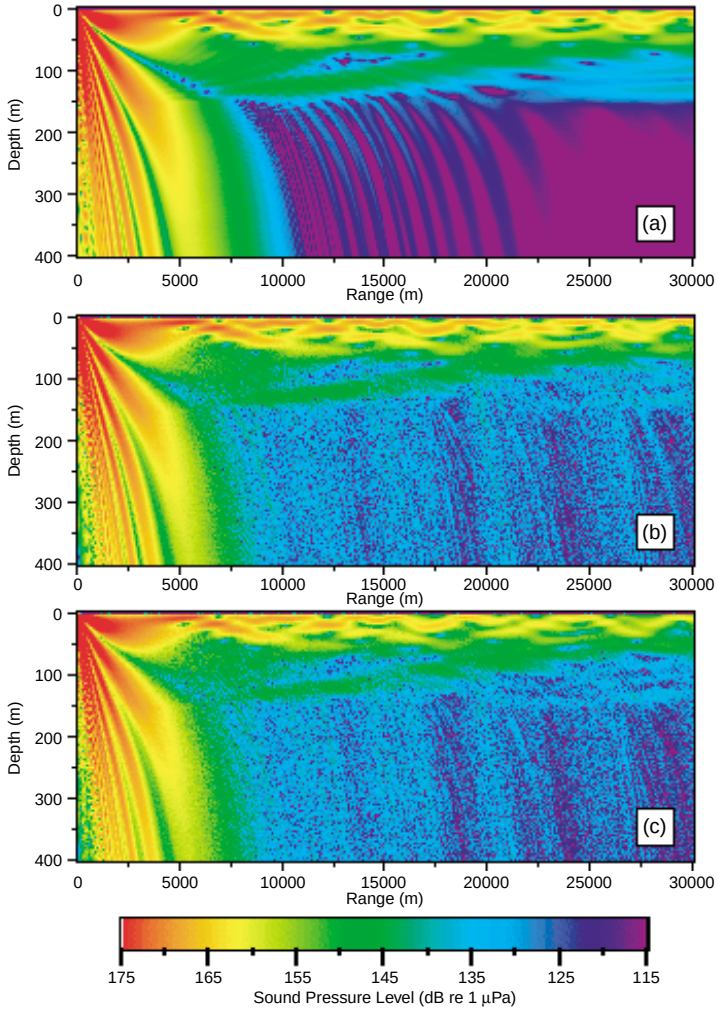

FIGURE 3
Simulated acoustic sound pressure level in dB re 1 μPa for a frequency of 2.6 kHz for three different ocean environments: (a) in situ sound speed, flat surface, and no bubbles; (b) in situ sound speed, deterministic rough surface, and no bubbles; (c) in situ sound speed, deterministic rough surface, and bubbles.

kHz hull-mounted sonar operating at a depth of 7.9 m (in the upper left corner of each figure). The false color indicates received sound pressure levels in dB re 1 μPa in water as a function of range and depth.

In Fig. 1(b), sound that propagates below the surface duct bounces off the bottom and the surface several times, quickly attenuating as it travels. The lobe structure observed at the source (known as the Lloyd's mirror effect) is the result of interference with the surface. The thin green layer across the top of this figure suggests the effect of the surface duct.

Figure 2(b) focuses on the sound field in the top 300 m of the water column and shows that sound is trapped in the top 50 m of the surface duct, slowly attenuating as it propagates to long ranges. This result is not affected by changes in bathymetry or bottom type. Effectively, this one figure could be used to describe the sound field in the top 50 m for the surface ship sonar located anywhere within the channel.

Sensitivity Studies: Numerous environmental effects, including scattering from surface roughness, scattering from near surface bubbles, scattering from biologics, internal waves, solitons, microstructure, detailed ocean bottom properties, three-dimensional effects, and basin reverberation, were evaluated for their effect on the acoustic propagation. These environmental effects generally acted to decrease the sound pressure level. Only surface roughness and near-surface bubbles have the potential to significantly impact the acoustic propagation within the surface duct in this case.

Figure 3 presents high-resolution modeling results using a variant of RAM that incorporates actual representations of the ocean surface roughness and near-surface bubbles.[2,3] Figure 3(a) shows a baseline case where the ocean surface is perfectly flat with no bubbles. It is similar to Fig. 2(b) except that for computational reasons, no energy returning from below 400 m is considered. Figure 3(b) shows the case where surface waves corresponding to observed wind and sea conditions have been included. The resulting surface roughness causes acoustic energy to be scattered out of the surface duct. At 30 km, the peak sound levels have been reduced by approximately 2 dB. Figure 3(c) shows that if near-surface bubbles are added to surface roughness, the sound pressure levels would have been further attenuated.

Conclusions: On 15 March 2000 in the Northwest Providence Channel, Bahamas, the acoustic propagation conditions for hull-mounted sonars were dominated by a surface duct. Also, due to calm seas, additional mechanisms for scattering or absorbing acoustic energy out of the duct were minimized. Consequently, acoustic energy from the sonars was concentrated near the ocean surface and propagated to significant distances. At press time, the role of these acoustic propagation conditions in the strandings was still under analysis. A final report, prepared in conjunction with marine biologists is due out in early 2001.

[Sponsored by ONR]

References:

[1] M.D. Collins, "A Split-Step Padé Solution for Parabolic Equation Method," *J. Acoust. Soc. Am.* **93**, 1736-1742 (1993).

[2] G. Norton, J. Novarini, and R.S. Keiffer, "Coupling Scattering from the Sea Surface to a One-way Marching Propagation Model via Conformal Mapping," *J. Acoust. Soc. Am.* **97**, 2173-2180 (1995).

[3] G. Norton, J. Novarini, and R.S. Keiffer, "Modeling the Propagation from a Horizontally Directed High Frequency Source in Shallow Water in the Presence of Bubble Clouds and Sea Surface Roughness," *J. Acoust. Soc. Am.* **103**, 3256-3266 (1998).

Ocean-Acoustic Soliton Modeling Predictions

S.A. Chin-Bing,[1] A.C. Warn-Varnas,[2] D.B. King,[1] Z.R. Hallock,[2] R.A. Zingarelli,[1] and J. Hawkins[3]
[1]*Acoustics Division*
[2]*Oceanography Division*
[3]*Planning Systems, Inc.*

Introduction: Large-scale sea floor topography can be viewed as a scarred surface made up of ripples, troughs, ridges, mountains, and valleys—all connected by gently sloping, near-planar surfaces.

In the deep ocean, these physical features do not significantly affect the flow of ocean water near the sea surface. However, in coastal regions, where the depth between sea surface and sea floor is less than a few hundred meters, sea floor protrusions combine with tidal flow to produce a substantial upwelling of water mass that creates internal waves. Waters in coastal regions can have sound speeds that vary sharply with depth and exhibit strong gradients between adjacent layers near the sea surface. These conditions define a *thermocline* region, and some internal waves generated in such regions can maintain their identity (shape, amplitude, and phase) while traveling hundreds of kilometers. These shallow-water, near-surface internal waves are known as *solitons*, and they produce subsurface "ripples" that travel along the thermocline over these long distances. Similar conditions with solitons are also found in straits. Computer simulations of the soliton phenomena have

been generated by primitive equation ocean (PEO) models. PEO computer models use "first principle" physics (conservation laws, fluid dynamic equations, etc.) and initialization conditions to produce computer simulations of solitons as the soliton packet evolves. Reasonably accurate computer simulations have been produced for solitons in the Strait of Messina using a PEO model.[1]

Large-amplitude solitons can have a significant effect on ocean acoustic propagation due to the acoustic mode conversions that occur when the acoustic field interacts with the soliton packets.[2] In some cases, these acoustic mode conversions can produce large losses in acoustic signal transmission. Studies of the effects of solitons on ocean acoustics have resulted in the development of a novel way of coupling oceanographic models with ocean acoustic models using dynamic feedback from the acoustic analysis. The following sections discuss this novel coupling of ocean models with acoustic models, present some initial results, and evaluate the suitability of using a PEO model for detailed acoustic studies.

Coupling Methodology: A two-layer, weakly nonhydrostatic PEO model was used to generate simulations of oceanographic soliton fields in the Strait of Messina. Figure 4(a) is a colored contour plot of one of the simulated soliton packets as it propagates away (left-to-right) from the Strait of Messina. These simulated soliton fields were used to study acoustic mode conversions as the acoustic field passed through the solitons (right-to-left) and propagated upslope.

Figure 4(a) shows the placement of the simulated acoustic source (S) and its proximity to the thermocline (T). Oceanographic parameters in the PEO model were adjusted so that the resulting amplitude and phase of the first two wavelengths of the simulated soliton fields were in agreement with measured soliton data. Figure 4(b) shows an expanded view of the simulated soliton packet. Only the color contours from Fig. 4(a) are shown in Fig. 4(b). The black contour lines in Fig. 4(b) are from measured soliton data.

A visual comparison of the soliton data with the PEO model simulations indicates that the peaks and troughs of the first two wavelengths in the soliton packets (on the right-hand side of Fig. 4(b)) are in good agreement in both phase and amplitude. Therefore, the soliton simulation generated by the PEO model might be considered as a fairly good simulation of the actual soliton packet. However, acoustic simulation studies in which the same acoustic signal was propagated through both the simulated and the

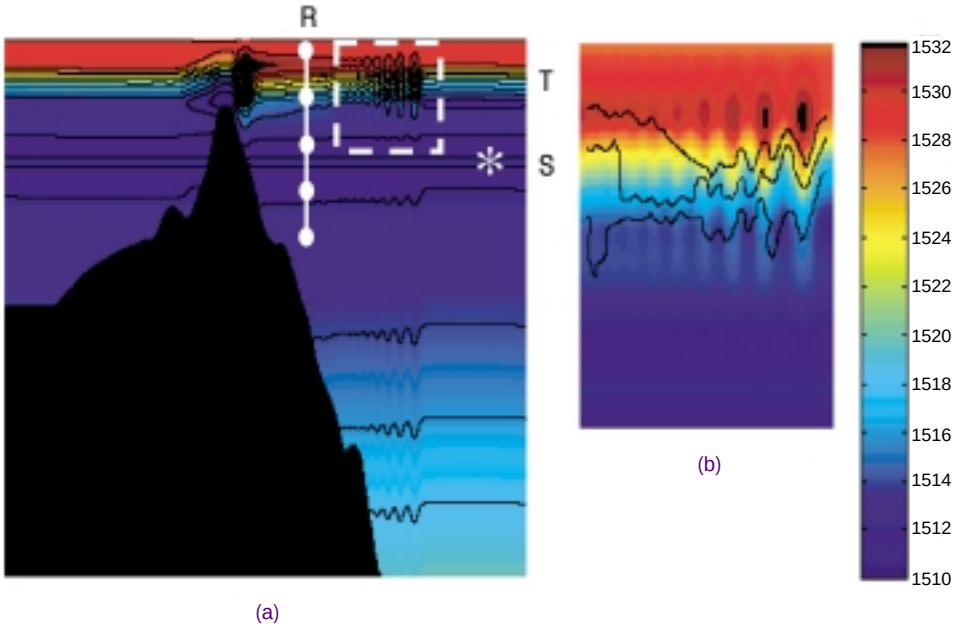

FIGURE 4
Figure 4(a) shows a computer simulation of a soliton packet as it is created by tidal flow over the Strait of Messina. A two-layer, weakly nonhydrostatic, primitive equation ocean model was used to generate the simulation. The ocean region contained in the broken line box is expanded and shown in Fig. 4(b) as color contours of sound speeds. The measured soliton sound speeds are overlayed in Fig. 4(b) as black contour lines. The color scale is given on the lower right-hand side in units of meters per seconds.

measured soliton fields produced different acoustic mode structures when calculated at the same vertical position (show in Fig. 4(a) as a vertical line array, labeled R). The acoustic mode structures were determined by performing Fourier transforms on the calculated complex pressures at R. Oceanographic parameter values used in the PEO model were adjusted until the differences in acoustic predictions were minimized. Thus, a feedback approach was used to dynamically couple the oceanographic and acoustic models.

Figure 5 is a flow chart detailing the logic used in applying this dynamic coupling of oceanographic and acoustic models. Figure 6 shows contour plots of simulated transmission loss (in decibels) for the acoustic wave field that was disturbed by the soliton packet. (The soliton packet was located near the surface at range 25 km). Acoustic field feedback adjustments were used in generating the soliton simulation used in Fig. 6(a). No acoustic field feedback adjustments were used in generating the soliton simulation used in Fig. 6(b). The soliton packet used in Fig. 6(c) came

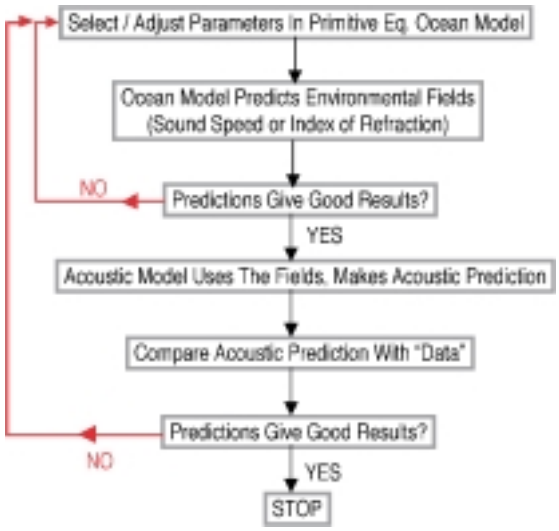

FIGURE 5
The approach that dynamically couples the primitive equation ocean model to the acoustic model. The approach may be viewed as using acoustic model simulations in a feedback loop to "fine tune" the results generated by the ocean model.

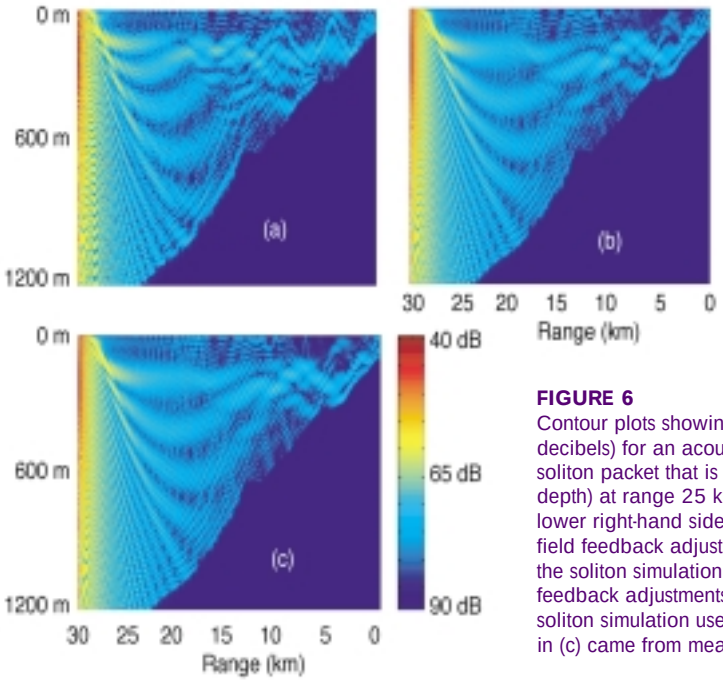

FIGURE 6
Contour plots showing the transmission loss (in decibels) for an acoustic wave field disturbed by a soliton packet that is located near the surface (zero depth) at range 25 km. The color scale is given on the lower right-hand side in units of decibels. No acoustic field feedback adjustments were used in generating the soliton simulation used in (a); acoustic field feedback adjustments were used in generating the soliton simulation used in (b); the soliton packet used in (c) came from measured data.

from measured data. The dynamically adjusted soliton simulation (used in Fig. 6(a)) gives a much better *acoustic* comparison to the acoustic fields generated with the actual soliton data (Fig. 6(c)).

Summary: Analysis of acoustic outputs can be used in a feedback loop to improve the fidelity of the output from a primitive equation ocean soliton model. This approach establishes a dynamic coupling between the oceanographic and acoustic models.

Examination of the acoustic and oceanographic fields in the vicinity of the soliton can provide limited insight for selection of ocean soliton parameters. However, the entire oceanographic field is needed, both in the vicinity of the soliton and throughout the water column, to obtain good coupling between the acoustic outputs and the critical parameters in the primitive equation ocean soliton model. A two-layer, weakly nonhydrostatic, primitive equation ocean soliton model may not be able to generate highly accurate soliton simulations when used as a standalone simulation model. However, using the dynamic coupling feedback method described here can extend the range of applicability of such a model.

[Sponsored by ONR]

References

[1] A.C. Warn-Varnas, S.A. Chin-Bing, D.B. King, S. Piacsek, and D. MacNaughton, "Modeling the Effects of Solitons on Acoustics," *Proceedings of the 1998 WHOI/IOS/ONR Internal Solitary Wave Workshop*, WHOI-99-07, Woods Hole Oceanographic Institute, Woods Hole, MA, 1999.

[2] S.A. Chin-Bing, D.B. King, R.A. Zingarelli, and A.C. Warn-Varnas, "A Search Algorithm for Resonance Anomalies (SARA)," *The 1999 NRL Review* (Naval Research Laboratory), 71-72, 1999.

Unifying Acoustic Boundary Scatter Modeling

R.C. Gauss, R.W. Nero, and D. Wurmser
Acoustics Division

Introduction: The increased importance of regional conflicts has focused Navy attention on littoral waters, with active sonars expected to provide crucial support to these operations. Major performance drivers of such systems are the acoustic interactions with the ocean boundaries and fish, whose strength and influence can vary greatly depending on the local oceanography, geology, and biology. Being able to determine the relative contributions of each scattering mechanism to the overall reverberation is very important for predicting and optimizing sonar performance. Because of their variety and dynamic nature, estimating the contributions of fish is particularly challenging. When fish are well separated from the sea surface or bottom, recognizable broadband acoustic signatures identifying their presence and strength have been observed. However, when fish are near the sea surface or bottom, as is common in littoral areas, these characteristic fish signatures can undergo significant modification.[1] Although several high-fidelity fish-scattering models exist, they neglect these important boundary-interference effects.

Fish Acoustics: At frequencies below 10 kHz, the primary scattering mechanism of most fish is their air-filled swimbladder, which typically occupies only about 5% of a fish's volume. The acoustic response depends on the bladder size, which in turn depends on the fish's size and its depth. Figure 7(a) illustrates how the frequency response of a particular fish, the salmon, changes with depth as its bladder compresses due to the increased water pressure at the deeper depths. For a layer of dispersed fish, their total scattering is simply the incoherent sum of scattering from the individuals, and so depends on their depths, sizes, and total number. (This free-field response is independent of the angle of ensonification.)

When a fish is near an ocean boundary, the scattering picture increases in complexity. In addition to backscattering from the rough interface itself, fish backscatter energy to a receiver along multiple paths (Fig. 7(b)). The relative time delay of these various paths generates a pattern of constructive and destructive interference, the intensity of which depends strongly on the surface grazing angle θ, the distance of the scatterer from the boundary, the acoustic frequency, and for the ocean bottom, its physical properties. This can significantly alter the fish's backscattered intensity (by a factor between 0 and 16).

Fish Near the Ocean Surface: Because the density of air is so small, the air-sea interface effectively reflects an incoming acoustic wave so that it is out of phase with the outgoing wave. The resultant interference pattern (Fig. 7(c)) modifies the free-field scattering response of the fish, leading to a rich variety of frequency and grazing-angle behaviors, especially at low angles. Figure 7(d) shows an example of this modification at $\theta = 10$ degrees for the salmon of Fig. 7(a). (Note the enhanced scale of Fig. 7(d).)

Figure 8 shows a real-world example of backscattering from salmon in the presence of the air-sea interface in the Gulf of Alaska. (Using the model, salmon depths were inferred to be 2 to 7 meters.)

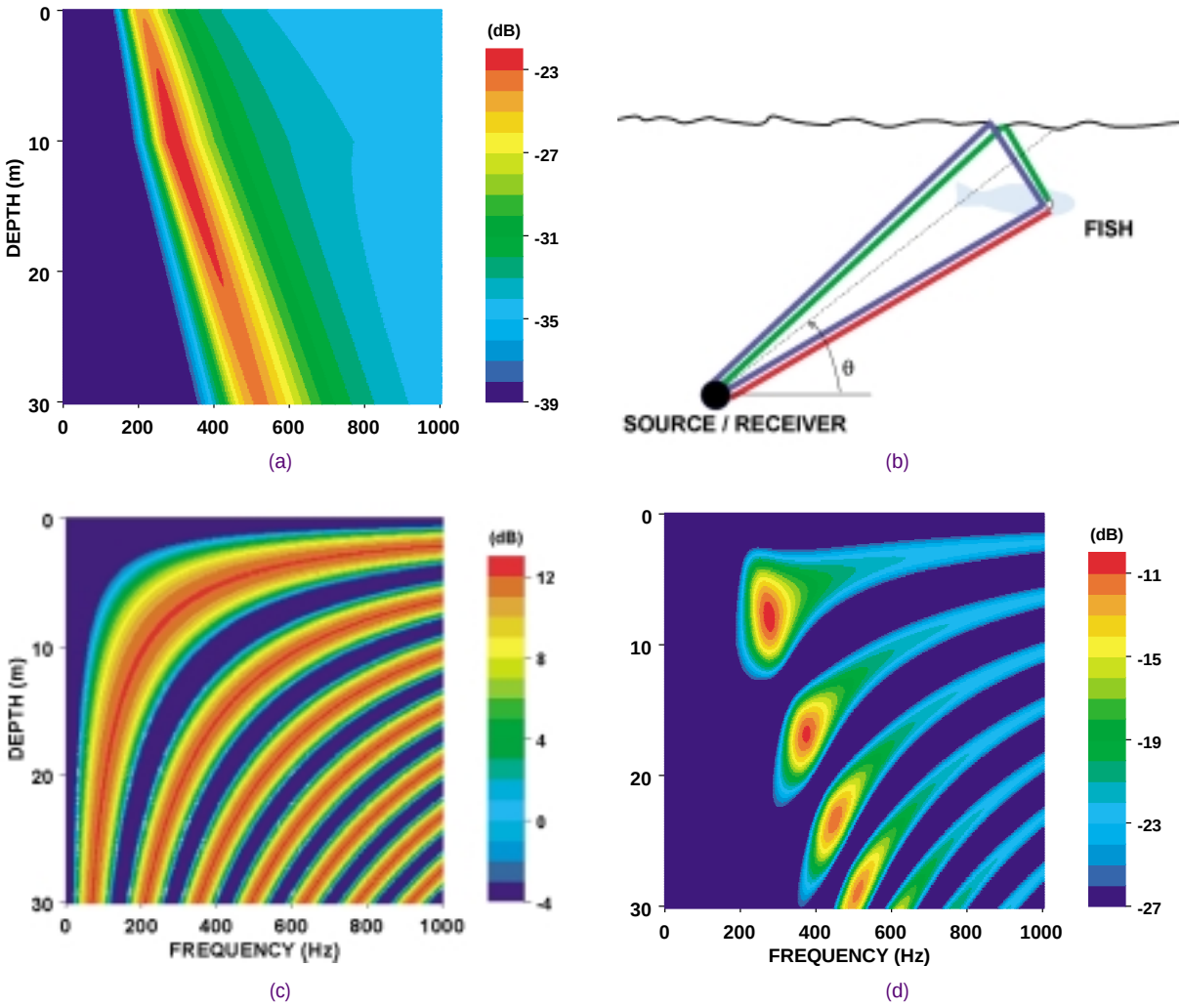

FIGURE 7
Near-surface fish scattering. (a) Free-field salmon scattering; (b) Near-boundary scattering paths; (c) Surface acoustic interference pattern; (d) Near-surface salmon scattering.

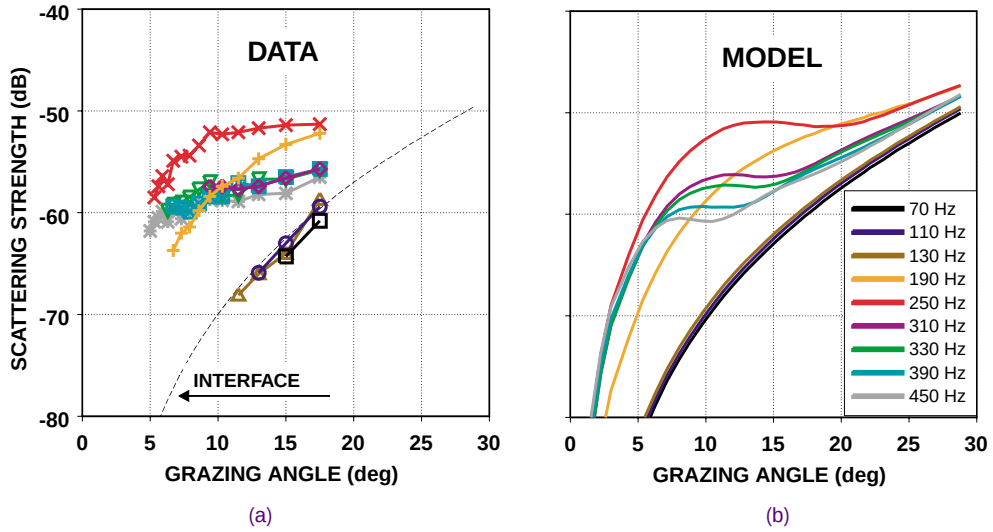

FIGURE 8
Data-model comparison for backscattering from salmon and the air-sea interface

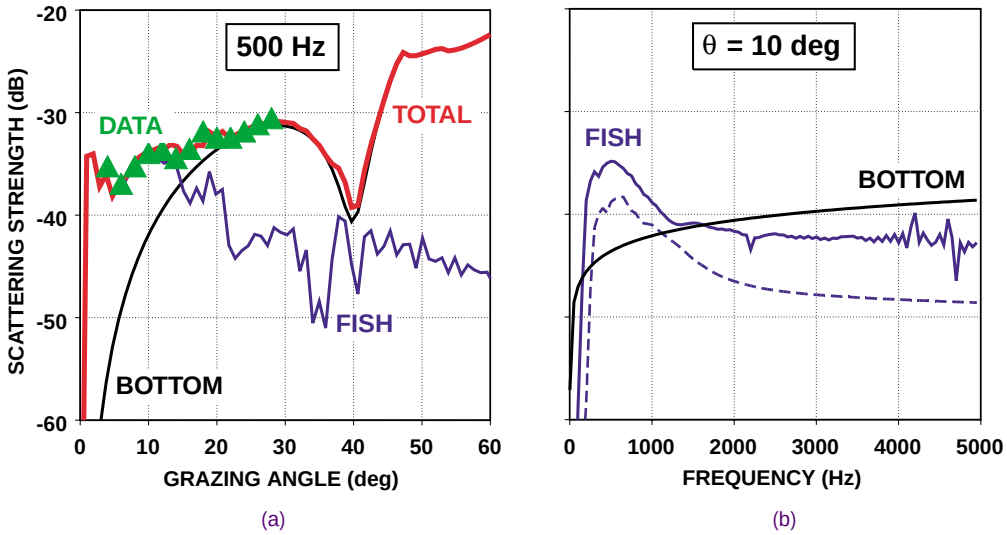

FIGURE 9
Backscattering from rockfish above a claystone bottom. (a) Modeled grazing-angle dependence compared with measured data; (b) Modeled frequency dependence, including (solid) and excluding (dashed) bottom-interference effects.

The (frequency-independent) contribution of the rough interface to the scattering is included in the modeling and is shown as a dashed line in Fig. 8(a). This figure shows that even at relatively low densities—a few hundred individuals per square kilometer during this measurement,[2] fish near resonance can dominate interface scattering at low grazing angles, e.g., in this case by a factor of 100 (20 dB).

Fish Near the Ocean Bottom: In contrast to the air-water interface, which effectively repels acoustic energy, the water-sediment interface has some rigidity and attracts acoustic energy. The result is that the proximity of the bottom has a milder influence on the free-field response of fish. In contrast to the sea-surface case, fish near the bottom are strongly ensonified. Hence, fish resting on the bottom not only can still be appreciable scatterers, but they can potentially be mistaken for bottom scattering.

As is the case for fish near the sea surface for most depths, the grazing-angle response for fish near the bottom is generally flat so that fish scattering is

primarily important at low scattering angles where the contribution of interface scattering typically drops off quickly. Figure 9(a) shows an example of backscattering from rockfish shoaling over a claystone bottom.[3] In this case, the low-angle scattering, which ordinarily would be attributed solely to bottom scattering, is in fact largely fish scattering. In general, the relative contributions of the scattering mechanisms can depend on a complex mix of factors. For example, Fig. 9(a) corresponds to the rockfish's resonance frequency. Off resonance (especially below), its target strength is reduced (Fig. 9(b)), so that at some angles and frequencies, fish scattering will dominate, and at other angles and frequencies, bottom scattering will dominate.

Significance: These new broadband scattering strength models will help advance the accuracy and robustness of predictions of sonar performance. By having a physics basis, the models allow extrapolation in frequency and to any 3-D scattering geometry. Moreover, they are essential for isolating scattering mechanisms and so advancing our understanding of the complex acoustic interaction processes at the ocean boundaries. In particular, the models have demonstrated not only that near-boundary fish can be significant scatterers at the low grazing angles of importance to sonar systems, but that scattering previously attributed to other mechanisms (ocean bubbles or sediment) may in some cases be due to fish. By being able to systematically identify and remove their contributions, this, in turn, has led to improved boundary scattering models.[1]

[Sponsored by ONR]

References

[1] R.C. Gauss, J.M. Fialkowski, D. Wurmser, and R.W. Nero, "New Broadband Models for Predicting Bistatic Surface and Volume Scattering Strengths," *Proceedings of the Environmentally Adaptive Sonar Technologies (EAST) Peer Review*, Office of Naval Research, Washington, DC (2000).

[2] R.W. Nero and M.E. Huster, "Low-Frequency Acoustic Imaging of Pacific Salmon on the High Seas," *Can. J. Fish. Aquat. Sci.* **53**, 2513-2523 (1996).

[3] E.L. Kunz and R.C. Gauss, "Bottom Backscattering Measured Off the Coast of Oregon During the Littoral Warfare Advanced Development 99-3 Experiment," NRL Memorandum Report 7140--00-8453, June 2000.

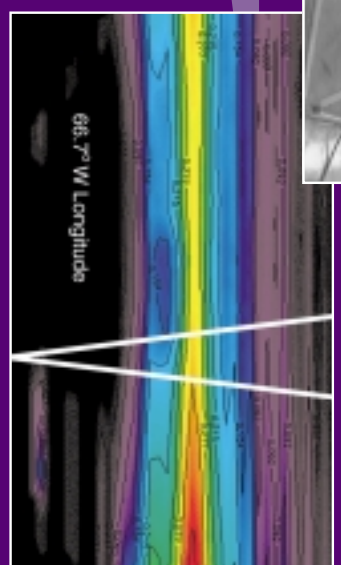

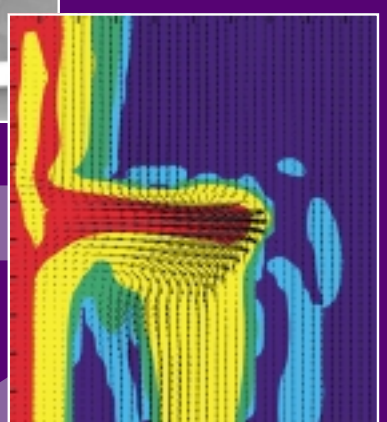

Atmospheric Science and Technology

Three-Dimensional, Tomographic Imaging of an Artificial Ionospheric Hole

P.A. Bernhardt,[1] C.A. Selcher,[2] and F.T. Djuth[3]
[1]*Plasma Physics Division*
[2]*Information Technology Division*
[3]*Geospace Corporation*

Introduction: Tomographic imaging of the ionosphere is a recently developed technique that uses integrated measurements and computer reconstructions to determine electron densities. The integral of electron density along vertical or oblique paths is obtained with radio transmissions from a low-Earth-orbiting (LEO) satellite transmitter to a linear array of receivers on Earth's surface. The reconstructed images using computerized ionospheric tomography (CIT) can be improved with additional data provided from ground-based sensors such as incoherent scatter radars (ISRs), which yield vertical profiles of electron density along a single line of sight.[1] CIT has previously been used to study the natural ionosphere, showing such features as high-latitude troughs, traveling ionospheric disturbances, and the equatorial "anomaly" consisting of a permanent trough near the magnetic equator. These features have typical scale sizes from 200 to 2000 km. Existing CIT chains of receivers can be found to extend over 1000s of kilometers in Europe, Asia, the U.S., and Russia.

The Naval Research Laboratory used CIT to diagnose an ionosphere that was artificially modified by the high-power transmitter located near Arecibo, Puerto Rico (18.476°N latitude, 66.666°W longitude). The experiments were carried out in January 1998. The Arecibo high-frequency (HF) facility transmitted a 3.175 MHz radio wave into a vertical beam with an effective radiated power of 80 MW. The cross section of the heater beam was elliptically shaped with a 7° by 14° antenna pattern. Nonlinear effects of the high-power radio waves have been known to produce large (~50 km) cavities in the ionosphere with density reductions on the order of 10 to 40%.[2] Several competing processes may produce the density cavities. The interactions of the powerful waves with the plasma elevate the plasma temperature from 800 K to above 2500 K. The hot electrons provide regions of enhanced plasma pressure, causing field-aligned transport out of the heated volume. The hot electrons also excite molecular nitrogen, which rapidly reacts with atomic oxygen ions to yield NO^+ ions. These ions recombine with electrons, leaving a large-scale electron density cavity. The cavity then acts like a large lens to focus the already powerful waves into an even more powerful beam. These processes dig out a large-scale hole in the plasma.

Experiment Description: To image the ionospheric cavities that have three-dimensional structures with scale sizes less than 100 km, it was necessary to deploy a two-dimensional array of receivers below the heated volume of the ionosphere. Figure 1 shows the locations of the CIT receivers on the island of Puerto Rico. Each receiver measured the integrated electron density by comparing the phase of 150 and 400 MHz transmissions from a TRANSIT satellite along the orbit shown by the solid line on the left in Fig. 1. The total electron content (TEC) accuracy with this measurement is typically one part in 1000. The receivers were organized into three north-south chains of three receivers each. The paths from the satellite to each linear array of receivers make a web in the plane containing the satellite orbit and the line of receivers. The electron densities were reconstructed in each of the three planes using an algebraic reconstruction technique (ART). In ART, the electron density image is broken up into pixels, and the TEC val-

FIGURE 1
Geometry for the ionospheric tomography experiment in Puerto Rico.

ues are written as the weighted sum of the electron density in each pixel where the weighting function is the length of a given path in the pixel. With this formulation, there is one equation for each TEC measurement. The resulting set of equations is solved numerically with algebraic iterations.[1]

The satellite-to-ground measurements contain no horizontal integration paths. Consequently, CIT is referred to as "limited angle" tomography and there is no unique reconstruction solution. From the measurements at Puerto Rico, the horizontal baseline for the receiver chains is only 80 km. With this short baseline, good horizontal resolution is obtained but very little information on the vertical structure of the ionosphere is contained in the observations. Fortunately, the Arecibo ISR can be used to provide a vertical profile through the ionosphere.

Transmissions at 3.175 MHz with effective radiated power of 80 MW were used to "heat" the ionosphere. The transmitter was operated continuously for greater than 30 minutes prior to each satellite pass to produce the maximum effects on the ionosphere. The Arecibo radar was pointed to the heated volume to provide electron density profiles during the experiments. Figure 2 illustrates the density profile during the time of the CIT measurements. The profile has a large "bight-out" produced by the ionospheric heater. A dashed line shows the profile without the effects of the high-power radio waves. The unmodified profile was included as an initial guess for the iterative solution.

After the experiment, the data from each CIT receiver were processed at NRL to produce images of the modified ionosphere (Fig. 3). The locations of the ionospheric intersection for each receiver chain are denoted by the diamond, plus, and triangle symbols in Fig. 1. Three slices through the ionosphere show density images where the ionosphere is (1) undisturbed outside the affected region, (2) slightly disturbed at the edge of the heater beam, and (3) strongly disturbed directly over the HF facility (Fig. 3). The western image at 67.3°W latitude shows almost no effects of the high-power radio waves. This is reasonable because this section of the ionosphere was about 30 km away from the cone of the heater beam. The image at 67.0°W latitude shows a localized effect of the HF beam centered about 25 km to the south of the main beam. The reconstructed image shows effects mainly on the bottomside of the layer. The ionospheric image at 66.7°W latitude shows the largest effects because it is obtained directly over the HF facility. In this case, there is a 50-km southward displacement of the maximum effects of the HF beam. The physical processes that can

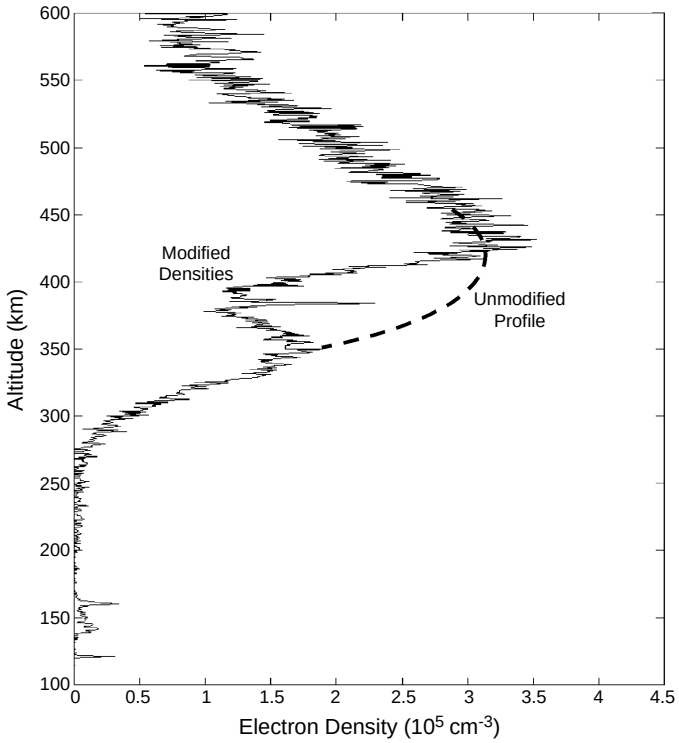

FIGURE 2
Electron density profile obtained from the Arecibo incoherent scatter radar, taken on 27 January 1998, 0337 UT.

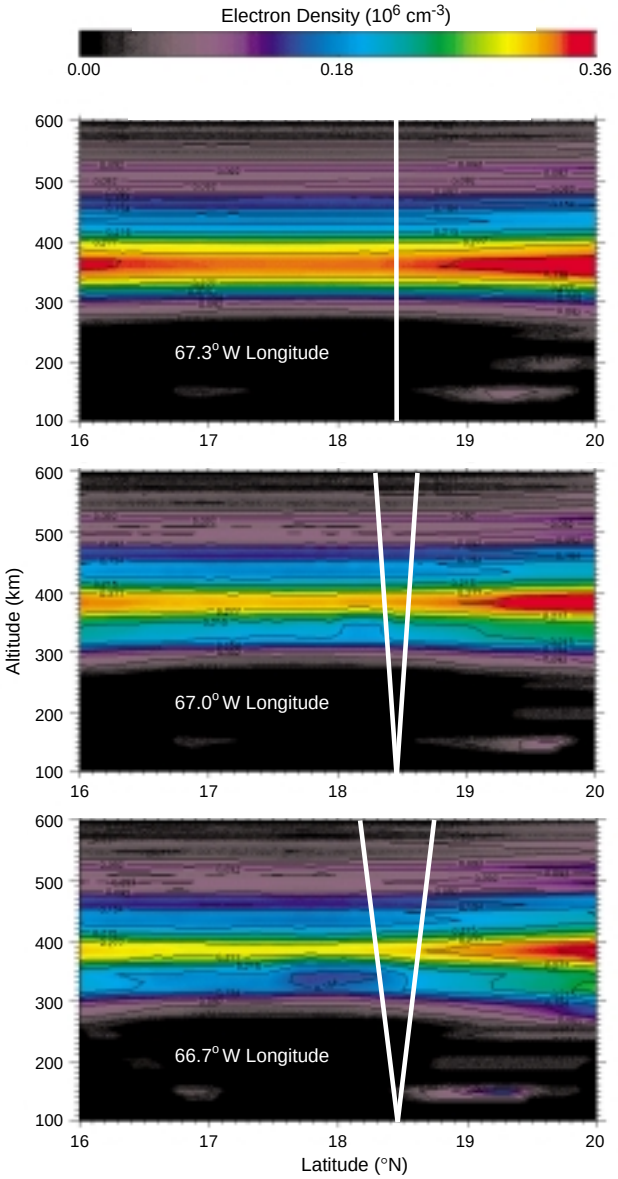

FIGURE 3
Reconstructed images of the modified ionosphere on 27 January 1998 at 0330 UT. The beam of high-power radio waves is outlined in white.

displace the heated volume to the south of the HF facility are under study.

Conclusions: Computerized ionospheric tomography has been shown to be a valuable tool to study electron density effects during ionospheric modification experiments. The experiments in Puerto Rico were performed on a campaign basis. Future applications of the technique will be used at the High Altitude Aurora Research Program (HAARP) facility under construction in Alaska. To continue these initial measurements as well as study the natural high-latitude ionosphere, The University of Alaska, North West Research Associates, the University of Texas as Austin, and the Naval Research Laboratory are deploying a permanent chain of CIT receivers along the meridian of the HAARP site.

New radio beacons for tomographic use are also being launched into orbit during the NRL Coherent Electromagnetic Radio Tomography (CERTO) program. Using support from the Air Force Space Test Program (STP), CERTO beacons have been flown on the ARGOS satellite in polar orbit and will be launched on the STRV-1d and PICOsat satellites in low inclination and 70-degree inclination orbits, respectively. These new radio tomographic systems will provide high-resolution, three-dimensional images of both the natural and modified ionosphere in the future.

[Sponsored by ONR]

References

[1] P.A. Bernhardt, C.A. Tepley, and L.M. Duncan, "Airglow Enhancements Associated with Plasma Cavities Formed During Ionospheric Heating Experiments," *J. Geophys. Res.* **94**, 9071-9092 (1989).

[2] P.A. Bernhardt, R.P. McCoy, K.F. Dymond, J.M. Picone, R.R. Meier, F. Kamalabadi, D.M. Cotton, S. Chakrabarti, T.A. Cook, J.S. Vickers, A.W. Stephan, L. Kersely, S.E. Pryse, I.K. Walker, C.N Mitchell, P.R. Straus, H. Na, C. Biswas, G.S. Bust, G.R. Kronschnabl, and T.D. Raymund, "Two-dimensional Mapping of the Plasma Density in the Upper Atmosphere with Computerized Ionospheric Tomography (CIT)," *Phys. Plas.* **5**, 2010-2021 (1998).

POAM III Observes Forest Fire Emissions in the Stratosphere

J. Hornstein,[1] K. Hoppel,[1] R. Bevilacqua,[1] E. Shettle,[1] M. Fromm,[2] J. Alfred,[2] B. Stocks,[3] Z. Li,[4] R. Servranckx,[5] and P. Wang[6]

[1]*Remote Sensing Division*
[2]*Computational Physics, Inc.*
[3]*Canadian Forest Service*
[4]*Canadian Centre for Remote Sensing*
[5]*Canadian Meteorological Centre*
[6]*University of Wisconsin*

Introduction: Every year huge tracts of forest in Alaska, northern Canada, Scandinavia, Russia, and China are racked by forest fires from May through October. Enormous quantities of smoke billow into the atmosphere, where high-altitude winds sometimes carry the smoke thousands of kilometers from the original fires.

Until data from NRL's Polar Ozone and Aerosol Measurement (POAM III) instrument proved otherwise,[1] no one believed that forest fire smoke could enter the stratosphere. This article describes how layers of forest fire smoke in the stratosphere were discovered, discusses how they may have entered the stratosphere, and sketches the discovery's implications.

POAM III: NRL's POAM III instrument[2] is carried by the SPOT-4 spacecraft, which is operated by the French Space Agency. As SPOT-4 orbits Earth, POAM III aims at the Sun and measures the changing attenuation of sunlight as SPOT's orbital motion causes the Sun to appear to rise and set behind Earth's atmosphere. By combining measurements from a variety of lines of sight through the atmosphere and for a variety of narrow slices in the near-ultraviolet, visible, and near-infrared portions of the spectrum, it is possible to deduce the vertical distribution of ozone, water vapor, nitrogen dioxide, and suspended particulates in the stratosphere and upper troposphere.

An instantaneous line of sight (Fig. 4) from POAM to the Sun samples a much longer path through the atmosphere than would a line of sight from an instrument that measures the atmosphere by looking down through it at the Earth's surface. As a result, POAM can detect trace chemicals, thin clouds, and aerosol layers that would be invisible to a downward-looking instrument. The viewing geometry also provides excellent vertical resolution—about 1 km. These two advantages were crucial in enabling the discovery of forest fire emissions in the stratosphere.

SPOT's orbit is such that POAM's measurements each day occur around a circle of latitude in each hemisphere, with about 14 measurement opportunities in each hemisphere every day. The two circles of latitude change slowly from week to week in a pattern that repeats every year. POAM's measurements in the Northern Hemisphere occur only between 55 and 72°N latitude.

POAM Sees Stratospheric Layers During the Summer of 1998: Figure 5 is an overview of POAM's observations of aerosols in the lower stratosphere during the Northern Hemisphere summer of 1998. The lower portion of the figure shows that in early and mid May 1998, POAM detected several brief intensifications of the aerosol in the lower stratosphere. The lower stratosphere then became rather

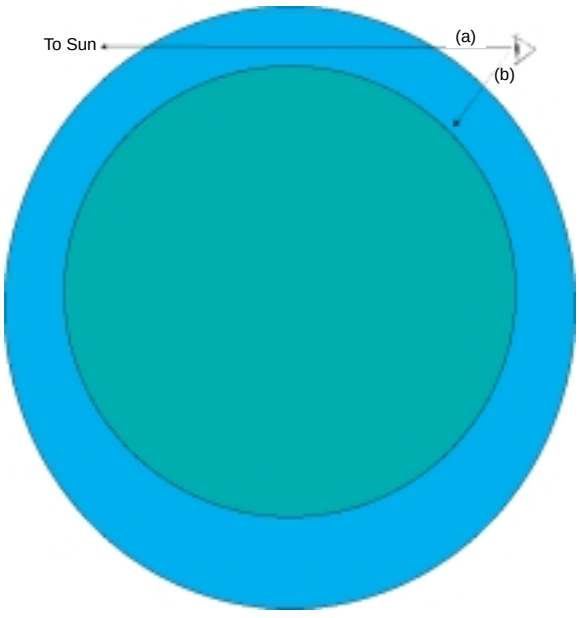

FIGURE 4
(a) POAM's measurement geometry. A downward-looking line of sight (b) samples a much shorter path through the atmosphere.

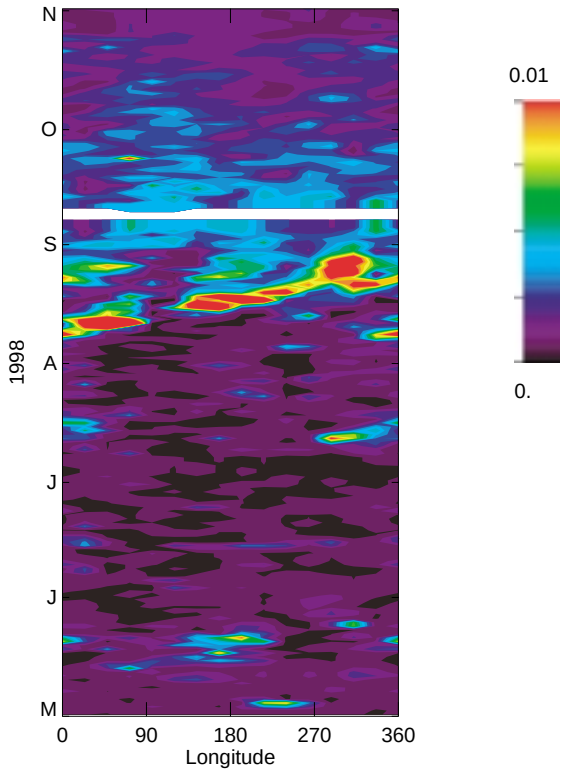

FIGURE 5
POAM III measurements of the aerosol optical depth at 1mm in a 5-km thick column whose base is 2 km above the tropopause, from May through October 1998. Horizontal white bar is a 5-day data gap.

clean, and remained so until July 9 when POAM detected a strong intensification spanning about 45° in longitude eastward of about 270°E, over Canada. The intensification slowly weakened as it moved eastward and then disappeared at about 40°E, over Russia. This first outburst was followed by another clean period, until early August, when a strong intensification occurred (the upper half of Fig. 5), soon spreading over all longitudes and lasting more than a month.

This article discusses the early to mid-July intensifications in detail and then points out the significant additional implications of the prolonged intensification in August and early September.

July 1998: The intensified aerosol seen by POAM during early to mid-July was also seen by the Stratospheric Aerosol and Gas Experiment (SAGE II), another space-based instrument that uses the same viewing geometry as POAM, and by a ground-based lidar[3] in Kiruna, Sweden.

Figure 6 shows the POAM, SAGE, and lidar measurements. The curves on the left of Fig. 6 are referred to the horizontal axis along the bottom of the plot and show the space-based measurements by POAM and SAGE. This axis shows the total attenuation of sunlight at a wavelength of 1 mm, in units of the attenuation caused by just the gas molecules in the atmosphere. Values greater than 1 indicate excess attenuation due to aerosol particles. The curve on the right of Fig. 6 shows the lidar data, referred to the horizontal axis along the top of the plot. This axis shows the strength of the atmospheric backscattering of the lidar beam in units of the backscatter due to gas molecules alone. Again, values greater than 1 are due to aerosols. Figure 6 shows that the aerosol intensifications were quite substantial relative to the background.

Horizontal bars in Fig. 6 indicate the tropopause, which is the boundary between the troposphere and the stratosphere. The aerosol layers are well above the tropopause, in the lower stratosphere.

The lidar also measures the change in polarization when atmospheric particles backscatter the lidar beam. The lidar found large changes in polarization, which means that the backscattering particles were not spherical, and hence must have been solid.

Except during the polar winter when polar stratospheric clouds may be present, intensifications of the stratospheric aerosol layer are usually ascribed to volcanoes. Indeed, on other occasions POAM and other space-based instruments using the same measurement geometry have seen layers that could be traced back to known volcanic eruptions. But in the present case in which wind fields provided by national meteorological services were used to trace back from the measurements shown in Fig. 6, there was no match to any known eruption.

All of the traced back air parcels did, however, traverse a region in northwest Canada between the Alaskan border and Great Bear Lake (in the Northwest Territories) at a time when particularly intense forest fires were raging there. The fires and their smoke were also observed by the spaceborne NOAA Advanced Very High resolution Radiometer (AVHRR) and Total Ozone Mapping Spectrometer (TOMS).

How Smoke Enters the Stratosphere: A mystery remained: how did the smoke overcome the buoyancy barrier to the entry of tropospheric air into the stratosphere?

Thunderstorms not only trigger forest fires, they can also be triggered by the wide-area heating produced by a large forest fire. Atmospheric soundings indicated that the air above the fires should be subject to strong vertical motions, and indeed AVHRR imagery showed several large thunderstorm complexes. The strong updrafts in the thunderstorms could bring smoky air up to the vicinity of the tropo-

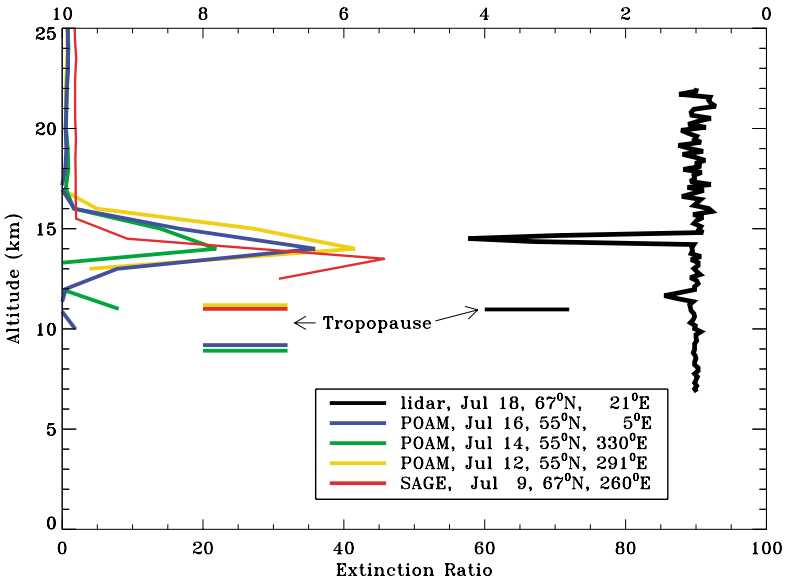

FIGURE 6
Vertical profiles of aerosol extinction and backscatter for selected locations and dates in 1998, ratioed to the corresponding values from atmospheric gas molecules alone.

pause. But the upflow hits a buoyancy ceiling when it strikes the tropopause and spreads out, forming an anvil-shaped cloud without necessarily injecting material into the stratosphere.

Satellite and other imagery show that in some thunderstorms a plume towers above the anvil, and that wakes resembling ship wakes sometimes form above the anvil. A detailed numerical model[4] of thunderstorms has recently explained these structures. Figure 7 shows output from the model for an actual thunderstorm (but not a storm associated with the July 1998 fires), with a plume extending well into the stratosphere above the anvil. Time sequences of such plots show that internal gravity waves form in and near the anvil, and that these waves sometimes break and cause material to irreversibly detach from the above-anvil towers and wakes instead of eventually subsiding back below the tropopause when the thunderstorm dissipates. In the future, the model will be applied to the storms associated with the July 1998 fires, but the results shown in Fig. 7 already make it likely that all of the missing links have been found in the mechanism for injecting forest fire smoke into the stratosphere.

Implications of the Stratospheric Smoke Layers of August 1998: The upper half of Fig. 5 shows that an unusually strong intensification of the lower stratospheric aerosol started in early August of 1998 and faded so slowly that traces of it could still be found in late October. The peak increase in the vertical optical depth of the lower stratosphere during August was more than three times the peak increase during July. The August-October intensification lasted so long that it encircled the globe at high latitudes.

Data from AVHRR, TOMS, and other sources indicated a large number of forest fires in Canada and Russia during this time. The strength and persistence of the August intensification appears to be the cumulative effect of multiple fires since, once injected into the stratosphere, smoke will remain there for a long time.

During the August-October event, the smoke would have reduced the average amount of 1-mm solar radiation reaching the ground at high latitudes by almost 0.3%. The decreases at shorter wavelengths would have been larger. Forest fire seasons like that of August 1998 might therefore affect climate.

A long-standing issue in atmospheric science is the origin of that part of the stratospheric aerosol layer that remains after the effect of any sporadic giant volcanic eruption has died away. The August-October 1998 layers suggest that, during certain seasons of certain years, some of the aerosol at high latitudes is due to the cumulative effect of large forest fires.

Smoke from the August-October 1998 fires would have reduced the horizontal visibility experienced by pilots or electro-optical systems flying at the altitude of the smoke, or satellites looking horizontally through the smoke. Typical reductions would

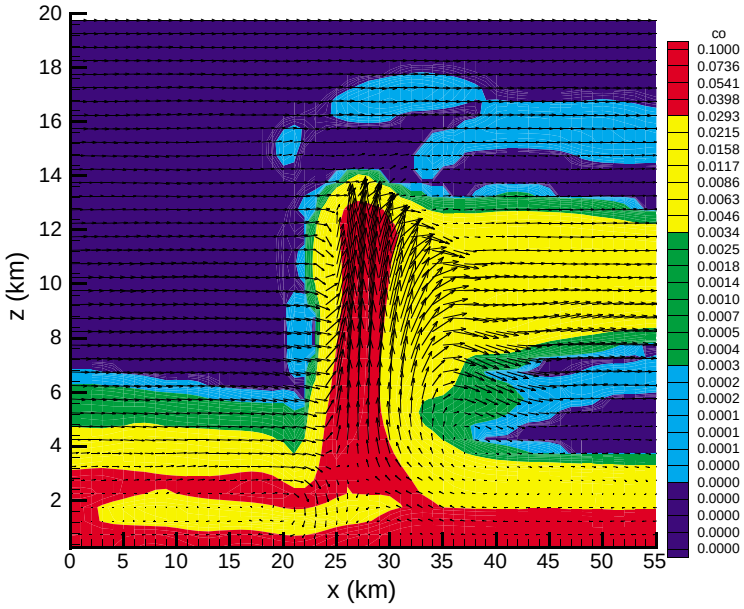

FIGURE 7
Numerical model of the concentration of an inert tracer 64 minutes after the beginning of the CCOPE thunderstorm on August 2, 1981. The original concentration of the tracer was 1% in the lowest kilometer.

have been 15% at 1 mm, with larger reductions at shorter wavelengths and at the smokiest times.

Summary: Large forest fires produce enormous quantities of smoke, but until data from NRL's POAM III instrument proved otherwise, no one believed that emissions from forest fires enter the stratosphere. Based on satellite imagery, the POAM group fingered intense thunderstorms as the likely mechanism for pushing forest fire emissions into the stratosphere. Subsequently, University of Wisconsin modeling and satellite observations of large thunderstorms provided strong support for this hypothesis. Once inside the stratosphere, forest fire emissions would be expected to remain aloft for a long time and the POAM observations bear this out. The POAM results indicate that some stratospheric layers that have previously been ascribed in the literature to unreported volcanic eruptions were actually due to large forest fires. Climate influences the frequency of large forest fires, and conversely, stratospheric layers due to forest fires may influence the temperature of the surface and lower atmosphere, so future climate models may have to take these feedbacks into account. Smoke from forest fires can reduce the horizontal visibility in the lower stratosphere.

[Sponsored by ONR]

References

[1]M. Fromm, J. Alfred, K. Hoppel, J. Hornstein, R. Bevilacqua, E. Shettle, R. Servranckx, Z. Li, and B. Stocks, "Observations of Boreal Forest Fire Smoke in the Stratosphere by POAM III, SAGE II, and Lidar in 1998," *Geophys. Res. Lett.* **27**, 1407-1410 (2000).

[2]R.L. Lucke, D.R. Korwan, R.M. Bevilacqua, J.S. Hornstein, E.P. Shettle, D.T. Chen, M. Daehler, M.D. Fromm, D. Debrestian, B. Neff, M. Squire, G. Konig-Langlo, and J.Davies, "The Polar Ozone and Aerosol Measurement (POAM) III Instrument and Early Validation Results," *J. Geophys. Res.* **104**, 18785-1879 (1999).

[3]J. Siebert, C. Timmis, G. Vaughan, and K. Fricke, "A Strange Cloud in the Arctic Summer 1998 Above Esrange (68N), Sweden," *Annales Geophysicae* **18**, 505-509 (2000).

[4]P.K. Wang, "Anvil Top Plumes – A Newly Discovered Transport Process of Stratospheric-Tropospheric Change," Talk A61A-08, Spring Meeting of the American Geophysical Union, May 30-June 3, 2000.

Chamber Studies of Processes Governing Atmospheric Aerosols

P. Caffrey,[1] J. Fitzgerald,[1] G. Frick,[1]
L. Pasternack,[2] and W. Hoppel[3]
[1]*Remote Sensing Division*
[2]*Chemistry Division*
[3]*Current affiliation: Computational Physics, Inc.*

Introduction: Interest in understanding the nature and effects of atmospheric particles has increased greatly over the last decade. Atmospheric aerosols, both natural and anthropogenic, scatter and absorb radiation. They, therefore, have a direct effect on global climate, the performance of military electro-optical (EO) systems, atmospheric visibility, and the accuracy of remote sensing measurements. Their effect on radiative transport, both directly (absorption, scattering) and indirectly (through changes in cloud reflectivity), represent the largest uncertainty in global climate change models. Additionally, extinction caused by aerosols and clouds is the primary cause

for performance degradation of EO systems used by DoD for surveillance, target detection, guidance and control. Many remotely sensed parameters (for example, sea-surface temperature) require significant corrections for aerosol scattering and extinction.

Whether produced either directly (injection from sea spray, wind-driven dust resuspension, etc.) or indirectly (formation from atmospheric gas-phase reaction products), atmospheric particles and their effects on the above systems depend on both individual and bulk particle properties (size, composition). Therefore, it is necessary to understand the processes governing the production, transformation, and transport of aerosols. Because it is virtually impossible to isolate and study these individual processes in the atmosphere, NRL scientists initiated and conducted a series of experiments in an environmental chamber. These experiments focused on aerosol processes relevant to the marine boundary layer (MBL), studying aerosol processing by clouds, formation and growth of new particles from organic gas-phase reaction products, and gas-particle reactions of SO_2 with humidified sea salt particles.

Under sponsorship of the National Oceanographic Partnership Program (NOPP), six weeks of collaborative experiments with scientists from six institutions were carried out in the Calspan Corporation (Buffalo, New York) 600-m^3 environmental chamber (Fig. 8). This chamber offers a unique capability in that it can function not only as a photolysis chamber, but also as a giant expansion cloud chamber, and is large enough to support the number of investigators required. Results from two of the six studies submitted for publication to date are summarized here.

Cloud Processing Results: Measurements in the 1980s made by NRL researchers[1] showed that the size distribution of submicron-size aerosols in the MBL was almost always bi-modal, with peaks at ~0.06 μm and 0.15 μm radius. NRL scientists proposed (now generally accepted) that this double-peaked feature is a result of cloud processing of aerosols. During cloud processing, a portion of the aerosol population serves as seed nuclei for cloud droplet formation. The cloud droplets then act as small chemical factories, converting soluble trace gases (such as SO_2, NO_x, etc.) into involatile material (sulfates, nitrates, etc.), which remains as increased particle mass upon evaporation of the cloud droplet. (On average, an aerosol particle is cycled through 10 non-precipitating clouds before it is removed by precipitation scavenging.) This mechanism is the most powerful transformation mechanism for moving particles from a size range too small to scatter visible light to a size where they become optically active. Since marine aerosols are known to contain a large amount of sulfate not naturally present in sea salt, the in-cloud conversion of SO_2 to sulfate by both H_2O_2 or

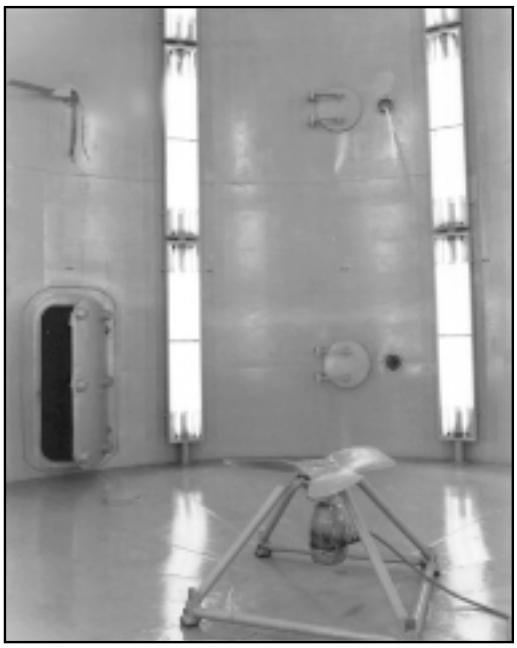

FIGURE 8
The Calspan Corporation 600-m^3 environmental chamber.

O_3 (with and without the presence of added NH_3) was of particular interest. Figure 9 shows a typical result when SO_2 was present at 2 ppb and the H_2O_2 concentration was 5 ppb. The solid line on the left is the (dry) particle size distribution prior to cloud processing, and the dashed line is the (dry) size distribution after cloud processing. The size distribution on the right, peaking at about 7 µm, is the cloud droplet distribution during the cloud portion of the cycle. The particles that acted as cloud condensation nuclei increased in radius from about 0.014 µm to about 0.08 µm, an increase in mass (volume) of about 125 times during a single cloud cycle. The double-peaked size distribution produced in the chamber looks much like those observed in the MBL, and the results give a very sensitive measure of the rate constants for liquid-phase conversion of SO_2 to sulfate by O_3 and H_2O_2. These rate constants can now be used in NRL aerosol models.

Nucleation Results: New particle formation (nucleation) in the atmosphere is initiated by the condensation of gases with very low vapor pressures. Typically, nucleation events are attributed to increases in gas-phase sulfuric acid formed from the gas-phase oxidation of SO_2. However, recent observations suggest that low-volatility organic acid vapors, produced from naturally occurring terpenes and pinenes reacting with O_3, may also be involved.

Figure 10 shows the evolution of the size distribution during an experiment in which 115 ppb of ozone was added to 20 ppb of alpha-pinene. A surprisingly large nucleation event was observed in which more than 54,000 particles cm^{-3} were formed in

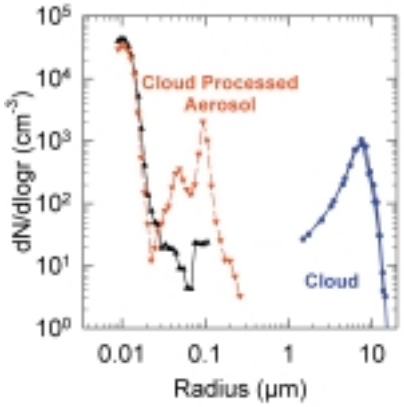

FIGURE 9
Measured size distributions before and after cloud processing are shown by solid and dashed lines. Cloud droplet spectra during cloud are shown by curve on right.

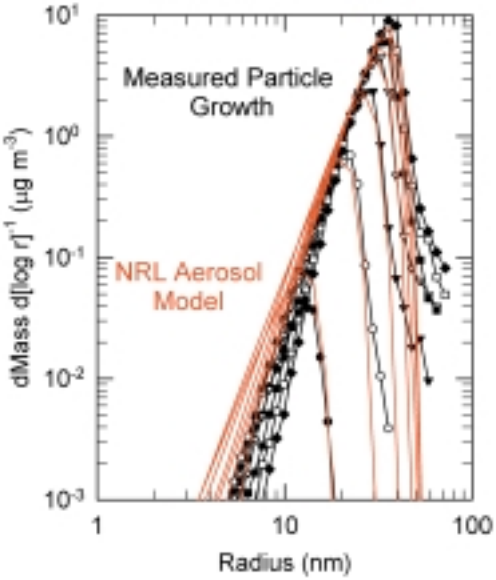

FIGURE 10
Evolution of the aerosol mass distribution vs radius during a nucleation event caused by ozonolysis of a-pinene. Black lines are measurements; red lines are modeling results.

about 15 minutes and grew to a radius of about 0.03 m before depleting the alpha-pinene. By modeling the nucleation and growth with the NRL microphysical aerosol model, it was determined that the condensing product was produced with a yield of about 5% and had a vapor pressure less than 0.01 ppb (7.6×10^{-9} torr) . This is much lower than the vapor pressure of known reaction products. This study has provided the first direct evidence that alpha-pinene, a common, volatile, naturally occurring organic compound, is involved in new particle formation in the atmosphere.

[Sponsored by NOPP]

References

[1] W.A. Hoppel, G.M. Frick, and R.E. Larson, "Effect of Nonprecipitating Clouds on the Aerosol Size Distribution in the Marine Boundary Layer," *J. Geophys. Res. Ltrs.* **13**, 125-128 (1986).

[2] J.W. Fitzgerald, W.A. Hoppel, and F. Gelbard, "A One-Dimensional Sectional Model to Simulate Multicomponent Aerosol Dynamics in the Marine Boundary Layer, 1, Model Description. *J. Geophys. Res. Ltrs.* **103,** 16085-16102 (1998).

Mountain Waves Over the Alps

J.D. Doyle,[1] A. Broad,[2] D.C. Fritts,[3]
G.S. Poulos,[3] R.B. Smith,[4] and H. Volkert[5]
[1]*Marine Meteorology Division*
[2]*The Meteorological Office*
[3]*Colorado Research Associates*
[4]*Yale University*
[5]*Institute für Physik der Atmosphäre, DLR*

Introduction: When stable air is forced to rise over a mountain, energy is radiated away from the barrier by internal gravity waves, or more specifically, mountain waves. Mountain waves may propagate vertically to high altitudes in the atmosphere, amplify (in part due to the decease of density with altitude), and subsequently overturn and break, somewhat analogous to shoaling ocean waves. Mountain wave breaking is known to play a crucial role in several aspects of atmospheric science, including the large-scale momentum budget, downslope windstorms, clear-air turbulence, and vertical mixing of trace constituents. Gravity wave theory has been extensively investigated in the past half century and continues to be one of the cornerstones of atmospheric dynamics. Recent progress with a new generation of numerical models, such as NRL's Coupled Ocean/Atmosphere Mesoscale Prediction System (COAMPS),[1,2] has rapidly advanced beyond our ability to fully evaluate these simulations from observational and theoretical perspectives.

Mesoscale Alpine Programme: The objectives of the Mesoscale Alpine Programme (MAP) include improving our understanding of mountain wave breaking and evaluating high-resolution numerical models over complex topography such as the Alps. The Alps are an isolated mountain range, 800 km in length, 200 to 300 km in width, and containing numerous peaks 3 to 5 km in height. Nearly every type of known atmospheric orographic phenomenon occurs in the Alps; not surprisingly, these mountains have an important influence on the weather of Europe. During the MAP observing period (fall 1999), mesoscale models such as COAMPS were used in real time to guide research aircraft missions to observe mountain wave breaking events above the Alps. Three aircraft were predominantly used to observe the mountain wave breaking: the National Science Foundation's Electra featuring a Scanning Aerosol Backscatter Lidar (SABL), the United Kingdom Meteorological Office's C-130, and the Deutsches Zentrum fur Luft and Raumfahrt Falcon, which had Differential Absorption Lidar (DIAL) onboard.

Observations and Simulations of Mountain Waves: Preliminary results from MAP highlight several emerging scientific issues that are important for the understanding and prediction of mountain wave breaking. Classical mountain wave theory has been established for simple orographic flows with free slip lower boundary conditions. However, in nature, MAP observations indicate that the boundary layer adjacent to the Earth's surface has a profound influence on the gravity wave response. Frequently during MAP, stagnant cold air in the low levels was entrenched upstream of the topography and within mountain valleys. In these situations, only mountain peaks extending into the strong flow above the stagnant region generated mountain waves. One dramatic example occurred when the three aircraft observed southwesterly flow over Mont Blanc, the highest peak in the Alps. The backscatter from the DIAL Lidar (Fig. 11) indicates mountain waves in the lee of Mont Blanc and very little wave activity downstream over the smaller peaks enshrouded in the stagnant air, which extended from the surface to 3 km. Vertically propagating mountain waves are discernible in the backscatter from cirrus clouds. Superimposed on the DIAL backscatter are high-resolution COAMPS-simulated isentropes, which are a surrogate for parcel trajectories in steady, adiabatic conditions. The simu-

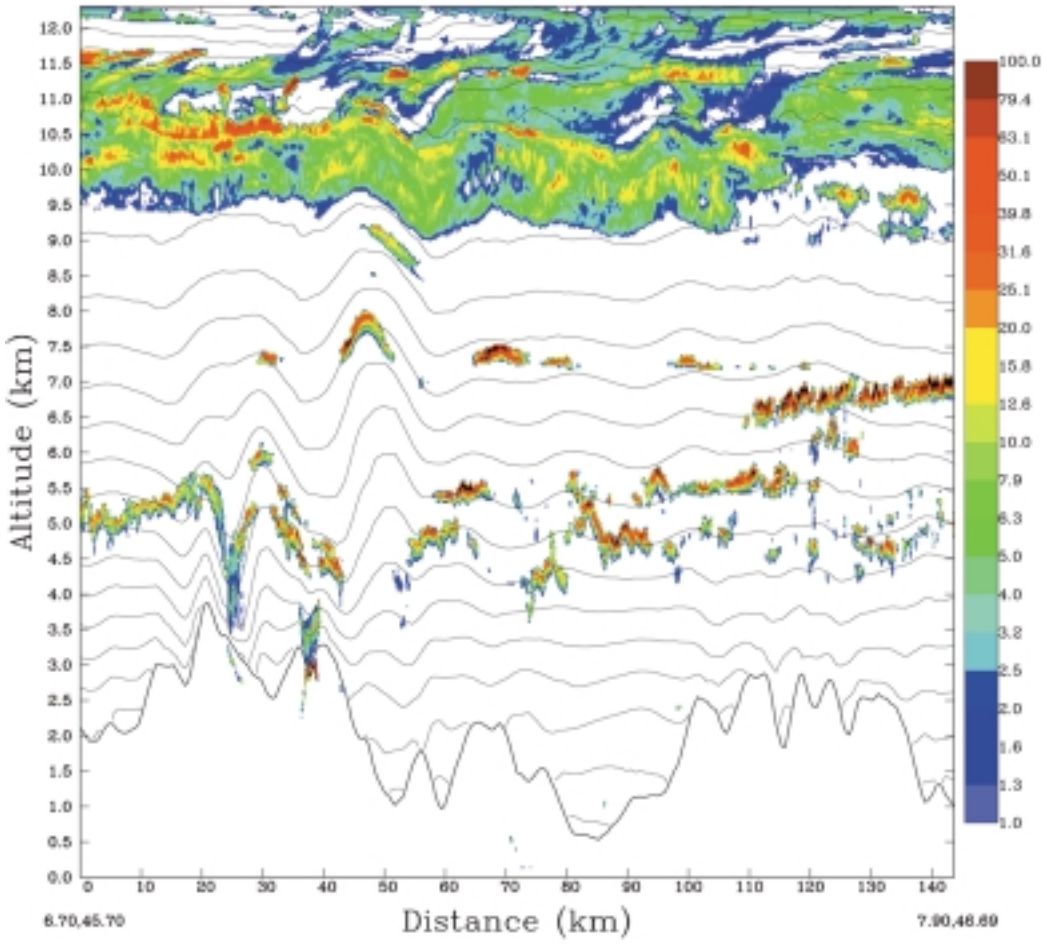

FIGURE 11
Simulated and observed mountain wave event over Mont Blanc on 2 November 1999. DIAL Lidar backscatter (color shading) and isentropes (contours) from a COAMPS simulation using a 1-km horizontal grid increment; the mean flow is from the southwest (left to right).

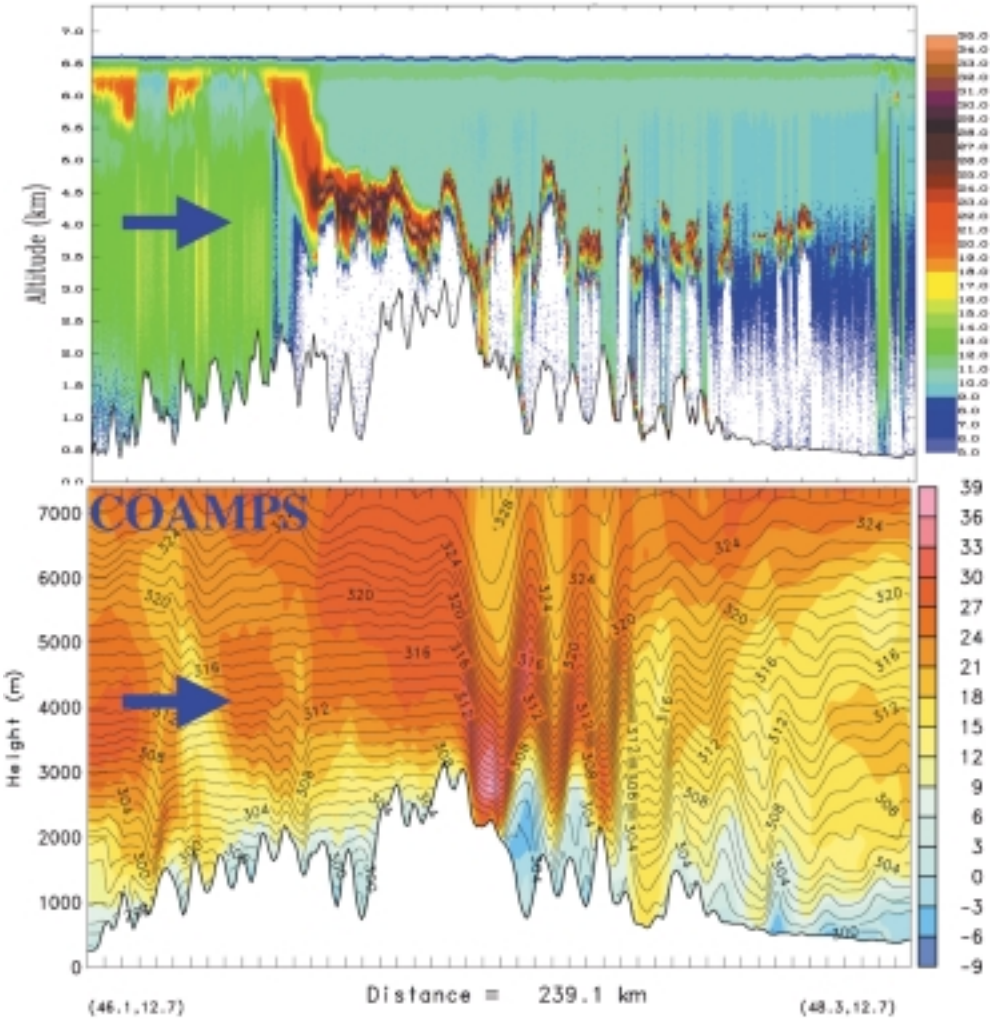

FIGURE 12
Simulated and observed mountain wave event over the eastern Alps on 20 September 1999. Top panel shows SABL Lidar backscatter (color shading); bottom panel shows isentropes (contours) and wind speed (m s^{-1}) from a COAMPS simulation using a 1-km horizontal grid increment. Mean flow is from the south (left to right).

lated wave structures, such as the Mont Blanc lee wave, are in remarkable agreement with DIAL backscatter.

Observations from MAP indicated the frequent presence of trapped waves, which were often not forecast by the real-time numerical models. One example occurred during southerly flow over the eastern Austrian Alps, for which the models predicted vertical mountain wave propagation. Measurements from the Electra indicated the existence of a train of quasi-periodic waves in the low levels, as apparent in the SABL backscatter (Fig. 12). The COAMPS simulated isentropes and winds, using a 1-km grid increment that was of higher resolution than that available in real time, are in reasonable agreement with the SABL backscatter (Fig. 12). These results highlight the importance of resolving the nonlinear processes that transfer energy from vertically propagating modes to trapped lee waves and the upstream stable air limiting mountain wave generation.

Summary: Preliminary results from MAP suggest that, in some cases, the mountain wave response in nature departs significantly from classical results and underscores the importance of boundary layer, nonlinear, and diabatic processes. To accurately predict the evolution of mountain waves and upper-level turbulence, local terrain features and nonlinear energy transport must be resolved, which requires fine resolution (<2 km). Next-generation techniques to represent mountain wave processes in large-scale models will undoubtedly need to consider these complexities. The data collected during MAP will provide valuable insight into the dynamics of mountain waves and the evaluation of sophisticated mesoscale numerical models such as COAMPS.

[Sponsored by ONR (for NLR's portion of research)]

References

[1] R.M. Hodur, "The Naval Research Laboratory's Coupled Ocean/Atmosphere Mesoscale Prediction System (COAMPS)," *Mon. Wea. Rev.* **125**, 1414-1430 (1997).

[2] J.D. Doyle, D.R. Durran, B.A. Colle, C. Chen, M. Georgelin, V. Grubisic, W.R. Hsu, C.Y. Huang, D. Landau, Y.L. Lin, G.S. Poulos, W.Y. Sun, D.B. Weber, M.G. Wurtele, and M. Xue, "An Intercomparison of Model Predicted Wave Breaking for the 11 January 1972 Boulder Windstorm," *Mon. Wea. Rev.* **128**, 901-914 (1999).

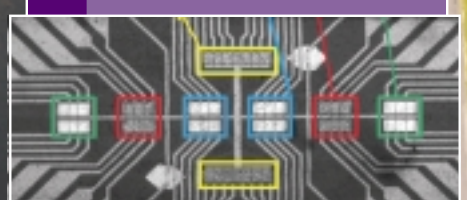

Chemical/Biochemical Research

The Search for Unexploded Ordnance

J.R. Deschamps
Laboratory for Structure of Matter

A.W. Kusterbeck
Center for Bio/Molecular Science and Engineering

Introduction: The Navy and other military organizations have instituted programs to remediate Formerly Used Defense Sites (FUDS). Often this means removing unexploded ordnance (UXO) from a site that was used for training, or was contaminated due to the sinking of a ship, or the unintentional destruction of storage or manufacturing facilities. Navy sites may be partially or completely under water. At any of these sites, UXOs need to be located and either removed or rendered harmless.

With current technologies, UXOs are located based on imaging (such as sonar) or metal content (magnetometers). These methods are very good at finding objects, but they cannot distinguish between UXOs and harmless debris. An explosive ordnance disposal technician makes this distinction by manually investigating each target. This process is dangerous, time-consuming, and expensive. Cleanup and site remediation would be greatly facilitated if an accurate means could be developed to identify those objects that contain explosives.

A major goal of the Chemical Sensing in the Marine Environment program (CSME) has been the development of novel means to detect and locate UXOs in marine environments. Research involves detection of very low concentrations of explosive residue, sampling strategies for data collection, and data analysis to locate the source of the explosive residue. Technologies developed in this program have several uses. Monitoring environmental remediation of explosive contaminants may be used to support the Navy's Mobile Underwater Debris Survey System and may be applied to monitoring manufacturing process streams.

CSME Strategy: A primary obstacle in developing strategies for UXO location in the marine environment is that no currently available chemical technique is capable of directly detecting trace explosive residues in seawater. Early efforts to measure low concentrations (i.e., high parts-per-billion (ppb) range) of explosives in seawater suffered from problems with sample handling and stability. Passivating the sample bottles and adding a preservative eventually solved these problems. This was not the final solution. A more realistic estimate for concentration of explosives leaching from a UXO is in the low ppb to high parts-per-trillion (ppt) range. As a result of a multidisciplinary effort involving NRL, other government laboratories, and several universities and private businesses, an effective technique for concentrating explosive residue contained in 100 liters of seawater by 5000-fold was developed. This method allowed measurement of the trace concentrations of explosives expected from UXOs. Various sources of explosive residue were then characterized to determine the actual concentration of explosives leaching from these targets in seawater, and the time course of the leaching. Based on these experiments, it was concluded that explosive residues leaching from UXOs could be used to locate UXOs.

Later work examined the characteristics of the plume resulting from chemicals released in the water. A typical plume was previously thought to have a Gaussian cross-section (Fig. 1, (A)). Although a Gaussian shape is a fair representation of the average behavior of a plume, the actual cross section is more complex (Fig. 1, (B) and (C)). There is some evidence that the extra information contained in these real cross sections is used by organisms trying to locate food or a mate. Thus, sensors with a rapid response time may allow this extra information to be used in locating UXOs based on their chemical plume.

The NRL Flow Biosensor: The Naval Research Laboratory has worked for many years to develop biosensors capable of detecting explosives. By using antibodies in a displacement assay to recognize an explosive and fluorescence to signal recognition, a fieldable sensor for detecting low concentrations of explosives in groundwater was developed. The first-generation biosensor (Fig. 2) was used in field trials to monitor groundwater contamination at military installations.[1,2] As with other chemical sensors, this sensor could not measure trace levels of explosive residue in seawater. Therefore, a program to improve the sensing element was initiated. Using the CSME data as a guide, improvements in the assay protocol and sensor format were made. These resulted in the ability to directly detect low concentrations of explosive residue in 90% seawater. In support of the CSME program, a second-generation biosensor is being miniaturized for deployment in the ocean. The prototype biosensor will be a stand-alone instrument that measures up to six chemicals simultaneously in seconds and can be operated at depths up to 100 meters.

Deployment of a Chemical Sensor: A number of methods can be used to deploy chemical sensors for locating the source of a chemical plume in the marine environment. These typically consist of

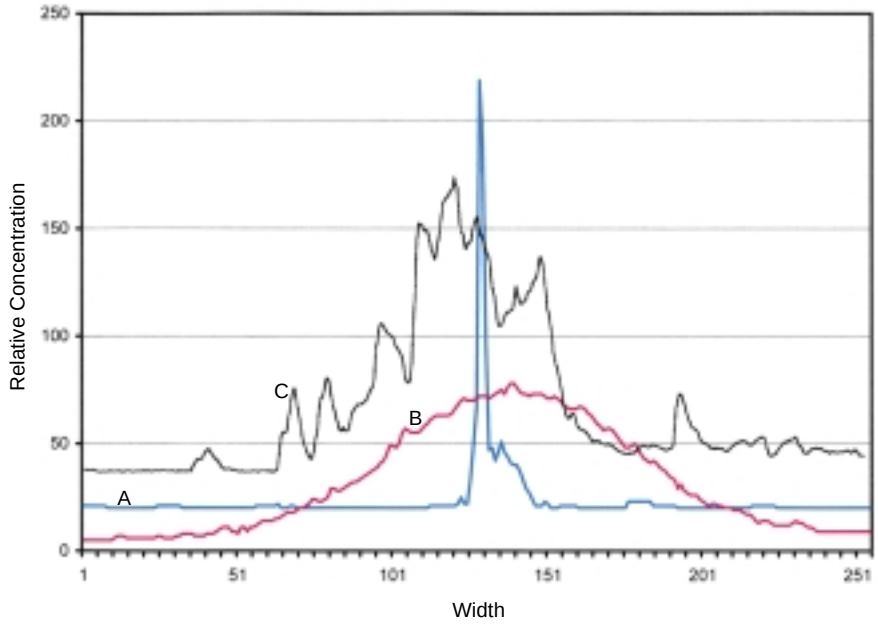

FIGURE 1
Plume cross-sections (off-set vertically for clarity): blue - time averaged showing typical Gaussian profile (A); magenta - instantaneous cross-section, part of series averaged to produce profile A (B); black - marine plume recorded during ONR-sponsored field test (C). [Cross section generated from data supplied by J. Crimaldi, M. Wiley, and J. Koseff (Stanford University).]

FIGURE 2
Setup for field operation of current-generation NRL flow biosensor. To assay for explosives and measure concentrations, samples are injected into the instrument and moved by a fluid stream to immobilized antibodies. Any increase in fluorescence is observed within minutes and stored on the computer for later data analysis.

FIGURE 3
AUV (REMUS) used in plume-mapping experiments. Sensing elements are contained in the white nose cone, a current profiler is in the green section, and vehicle controls and batteries are in the central yellow section. The inset shows the AUV while deployed in a plume mapping experiment. [Images courtesy of SPAWAR.]

towed systems or diver-deployed systems. A recent development in experiments aimed at mapping and tracking plumes has been the use of autonomous underwater vehicles (AUVs) for data collection (Fig. 3). Using an AUV, all data required for locating the source of a chemical plume can be rapidly collected from a single platform. The miniaturized flow biosensor can be deployed on such a platform.

Future Plans: Through continued improvements in the sensing element, it is expected that the biosensor will have sufficient sensitivity to directly detect plumes from UXOs in the marine environment. Over the next one to two years, NRL will be field testing the next-generation biosensor and working to integrate the sensor into an AUV. This combination will provide the desired novel means of detecting UXOs and will remove the Navy diver from the location and identification phases in any cleanup effort.

Acknowledgments: Research described in this report was supported by the Office of Naval Research

and represents the results of a collaboration among NRL, NSWC-CSS, SPAWAR, NAVEODTECH, ORNL, CRREL, Sandia, Areté Associates, Thorleaf Research, Stanford University of California at Berkley, and Rutgers University.

[Sponsored by ONR]

References

[1] P.T. Charles, P.R. Gauger, C.H. Patterson, Jr., and A.W. Kusterbeck, "On-Site Immunoanalysis of Nitrate and Nitroaromatic Compounds in Groundwater," *Envir. Sci. Tech.* **34**(21), 4641-4650 (2000).

[2] U. Narang, P.R. Gauger, A.W. Kusterbeck, and F.S. Ligler, "Multianalyte Detection Using a Capillary-based Flow Immunosensor," *Anal. Biochem.* **255**, 13-19 (1998).

Low-Cost, High-Sensitivity Atmospheric Ozone Detector

C.M. Roland and P.H. Mott
Chemistry Division

Introduction: Ozone, the triatomic allotrope of oxygen, occurs naturally from exposure of atmospheric oxygen to ultraviolet sunlight or electric discharge. Indeed, the characteristic fresh odor following thunderstorms is due to the ozone produced by lightning. Among common oxidants, ozone has the highest oxidation potential (2.1 V), leading to various commercial uses. These include as a disinfectant in the medical and food industries, for drinking and wastewater treatment, to suppress mold in storage facilities, and as a bleach. An increasingly popular application of ozone is as a deodorant. Hotels, for example, use ozone to purge tobacco odors, where it functions by oxidizing the phenol byproducts in the smoke. As a measure of its deodorizing effectiveness, one gram of ozone is reputed to neutralize the odor from a liter of hog manure.

There is a downside to the high reactivity of ozone. It is a strong respiratory irritant and is even toxic at high concentrations. The smog cycle, common to urban areas, is initiated by the photodissociation of atmospheric oxygen to produce ozone in the presence of hydrocarbons. The American Lung Association considers ozone to be the greatest airborne public health threat in the Washington, D.C. area. During the summer of 1994, for example, 600 hospital admissions in the region were attributed to high ozone levels. Metropolitan areas throughout the United States habitually fail to comply with the Environmental Protection Agency's air quality standard of 120 ppb average ozone level.

The environmental hazards of ozone, along with industry's increasing use of it, have led to the demand for a sensitive, inexpensive method of ozone detection. Existing analytical instruments are expensive and ill-suited for field use, while portable methods (e.g., the Draeger tube) suffer from poor accuracy and interference by other chemicals. Recently, work at NRL has shown that ambient ozone levels can be quantified by measuring the opacity that accompanies ozone-cracking of rubber films. This has been developed into a technique for detecting atmospheric ozone that is portable, inexpensive (few dollars), and combines high sensitivity (1 ppb atmospheric ozone, 100 times less than the OSHA safety limit) with a broad dynamic range (at least six decades).[1]

Background: When an unsaturated hydrocarbon elastomer is exposed to ozone, rapid reaction occurs to form an unstable ozonide ring (Fig. 4). This structure rapidly dissociates, severing the polymer backbone. If the rubber is stretched during this process, a surface crack is produced. As these cracks accumulate, light scattering from the rubber surface gives rise to a translucent ("frosted") appearance. The rate at which the surface cracks grow is governed by the availability of ozone; thus, the loss of optical transparency can be directly related to the ambient ozone concentration.[2]

Results: The sensing material is an initially transparent, elastomeric film (e.g., 1,4-polybutadiene crosslinked with dicumyl peroxide). The degree of crosslinking and the applied strain determine the mechanical stress, and hence the ozone-sensitivity of the rubber. A minimum level of stress (ca. 0.2 MPa) is necessary for crack initiation; ozone-induced hazing will not occur if the rubber is unstretched.

The spacing of cracks on the rubber's surface is determined by the number of nucleation sites, which in turn depends on the applied stress. To produce a

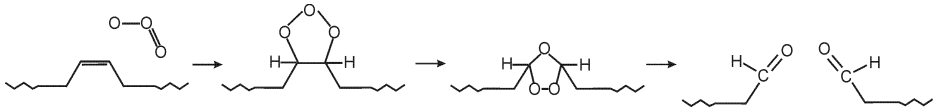

FIGURE 4
Ozonolysis of stretched rubber involves formation of a molozonide structure, then an ozonide ring. The latter rapidly decomposes, propagating a surface crack.

uniformly frosted appearance, crack initiation must be profuse, requiring somewhat greater stress than the minimum necessary for any cracks to initiate. This is illustrated in Fig. 5. If the stress is too small, only large, isolated cracks appear, while higher stresses produce a plethora of mutually interfering cracks, roughly 10 mm in size.

The ozone level associated with loss of transparency in the material is also governed by the stress. Using a tapered geometry to vary the strain, a range of sensitivities can be obtained from a single test specimen (Fig. 6). The narrower section of the sample, where the stresses are higher, becomes opaque before the wider parts. The result is a "frosting front" that propagates from along the sample. The same effect can be accomplished by changing the crosslink density within the sample.

Two modes of operation are envisioned for this technology:[3] a simple, disposable "litmus paper" type detector, and a more elaborate device, using, for example, a spool that dispenses the rubber for stretching and measurement, in combination with a take-up spool that unstretches it for archival storage.

Figure 7 shows relative transmission as a function of exposure time for five ozone concentrations. The conversion of the measured opacity to ozone concentration is done by means of a calibration curve. The rubber's response to different conditions, such as strain or exposure time, can be superimposed to yield a "master curve." This facilitates implementa-

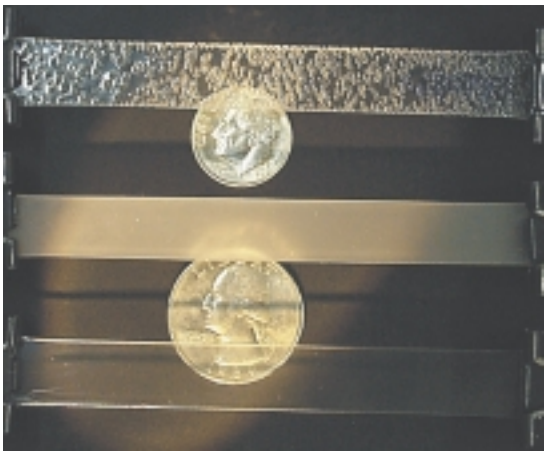

FIGURE 5
Polybutadiene exposed to 10 ppb ozone for 24 hours. The lower strip is unstrained, and remains identical in appearance to unexposed rubber. The middle strip, stretched 121%, is almost opaque, due to a uniform coverage of surface cracks, 5-10 mm in depth and spaced about 20 mm apart. The strip at the top had a strain of 18%. The resulting stress was only sufficient to induce distinct, well-separated cracks, corresponding to the largest inherent flaws.

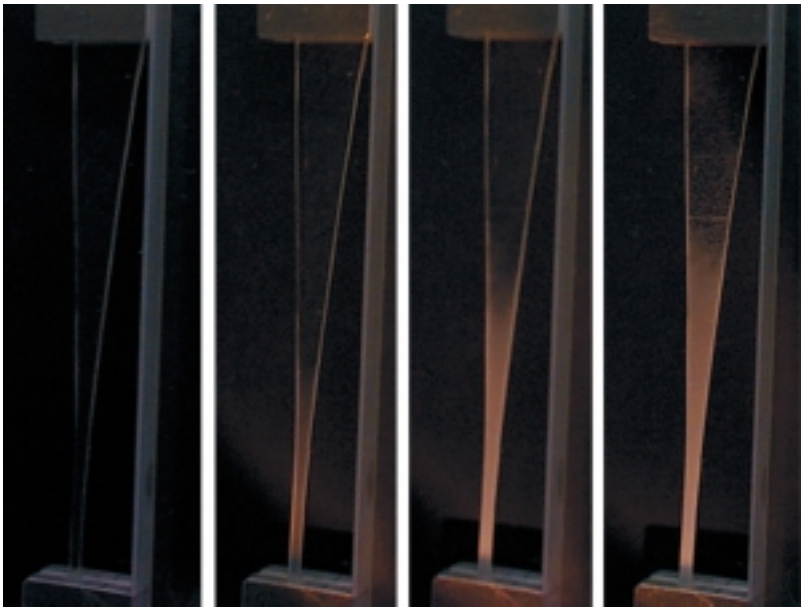

FIGURE 6
Stretched polybutadiene exposed for 0, 4, 8, and 120 minutes to 200 ppb ozone. The cross-sectional area varies by a factor of four along the specimen length. The consequent variation in stress causes the observed varying response to ozone.

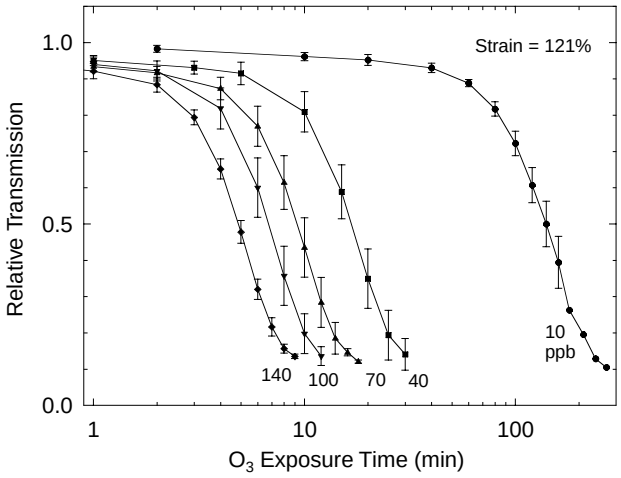

FIGURE 7
Change in optical transparency of polybutadiene stretched 121% while exposed to the indicated levels of ozone.

tion of the method, enhancing both the sensitivity and dynamic range.

Since ozone will not necessarily be the only air pollutant present, it is important to demonstrate that the test method is free from interference. We have determined that exposure to specific pollutants (sulfur dioxide, carbon monoxide, methane, nitrogen dioxide, nitrogen monoxide) has no influence on the response of the stretched elastomer to ozone. This is not surprising, since ozone is much more reactive than these gases.

Summary: Transparent rubber stretched in an ozone-laden environment initially develops micron-sized surface cracks due to ozone-induced chain scission. The consequent reduction in the transparency of the rubber provides a facile method for measuring ambient ozone levels. The loss of light transmission is linearly dependent on the ozone concentration, and is an increasing function of the strain. This method of detecting atmospheric ozone has high sensitivity (1 ppb) and a broad dynamic range. Environics, Inc. of Tolland, Connecticut, has obtained a license from the Navy to market the technology.[4]

Acknowledgments: We thank Environics, Inc. for the loan of their ozone generator and analyzer.

[Sponsored by ONR]

References

[1] C.M. Roland and P.H. Mott, "Atmospheric Ozone Concentration Detector," U.S. Patent #5,972,714, October 26, 1999.

[2] P.H. Mott and C.M. Roland, "Ozone Detection by Crack-Induced Opacity in Rubber," *Rubber Chem. Tech.* **72**, 769 -778 (2000).

[3] P.H. Mott and C.M. Roland, "Disposable Elastomeric Ozone Detector," *NASA Tech. Briefs* (September 1997).

[4] "Partially Exclusive License Between Environics, Inc. and the United States of America," NRL-LIC-98-2-039, October 19, 1998.

The BARC Biosensor

L.J. Whitman,[1] P.E. Sheehan,[1] R.J. Colton[1], M.M. Miller,[2] R.L. Edelstein,[3] and C.R. Tamanaha[3]
[1]*Chemistry Division*
[2]*Materials Science and Technology Division*
[3]*Geo-Centers, Inc.*

Recent events in Yemen have made disastrously clear that acts of terrorism are one of the greatest threats to our Armed Forces. One of the most insidious threats is exposure to biological warfare agents. Unfortunately, treatments for infection by likely pathogens are currently limited, and may require treatment before any symptoms appear—the case for anthrax, for example. The invention of highly sensitive sensors for early detection of biological warfare agents is crucial. The Bead ARray Counter (BARC) system is a revolutionary tabletop biosensor we are developing at NRL to help solve this urgent national problem.

Gene Chips: The BARC biosensor is based on a so-called "gene chip." The function of a gene chip is to simultaneously look for a large number of distinct segments of deoxyribonucleic acid (DNA), the unique genetic material of life. Identification is accomplished by taking advantage of the unusual structure of DNA: two complementary strands that recognize one another, even in a complex mixture. An array of DNA spots (the "probes") is deposited on a surface (the "chip"), with each spot containing *single* strands of one particular segment of interest. When matching segments are present in a sample, they combine (hybridize) with their complements on the chip. The resulting double-stranded DNA molecules are typically labeled with fluorescent molecules. Then

a bright light is focused on the chip, and a special optical system "reads" which spots fluoresce.

Although the first commercial gene chips are proving useful for medical research, they fall short for biological warfare defense. Because very little light is emitted by the labeled DNA, a large, powerful, and complex optical system is needed to read a chip. Furthermore, to achieve the desired sensitivity—the detection of a few thousand DNA molecules or less per milliliter in the original sample—fluorescence-based systems require extensive sample preparation that may take hours to complete.

The BARC Approach: In the BARC biosensor, the fluorescent labels are replaced by magnetic labels that can be detected *individually* using an array of magnetic field microsensors embedded in the chip (Fig. 8).[1,2] The magnetic labels are commercial beads, 1 to 2 microns in diameter, containing some magnetic material. The magnetic field sensors are wire-like structures on the chip, a few microns wide, made of a special metal alloy that displays giant magnetoresistance (GMR). When a magnetic bead is present above a sensor wire, the wire's resistance decreases by a small, but detectable, amount. The more beads present, the larger the change in resistance. Hence, the BARC approach eliminates the optical system required for fluorescence-based detection, replacing it with simpler, more sensitive, and less expensive microelectronics.

The biochemistry underlying the BARC biosensor is illustrated in Fig. 8. The chip containing the GMR sensors is coated with thin layers of silicon nitride (~1 μm) and gold (~50 nm) to protect the electronic circuitry from the saline solution containing the DNA. A custom-designed arraying system then deposits 0.3 mm-diameter spots of single-stranded probe DNA over the GMR sensors, with one end of each DNA molecule specially modified with a sulfur atom to bond to the gold surface. The DNA segments are from genes of pathogens likely to be used for biological warfare, such as *Botulinum*, *Francisella tularensis*, and *Yersinia pestis* (responsible for botulism, tularemia, and plague, respectively). The genetic information was provided by the Naval Medical Research Center.

After depositing the probes, the remaining surface is coated with polyethylene glycol, a polymer that inhibits the sticking of DNA or microbeads in the areas outside of the spots. The sample is then introduced and allowed to hybridize with the probes. At this point in our system development, the sample DNA must first be prepared so that it is single-stranded and tagged with biotin, a small ligand molecule that binds very selectively (and strongly) with a special receptor molecule, streptavidin. Magnetic microbeads precoated with streptavidin are then allowed to settle on the chip, bonding strongly with any biotin present and thereby labeling the captured sample DNA. The beads that are not bonded in this way are easily rinsed off, and the remaining beads are counted by the GMR sensors, indicating the identity and concentration of any pathogens present.

The Sensor System: The BARC assay is done in a small, glass flow cell mounted on the sensor chip (Fig. 9). The chip carrier board is housed in a disposable plastic cartridge that contains the reagents for the assay. The cartridge plugs into the electrical control system and interfaces with a miniature pump (not shown) that regulates the fluid flow. The overall system is operated with a laptop computer. A demonstration of the BARC biosensor is illustrated in Fig. 10. The eight sensor regions on the chip were each coated with gold. Two of each were arrayed with four different probes (one a positive control), and an assay

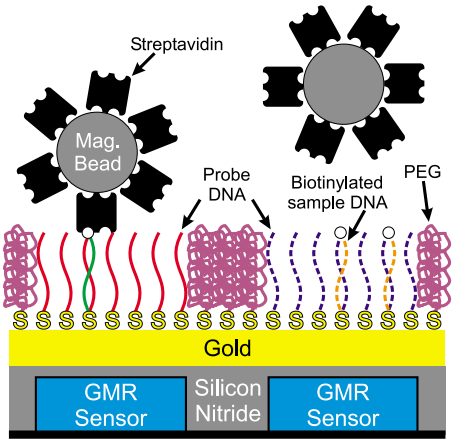

FIGURE 8
The BARC biosensor approach. Note that the elements are not to scale; in particular, the beads and sensors are much larger in proportion to the molecular components.

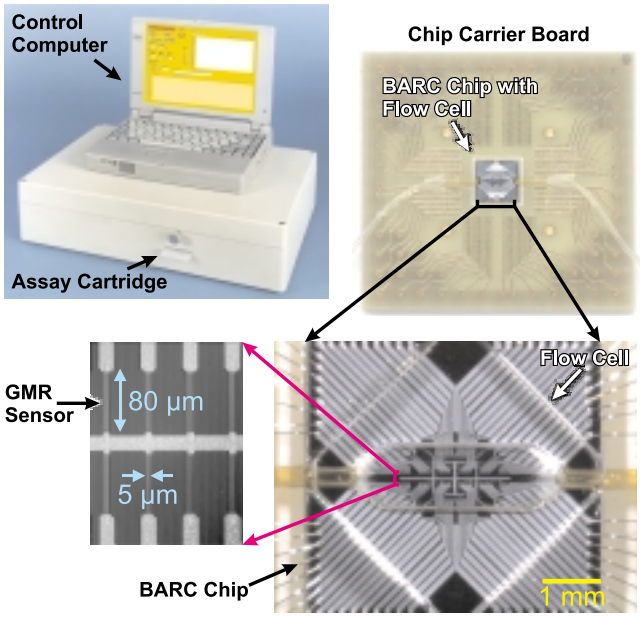

FIGURE 9
The BARC system and some of the internal components. The 5-mm-wide BARC chip (with the flow cell on top) is mounted on the chip carrier board, which is housed within the assay cartridge. The prototype chip shown has 64 GMR sensor strips, 5 × 80 μm each, in groups of eight.

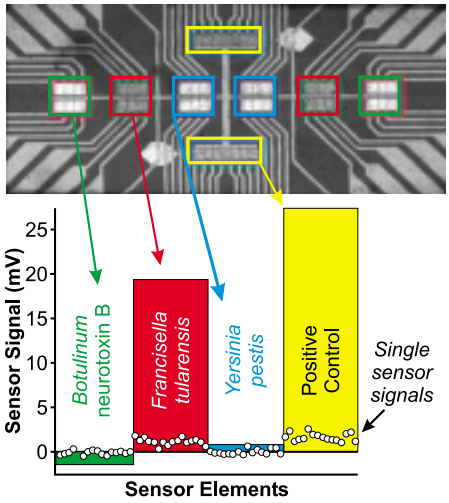

FIGURE 10
The results of a three-analyte assay. A view of the chip surface after the assay is shown, with the eight sensing regions outlined. The dark regions are almost completely covered with microbeads. For each analyte, the graph shows the measured signals from the individual sensing elements (symbols) and the integrated signal for all 16 elements (colored bar). The assay for *Francisella tularensis* was performed with 10 nM DNA hybridized for 30 min. The total assay required about 60 min.

was performed for *Francisella tularensis*. Afterward, the control and *tularensis* regions are densely covered with beads, while the other four sensor regions are nearly bead-free. The amount of DNA in the sample is measured by summing the signals from the sensors addressing each probe type (16 each).

Prospects for Further Development: The GMR sensor used in the BARC system is similar to technology being developed for a new type of computer memory, magnetic RAM. It should be possible to adapt this technology to make inexpensive BARC chips with millions of sensors. Ultimately, we hope to develop a small cartridge that can be plugged into a hand-held computer for rapid, sensitive detection of all known biological warfare agents. Such a system would also have broad commercial applications in the fields of biomedical research, diagnostics, drug discovery, forensics, agriculture, and environmental testing.

[Sponsored by DARPA and ONR]

References

[1] D.R. Baselt, "Biosensor Using Magnetically-detected Label," U.S. Patent 5,981,297, issued November 9, 1999.

[2] R.L. Edelstein, C.R. Tamanaha, P.E. Sheehan, M.M. Miller, D.R. Baselt, L.J. Whitman, and R.J. Colton, "The BARC Biosensor Applied to the Detection of Biological Warfare Agents," *Biosens. Bioelectron.* **14**, 805 (2000).

Better Use of Water for Fire Suppression

E.J.P. Zegers, P. Fuss, J.W. Fleming, B.A. Williams, A. Maranghides, and R.S. Sheinson
Chemistry Division

Introduction: Environmental concerns over the past decade have provided new impetus for expanding and improving the use of water for Navy fire protection. Traditionally, fire suppression in selected Navy shipboard compartments has been provided by Halon 1301 (CF_3Br), whose production has been banned in the United States and other developed countries because of its depletion of stratospheric ozone. Nonbrominated fluorocarbons, while ozone safe, are less effective, carry space and weight penalties for Navy platforms, are significant global warming agents, and produce toxic hydrogen fluoride (HF) gas in extinguishing a fire.

Water is perhaps the oldest firefighting agent, but it can be difficult to implement in many situations; because, unlike Halon, it is a liquid. Droplet size, transport, evaporation rate, and suspension time are all critical parameters in determining the effectiveness of a water-based suppression system against a given fire threat. Although water-based fire suppression has been the subject of empirical tests for many years, the interaction of liquid water droplets with flames has received surprisingly little systematic study in laboratory settings. The identification of the factors important in determining water's effectiveness as a fire extinguishing agent is a prerequisite for better implementation. The Navy Technology Center for Safety and Survivability has a coordinated program, combining fundamental laboratory studies of water/flame interactions with real-scale fire tests, to provide the Navy with implementation particulars for water mist-based fire protection systems.

Water Mist Fire Suppression: Traditionally, water has been used as a firefighting agent in the form of relatively large drops. Typical sprinkler systems produce water drops having diameters on the order of a millimeter. Such droplets are useful at cooling smoldering surfaces, but are relatively ineffective at suppressing combustion of gaseous or liquid fuels. The large size and low surface area/volume ratio means that relatively little of the water evaporates in the length of time the droplet spends near the fire. Thus the cooling provided by the water evaporation and dilution of the oxygen and fuel by the resulting water vapor are not efficiently achieved. For this reason, most water-based fire suppression systems use more water than would be needed if the thermal and dilution effects could be properly utilized.

Fine water mists, having diameters of 200 microns or less, circumvent these difficulties by allowing better droplet vaporization, but they are more difficult to produce. The tradeoffs between efficiency and engineering difficulties in droplet generation and delivery must be determined.

Laboratory Studies: In assessing the applicability of water mist fire suppression systems, one must answer the question "how effective can water be under ideal conditions?" We have investigated water mist inhibition and extinguishment in two types of laboratory flames and find that, under suitable conditions, water mist can be as effective as Halon 1301.

Figure 11 shows data taken in a nonpremixed propane/air counterflow flame, to which suppressants (Halon and water droplets of various sizes) were added to the air stream.[1] Addition of the suppressant to the air stream is the most typical scenario for most fire threats. The extinction strain rate plotted in Fig. 11 is a measure of flame stability. Effective fire suppressants lower the extinction strain rate as shown. Data for water and Halon, plotted on a mass basis, show that over the range of droplet sizes tested (20 to 50 microns), smaller droplets are more effective. Furthermore, water droplets of 14 and 30 micron diameter are considerably more effective than Halon, while droplets of 42-micron diameter are comparable to Halon in extinguishing this particular flame.

The degree of burning velocity reduction is also an indication the effectiveness of a fire suppressant. Figure 12 shows data on the burning velocity of premixed methane/air flames containing submicrometer diameter water droplets.[2,3] These droplets are small enough to completely evaporate during the short residence time (approximately one millisecond) in the flame region. In this type of flame, the effectiveness of the submicron water droplets is comparable to the findings for Halon 1301 in Refs. 2 and 3. Comparison of the water data to measurements with nitrogen and CF_4, two well-studied gaseous agents that are chemically inert and inhibit combustion by cooling and dilution of the available oxygen, indicates that the expected effect of water evaporation is achieved in this environment.

Achieving the maximum effectiveness of water in real fire scenarios is more challenging. The small drops that are most effective in the flame may evaporate before they reach the fire, while larger drops may be too large to be entrained in the air flow and get to the fire, especially for obstructed or cluttered areas. The key issues to understand are mist drop size and distribution in the protected space.

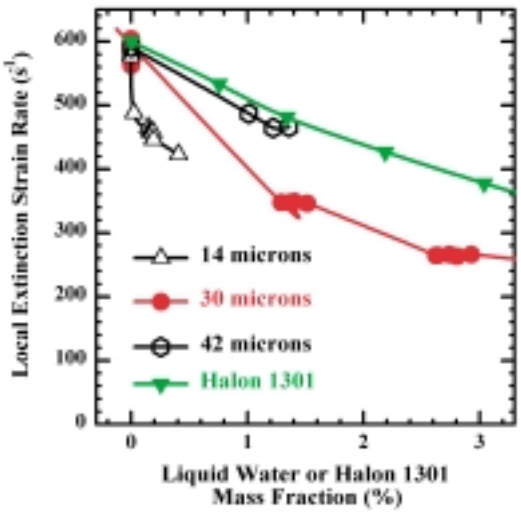

FIGURE 11
Measurements of extinction strain rate in nonpremixed propane/air flames inhibited by Halon 1301 (CF_3Br) and by monodisperse water droplets of various sizes (from Ref. 1).

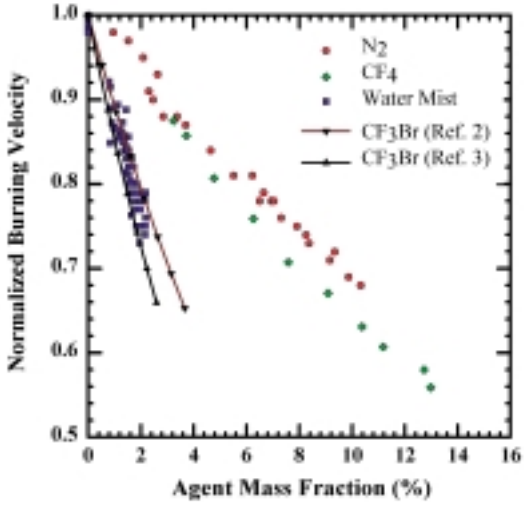

FIGURE 12
Measurements of burning velocity reduction in a methane/air mixture by addition of nitrogen, CF_4, and submicron water mist. Published measurements for Halon 1301 (CF_3Br) are also shown.

FIGURE 13
Fire test facility at the NRL Chesapeake Bay Detachment. The two enclosures at the rear (285 cubic meters) and the right (27 cubic meters) of the picture are used for testing different sized shipboard compartments.

Toward Implementation: Realistic large-scale tests are currently underway at NRL's Chesapeake Bay Detachment to develop water mist system implementation solutions to protect Navy shipboard flammable liquid storerooms against different fire threat scenarios (Fig. 13). These tests combine a powerful array of instruments to determine droplet sizes, velocities, and number densities at various locations in the test compartment, as well as the in situ measurement of oxygen dilution by the evaporating water mist, for truly understanding suppression by water mist. The detailed suppression mechanisms studies in laboratory flames combined with well instrumented full-scale studies is providing design guidance to the Navy for implementing water mist as an effective and reliable Halon alternative.

[Sponsored by SERDP and NAVSEA]

References

[1] E.J.P. Zegers, B.A. Williams, R.S. Sheinson, and J.W. Fleming, "Dynamics and Suppression Effectiveness of Monodisperse Water Droplets in Non-Premixed Counterflow Flames," *Proceedings of the Combustion Institute* **28** (2000) (in press).

[2] T. Noto, V. Babushok, A. Hamins, and W. Tsang, "Inhibition Effectiveness of Halogenated Compounds," *Combust. Flame* **112**(1-2) 147-160 (1998).

[3] D.J. Parks, N.J. Alvares, and D.G. Beason, "Fundamental Flame-speed Measurements in Combustion Gases Containing CF_3Br," *Fire Safety J.* **2**(4) 237-242 (1980).

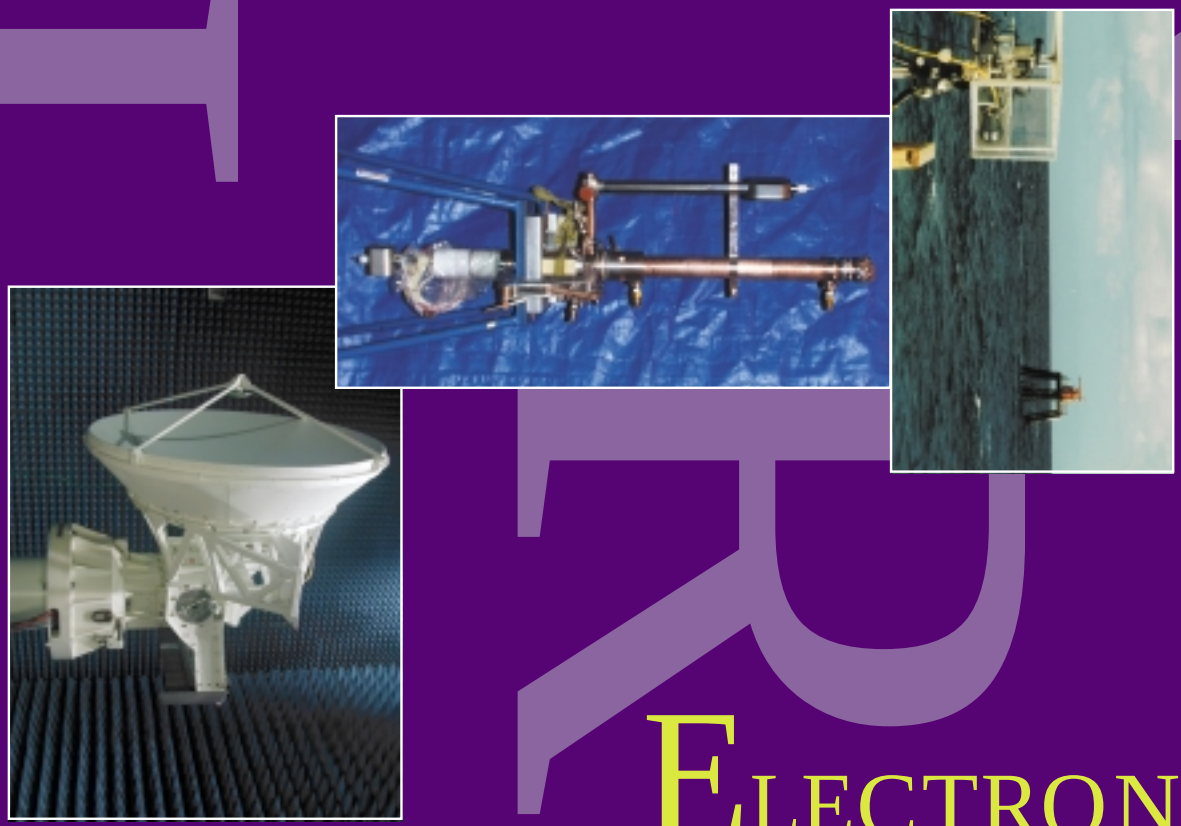

Electronics and Electromagnetics

WARLOC: A New 94 GHz High-Power Coherent Radar

V. Gregers-Hansen,[1] G.J. Linde,[1] W.-J. Cheung,[1]
B.G. Danly,[2] M.T. Ngo,[3] and R. Myers[4]
[1]*Radar Division*
[2]*Electronics Science and Technology Division*
[3]*Mission Research Corporation*
[4]*Dyncorp ENSP, Inc.*

Introduction: Extremely high resolution in the combined space of range, velocity, and angle measurement requires a radar operating at a very high frequency.[1] In the past, the lack of high-power sources, as well as low-loss microwave components, has slowed the development of such high-performance millimeter-wave (MMW) radars, and system designers have looked for needed performance improvements at infrared and visible frequencies. Current urgent military requirements for airborne target identification, debris and decoy discrimination in theater ballistic missile defence (TBMD), and improved missile or projectile guidance, have generated a renewed interest in MMW radars and the associated technology.

Two programs at the Naval Research Laboratory (NRL), are currently developing a new level of capability in W-band (94 GHz) MMW radar. In the Electronics Science and Technology Division, a high-power gyroklystron power amplifier has been developed in a joint program with industrial partners at Litton and CPI. This development effort is described separately in this issue.[2] A companion program, in the Radar Division, is using this tube in the development of the high-power, coherent WARLOC (W-band advanced radar for low observable control) radar, which is using enabling technology in the areas of low-loss transmission lines, quasi-optical duplexing, and new W-band semiconductor technology.

The WARLOC Radar: The NRL WARLOC radar is being developed as a transportable, land- or sea-based system, using a high-power gyroklystron, quasi-optical transmission line and duplexer components, a Cassegrain antenna, and associated low-noise receiver and signal processor subsystems. The complete system will be housed in two trailers, 40 by 8 ft and 20 by 8 ft, respectively.

Figure 1 is a block diagram of the radar, and Table 1 lists major radar characteristics. The 70 kV power supply and associated 20 kV modulator, which are needed to operate the gyroklystron, were developed by Electromatics (ETM) Inc. The power supplies are accurately regulated for optimum system stability and will permit operation in modes with widely varying pulse repetition frequency (PRF) and pulsewidth. Currently instrumented waveforms will use PRFs of 1 to 5 kHz with pulse widths in the 1 to 100 ms range. Waveforms will support a number of different modes of operation.

Transmission lines and rotary joints for azimuth and elevation tracking use over-moded waveguide, 90-degree miter bends, and mode-converters to transform the waves between the TE_{01} output mode of the gyroklystron to the final linearly polarized input to the duplexer. The transmission line components were supplied by General Atomics Corp.

The duplexer is implemented using quasi-optical Gaussian beams and a Faraday rotator.[3] It was developed at MIT Lincoln Laboratory in a joint effort. A transmit-receive isolation of ~35 dB has been measured, and the total transmit and receive losses are

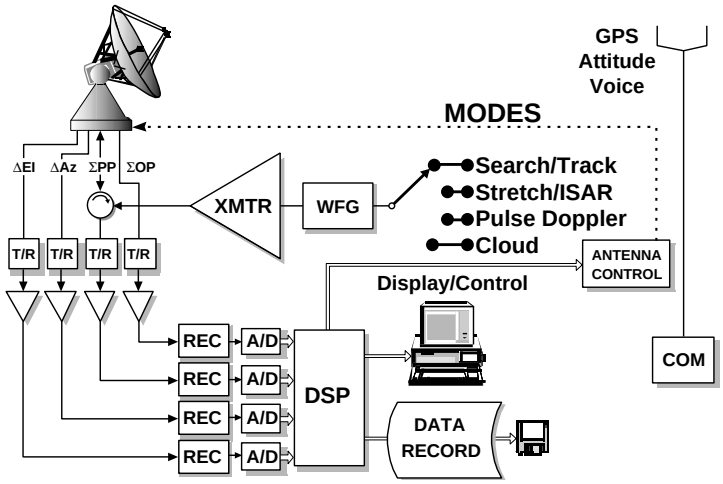

FIGURE 1
Block diagram of WARLOC radar.

Table 1 — Major Parameters of the WARLOC Radar

Radar Parameter	Value
Center frequency	94 GHz
Bandwidth	>600 MHz
Peak power	80 kW
Average power	10 kW
Antenna diameter	1.8 m
Antenna gain	63 dB
Polarization	Horizontal/Vertical
Az and El monopulse	Yes
Transmit loss	1.5 dB
Receive loss	0.5 dB
Noise figure	5 dB

less than 1.5 dB. The duplexer generates a circular polarized transmit beam and separates co- and cross-polarized returns into independent channels. Azimuth and elevation monopulse is implemented on the co-polarized channel.

The radar antenna is a 1.8-m parabolic reflector with a Cassegrain subreflector feed system illuminated by the output from the duplexer. The fabrication tolerance of the antenna is around 65 μm rms, with a first sidelobe goal of –20 dB. An antenna gain of 62 dB has been measured in the Radar Division compact antenna range. The pedestal for the WARLOC radar is a high-precision director built by Contraves. Figure 2 is a photograph of the antenna and pedestal.

The receiver is triple conversion with IF frequencies at 10 GHz, 1800 MHz, and 60 MHz. Narrow and medium bandwidth chirp waveforms, as well as the wideband FM stretch signal, are generated using arbitrary waveform generators (AWGs) and multipliers. The 84 GHz local oscillator is generated in a phase-locked oscillator using a reference input at 100 MHz. The W-band receiver will be mounted on the antenna to minimize RF losses and will consist of four channels with low-noise preamplifiers and mixers to 10 GHz. The noise figure value quoted in Table 1 is for a planned upgrade to W-band low-noise amplifiers using integrated circuits developed by TRW during Phase III of the DoD MIMIC program. These amplifier chips are being packaged in a joint program with the Army Research Laboratory.

The signal data processor (SDP) is contained in a VME 6U chassis. The SDP incorporates several different cards, including programmable digital signal processing (DSP) SHARC cards from Mercury Computer Systems, A/D converters (four channels at 12 bits, 20 MHz), a Power PC system controller, data I/O circuit cards, a GPS and IRIG time code generator, and an interface to the data recording and real-time display system. The RACEway Interlink ports provide a high-bandwidth data path in this system. Firmware development for the SDP is developed under VXWorks/Tornado through a SUN Workstation. The DSP receives A/D dwell data and performs pulse-compression, Doppler processing, range-Doppler image processing, and range and angle-error processing and will provide position updates to the antenna pedestal.

The radar also includes a data recording system that will permit coherent data recording in all four channels simultaneously.

Additional equipment needed for the operation of the radar includes the coolant group for the transmitter, a diesel generator for operation at remote sites, and communication equipment for test coordination and test target communication. Figure 3 is a photograph of the two radar trailers.

Applications: There are a number of candidate applications of a high-performance W-band system such as the WARLOC radar. These include non-cooperative target recognition (NCTR) using

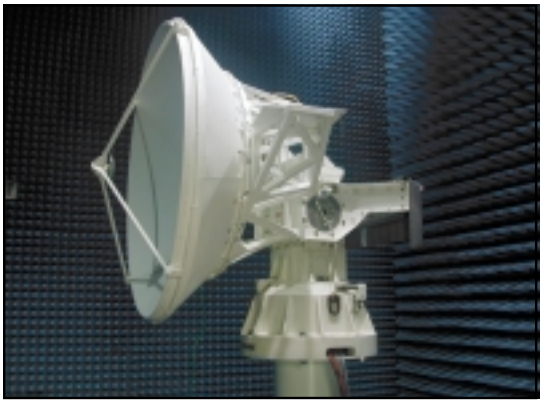

FIGURE 2
WARLOC radar antenna.

FIGURE 3
The two trailers housing the WARLOC radar.

high-definition range-Doppler imaging and jet engine modulation (JEM) exploitation, debris and decoy discrimination for TBMD, guidance and control for ship self-defense against very low altitude threats, enhanced ECCM, and improved detection of low cross-section targets. In addition, there are several promising applications of W-band radar to remote sensing (cloud studies) and in basic research.

Radar Testing: The WARLOC radar will be moved from its current location at NRL-DC to the NRL Chesapeake Bay Detachment (CBD) in January 2001 for final integration. Once operational status is achieved, the radar will initially support planned cloud physics research, propagation measurements, and imaging experiments against aircraft targets. Other test efforts currently being planned are support of TBMD testing, target cross section measurements of low or reduced cross section aircraft and missiles, and tracking tests against very low altitude targets over water.

Summary: An advanced high-power, coherent W-band radar system is being developed by the Radar Division. This radar uses a high-power gyroklystron developed by the Electronics Division along with other critical W-band microwave components. Potential applications of such a radar were discussed and the planned experimental program was outlined.

[Sponsored by ONR]

References

[1] N.E. Currie and C.E. Brown, *Principles and Applications of Millimeter-Wave Radar* (Artech House, Norwood, MA, 1987).

[2] B.G. Danly, J.P. Calame, B. Levush, K.T. Nguyen, and D.E. Pershing, "High-Power 94 GHz Gyroklystron Amplifier," *2001 NRL Review*, p. 113.

[3] W.D. Fitzgerald, "A 35-GHz Beam Waveguide System for the Millimeter-Wave Radar," *The Lincoln Lab. J.* **5**(2), 245-272 (1992).

Directly Measuring Forward Scatter with an Ultra Wideband Radar

J.P. Hansen, K.M. Scheff,
E.L. Mokole, and E. Tomas
Radar Division

Background: Knowledge of the behavior of radar forward scatter from the ocean surface is important for designing Navy radar systems and defining their performance. Radar targets physically located close to the ocean surface can be illuminated by radiation coming both directly from the radar and, by reflection, from the ocean surface. The surface-reflected components are described as having experienced forward scatter. Interference between the direct and forward-scattered components causes fluctuations in the amplitude of the detected radar signal and distorts the measured phase front. When a radar at a low elevation illuminates a target that is also close to the ocean surface, the geometry tends to include small grazing angles, with inherently small differences in both path length and direction between the direct and surface-reflected signal components. Experimental measures of the forward-scattered signals are challenging since they require either ultra high resolution in time or angle or must be inferred from the combined signal. Historically, past estimates of ocean forward scatter have largely been based on examining heavily averaged data and looking for a spatial interference pattern.

Experiment: To meet the experimental challenge, an ultra wideband, ultra high-resolution, dual-polarized measurement radar system has been used in a field experiment to measure ocean forward scatter at a 9 GHz center frequency. Figure 4 shows a simplified block diagram of the measurement radar. The field-deployable, dual-polarized system used a video impulse excited traveling wave tube to produce transmit pulses with 2 kW peak power and 150-ps duration. This very short pulse length provides range resolution of the order of 2 cm. Separate, ultra wideband, dual-polarized transmit and receive horn antennas are used to maintain receiver isolation without the use of a duplexer. The receive system detects signals with a unique direct sampling detector based on a multiple sampling head, 8-bit digital sampling oscilloscope. This detection technique supports an overall instantaneous receive bandwidth in excess of 5 GHz.

Figure 5 shows a field experiment with the radar illuminating a retroreflecting target mounted on a tower. The tower is situated in the ocean at a range of 242 m from the radar. The dynamically changing ocean surface located between the radar and the tower reflects a portion of the radar signals going toward and returning from the retroreflecting target.

Figure 6 shows an example of measurements of the return signal from the retroreflector. Each range point was sampled for both linear transmit and receive polarization states (VV and HH) within a time period of 25 μs before moving to the next range point, and each full range profile was completed within 3.7 ms. Five hundred consecutive range profiles, performed at intervals of 0.3 s and spanning a

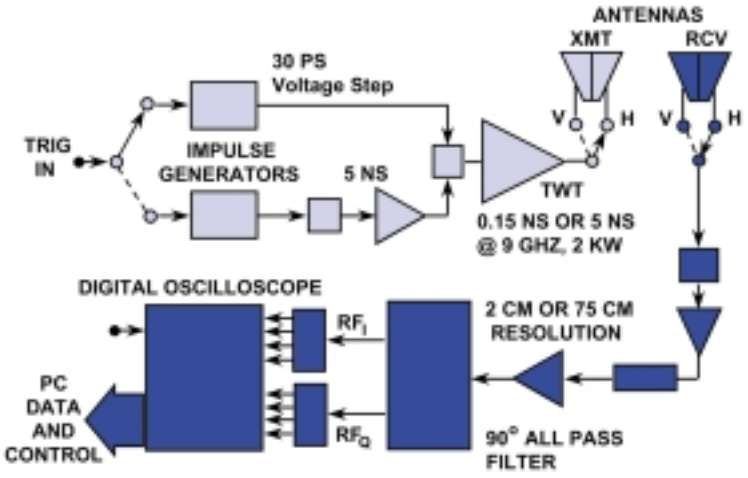

FIGURE 4
Block diagram of measurement radar.

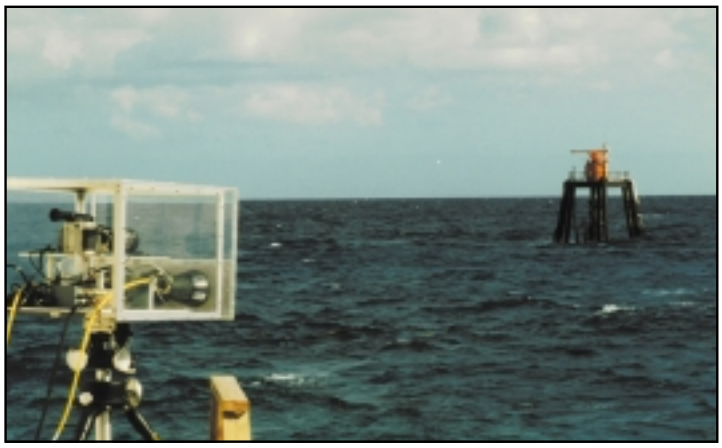

FIGURE 5
Radar (left) illuminating retroreflector on tower (right).

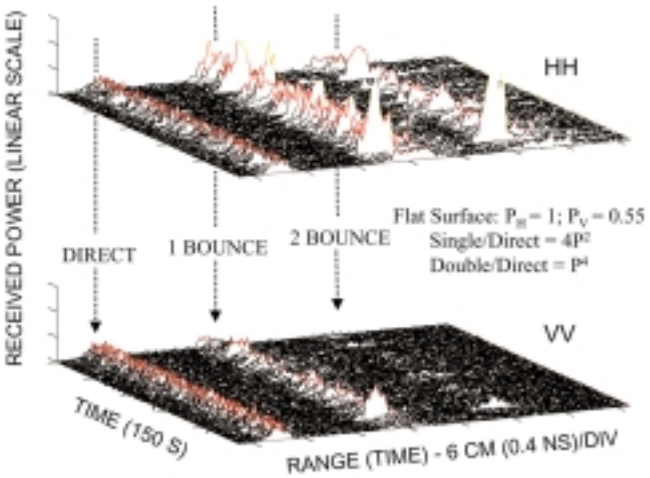

FIGURE 6
Returning signals from retroreflector.

total time period of approximately 150 s, are shown. Figure axes are range in centimeters, time in seconds, and received peak power on a linear scale. As shown in this data record, signals that have experienced one bounce travel a slightly longer path and are consequently delayed in time by approximately 1 ns with respect to the direct path signals. Similarly, signals that have experienced double bounces are delayed by 2 ns. Note that the amplitudes and locations of the bounce path signals exhibit the influence of the changing ocean surface during the time span of the data record. The equivalent surface-reflection coefficients are directly found by comparing the amplitudes of the time-resolved direct and bounce path signals.

This particular data sample, taken for a crosswind orientation (with the wind moving perpendicular to the line of sight between the radar and the tower), presents some new results with regard to conventional wisdom concerning radar forward scatter. First, there is evidence of a focusing phenomena, where the forward scatter path occasionally presents an equivalent reflection coefficient greater than unity. Second, the measurements show an unexpected dependence on wind orientation, with the average forward scatter being significantly greater for a crosswind orientation than for a comparable upwind orientation.

Summary: An ocean forward-scatter experiment has been described that used an ultra wideband, dual-polarized, instrumentation radar. The ultra high range resolution of the radar system has served to separate the direct and surface-scattered components of signals reflected from targets oriented close to the ocean. The ability to achieve this separation and examine the signal components in isolation is leading to a better understanding of the composition and behavior of low grazing angle forward scatter.

[Sponsored by ONR]

A Wideband Beamformer Using True Time Delay and FPGAs

J.J. Alter, M.G. Parent, J.O. Coleman,
J.P. McConnell, D.P. Scholnik, and W.R. Pickles
Radar Division

Introduction: Many military and commercial applications require the formation of wideband beams in space, including high-range-resolution radar for imaging and target identification, wideband communications, and electronic surveillance. Wideband digital beamforming techniques allow the possibility of forming multiple beams and tracking several targets simultaneously. In an array antenna, a beam in space is formed by delaying the signal from each element of the array by the appropriate amount so that when the delayed signals are combined, they add constructively to form a beam in the desired pointing direction. In narrowband systems, where the signal bandwidth is typically less than 3% of the RF center frequency, these delays can be implemented using phase shifters. However, in wideband systems (percentage bandwidths greater than about 3%) with electrically large antennas, these delays must be implemented using true time delay techniques to avoid dispersion effects. Historically, the high cost of implementing true time delay beamforming has prohibited its use in actual systems. The purpose of this project is to demonstrate that the state of the art in RF and digital components has advanced to the point where commercially available devices can be used to make an all-range, wideband beamformer more affordable.

Approach: The system under development is a receive-only beamformer that accommodates a 400 MHz instantaneous bandwidth over a 1-4 GHz operating frequency.[1,2] As shown in Fig. 7, the array consists of 576 active receive elements configured as 16 36-element subarrays. Due to the high percentage bandwidths (10-40%), true time delay techniques are required. The technique for implementing true time delay in the system is outlined in Fig. 8. To steer the beam in the direction of the indicated wavefront, a linear time delay is required across the array (green solid line). Each subarray provides a portion of the time delay using switched line-length circuits behind each element (dashed blue lines). The signal from each subarray is then delayed digitally (dotted red lines) to offset each subarray's output to match the desired overall time delay.

Subarray Design: Each subarray is composed of six circuit boards, each of which incorporates six wideband Vivaldi elements, as shown in the blowup in Fig. 7. The signal from each element is passed through a low-noise amplifier, a switched-line-length network for analog true time delay, and a digital attenuator. It is then summed with the other element outputs on the board to form a combined six-element output. The outputs of six of these circuit boards are combined to form a single, 36-element subarray output. The 16 RF subarray outputs are then sent to the digital beamformer.

FPGA Technology: The digital beamformer is implemented using field programmable gate array

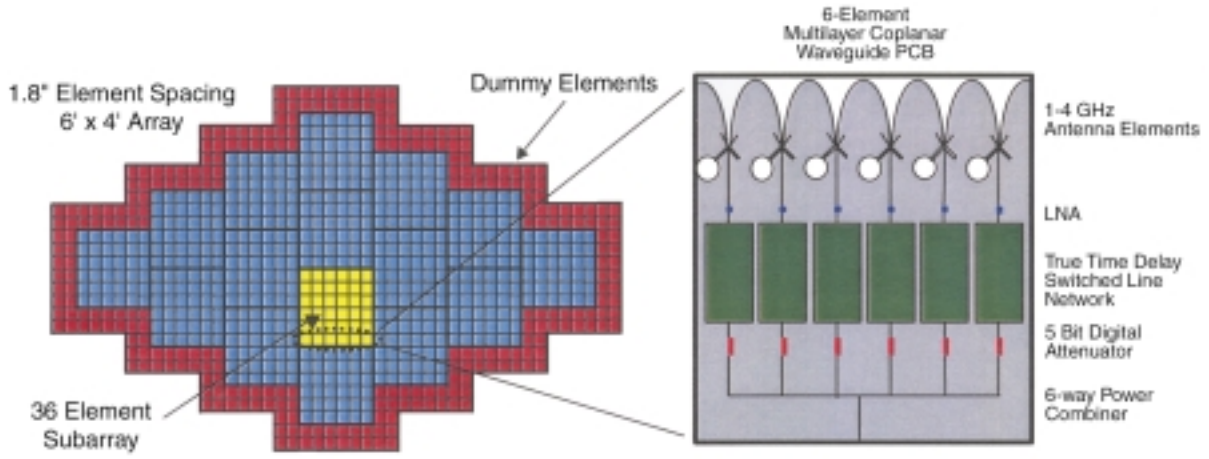

FIGURE 7
Wideband array architecture.

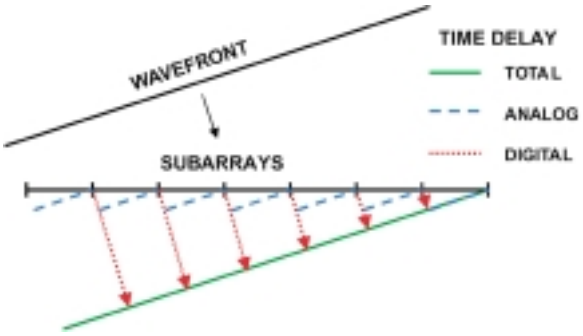

FIGURE 8
True time delay implementation.

(FPGA) technology. FPGAs are integrated circuits that incorporate a large number of logic gates that a circuit designer can arbitrarily connect to implement specific functions. The circuit is designed in a high-level hardware description language, which is interpreted by software tools that map the design onto the FPGA. Today, FPGAs with more than two million logic gates and more than 100 MHz clock rates are in production. Devices with ten million gates and 200 MHz clocks will soon be available.

RF and Digital Processing: As seen in Fig. 9, the RF output of each subarray is sent to a receiver, which downconverts the signal to produce a 400 MHz bandwidth IF signal centered at 750 MHz. The IF signal is then digitized to 8 bits at a 1 gigasample/second (GSPS) rate. Since the FPGAs cannot support this data rate, the processing is performed using polyphase techniques. The 8-bit, 1 GSPS output of the A/D converter first passes through a DEMUX process, which demultiplexes the data stream by a factor of 8, producing 64 bits (representing eight consecutive 1 GHz data samples) at 125 MHz. These data then pass through several FPGAs that implement the polyphase digital filters required for equalization and time delay and the running sum for the beamformed output. After the beam is formed, another FPGA implements the filters required for I/Q demodulation. Multiple beams can be formed by duplicating the hardware after the equalization filters, as demonstrated by the second string of time delay and adder blocks. This digital beamformer delivers more than 1.5 trillion operations/second (teraops, or TOPS) and resides in a single 6U VME cardcage.

Summary: The Radar Division is developing a wideband receive array that incorporates analog true time delay beamsteering at the element level to form directional subarray beams, and digital true-time-delay beamsteering to combine the subarray outputs. The system supports a 400 MHz bandwidth over a 1-4 GHz operating frequency and uses commercially available components. The FPGA-based digital processor delivers more than 1.5 TOPS of performance. The system will be used as a testbed to demonstrate optimal beamforming techniques that are currently under development. Wideband digital beamforming is essential to the success of programs such as AMRFS[3] (now AMRF-C), which is attempting to execute communications, electronic warfare, and radar functions through a single antenna aperture.

[Sponsored by ONR]

References

[1] J.J. Alter, M.G. Parent, J.O. Coleman, D.P. Scholnik, and F.J. Caherty, "Implementation of Wideband Beamformers Using FPGAs," in *Proc. Military Sensing Symp. (MSS99)*, North Charleston, SC, Nov. 1999.

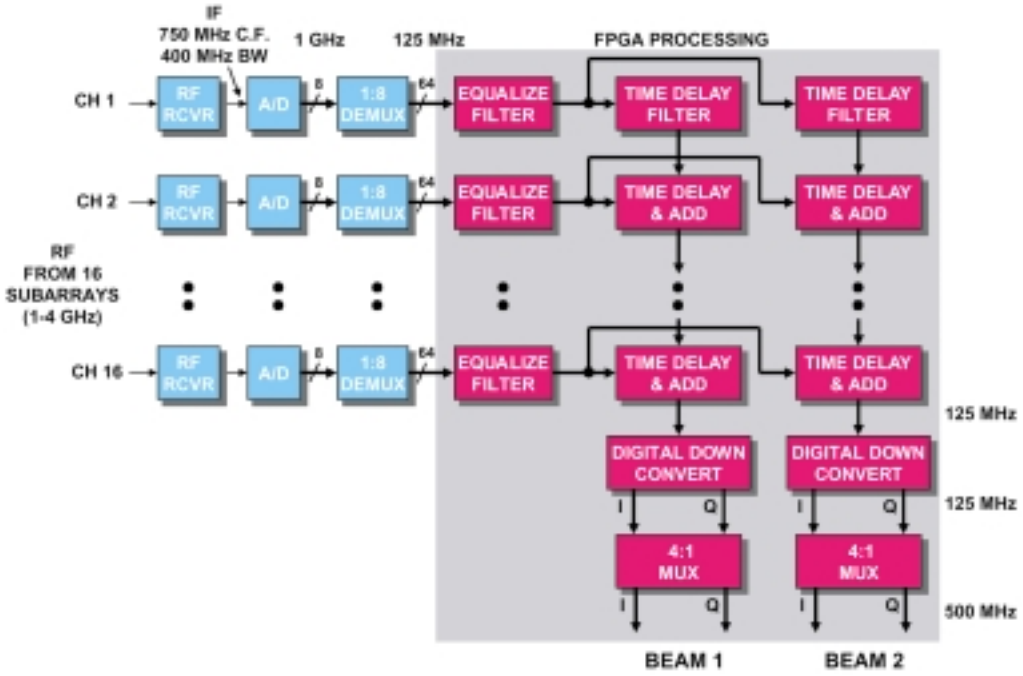

FIGURE 9
FPGA-based digital beamformer architecture.

[2] M.G. Parent, J.J. Alter, R. Pickles, J.B.L. Rao, J.O. Coleman, and D.P. Scholnik, "Wideband Digital Subarray Beamforming Using True Time Delay Steering at the Element Level," in *Proc. 2000 Antenna Applications Symp.*, Monticello, IL, Sept. 2000.
[3] P.K. Hughes II, J.Y. Choe, J.B. Evins, J.J. Alter, J.P. Lawrence III, D.C. Wu, G.P. Hrin, W. Habicht II, and P.J. Matthews, "Advanced Multifunction RF Systems (AMRFS)," *2000 NRL Review*, pp. 37-50, June 2000.

High-Power 94 GHz Gyroklystron Amplifier

B.G. Danly,[1] J.P. Calame,[1] B. Levush,[1] K.T. Nguyen,[2] and D.E. Pershing[3]
[1]*Electronics Science and Technology Division*
[2]*KN Research, Inc.*
[3]*Mission Research Corp.*

Introduction: The millimeter wave (MMW) frequency band, extending from 30 to 300 GHz, lies in the regime between microwaves and light. Although the majority of Navy, Marine Corps, and DoD radar, communications, and electronic warfare systems make predominant use of the microwave part of the spectrum, there are increasing numbers of applications in the MMW bands. In many cases, the technology for the generation and amplification of high-power millimeter waves is an extension of traditional technologies used in the microwave bands. Such traditional technologies include RF transistor technologies with a variety of materials, and vacuum electronic technologies with a variety of device types. However, in many cases these traditional technologies are limited in power when pushed to operate in the millimeter-wave bands.

Traditional vacuum electronic amplifiers, such as helix and coupled-cavity traveling wave tubes (TWTs) and klystrons, used in the MMW bands are all slow-wave devices. This means that in order to achieve the coupling between the electron beam and the electromagnetic (EM) wave necessary for the wave amplification, the EM wave must have its phase velocity slowed to roughly the beam velocity by the circuit. To do this and to operate in a low-order mode, the circuit dimensions are typically 10% to 20% of a free space wavelength. This limits the amount of electron beam power that can be propagated through the circuit, and thus limits the achievable MMW RF power obtainable from the device. Typical state-of-the-art average powers for slow-wave devices in the MMW bands range from tens of watts to a few kilowatts. For the situations where higher power is required, one must turn to alternate technologies.

The gyro-devices are a class of vacuum electronic devices in which the EM waves are fast-waves rather than slow-waves. In these devices, the beam-wave coupling is obtained by modification of the electron beam propagation, where the electrons are made to spiral in helical orbits around axial magnetic field lines

from a solenoid magnet. The circuits have transverse dimensions of order a wavelength, and thus are compatible with higher power operation than are slow-wave devices. Gyro-devices come in both oscillator and amplifier configurations. The most studied gyro-amplifier configuration is the gyroklystron.

A variety of radar applications require the development of high-power millimeter-wave amplifiers such as gyroklystrons. Because of the many applications, the NRL Radar Division has embarked on a project to build a high-power W-band (94 GHz) radar, named WARLOC (W-band advanced radar for low observable control), based on this gyroklystron technology. This project is described in a companion article in this *NRL Review*.[1] These radar applications have resulted in continuing interest in gyro-amplifiers, including their many variants, such as the gyroklystron, gyro-twystron, and gyro-TWT.

Gyroklystron Development: To meet the needs of the WARLOC project and other DoD radar needs, the development of a high average power 94 GHz gyroklystron was begun in 1996 with a team formed from NRL personnel, U.S. industry (Communications and Power Industries (CPI) and Litton), and the University of Maryland. Following early successful low-average power prototype demonstrations at NRL,[2] the engineering work on the full 10 kW average power device was carried out by the development team. An extensive suite of engineering codes was used to design this device, including generic commercial codes as well as many specialized codes to model the physics of the gyroklystron performance.

The first device went on test in summer of 1998 at CPI. In this first gyroklystron, an average power of 10 kW was obtained with 11% RF duty factor and 92 kW peak power in the TE_{01} circular cavity mode. At this 10 kW operating point, the instantaneous (3 dB) bandwidth was 420 MHz, and the efficiency was 33.5%. Low-duty-factor testing also yielded a peak power as high as 115 kW with 600 MHz instantaneous bandwidth. This success represents record average power performance in an amplifier at this frequency.

In spite of the success of the first device, several improvements were needed. The gain of the first device was lower than desired, and there was gain ripple on the frequency response due to window reflections. As a result, a second device was designed with five cavities rather than four to increase the gain, and the window match was improved. This second device (Fig. 10) was tested during the spring of 2000.

This second gyroklystron produced 10.2 kW average output power, corresponding to 102 kW peak output power and 31% efficiency. The measured bandwidth was 700 MHz. The maximum output power was achieved with 50 W peak power at the gyroklystron input flange, which corresponds to 33 dB saturated gain.

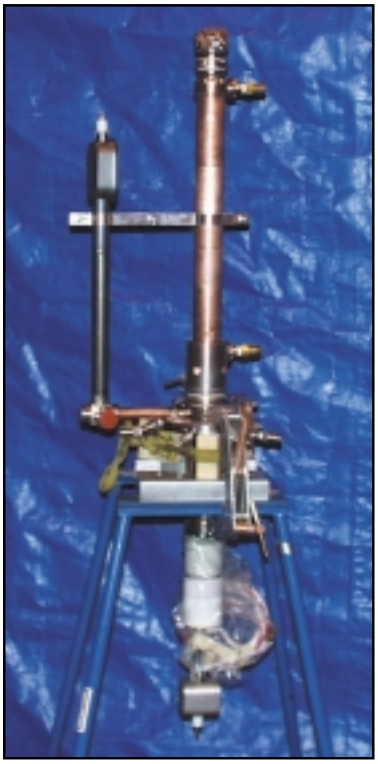

FIGURE 10
The second 94 GHz gyroklystron (VGB-8194 S/N2).

This gyroklystron was also operated at higher magnetic fields, for wider bandwidth and lower power. For example, at a magnetic field of 36.6 kG, with a 55 kV and 6 A beam, the amplifier produced 4 kW average power at 10% RF duty factor with a 3 dB bandwidth of 1050 MHz. At lower voltages, for example 50 kV and 6 A, 8 kW average output power and 95 kW peak output power were achieved at 8.5% RF duty factor. The bandwidth at this point was 775 MHz and the saturated gain was 33 dB. This second device, like the first, has been made available to the NRL Radar Division for the WARLOC radar project.[1]

Summary: The development of gyroklystron amplifier technology now makes possible the many Navy and DoD MMW radar applications that were heretofore limited by the availability of powerful amplifiers in these frequency bands. This development activity has resulted in a twenty-fold increase in MMW average power at 94 GHz compared with prior existing TWT technology.

Acknowledgments: The authors acknowledge their coworkers on this team effort from Communications and Power Industries (M. Blank, K. Felch, B.G. James, P. Borchard, P. Cahalan, and T.S. Chu), and their coworkers on the first development tube from the University of Maryland (W.G. Lawson and T. Antonsen, Jr.), and Litton (T. Hargreaves and R. True).

[Sponsored by ONR]

References

[1] V. Gregers-Hansen, G.J. Linde, W.J. Cheung, B.G. Danly, M.T. Ngo, and R. Myers, "WARLOC: A New High Power 94 GHz Coherent Radar," *2001 NRL Review*, p. 107.

[2] M. Blank, B.G. Danly, and B. Levush, "Demonstration of W-Band Gyroklystron Amplifiers for Radar Applications," *1998 NRL Review*, p. 55-62.

Coherent Operations on the Spin of the Nitrogen-Vacancy Center in Diamond

F.T. Charnock and T.A. Kennedy
Electronics Science and Technology Division

Introduction: Recently, excitement has spread throughout the scientific community over the possibility of creating a quantum computer.[1] "Classical" computers store and operate on information as binary bits: 1's and 0's. However, a quantum computer would use quantum bits (or qubits), which exploit the quantum mechanical property of superposition. A qubit can be 1 or 0, or it can be a superposition of both 1 and 0 at the same time. This permits implementation of new quantum algorithms that can be exponentially faster than their classical counterparts. A example is polynomial factorization, which is at the heart of modern encryption and code breaking, crucial issues to both the defense and public sectors.

However, no practical quantum computing device yet exists. The biggest hurdle is creating a physical qubit that can be controlled over a time long enough to perform useful operations, i.e., a qubit must have a long coherence time. A qubit must also be able to interact with other qubits in a controllable fashion. A quantum spin system makes a particularly good candidate for a qubit, with an "up" spin representing 1 and a "down" spin representing 0. To date, the most successful qubit demonstrations have used the nuclear spin states of simple molecules. However, a solid state qubit would have several advantages, such as compatibility with solid state electronics and scalability to large arrays of qubits.

We are investigating the spin dynamics properties of several solid state systems; the nitrogen-vacancy (N-V) center in diamond has proved to be the most successful so far. This center consists of a substitutional nitrogen atom plus a neighboring carbon vacancy. It is very stable and fluoresces efficiently, and it contains two quantum spins: an electronic spin centered on the vacancy and a nuclear spin due to the nitrogen.

Measuring Coherence: We have performed single qubit operations on the electronic spins in diamond using a combination of optics and microwaves. In the first step, we polarize the spins by moving them into a single spin state. We do this by illuminating the sample with laser light, which creates the spin polarization through the selection rules for absorption and fluorescence (see Fig. 11). Once the spins are polarized, we use microwave pulses to perform operations on them, such as flipping the spins or creating a superposition of up and down spins. Since the intensity of the fluorescence depends on the spin polarization of the ground state, we monitor the resulting spin polarization optically.

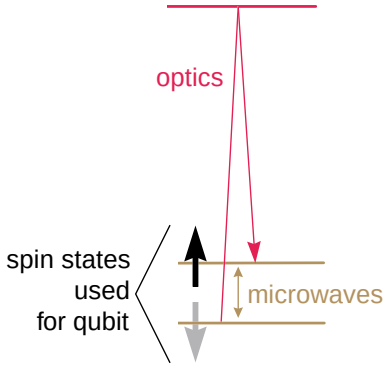

FIGURE 11
Energy level diagram illustrating the transitions used. Spin-dependent optical excitation and decay polarize the spin in the ground state. Microwaves then manipulate the polarization of the spins. The resulting polarization is reflected in the intensity of the fluorescence emitted by the sample.

To measure the spin coherence time of the center, we applied the microwaves in a so-called Hahn spin echo sequence. This is a series of microwave pulses that first moves the spins into a superposition state (both up and down) and then returns them to their original orientation after a delay t_e (the echo). Figure 12 illustrates the results for echoes with three different delays. As the delay increases, various decoherence processes reduce the intensity of the observed echo.

In our sample, we find the N-V center has a coherence time of 3.3 µs. This is much longer than the

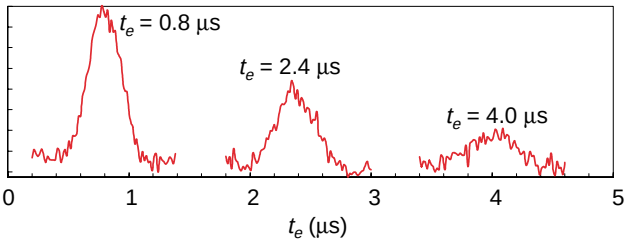

FIGURE 12
Measured spin echoes for electronic spins with increasing delay times. As the echo delay increases, the coherence of the spins and the intensity of the echo decreases.

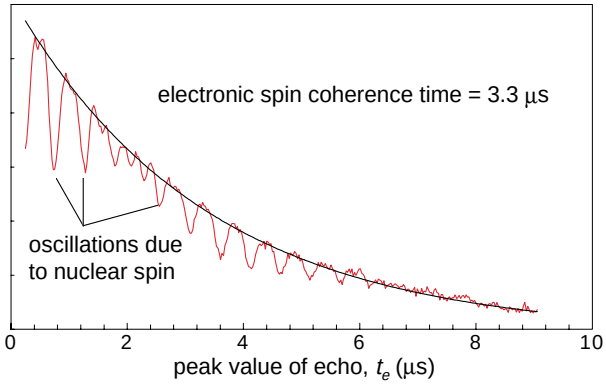

FIGURE 13
Peak values of the spin echo as a function of echo delay. The overall envelope of the spin echo decays with a time constant of 3.3 µs (note black curve). Within this envelope are oscillations arising from magnetic interactions with the nuclear spin of the nitrogen.

coherence times of most other solid state systems. One measure of the technological potential of a spin system is the number of operations that can be performed within the coherence time. Using 3-ns microwave pulses, 1000 spin operations can be performed before coherence is lost. This approaches the number of operations required for simple quantum computations. Better understanding of the sources of decoherence in diamond will permit the development of materials with even longer coherence times.

Qubit Interaction: In addition to single qubits, a practical computer will also require two qubit gates. These are formed from two single qubits with a controllable interaction between them. In the N-V center, such a pairing is possible due to the coupling of the electronic spin and the nuclear spin of the nitrogen. A detailed look at the decay envelope of the electron spin echo reveals oscillations arising from the coherent interaction of the two spins (Fig. 13). The strength of this interaction can be varied with the intensity of the applied microwave pulse. This is the first observation of this type of interaction between these spins in the N-V center, and it permits the implementation of a two-qubit gate.

Conclusion: Our work has shown both the potential of the N-V center as a qubit and the value of a combined optical/microwave approach to working with qubits. A 3.3 ms coherence time sets a standard for qubit lifetimes in the solid state, and the interaction of the electronic and nuclear spins provides the potential for a two-qubit gate. Microwave manipulation permits wide flexibility in controlling the spins. Optical detection provides unmatched sensitivity in observing spin states. This approach allows the extension of this work to single N-V centers and moves the state of the art closer to a practical quantum computer.

Acknowledgments: We thank Steve Rand of the University of Michigan for providing the diamond.
[Sponsored by ONR]

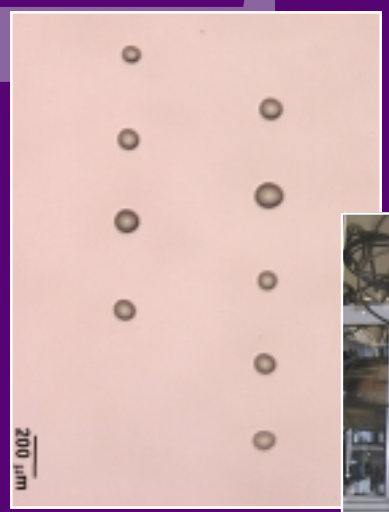

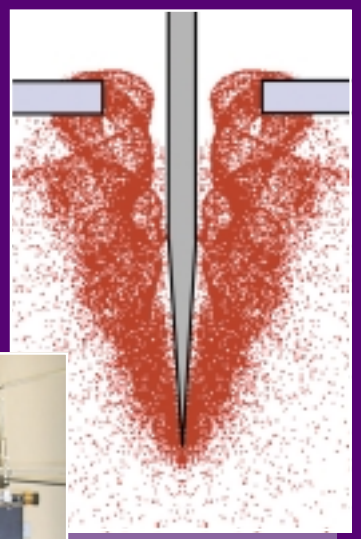

Energetic Particles, Plasmas, and Beams

Laser Direct Writing of Living Cells and Active Biomaterials

B.R. Ringeisen,[1] D.B. Chrisey,[1] B. Spargo,[2] and A. Piqué[1]
[1]*Materials Science and Technology Division*
[2]*Chemistry Division*

Introduction: Methods to generate mesoscopic patterns of viable cells and active biomaterials are required to fabricate next-generation cell, protein, or antibody-based microfluidic biosensor arrays; gene and protein recognition microarrays; and three-dimensional (3D) cellular structures for advanced tissue engineering. They are also required for selectively separating and differentially culturing microorganisms for a variety of basic and applied research applications. Specific DoD applications include the fabrication of miniature biological and chemical warfare agent sensors, environmental contaminant sensors, advanced materials coatings on controlled biological systems (i.e., remote sensing devices attached to insects), and microscopic implantable systems that could sense fatigue or pain and activate drug release in the body to extend human ability in key individuals (surgeons, astronauts, warfighters, etc.). Potential commercial applications include the fabrication of microfluidic chemical and biosensors, miniaturized chemical and biological analytical tools ("lab-on-a-chip" technology), and DNA and antibody microarrays for genomics and proteomics analysis, respectively. Each of these applications requires a technique that forms biomaterial patterns adjacent to or compatible with electronic platforms or various detection devices.

At present, only limited technologies are capable of writing adjacent patterns or three-dimensional structures of different biomaterials, much less patterns that are software-generated, have micron resolution, and can be written at submillisecond times. We have developed a laser-based transfer process that is capable of forming patterns and 3D structures of living cells and active biomaterials with resolution of less than 10 microns. This laser transfer technique is capable of forming interfaces between biological and electronic materials by patterning biotic (living microorganisms, active proteins, enzymes, DNA, antibodies, etc.) and abiotic (passive electronic devices and other inorganics) material adjacently on the same substrate. This technology also eliminates the need for masks or moulds when fabricating surface patterns of biomaterials, can be driven by computer-aided design/computer-aided machining (CAD/CAM), allows rapid prototyping without the use of mask patterning and/or photolithography steps, and is compatible with almost any substrate.

Method: Matrix-assisted pulsed laser evaporation direct write, or MAPLE DW, is a laser-based processing technique that was originally designed to fabricate and rapidly prototype mesoscopic electronic devices from composite materials.[1,2] We also find that this process is gentle enough to successfully transfer a wide variety of organics including polymers and active proteins. Figure 1 is a schematic of the MAPLE DW technique. The material to be transferred is mixed in an ultraviolet (UV)-absorbent matrix and coated onto a quartz disk that is UV transparent. A focused UV laser pulse is directed through the backside of the quartz support so that the laser energy first interacts with the matrix at the quartz interface. The laser pulse is focused at the matrix-support interface by a UV microscope objective that also serves as an optical guide to determine the area of the matrix to transfer. Layers of matrix near the support interface evaporate due to localized heating from electronic and vibrational excitation. This sublimation releases the remaining material farther from the interface by gently and uniformly propelling it away from the quartz support to a substrate positioned 25 to 100 microns

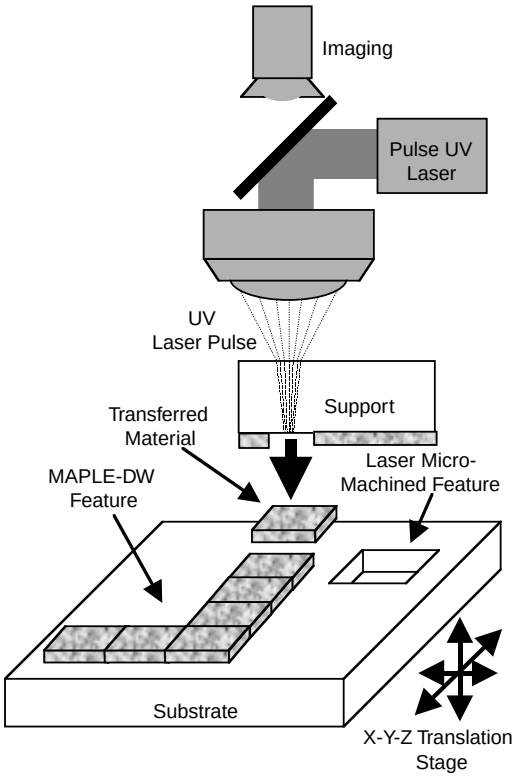

FIGURE 1
MAPLE DW is a laser-based technique that transfers patterns of inorganic materials. A novel variation of this laser transfer technique is not only capable of optically imaging and directly writing micron-scale patterns of passive electronic devices, but is also capable of forming patterns of polymers, active proteins, and living cells.

away. MAPLE DW is capable of producing passive electronic devices (i.e., interconnects, resistors, capacitors) with line widths under 10 microns. By removing the quartz support and allowing the laser pulse to interact with the substrate, this approach is also able to micromachine channels and through vias into polymer, semiconductor, and metal surfaces, as well as to trim passive devices to meet design specifications. All micromachining and material transfer can be controlled by computer (CAD/CAM), which enables this tool to rapidly fabricate complex structures without the aid of masks or moulds.

Biomaterial Patterns: We have successfully used a novel variation of MAPLE DW to directly write patterns of living *Escherichia coli*, living Chinese hamster ovaries (CHO), and bovine serum albumin onto various substrates ranging from nutrient culture plates to semiconductors and functionalized glass slides.[3 4]

Bovine Serum Albumin: Figure 2 is an optical micrograph of an array of active biotinylated bovine serum albumin deposited onto an aldehyde-treated glass slide by our laser-transfer technique. The spot size of deposited protein by our method ranges from 50 to 100 microns, whereas current available techniques produce spots with a minimum diameter of several hundred microns. This test experiment demonstrates that our technique is capable of fabricating a high-density microarray. Future experiments using the same procedure will deposit microarrays of antibodies specific to a variety of classes of cancer-related proteins including intracellular and extracellular matrix proteins, signaling proteins, cell cycle proteins, growth factors, and growth factor receptors.

E. Coli Bacteria: Figure 3(a) is an optical micrograph of an *E. coli* pattern transferred using MAPLE DW. The line width of the pattern is approximately 100 microns and demonstrates the ability of our approach to accurately place biomaterials on a glass substrate. *E. coli* cells containing the jellyfish *Aequorea victoria* green fluorescent protein (GFP) have been used to assess cell viability and to positively identify the transferred microorganisms from possible contaminants. Figures 3(b) and 3(c) are micrographs of a ceramic/*E. coli* composite patterned to write "NRL" (portion of "R" shown) under white and UV light, respectively. The characteristic fluorescence of the GFP is emitted only in the areas where *E. coli* was written. This relatively large pattern was written to transfer enough bacteria to observe the green fluorescence shown in Fig. 3(c). When the pattern was submerged in Luria-Bertani (LB) broth, fluorescence remained over a period of several days, indicating the bacteria were viable after transfer and that the composite material used as a matrix acted to immobilize the transferred cells.

Patterns of cells were also formed using a variety of different materials as stabilizing agents for the transfers. Mixing *E. coli* and cell media with nutrient agar or other composite materials provided a stable platform for room temperature experiments. Successful transfers were also performed without adding solidifying materials by freezing a thin film of cells and cell media to the support. This versatility in the types of materials that can be transferred by this technique is an advantage over current approaches that are only capable of patterning cells alone. Our method, for example, could be used to transfer cells with the nutrients, proteins, or amino acids needed to grow, adhere to the substrate, multiply, or maintain functionality. By using a rigid, biocompatible matrix such as collagen or sol-gels, our method could also form 3D cellular structures that encapsulate the transferred cells and maintain the desired structure in various environments. In addition, the serial nature of this technique enables multiple layers to be constructed step-by-step from various biomaterials.

Chinese Hamster Ovaries (CHO): The next step in complexity for transferring living cells is to form patterns of mammalian cells. These cells are

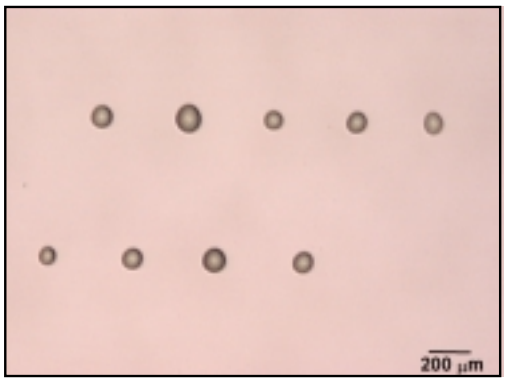

FIGURE 2
Microarray of biotinylated bovine serum albumin fabricated by our laser transfer technique. Spot sizes range from 50 to 100 microns.

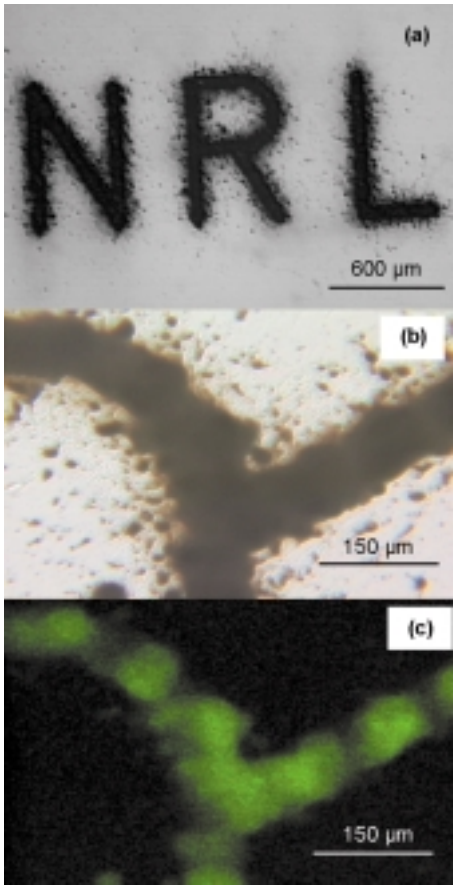

FIGURE 3
(a) Optical micrograph of laser-transferred ceramic/*E. coli* composite pattern. Scale equals 600 microns. (b-c) Transferred *E. coli* under white light (b) and 365 nm UV exposure (c). Green fluorescence is observed from viable cells expressing the green fluorescent protein (GFP). Scale is equal to 150 microns.

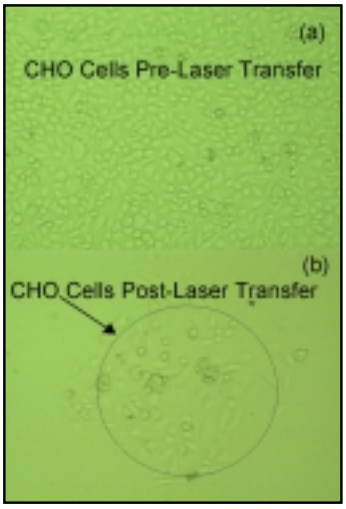

FIGURE 4
(a) Micrograph of living Chinese hamster ovaries (CHO) before laser transfer. (b) Laser-transferred 200-microns diameter pattern of living CHO cells.

generally larger and more fragile than bacteria, and would therefore be more susceptible to the shear forces present during the laser transfer. Figure 4(a) is a micrograph of native (pre-transfer) CHO cells, while Fig. 4(b) is an optical micrograph of several CHO cells after laser transfer (dotted circle outlines the 200-micron spot of transferred cells). Figure 4(b) shows the growth and reproduction of the transferred CHO cells after three days in growth media. We observe no damage to the plasma membrane post-transfer, and the transferred cells appear very similar to the native cells in panel (a). The increased size and stretched appearance (attachment to the substrate) verify the viability of the transferred species.

Summary: We have demonstrated the formation of novel patterns of living cells and active proteins by a new laser transfer technique. In the future, we will use this approach to produce improved microfluidic biosensor arrays, to fabricate protein identification antibody arrays, to electronically probe intercellular signaling, to control the transfer and placement of pleuripotent mammalian cells for differential culturing, and even to form 3D biological structures not found in nature (e.g., combinations of unique cells or cell arrays).

Acknowledgments: B.R. Ringeisen thanks the National Research Council for his postdoctoral fellowship. We thank R.A. McGill for discussions pertaining to the approach presented in this article and D. Krizman (Advanced Technology Center, National Cancer Institute, National Institutes of Health) for collaborating with NRL to help accomplish this work.

[Sponsored by ONR]

References

[1] A. Piqué, et al., "A Novel Laser Transfer Process for Direct Writing of Electronic and Sensor Materials," *App. Phys. A - Mat. Sci. Proc.* **69**, S279-S284 (1999).

[2] D.B. Chrisey, et al., "New Approach to Laser Direct Writing Active and Passive Mesoscopic Circuit Elements," *App. Surf. Sci.* **154**, 593-600.

[3] B.R. Ringeisen, D.B. Chrisey, A. Piqué, and R.A. McGill, "Generation of Living Cell and Active Biomaterial Patterns by Laser Transfer," patent pending, Navy Case #82,621.

[4] B.R. Ringeisen, et al., "Generation of Mesoscopic Patterns of Viable *Escherichia coli* by Ambient Laser Transfer," submitted to *Biomaterials* (2000).

Breakthroughs in Concentrating Pulsed, High-Power Electron Beams for High-Intensity X-Ray Applications

B.V. Weber, R.J. Commisso, G. Cooperstein, D.D. Hinshelwood, D. Mosher, P.F. Ottinger, J.W. Schumer, and S.J. Stephanakis
Plasma Physics Division

J.R. Boller, S.B. Swanekamp, and F.C. Young
JAYCOR

A New X-ray Source for Pulsed Hydrodynamic Radiography: Pulsed-power generators, such as NRL's Gamble II, drive vacuum diodes that produce short-duration (< 100 ns), high-power (> 10^{12} W), high-voltage (> 1 MV) electron beams. X rays are generated when the electrons deposit energy in a high-atomic-number (e.g., tungsten) anode. If the x-ray source is sufficiently intense and penetrating and if the source size is sufficiently small, it can be used to radiograph dense matter under extreme conditions. We recently made two breakthroughs in this area: (1) The "rod pinch" diode concentrates electrons at the end of a small diameter (< 1-mm) rod, achieving electron power densities in excess of 10^{12} W/cm^2, suitable for the radiography application. (2) A variation of this technique, called a "plasma-filled rod pinch" diode increases the concentration of beam energy 10 to 100 times and may lead to superior radiography sources.

The rod pinch diode was invented at NRL in the 1970s.[1] The device had no important application at that time, but new results at NRL have made it an important part of the DOE Stockpile Stewardship Program,[2] where it will be used in underground experiments to diagnose subcritical nuclear weapon experiments. The rod pinch diode generates high-energy X rays (100 keV to 2 MeV) that can penetrate through high-density objects to create a radiograph on a detector (film or an active device). The short duration of the x-ray pulse "freezes" the motion of the moving mass. The x-ray source must be small enough to obtain adequate resolution on the detector, and intense enough to be detected with adequate signal-to-noise ratio. The rod pinch diode has been selected as the radiography source for subcritical tests requiring x-ray energy < 2 MeV based on its demonstrated x-ray production and small source size.

Rod Pinch Diode Physics: Figure 5 shows the setup and operation of the rod pinch diode on Gamble II. The parts are inside a vacuum chamber and are connected to the output terminals of the generator.

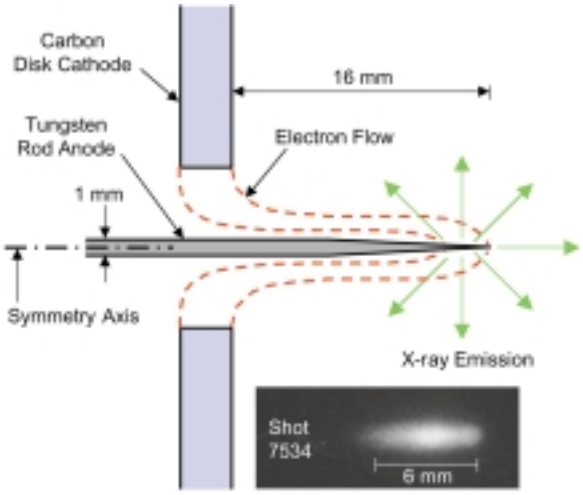

FIGURE 5
Gamble II rod pinch experiment with x-ray image for shot 7534. Electrons (red dashed lines) emitted from the disk cathode (blue) flow to the tip of the tapered rod anode (gray) producing X rays (green) over the last 6 mm. (Note: the axial and radial extent of the x-ray emission is less than indicated in the photograph by 0.9 mm due to pinhole blurring.)

The central tungsten rod is pulsed to a high positive voltage (1.85 MV for shot 7534) while the outer carbon cathode is kept at ground potential. Electrons emitted from the cathode accelerate radially inward toward the rod across the 4.5-mm gap. The electrical current in the rod (48 kA for shot 7534) creates an azimuthal magnetic field that bends the electron orbits toward the tip of the rod, as indicated by the "electron flow" lines in the figure. The x-ray emission recorded on film for shot 7534 indicates that the beam deposition is concentrated in the last 6 mm of the tapered rod. When viewed end-on, the x-ray source is circular, with less than 1 mm diameter. The combination of high x-ray dose (2.8 R at 1 m for shot 7534) and small source diameter (less than 1 mm) catapulted this technique ahead of its competitors, making it the chosen technique for radiography diagnostics at the 2-MV level for subcritical underground tests.

Rod pinch operation is understood using a combination of analytic theory and computer modeling.[2] Computer simulations based on electrical waveforms and electrode configurations from Gamble II predict the motion of electrons and ions. Figure 6 is an example showing electron positions at a moment in time. The electrons are impeded from crossing directly from the cathode to the rod by the large self-generated magnetic field. Instead, the electrons flow to the tip of the rod where they are absorbed. Ions emitted from the rod (not shown in Fig. 6 but included in the calculation) neutralize

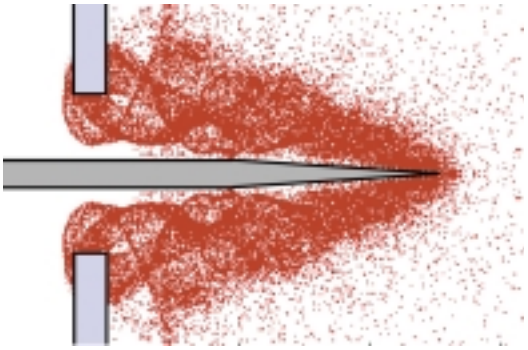

FIGURE 6
Numerical simulation of Gamble II rod pinch experiment showing electron positions (red) at a moment in time.

the electron charge to a great extent, a necessary condition for beam propagation to the tip. Theory and modeling play an important role in understanding and exploiting the rod pinch phenomena for all applications.

Plasma-Filled Rod Pinch Diode: An exciting improvement to the rod pinch occurs when the anode-cathode gap is initially filled with a plasma (a low-density gas consisting of electrons and ions). This configuration, as fielded on Gamble II, is depicted in Fig. 7. Two cathode disks are used to collimate the injected plasma. The plasma acts as an initial short circuit, allowing the current to increase while keeping the voltage small. The magnetic pressure displaces the plasma toward the tip of the rod. After a short-circuit phase that lasts 10 to 30 ns, the impedance of the diode increases to a value that typically is small compared with the standard rod pinch. We hypothesize that a vacuum gap forms between the plasma and the rod, in the vicinity of the rod tip, with the gap size much smaller than the gap between the metal electrodes. Low impedance means that much more current can be coupled to the diode at a given voltage. In the first Gamble II experiments, the coupled current and voltage varied from 260 kA and 1.8 MV to 770 kA and 0.45 MV, depending on the initial density of the injected plasma. This represents an order-of-magnitude increase in coupled energy and power compared with the standard rod pinch, and indicates that the plasma-filled rod pinch diode is a versatile x-ray source. The x-ray dose is greater by an order of magnitude and the spot size remains small, about equal to the rod diameter (0.5 mm for shot 7813). The x-ray emission is concentrated near the tip of the rod, even when the rod extends 50 mm from the plasma injection region. Analytic theory and computer simulation of this configuration are much more difficult than for the standard rod pinch diode. Techniques to address this problem are under development.

We speculate that the high currents and voltages, combined with the small diameters, may produce record energy densities and interesting plasma conditions at the tip of the rod. Estimated values of some relevant parameters using typical Gamble II data are: B = 2 to 6 MG (magnetic field near the rod surface); J = 50 MA/cm^2 (current density at the rod tip); P = 100 TW/cm^2 (electron power incident on the tip); and solid-density tungsten plasma with T > 100 eV (assuming the electron energy is absorbed in a 0.5-mm diameter sphere).

Future Applications: The rod pinch diode is now established as the best x-ray source for pulsed, 1 to 2 MV radiography for subcritical underground

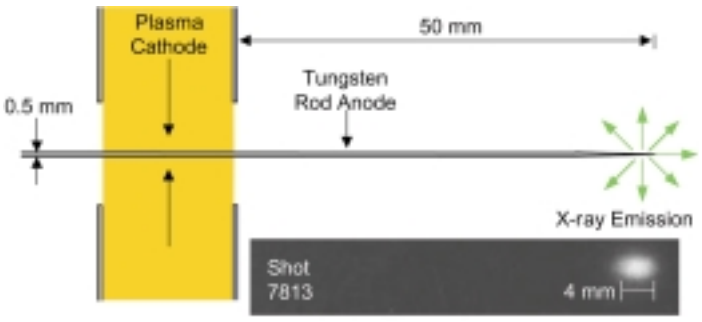

FIGURE 7
Gamble II plasma-filled rod pinch experiment with x-ray image for shot 7813. Plasma (yellow) injected between two disks (blue) connects the cathode and rod anode (gray). After a gap forms between the plasma and the rod, X rays (green) are emitted from the tip of the tapered 0.5-mm diameter rod. (Note: the axial and radial extent of the x-ray emission is less than indicated in the photograph by 1.7 mm due to pinhole blurring.)

tests. The utility of this source for future radiography applications depends on its ability to scale to even higher voltage. The plasma-filled rod pinch diode is truly a breakthrough in concentrating electron beam energy into a small volume. Its impedance time history makes it an ideal candidate to be driven by compact, high-voltage pulsed power devices. Applications for this device include improved radiography, x-ray-matter interaction studies, and high-energy-density plasma generation.

[Sponsored by ONR and DOE]

References

[1] R.A. Mahaffey, J. Golden, S.A. Goldstein, and G. Cooperstein, "Intense Electron-Beam Pinch Formation and Propagation in Rod Pinch Diodes," *Appl. Phys. Lett.* **33**, 795-797 (1978).

[2] R. Jeanloz, "Science-Based Stockpile Stewardship," *Phys. Today* **53**, 44-50 (2000).

[3] S.B. Swanekamp, R.J. Commisso, G. Cooperstein, P.F. Ottinger, and J.W. Schumer, "Particle-in-Cell Simulations of High-Power Cylindrical Electron Beam Diodes," *Phys. Plasmas* **7**, 5214-5222 (2000).

Electron Beam-Produced Plasmas for Materials Processing

R.A. Meger
Plasma Physics Division

Introduction: Advances in materials processing are, to a large extent, responsible for the technological revolution that has driven the world's economy over the last decade. Much of this is due to the development of plasma processing to etch circuits or deposit layers of material on surfaces. Plasma processing uses low-pressure ionized gases rather than liquids to deposit or remove materials from surfaces. These techniques are responsible for the shrinking size and increased capability of computers that now appear in nearly every aspect of military and civilian life. To maintain and extend this revolution, there is a continuous search for improved manufacturing techniques to further decrease integrated circuit feature size while increasing the size of the surface processed. Smaller features allow more complex circuits that operate at lower power, while larger areas are good for manufacturing economics and new applications such as flat panel displays.

Conventional plasma generation techniques use various kinds of electrical discharges driven in a low-pressure gas. This technology is well developed, but it may not be able to scale to finer features and larger areas. NRL has been developing a new technique that may remedy some of the scaling difficulties. This new technique uses energetic electron beams to create a large-area plasma sheet that can be used to process large-area surfaces. The beam-generated plasma is at the heart of NRL's Large Area Plasma Processing System (LAPPS).[1] The technique offers a means to better control the etch process for smaller feature size, while also offering larger area plasmas for larger circuits or manufacturing efficiency.

Beam-Generated Plasma System: Figure 8 shows a schematic side view of a LAPPS processing reactor. The electron-beam source at the left is used to produce a 2 to 3 kV, ~5 mA/cm^2, 1-cm thick sheet beam of electrons.[2] The source can be pulsed or continuous, depending on the type of processing to be done. The 30 to 100-cm wide beam of electrons is injected into a 1-m long rectangular cross section, low-pressure gas chamber. The beam electrons follow a 100 to 300 Gauss magnetic field as they cross the chamber, ionizing the background gas, and eventually being collected by the beam dump at the far side. The ionization process is efficient because of the large beam energy. The result is a cold, dense plasma sheet within the beam channel. Materials placed on a processing stage close to the plasma sheet are exposed to the plasma. Ions, excited neutrals, and free radicals (e.g., oxygen atoms) flow out from the plasma, striking the surface. A radio frequency bias voltage can be placed on the stage to control their impact energy. The ion and free radical fluxes can be controlled by varying the background gas fill and the location of the plasma relative to the surface. The plasmas produced using this technique can have square meters of area suitable for processing. The technique can also be used to ablate material from surfaces and deposit it on others for precision coatings. Experiments to date have produced uniform, 1-cm thick plasmas with up to 10^{12} cm^{-3} density, 60 × 60-cm areas, and electron temperatures ~1 eV. Figure 9 shows a portion of the LAPPS processing chamber with the magnetic field coils and diagnostics stuck through different ports in the ultra-high vacuum chamber. Figure 10 shows views of a plasma layer through a vacuum port. The side view (Fig. 10(a)) shows how thin the plasma sheet is; the top view (Fig. 10(b)) shows its large area.

Summary and Prognosis: LAPPS represents a radically different means of making a plasma suitable for processing. It offers advantages over other techniques such as high plasma production efficiency, low plasma temperature, improved control of plasma composition, additional parameters for processing control, and much larger area. It shows promise for coating large areas for production of new materials,

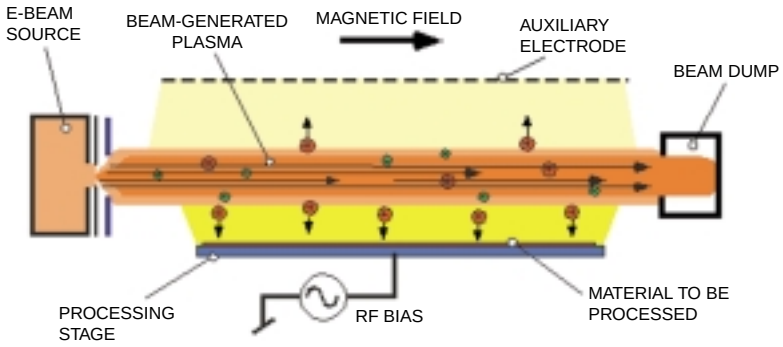

FIGURE 8
Schematic of LAPPS processing system.

FIGURE 9
Vacuum chamber used in LAPPS research.

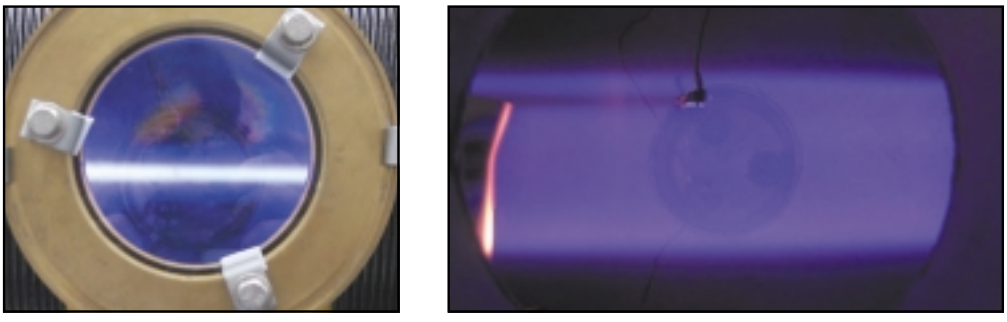

(a) Side view (b) Top view

FIGURE 10
Beam-produced plasma sheet.

improved wear resistance, or better surface adhesion properties. Spin-offs of the technology also show promise in waste gas treatment for biohazards or chemical pollutants and in non-equilibrium gas chemistry. The Navy will benefit from advances in all of these areas.

Acknowledgments: Co-investigators include R. Fernsler, M. Lampe, D. Leonhardt, W. Manheimer, and D. Murphy of NRL and D. Blackwell and S. Walton, NRC Postdoctoral fellows.

[Sponsored by ONR]

References

[1] R.A. Meger, R. F. Fernsler, M. Lampe, and W. Manheimer, U.S. Patent No. 5,874,807, dated February 23, 1999.

[2] W.M. Manheimer, R.F. Fernsler, M. Lampe, and R.A. Meger, "Theoretical Overview of the Large-Area Plasma Processing System (LAPPS)," *Plasma Sci. Technol.* **9**, p. 370-386 (2000).

Compact Source of Tunable, Monochromatic, Picosecond X rays

A.C. Ting, R. Fischer, C.I. Moore, and P. Sprangle
Plasma Physics Division

M. Baine and S. Ride
University of California at San Diego

Many applications in medicine, material studies, and basic scientific research can benefit tremendously from a source of tunable, monochromatic, polarized, and picosecond X rays. These include K-edge differential angiography, high-contrast mammography, x-ray magnetic circular dichroism, picosecond resolution of phase transitions and energetic dynamics, and many others. At present, some of these applications can only be carried out at the few national synchrotron laboratories using elaborate filtering techniques on the synchrotron radiation. NRL has proposed a unique tunable, monochromatic x-ray source, the Laser Synchrotron Source (LSS).[1,2] It can produce these valuable X rays in a compact configuration. Demonstration experiments at NRL have produced X rays at 370 eV (3.37 nm) with good agreement to theoretical predictions.

Introduction: The LSS mechanism relies on the Thomson scattering of electromagnetic radiation, such as from a laser, by electrons traveling at relativistic velocities. The electrons oscillate in the field of the radiation, which is Doppler-shifted to about twice its original frequency in the rest frame of the relativistic electron. As the electron reradiates, the observed frequency of the radiation from this source is further Doppler-shifted. The laser radiation can be Doppler upshifted to x-ray frequencies by as much as $4\gamma^2$ (in a backscattering geometry), where γ is the relativistic mass factor of the electrons. For example, a 527-nm photon (2.35 eV, frequency doubled Nd:YAG laser), when backscattered from a 30-MeV electron, is upshifted to an x-ray photon of 33.55 keV (a suitable energy for iodine K-edge differential angiography). Since the laser radiation is monochromatic and polarized, these X rays are also monochromatic and polarized. With the advent of picosecond electron beams and laser beams, subpicosecond x-ray pulses can be generated for picosecond time-resolved diagnostics of fast kinetics and reactions. Figure 11 is a schematic of the interaction configuration. The X rays are emitted in the forward direction of the electron beam and are confined to an angular region of $\sim 1/\gamma$ radians due to relativistic effects.

Demonstration Experiment: We have performed an experiment to demonstrate the production of X rays in the water transmission window at a wavelength of ~3 to 4 nm. The laser photons are derived from a Nd:Glass laser in a 10-ns pulse with ~5 J of energy. The relativistic electrons are gener-

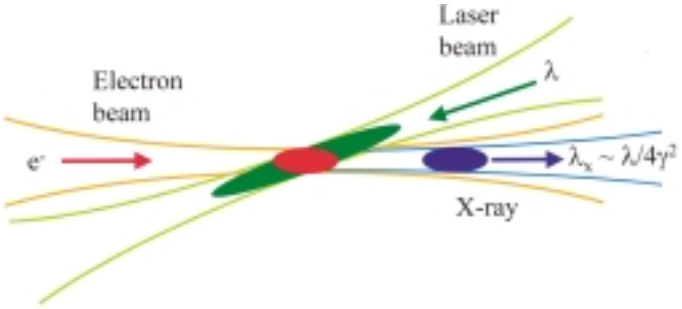

FIGURE 11
LSS interaction configuration.

ated by a radio-frequency (RF) electron gun driven at the S-band frequency of 2856 MHz. A 300-mA, 500-ns pulse of relativistic electrons at 4.1-MeV energy is produced. This high-quality electron beam, with an energy spread $\Delta E/E \sim 1\%$, is focused to less than 1 mm at the interaction region where the counter-propagating laser pulse is also focused. Figure 12 shows the electron beam line during construction. The interaction region is in the vicinity of the yellow beam dump magnet on the right. The beam line is now inside a concrete block enclosure for radiation safety shielding.

The laser pulse is synchronized to arrive at the interaction region near the center of the electron beam pulse. Electron beam and laser monitors at the interaction region allow spatial alignment of the two beams. The x-ray photons that are generated travel in the same direction as the electron beam and propagate forward while the spent electron beam and laser beam are dumped separately. The x-ray detector is a 21-stage electron multiplier tube (EMT). The first stage of the multiplier with its aluminum oxide coating is an excellent x-ray photocathode. It is insensitive to both the infrared radiation from the laser and the high-energy bremsstrahlung X rays from the electron beam. The EMT is calibrated separately to convert its signals to an absolute measurement of x-ray photon numbers. The number of photons per pulse is measured to be 1×10^7. The results are shown in Fig. 13, where the experimental data lie close to the predicted values for the range of laser beam energies used in the experiment. Energy measurements of the X rays confirmed the 370-eV (3.37-nm) photon energy predicted by the Doppler upshift formula at our measured electron beam energy. The energy spread of the x-ray photons was measured to be 2%, which agrees very well with the prediction using the electron beam's energy spread. Ongoing experiments include measurements of the angular distribution of the X rays and harmonic production due to intense laser excitation of nonlinear electron oscillations.

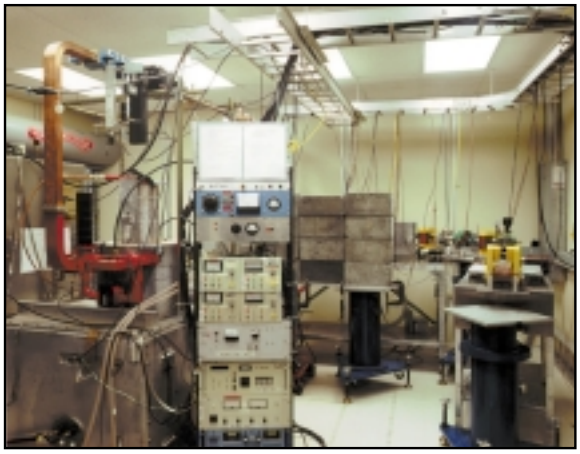

FIGURE 12
The NRL 4 MeV RF electron gun beam line. The 20 MW S-band klystron is shown on the left and the electron beam propagates toward the reader on the right.

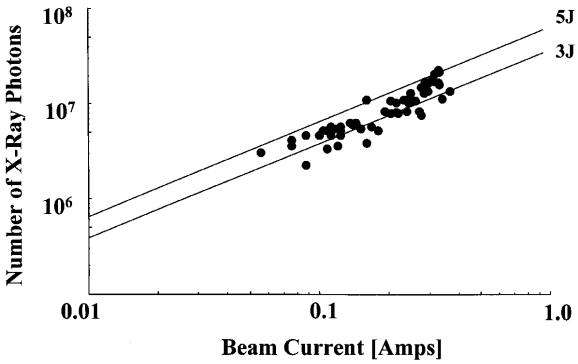

FIGURE 13
Number of x-ray photons generated per pulse as a function of electron beam energy and laser beam energy. The two straight lines indicate the predicted photon numbers for laser beam energies of 3 J and 5 J, respectively.

Summary: The LSS is a unique scheme of generating tunable and monochromatic X rays. A compact x-ray source with the desirable characteristics of a tunable, monochromatic, polarized, and ultra-short x-ray pulse is very useful in many applications relevant to both Navy missions and civilian benefits.

Acknowledgments: The authors thank Ray Elton and Ray Burris for their technical assistance in the experiment.

[Sponsored by ONR and MFEL]

References

[1] P. Sprangle, A. Ting, E. Esarey, and A. Fisher, "Tunable, Short-pulse Hard X-rays from a Compact Laser Synchrotron Source," *J. Appl. Phys.* **72**, 5032 (1992).

[2] A. Ting, R. Fischer, A. Fisher, K. Evans, R. Burris, J. Krall, E. Esarey, and P. Sprangle, "Observation of 20 eV X-ray Generation in a Proof-of-Principle Laser Synchrotron Source Experiment," *J. Appl. Phys.* **78**, 575 (1995).

Information Technology and Communication

The Multicast Dissemination Protocol

J.P. Macker
Information Technology Division

R.B. Adamson
Newlink Global Engineering Corp.

Background: An ever-increasing number of Navy, Department of Defense (DoD), and commercial information network systems are relying on the Internet Protocol (IP) suite of protocols for support of information systems operations. While historical IP applications and network services focused on data exchange between fixed pairs of end points within the network, recent IP multicasting technology standards support group-based (one-to-many or many-to-many) communications. While providing powerful building blocks for a wide range of group networking applications, present IP multicast core building blocks and standards lack functionality in data transport reliability and dynamic congestion control. The NRL Multicast Dissemination Protocol (MDP) addresses these technology gaps by functioning as a reliable multicast transport protocol and by directly supporting research efforts in multicast transport congestion control.

Technical Overview and Software Tools: In designing MDP, we considered a broad range of operational goals, including

- use in heterogeneous, internetworking infrastructures;
- use in mobile and wireless network environments;
- operation in asymmetric delivery scenarios;
- support for scaling from small to large multicast group sizes; and
- support for significant group membership dynamics.

These factors are important general considerations for any scalable or flexible multicast protocol design, but they also provide additional design focus on particularly challenging military environments and applications areas.

Figure 1 is a high-level representation of MDP operating within a heterogeneous internetworking architecture. MDP mainly relies on receiver group feedback techniques to enforce data transport reliability, but it also supports improved reliability for groups of silent receivers when appropriate. Primary data transport reliability is accomplished by using multicast-oriented, selective negative-acknowledgment (NACK) techniques and by incorporating NRL-developed multicast parity-based repairing mechanisms based on packet-level information coding concepts.[1] (Previous multicast research has shown that selective NACK protocols are more scalable and efficient than those based on positive acknowledgment (ACK).[2]) These information coding extensions to the protocol have dramatically improved overhead efficiency, delivery delay, and robustness. Also, the hybrid protocol and coding techniques demonstrate additional performance advantages in error-prone wireless environments and across scaled wide-area network (WAN) sessions (e.g., use in the Internet backbone).

Reliable multicast transport protocol design is a rich area of research, and a variety of solutions and performance issues are widely discussed in the literature.[3,4] General research consensus holds that no "one size fits all" solution across the myriad of application semantics and networking architectures is foreseen. MDP, for example, was initially designed as a reliable multicast bulk transfer protocol for use in heterogeneous network environments. In addition to reliably transporting bulk data, recent MDP enhancements support the effective transport of small, self-contained application data messages within a multicast session. MDP operation assumes no special structure in the network architecture, and typically works in a completely end-to-end fashion with minimum system complexity and cost impact.

MDP and its software toolkit[5] have recently been adapted to a number of real uses and applications within both military and commercial systems. The software toolkit (<http://manimac.itd.nrl.navy.mil/MDP>) works across a wide set of existing operating systems and is relatively simple to install, since it builds on top of the existing UDP/IP multicast functionality. Network applications demonstrated with the protocol toolkit include Web content multicasting, imagery dissemination, directory replication, generic multicast file transfer, shared data spaces, and integration into distributed situational awareness applications (e.g., U.S. Army FBCB2, Navy GCCS-M). The MDP Application Programming Interface (API) provides a common programming method for application designers to use and control protocol features. Figure 2 is a screenshot of an MDP application providing Web-based hypertext content and imagery during worldwide Internet Multicast Backbone (MBone) testing, using a standard Web browser as a multicast media content viewer (winMDP operates with Netscape or Internet Explorer).

Congestion Control Research Support: Present MDP and related simulation tools developed

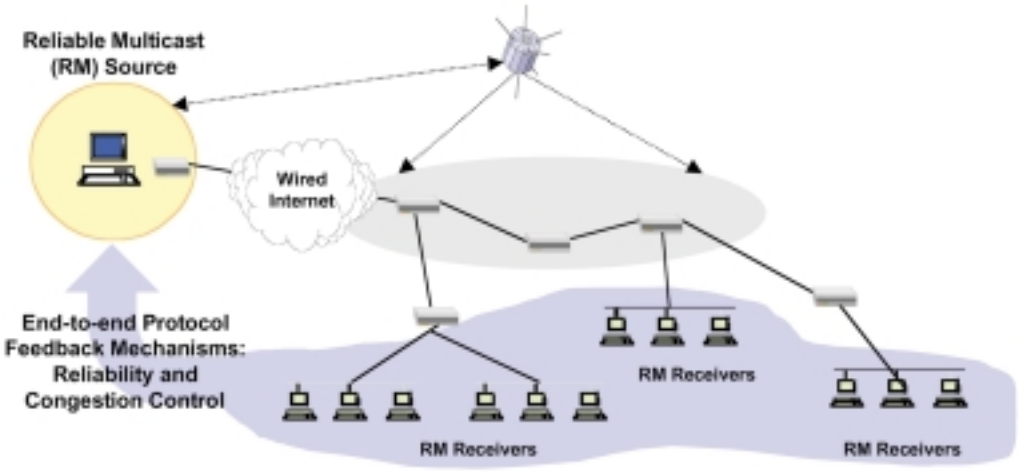

FIGURE 1
High-level functional view of reliable multicasting within an example internetworking architecture. MDP is designed to act as an end-to-end reliable multicast data transport protocol. ADP addresses the needs of both high-speed wired networking infrastructures and more challenging satellite and wireless network operational characteristics.

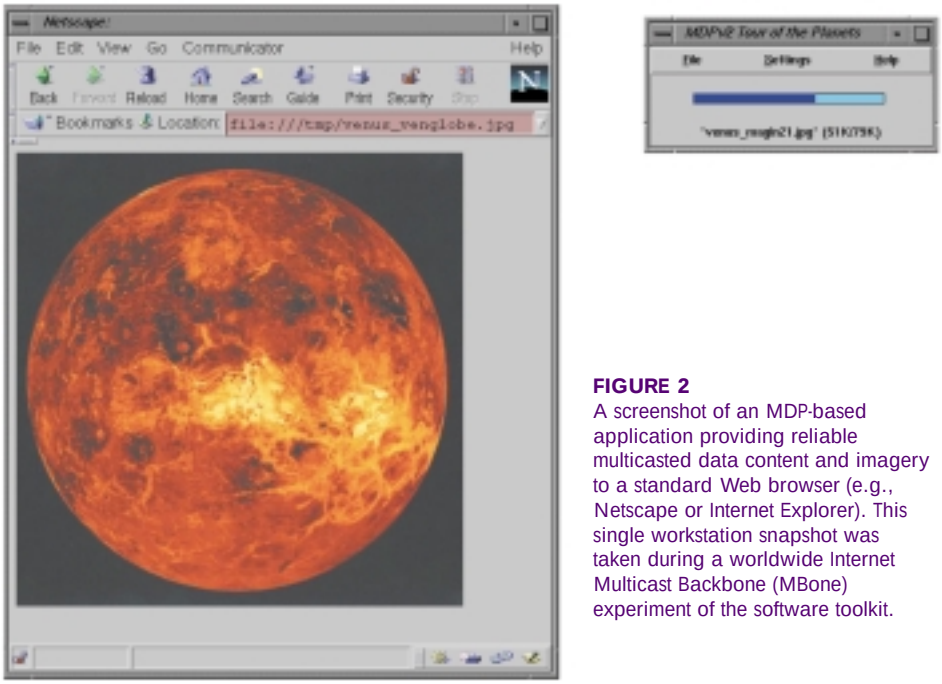

FIGURE 2
A screenshot of an MDP-based application providing reliable multicasted data content and imagery to a standard Web browser (e.g., Netscape or Internet Explorer). This single workstation snapshot was taken during a worldwide Internet Multicast Backbone (MBone) experiment of the software toolkit.

by NRL are also being used as a framework to support research in multicast-based congestion control algorithms. Multicast congestion control is essential to achieve safe and robust wide-scale deployment of multicast network services. Progress in this challenging research area is poised to have a catalytic effect on the future proliferation of multicasting technology. Our recent accomplishments include a working protocol design and extensive network simulation analyses of a congestion control extension model. Figure 3 is a simulation result demonstrating friendly co-existence of MDP-based congestion control algorithms with a set of dynamic unicast TCP flows.

In addition to providing a number of technology transitions of MDP work into commercial (e.g., VSAT) and DoD systems (e.g., Navy, Army), we are also serving a technical contribution role within the Internet research and standards community. Working with

other key researchers in the field, we are helping to transition sound and robust design concepts for the future Internet community and targeting related protocol standards involving both reliable multicast and multicast congestion control.

Conclusions: In summary, MDP is reliable multicast software technology supporting a broad range of networking conditions and applications, both military and commercial. Application of MDP dramatically improves present network capacity utilization, provides needed reliability and robustness for group-based network applications, and is helping the R&D process to develop multicast congestion control that is safe and robust within existing ubiquitous TCP/IP network infrastructures. The growing emphasis on "network-centric" operational concepts and the increasing demand for effective warfighter information exchange and dissemination will likely further increase the need for these technical concepts and research products in years to come.

Acknowledgments: The Office of Naval Research (ONR) partially sponsored recent research and design work reported here, and we acknowledge the support of Dr. James Freebersyser and other ONR personnel during this period. A host of NRL scientists and other organizations have contributed to the demonstration and analysis effort over the years. Also, recent activities and members of the Internet Research Task Force (IRTF) Reliable Multicast Research Group were instrumental in contributing to the multicast congestion control research direction.

[Sponsored by ONR]

References

[1] J. Macker, "Reliable Multicast Transport and Integrated Erasure-based Forward Error Correction," *Proc. IEEE MILCOM 97*, Oct. 1997.

[2] S. Pingali, D. Towsley, and J. Kurose, "A Comparison of Sender-Initiated and Receiver-Initiated Reliable Multicast Protocols," *Proc. INFOCOM*, San Francisco, CA, Oct. 1993.

[3] B.N. Levine and J.J. Garcia-Luna-Aceves, "A Comparison of Known Classes of Reliable Multicast Protocols," *Proc. International Conference on Network Protocols (ICNP-96)*, Columbus, Ohio, Oct. 29-Nov. 1, 1996.

[4] J.P. Macker, M.S. Corson, and E. Klinker, "Reliable Multicast Data Delivery for Military Internetworking," *Proc. IEEE MILCOM 96*, Oct. 1996.

[5] J. Macker and R.B. Adamson, "The Multicast Dissemination Protocol Toolkit," *Proc. IEEE MILCOM 99*, Oct. 1999.

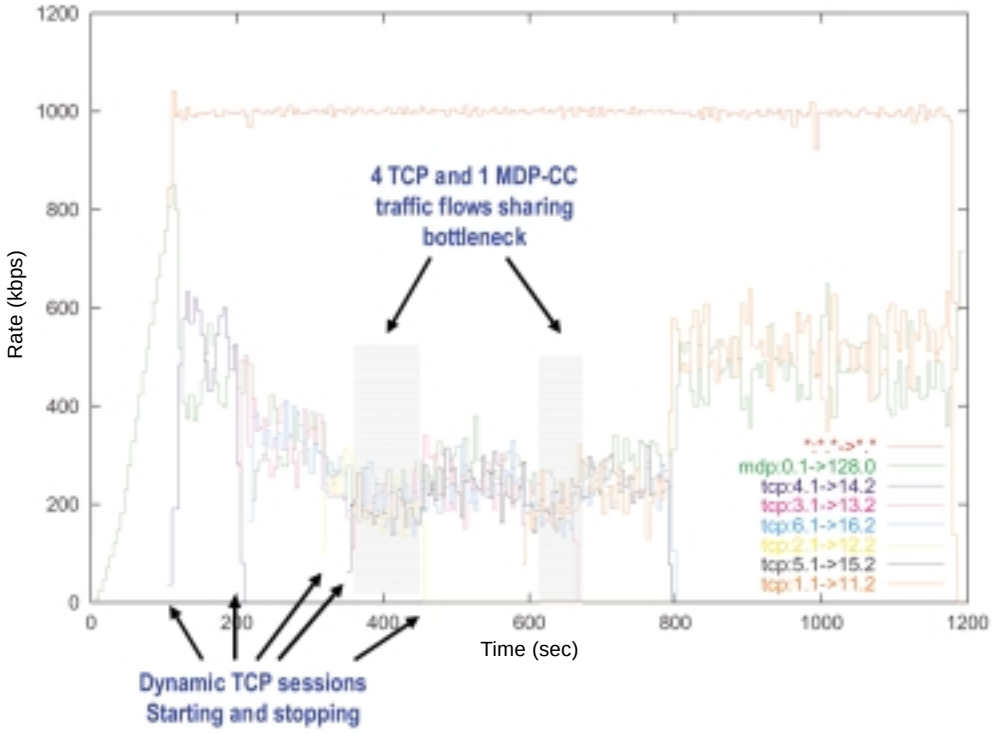

FIGURE 3
Example throughput measurement of a bottleneck queue being dynamically shared by a single multicast MDP session (20 receivers) and 6 TCP unicast transport sessions with randomized start and stop times. These early results demonstrate end-to-end congestion control algorithm friendliness between a dynamic multicast data flow and multiple unicast data sessions.

Internet-Like Service for the Mobile Warfighter

D.L. Tate and R. Cole
Information Technology Division

As we enter the 21st century, the use of the Internet is commonplace in many offices, schools, and homes. The Navy and Marine Corps have embraced the Internet as a rapid, convenient mechanism for conducting much of their business in offices, on ships, and even on the battlefield in peacetime and in war. However, the Internet is primarily designed for stationary computer systems located within a fixed network topology defined by each computer's Internet Protocol (IP) address. Much of the infrastructure that is necessary to make the Internet function effectively relies on routers that know how to move information from one location to another and how to locate computers based on their IP address. Most of the Internet is connected via wires and fiber cables, so the routing information remains relatively static. Today's warfighters are highly mobile and need wireless communication systems to perform reconnaissance, maintain situation awareness, or report mission preparedness. Standard Internet routers and protocols cannot provide the uninterrupted connectivity to a unified tactical communications infrastructure to support the voice, video, situation awareness, and Internet browsing requirements of the mobile warfighter.

Where No Network Has Gone Before: The Communication Systems Branch, Code 5520, is developing network architectures, protocols, and applications that will allow sailors and Marines to maintain uninterrupted network connectivity even when they are highly mobile and in remote areas. Wireless networks are crucial to allow them to be geographically dispersed if conditions require it, yet maintain good communication. Network technologies that are tailored to meet military requirements are being developed to support operations in parts of the world where good communication infrastructures (such as cell phones or fiber optic networks) do not exist.

The On-Board Switch Wireless Network Architecture: The On-Board Switch (OBS) project is developing a wireless network architecture that provides a unified tactical communication infrastructure to support a variety of applications through mobile routing services between end-user terminals (EUTs) and other computers on private networks or the Internet. The EUT is a wearable computer that will be part of the future warfighter's standard equipment. With this technology, mobile warfighters will have Internet-like connectivity throughout the battlespace. OBS enables mobile routers to automatically establish a robust network backbone that permits dismounted tactical users and mobile air and ground vehicles to maintain continuous over-the-horizon communications while moving.

With the mobility of wireless networks comes susceptibility to adversaries trying to surreptitiously join the network. The OBS architecture provides a measure of protection against this threat by using host authentication security procedures. OBS also provides prioritized data traffic control through quality of service (QoS) mechanisms that guarantee that high-priority traffic can preempt lower priority traffic when bandwidth resources are limited. An important feature of OBS is that as units roam freely among various networks and geographic locations; no IP address change or system reboot is required by the user. This is a significant improvement over the procedures used with tactical mobile computer systems today.

Field Exercise Gives Successful Proof of Concept: A field exercise was performed at Camp Upshur, Quantico Marine Corps Base, Quantico, Virginia, on 28-29 September 1999 to demonstrate how the OBS mobility architecture would perform under realistic conditions using airborne, vehicular, and dismounted units. Figure 4 is a diagram of the various components and links used for the exercise. The Marine Corps Warfighting Laboratory (MCWL) provided personnel and equipment for the Enhanced Combat Operations Center (ECOC) and tactical users, and a shipboard node was emulated with NRL's *USS Winnebago* test van. Mobile routers were located in the airborne and vehicular units, and tactical users (both on foot and in vehicles) were equipped with EUTs. EUTs were connected to the routers and other EUTs by 2 Mbps WaveLAN links. A wideband UHF 512 Kbps link between aircraft completed the robust backbone network. Emulated "reach-back" capability was provided from the *USS Winnebago* through a 512 Kbps satellite communication (SATCOM) link to the Air Force Research Laboratory, Rome Research Site (AFRL/RSS) in Rome, New York. The Defense Research and Engineering Network (DREN) provided connectivity from AFRL/RSS to NRL. The entire mobile network interfaced to the Internet at NRL.

The field exercise successfully demonstrated that OBS meets the mobile warfighter's requirements for voice, video, situation awareness, and Internet browsing. While data and voice traffic was being transferred on the network, live video from an overhead Extender unmanned air vehicle (UAV) was relayed from its ground control station through a video server into the tactical net. Figure 5 shows how this was done

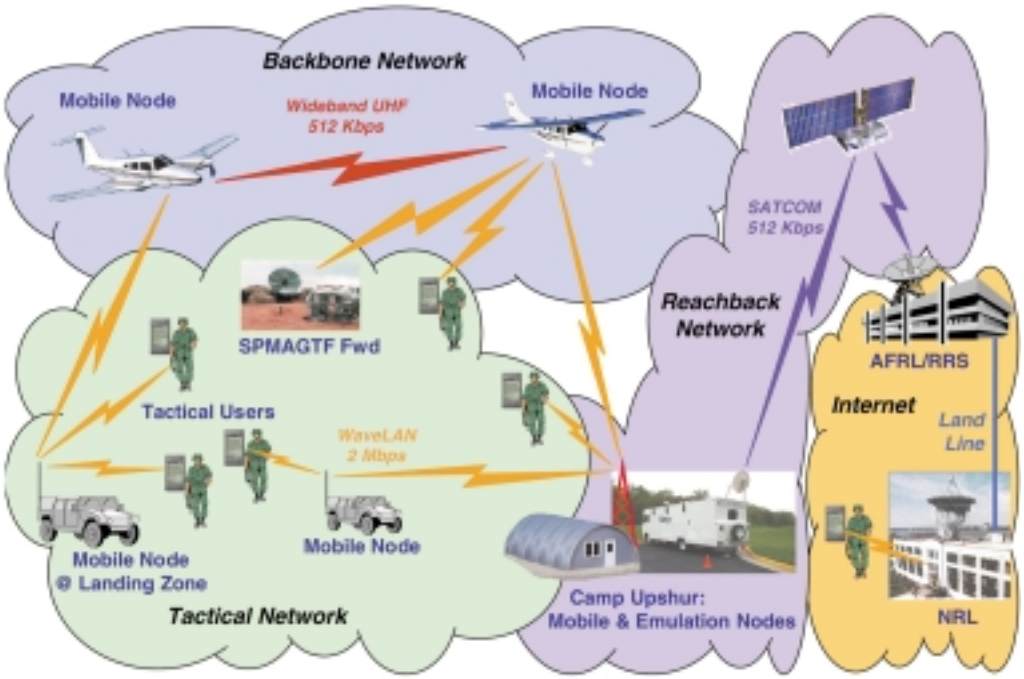

FIGURE 4
System diagram for the OBS field experiment at Quantico Marine Corps Base.

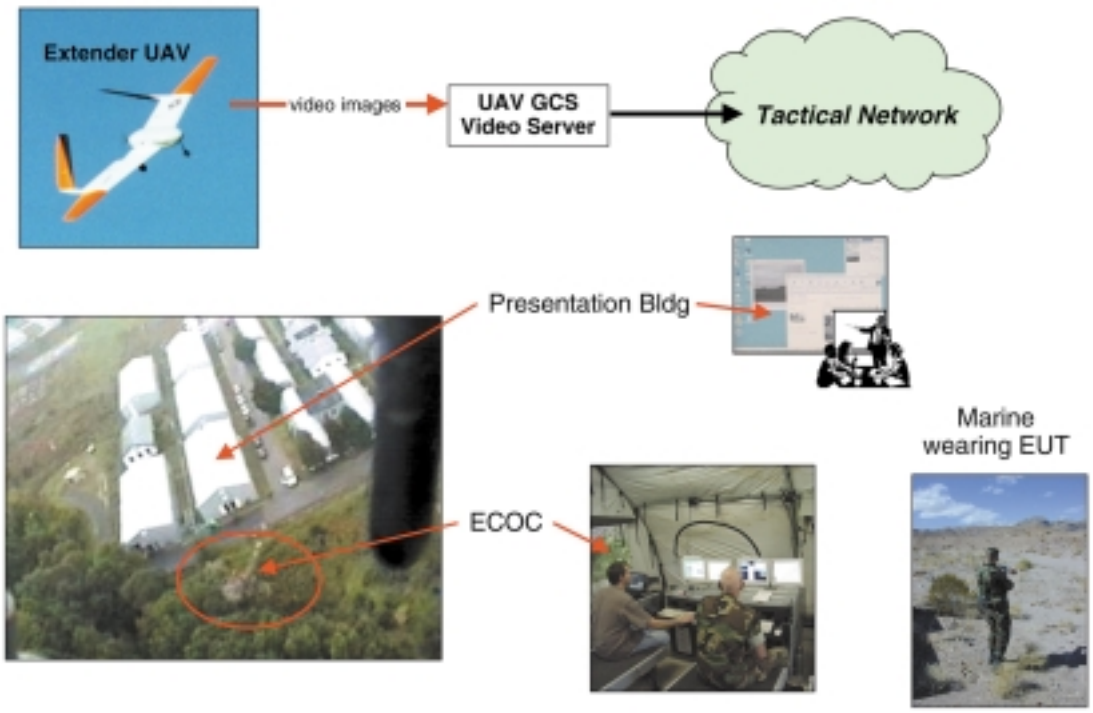

FIGURE 5
Live video fed to the Tactical Network allows viewers to watch from any location in the battlespace.

so that viewers in the presentation building, the ECOC, and throughout the battlespace could watch the video simultaneously.

NRL's Communication Systems Branch continues to develop advanced mobile networking techniques to meet the demands of tomorrow's mobile warfighters.

Acknowledgments: The development of the OBS mobility architecture and the success of the field exercise was a joint effort between several government agencies and private contractors. Sponsorship was provided by the Defense Advanced Research Projects Agency (DARPA), AFRL/RSS, NRL, and the Army Communications and Electronics Command (CECOM). MCWL and the Extended Littoral Battlefield (ELB) Program Office were participating activities in the field exercise. TRW, BBN Technologies, L-3 Communications, and Hughes Research Laboratories were the contractors responsible for the OBS development.

[Sponsored by DARPA and ONR]

Augmenting the Urban Battlefield

L.J. Rosenblum,[1] S.J. Julier,[2] Y. Baillot,[2]
D. Brown,[2] and M. Lanzagorta[3]

[1]*Information Technology Division*
[2]*ITT Systems Corporation*
[3]*Scientific and Engineering Solutions*

The urban environment is perhaps the most difficult environment that the warfighter faces. First, it is extremely complicated and inherently three-dimensional. Above street level, buildings can harbor many risks (such as snipers or mines) that can be on many floors. Below street level, there can be networks of sewers and tunnels. Second, coordination between team members can be difficult. In narrow, crowded streets it is unlikely that all members of a team will be in direct line of sight of one another.

Third, the urban environment is highly dynamic. Not only do the locations of threats change (e.g., a sniper repositions) but also the infrastructure itself can change (e.g., damaged buildings can fill a street with rubble, making a once-safe route impassable). All of these difficulties are compounded by the need to minimize civilian casualties and damage to civilian targets. The effects of these problems have been illustrated in many examples, from Berlin in World War II to Mogadishu and even to Grozny. In principle, many of these difficulties can be overcome through better situational awareness. To meet these needs, NRL is developing the Battlefield Augmented Reality System (BARS).

Background: BARS uses a display paradigm known as *augmented reality* (AR). The user's position and head orientation is tracked, so that the system knows where the user is located and the direction of the user's gaze. The user wears a see-through, head-mounted display and computer-generated imagery is aligned (from the user's point of view) with the real world. The advantages of AR can best be appreciated by considering the (far easier) problem of providing jet pilots with a heads-up display. A pilot must be aware of the full 3D environment and, in particular, the location of aircraft. A 2D display (such as a map or a personal digital assistant (PDA)) would divert the pilot's attention away from the environment, leading to a possibly critical loss of situational awareness. AR allows a mobile user to maintain continual awareness of the environment. At the same time, 3D information can be provided in a hands-free and intuitive manner.

The BARS System: BARS pushes the state of AR research in several directions.[1] First, the application domain—delivering situational awareness to a mobile user in the urban environment—is complex and a great deal of attention must be paid to what is to be displayed, how it is to be aligned, and how it is to be represented. Second, the outdoor system must be wearable and self-contained. Third, the system must be multi-user and must allow multiple mobile users to collaborate directly with one another and with a fixed base station.

Figure 6 shows the current development system; Fig. 7 is a typical output from the system. This mobile system is capable of showing buildings, windows, doors, routes, maps, and situation awareness information such as the location of other mobile users.

BARS Research: AR research is complicated by its intrinsically multidisciplinary nature. Topics covered include computer graphics, human-computer interface, system design and engineering, robotics and machine vision, and evaluation. Our major research thrusts are:

- *Tracking*. To accurately register the graphics against features in the environment, the system must accurately measure the position and orientation of the user's head. "Open loop" tracking systems (such as GPS and inertial systems) are not sufficiently accurate, and we are currently in-

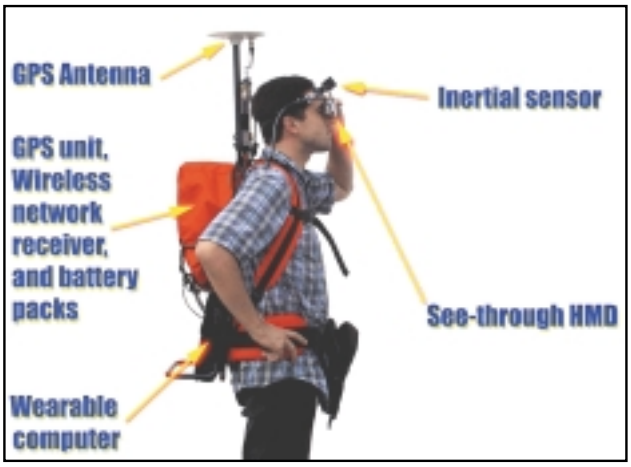

FIGURE 6
Current BARS development system. This system is developed using COTS products, hence its size. (This system might be a familiar sight to regular users of the Building 28 cafeteria.)

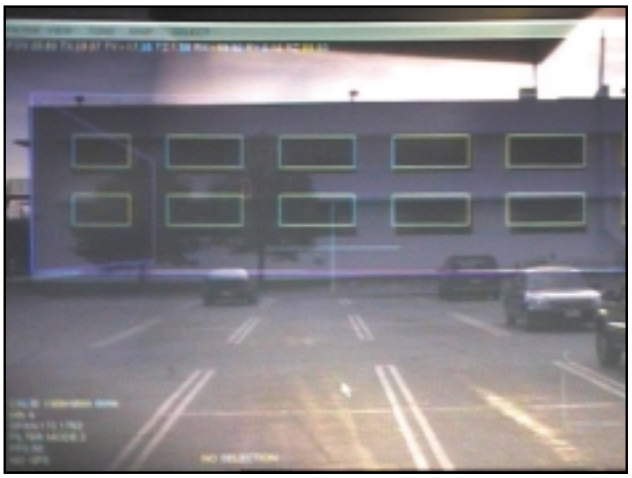

FIGURE 7
Output from AR system, captured by camera aligned with the head-mounted display.

vestigating vision-based tracking systems developed at the University of Southern California and MIT.

- *Calibration*. Different users wear the system differently, and subtle differences in the placement of the display can lead to significant registration errors. Therefore, we have developed tools and techniques for interactively calibrating the display.

- *User interface design*. Many different types and kinds of data can be shown to a user, and we explore the use of various types of representations and their effectiveness.

- *User interaction*. Users will have the capability to query and enter data into the system. To date, most systems have focused on the use of handheld displays and wrist-mounted keyboards. We are exploring the use of multimodal interactions (integrated speech and gesture recognition).

- *Information filtering*. Due to its complexity, the urban environment contains reports of many objects in a small space. We are developing tools that automatically determine what information should be shown to a user at any given time.[2] Metrics include the type of mission, the types of objects, and training manuals.

- *Software architecture and data distribution*. We are developing flexible software architectures and data distribution systems for delivering the appropriate subset of information to a particular user at the right time and the right place.

- *Virtual Reality "Command Center."* To explore the interaction between a command center and

several outdoor, mobile BARS users, we are modeling a portion of NRL and displaying it in our virtual reality CAVE facility (a full-sized, fully immersive room). While good techniques exist to model urban areas for fly-throughs, new methods are required to model urban areas with geophysical accuracy.

Conclusions and Future Developments: We have built one of a handful of systems that is capable of outdoor, mobile AR. The system contains many advanced features such as the information filtering discussed above. We expect to shortly perform a seminal demonstration of multiple outdoor users working together using BARS. Within the next year, we will be demonstrating the interplay between the outdoor users and the VR Command Center. Longer-term issues we are starting to address include user evaluation to optimize the effectiveness of the system and the use of automated tools to construct accurate and detailed models of an urban environment.

Acknowledgments: BARS has been sponsored by ONR-base and ONR-311 funding, for which we thank our sponsors. We also acknowledge the efforts of our colleagues at Columbia University (Professor Steven Feiner, Tobias Höllerer, Drexel Hallaway, Sinem Gupta, and Elias Gagas) who contribute to the BARS project. For additional detail and research articles, see www.ait.nrl.navy.mil/vrlab.

[Sponsored by ONR]

References

[1] S. Julier, S. Feiner, and L. Rosenblum, "Mobile Augmented Reality: A Complex Human-Centered System," to be published in *Frontiers of Human-Centered Computing, Online Communities and Virtual Environments*, R. Earnshaw, R. Guedj, A. van Dam, and J. Vince (editors), (Springer-Verlag, NY, 2000).

[2] S. Julier, M. Lanzagorta, Y. Baillot, L. Rosenblum, S. Feiner, T. Höllerer, and S. Setito, "Information Filtering for Mobile Augmented Reality," to be presented at the 2000 International Symposium on Augmented Reality.

End User Terminal and Wearable Ground Control Station

J.G. Durbin, B.T. Solan, and G.D. Stern
Tactical Electronic Warfare Division

Under Office of Naval Research and United States Marine Corps (USMC) sponsorship, the Tactical Electronic Warfare Division (TEWD) has developed a unique capability for the USMC. The End User Terminal (EUT+) is a lightweight, ruggedized, wearable computer. This capability was developed to provide a wearable computer for Marine Corps Warfighting Laboratory (MCWL) experimentation. MCWL has been developing a suite of hardware, software, and communications infrastructure to determine the efficacy of enhanced situational awareness at the battalion level and below. The EUT+ is seen as meeting the needs at the individual rifleman, fireteam, squad, and platoon levels. More recently, TEWD was asked to develop a squad-level unmanned air vehicle (UAV). Because of the likely forward deployment of this asset, a wearable ground control station (GCS) was seen as being advantageous. The development of the EUT+ and the wearable GCS are explored, as are the salient specifications and expected future deployments.

Development: Crucial in the development of an advanced wearable computer is the recognition that it must be rugged, lightweight, easy to use, and easily maintained by the Marine in the field. The system developed by NRL meets these criteria, and it provides the performance required to run developmental software. To understand what features the Marines would need, NRL deployed on numerous limited objective experiments (LOEs) that were run by MCWL. Feedback and lessons learned from participating in the LOEs and from conversations with individual Marines have been folded into the current system.

Hardware: The EUT is a ruggedized, wearable computer configured on a modular lightweight load-carrying equipment (MOLLE) vest. The EUT is a full-function 550 MHz Pentium III processor (Fig. 8), Windows NT touch screen computer. The system uses both a GPS receiver and a simple inertial navigation system (INS) to provide the wearer with current location. The INS is a pedometer coupled with a digital compass and inclinometer. This combination provides location updates in the absence of a GPS signal, such as indoors or underground. An internal 6 watt 2.4 GHz amplifier can be used to communicate via the IEEE 802.11 local area network protocol or to communicate with the Dragon Eye unmanned air vehicle. The 6-inch LCD display is heavily ruggedized and fits into a pocket on the MOLLE vest. The computer system, GPS, and RF transmitter are all powered from a Mil-Spec battery that provides approximately 3 to 5 hours of continuous operation. By using the SINCGARS family of batteries, the EUT user has access to the normal supply chain of BA-5590 LiSO2, BB-390 NiMH, and the new LiON BB-2590 batteries. Figure 9 shows a U.S. Marine wearing the EUT in the field; Fig. 10 shows a Marine holding the Dragon Eye UAV while wearing the GCS. He is also

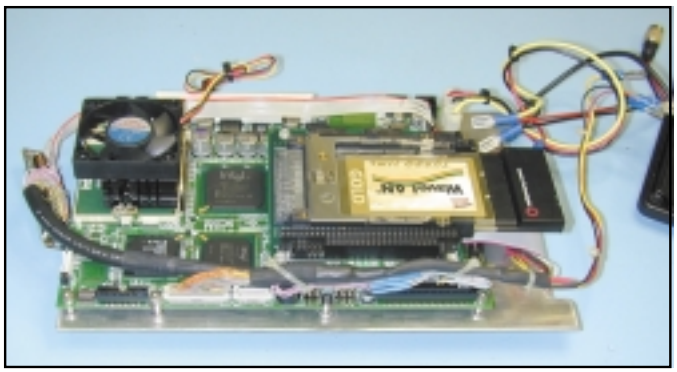

FIGURE 8
Wearable computer complete with IEEE 802.11 RF local area network.

FIGURE 9
A U.S. Marine using an EUT.

FIGURE 10
A U.S. Marine wearing the ground control station while holding the Dragon Eye UAV.

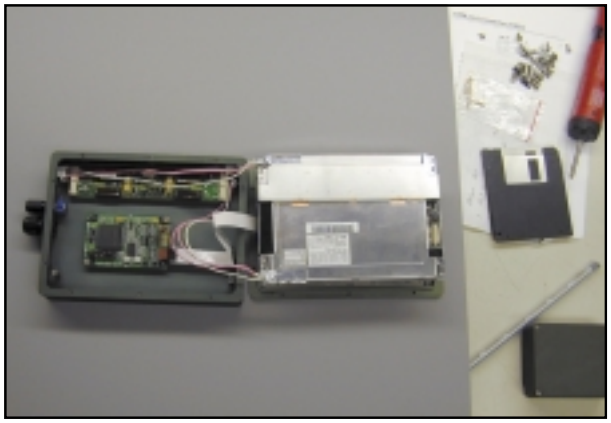

FIGURE 11
Internals of the ruggedized display.

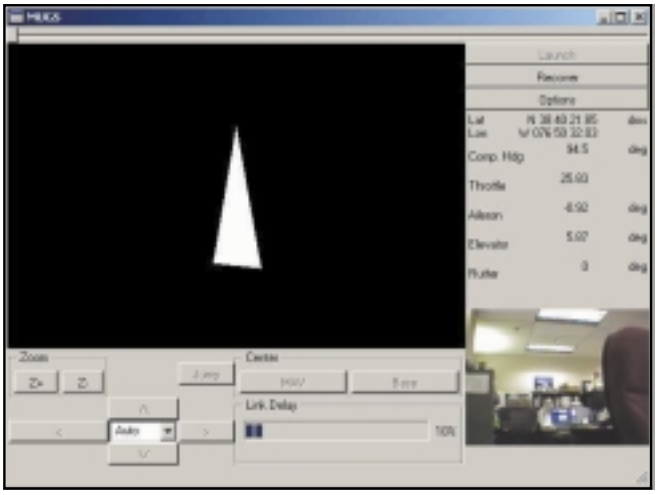

FIGURE 12
The ground control station user interface and data display.

holding the ruggedized display unit, the internals of which are shown in Fig. 11.

Software: Current applications of the NRL wearable computer include MCWL's Battlefield Visualization Toolkit (BVT) and Dragon Eye ground control station. The End User Terminal is part of the Marines effort to provide enhanced situational awareness to the individual Marine. Locations of the user, other Marines, and threat information are displayed on a 6-inch color LCD display. Software written in JAVA by Spawar Systems Center, San Diego, California, provides an intuitive display with military icons overlaying a moving map display. When used as a Dragon Eye ground control station, the software provides a means to control the UAV, receive via a downlink the location of the UAV, and video from the onboard camera. Figure 12 shows the user interface of the GCS software.

Future Deployments: TEWD is committed to delivering wearable end user terminals and ground control stations to MCWL. The Marine Corps Systems Command is scheduled to procure 2,000 wearable computers beginning in FY 02. It is expected that the EUT will provide further insight into wearable computing, and possibly be a benchmark for Marine Corps procurement. NRL is scheduled to deliver wearable GCS systems that will accompany the Dragon Eye UAV when it is delivered to the 1st and 3rd Marine Expeditionary Forces.

[Sponsored by ONR and USMC]

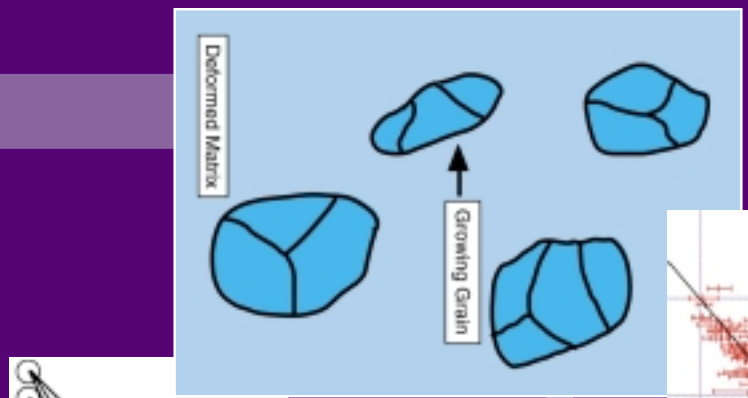

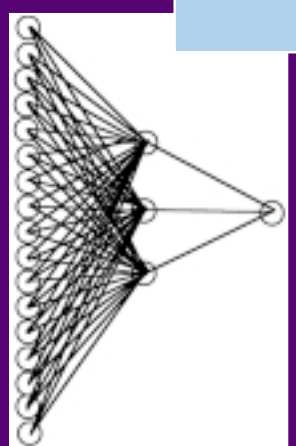

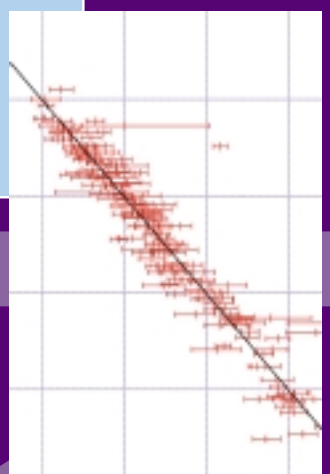

Materials Science and Technology

Weld Metal Strength: A Neural Network Analysis

E.A. Metzbower
Materials Science and Technology Division

Introduction: The U.S. Navy has been working to replace high-yield (HY) and high-strength low-alloy (HSLA) steels for surface ship construction. The compelling reason for this substitution is the cost savings associated with the reduction or elimination of preheat during welding operations. An associated program was instituted to provide an integrated approach to the development and certification of improved filler metals for welding 550-690 MPa steels for surface ships and submarines. The goal of the program was to develop, optimize, and certify improved filler metals for welding HSLA and HY steels. This research program to develop a suitable welding consumable has generated significant quantities of experimental data that provide an opportunity for creating a quantitative model for estimating weld mechanical properties. Such a model could be useful in understanding the effect of each variable on the properties, and may be used to assess the behavior of the welds over a wider range of parameters than covered by the experimental data. It should, in principle, be possible to improve on the current or proposed welding consumables.

Neural Network Modeling: The methodology used here is neural network modeling. A neural network is capable of realizing a great variety of nonlinear relationships. Data are presented to the network in the form of input and output parameters. The optimum nonlinear relationship is found by minimizing the difference between the measured value and the predicted value. As in regression analysis, the results then consist of a series of coefficients (called weights) and a specification of the kind of function that, in combination with the weights, relates the inputs to the output.

The experimental data generated in the weld wire program have been used to create the neural network. They include the chemical composition of the as-deposited weld beads, the measured yield and ultimate tensile strengths, and the cooling rate at 538 °C. The input data included alloys that did not satisfy the acceptance criteria for yield strength or ultimate tensile strength in the context of ship construction. Nevertheless, all data were included so that the best predictive capability over the widest chemistry and cooling rate range could be developed. The major alloying additions, i.e., carbon, manganese, silicon, nickel, and molybdenum, affect the transformation products and, consequently, the strength and toughness. Impurity elements (sulfur, phosphorous, aluminum, nitrogen, oxygen) are included because of their known tendency to embrittle or because of their importance in the formation of nonmetallic inclusions in welds. The total number of input variables for the yield and ultimate tensile strength models was 17.

The complexity of the models is controlled by the number of hidden units and the values of the regularization constants—one associated with each input variable, one for biases, and one for all weights connected to the output. Figure 1 describes a typical network used in the analysis.

A potential difficulty with the use of powerful regression methods is the possibility of overfitting data. To avoid this, the experimental data can be divided into two sets, a *training* dataset and a *test* dataset. The model is produced using only the training data. The test data are then used to check that the model generalizes well when presented with previously unseen data. The test error will be large if the model is so simple so that it is unable to capture the real complexity in the data, or if the model is so complex that it is erroneously modeling the noise in the experimental data. The optimum model corresponds to some case in between these two undesirable states. The training process involves a search for the optimum nonlinear relationship between the input and the output data and is computer-intensive. Once the network is trained, estimating the outputs for any given input is very fast.

Committee of Best Models: This analysis uses a committee of best models to make predictions. It is possible that a committee of models can make a more reliable prediction than an individual model. The best models are ranked using the values of the test errors. Committees are then formed by combining the predictions of the best L models, where L=1,2,…: the size of the committee is therefore given by the value of L. Using this procedure, the optimum size of the yield strength committee was found to consist of 11

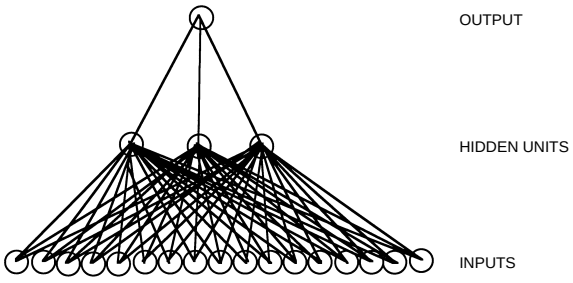

FIGURE 1
Schematic illustration of the structure of the network, the input nodes, the hidden units, and the output node.

of the top-ranking models, whereas the committee for the ultimate tensile strength (UTS) consisted of six of the top-ranking models. Once the optimum committee is chosen, it is retrained on the entire dataset without changing the complexity of each model, with the exception of the inevitable although relatively small adjustments to the weights.

Figure 2 shows the correlation between the experimental measurements and data predicted using the committee of models. The committees clearly perform rather well.

The minimum required yield strength is 607 MPa. Figure 2 shows that about one quarter of the data points generated in the program of experiments do not satisfy the design. There is not a requirement specified for the ultimate tensile strength.

The best way to examine the performance of the models is to use them to make predictions about trends as a function of each of the inputs, for a reasonable choice of baseline inputs. Table 1 lists the set of baseline inputs. The cooling rate was set at 61.2 °C/s. An alloy such as this should have a mixed microstructure of bainite and some martensite, given the combination of high manganese, high nickel, and molybdenum concentrations.

It is not surprising that an increase in the cooling rate causes an increase in strength (Fig. 3(a)). The high hardenability of the alloys (Table 1) must lead to a greater amount of martensite as the cooling rate increases. This is consistent with the observed larger sensitivity of the yield strength to the carbon concentration at high cooling rates (Fig. 3(b)) since the effect of carbon on hardness is greatest when it is in solid solution in martensite. Apart from the sensitivity to carbon, Fig. 3(b) also shows that, for any given carbon concentration, the yield strength is much greater at the higher cooling rate. This can only happen if the higher cooling rate leads to a harder microstructure, i.e., one with a larger fraction of martensite.

Finally, Fig. 3(b) shows an important feature of nonlinear modeling, which captures the interdependence of the variables. Thus, the predicted behavior is different at high cooling rates.

Summary: A neural network method within a Bayesian framework has been used to model experimental data on the yield and ultimate strength of ferritic steel weld metals that are appropriate for welding high-strength low-alloy steels. The inputs for the

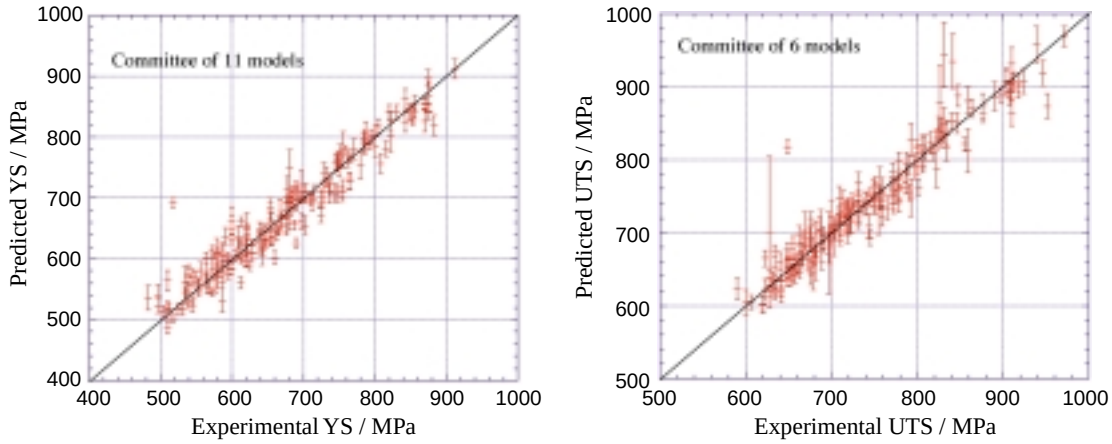

(a) Yield strength.

(b) Ultimate tensile strength.

FIGURE 2
Comparison of the predicted and measured values of the strength of the as-deposited weld metal. The calculations were done using the committee of models. The error bars represent ±1σ values.

Table 1 — Standard Set of Inputs Used to Observe Trends

C/wt%	Mn	Si	Cr	Ni	Mo	Cu	S
0.036	1.72	0.31	0.03	2.63	0.59	0.061	0.004
P	Al	Ti	Nb	V	B	O/ppm	N/ppm
0.001	0.005	0.007		0.001	0	181	8

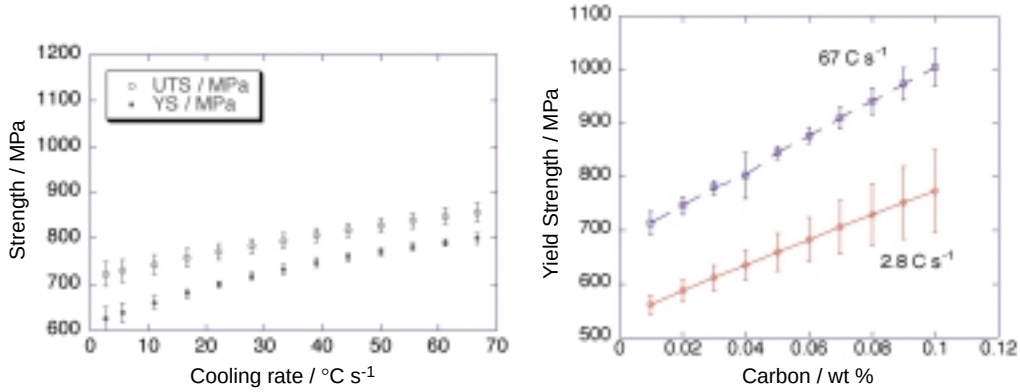

FIGURE 3
Trends in the yield and ultimate tensile strength, predicted using committee models, as a function of (a) the weld cooling rate, (b) the carbon concentration and the cooling rate. The error bars represent ±1σ values.

neural network were the concentrations of 16 chemical elements and the cooling rate at 538 °C. The models are found to be well-behaved, with a demonstrated ability to reproduce known metallurgical trends.

[Sponsored by ONR]

A Model of Grain Size Distribution During Primary Recrystallization

C.S. Pande
Materials Science and Technology Division

Background: During the annealing of a sufficiently cold worked metal or alloy, discrete and localized grain nuclei appear and subsequently grow. They gradually consume the deformed structure and eventually replace it by a network of strain-free grains. This process is called *primary recrystallization*.[1] Recrystallization strongly affects the microstructure and mechanical properties of many structural components.

Surprisingly, computer simulations of this process are not found to be consistent with experiments.[2] For example, all the experimental distributions of grains in partially or fully recrystallized materials are approximately lognormal, given by

$$F(A) = \frac{1}{\sqrt{2\pi\sigma^2}}\,\frac{1}{A}\,\exp\left[-\frac{1}{2\sigma^2}\left(\log A - \mu\right)^2\right],$$

where A is the area of the grain, σ^2 is variance of the equivalent Gaussian distribution, and μ is the median of the distribution. None of the computer simulations appear to reproduce these distributions. It has been concluded that computer simulation would be of limited value in elucidating the detailed mechanism of recrystallization. Also, due to the complexity of the process, no analytical theory is available.

The aim of our work was to develop a simple theory of recrystallization that would predict the observed distribution and satisfactorily explain other experimental results. However, it should be general enough to explain experimental observations in a variety of materials under somewhat varied circumstances.

A Stochastic Model of Recrystallization: It appears that the grain size distributions are invariably lognormal in a variety of different situations and experimental conditions. This leads us to believe that, despite the complexity of the recrystallization process, some very simple and fundamental mechanism must be dominant and would lead to unique and persistent size distributions. It should be noted that even during a later stage of annealing i.e., during normal grain growth, the grain size distribution continues to be lognormal. However, there is one important difference. During grain growth, the variance of the normalized grain size distribution is essentially constant for a given material and initial conditions, whereas during recrystallization, the variance of the distribution is found to increase with time.

The actual mechanism of recrystallization may involve a variety of processes, such as rate-controlling atomic mechanisms, impurity effects, grain boundary energies, and curvature. We consider grain nuclei growing in a matrix of deformed material (Fig. 4). Based on our review of experimental results, we surmise the following as the key to understanding the growth of these nuclei during primary recrystallization.

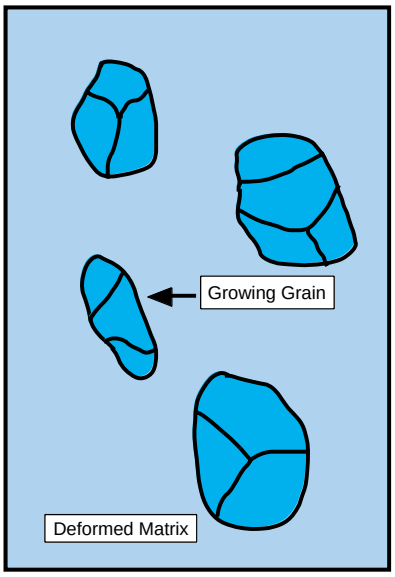

FIGURE 4
Schematic diagram illustrating the mechanism assumed in the model.

At any instant, during primary recrystallization, the change in area of a given grain is a random proportion of the previous area, i.e.,

$$\frac{dA}{dt} = A\,T(t)f(t),$$

where $T(t)$ is a random function and $f(t)$ is a function of time related to the volume fraction of grains transformed. This equation contains the main assumption in the model. It is a stochastic equation and leads to a Fokker-Planck equation for grain size distribution F,

$$\frac{\partial F}{\partial t} = -\frac{\partial}{\partial A}\left(AF\right) + \frac{\partial^2}{\partial A^2}\left(A^2F\right)$$

whose solution has been given by Pande (Ref. 1, p. 491).

The two main predictions of the model are: (1) the grain size distribution that forms during primary recrystallization is lognormal; and (2) the distribution broadens with increasing time.

This result is based on our assumption that, although plausible, needs careful experimental scrutiny. Our main justification is that it leads to correct predictions of experimental results.

Comparison with Experiments: All experimental observations are consistent with predictions of the model. Figure 5 shows the grain size distribution of Ref. 2 for partially and fully recrystallized aluminum. It shows that the grain size distributions are lognormal (bell-shaped when plotted in log of grain area) and broaden with time. Comte and Form[3] have investigated whether the lognormal grain size distribution is fully established during the early stages of

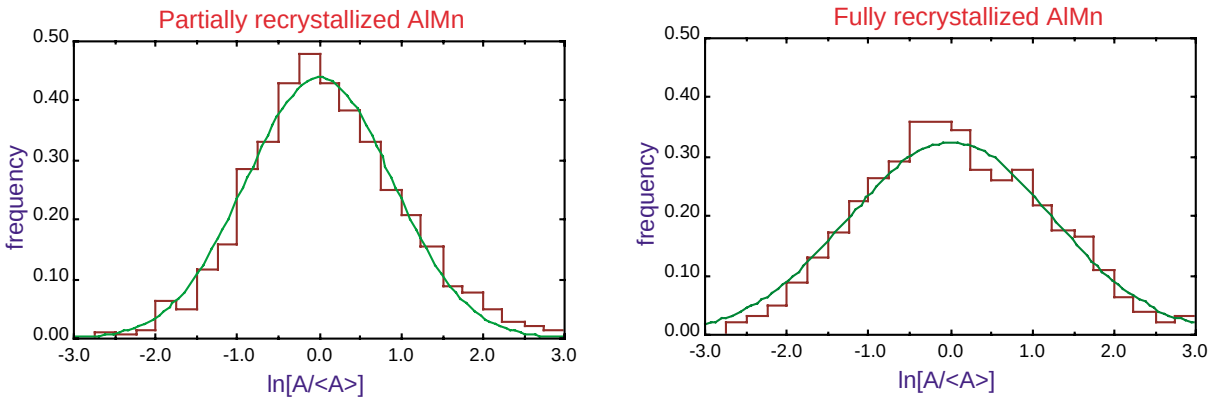

FIGURE 5
Comparison with experiments of area distribution of grains. (Histogram - experimental data from Ref. 2, curve - theory.)

recrystallization or whether it develops gradually as recrystallization proceeds. For this purpose they heated a previously deformed oxygen-free Cu specimen and observed the recrystallization kinetics at 320 °C. They found that the grain size distribution is log-normal at the early stages of recrystallization, as predicted in our model.

Summary: A new model of grain growth distribution during recrystallization has been proposed that is consistent with experiments. The theory is based on the assumption that, despite the complexities of the process, a simple mechanism common to all recrystallization process exists that explains the grain size distribution and its evolution in fine detail.

[Sponsored by ONR]

References

[1] N. Hansen, editor, *Recrystallization—Fundamental Aspects and Relations to Deformed Microstructure* (Risoe National Laboratory, Denmark, 2000).

[2] K. Marthinsen, O. Lohne, and E. Nes, "The Development of Recrystallization Microstructures Studied Experimentally and By Computer Simulation," *Acta. Metall.* **37**, 135 (1989).

[3] P.A. Comte and G.W. Form, "Statistical Aspects of Recrystallization and Grain Growth Kinetics," *Practical Metall.* **13**, 9 (1976).

Giant Internal Magnetic Fields in Mn-Doped Semiconductor Nanocrystals

A.L. Efros and M. Rosen
Materials Science and Technology Division

We predict the existence of a huge internal magnetic field in manganese (Mn)-doped semiconductor nanocrystals (NCs) that splits electron- and hole-spin sublevels by as much as 100 meV. The splitting exists even in zero external field. This internal field is the result of a giant enhancement of the short-range contact interaction of electron and hole spins, with the dopant magnetic ion (MI) spin arising from the strong confinement of carriers inside the extremely small NCs. This interaction is proportional to the square of the value of the electron and hole wave functions at the MI. It grows dramatically as the inverse of the NC volume. The magnetic field of the MI acting on the electron and hole spins depends on the position of the MI in the NC and on the NC radius, but it can be as much as 1000 Tesla. Our theory successfully describes the splitting as measured by magneto-circular dichroism experiments in cadmium sulfide (CdS) NC ensembles. Analysis of these data indicates that a splitting of 72 MeV occurs in some NCs.

Introduction: Particle confinement plays an all-important role in the optical and opto-electronic properties of nanometer-scale semiconductor crystallites —the so-called nanocrystals or quantum dots. Confinement causes the energy spectra of electrons and holes to be discrete, with optical transition strengths concentrated at these discrete levels. On the other hand, because it only takes a small number of confined electrons or holes to reach a high charge density, confinement also leads to the low threshold enhancement of nonlinear nonradiative transitions, e.g., Auger transitions that compete with radiative recombination. In this paper we draw special attention to another important effect of particle confinement: the great enhancement of a particular class of interparticle interactions—short-range (contact) spin-spin exchange interactions. Because they are contact, δ-function interactions, their magnitude depends on the overlap of the wave functions of the two particles and varies as the inverse cube of the nanocrystal radius. This results in an enhancement by some three orders of magnitude in quantum dots over that in the bulk.

Giant Splitting of Electron Spin Sublevels by Dopant Mn Ion Magnetic Field: The electron/hole short-range spin-spin contact interaction with a dopant Mn ion in an NC can be written

$$H_{e,h} = \frac{\alpha_{e,h}}{2}\frac{v_0}{4}(\boldsymbol{\sigma}\cdot<\mathbf{S})\delta(\mathbf{r}_{e,h}-\mathbf{R}_I)\,, \qquad (1)$$

where $\mathbf{S}$ is the spin of the Mn ion ($\mathbf{S} = 5/2$) located at the coordinate $\mathbf{R}_I$ in the NC, the $\boldsymbol{\sigma}$ are the Pauli spin matrices, $\alpha_{e,h}$ are the exchange integrals averaged over the Bloch functions of the conduction and valence bands, respectively, and v_0 is the volume of the NC unit cell. Equation (1) describes the interaction of the spin of the electron or hole with the magnetic field of the MI, from which we can obtain the splitting of their spin sublevels. From first-order perturbation theory we find for the electron levels

$$\Delta E_e = |\alpha_e|\frac{5}{2}\frac{v_0}{4}\psi_e^2(\mathbf{R}_I)\,, \qquad (2)$$

where $\psi_e(\mathbf{R}_I)$ is the value of the electron wave function at $\mathbf{R}_I$. It is important to emphasize that this splitting exists in the absence of any external magnetic field! Because the square of the electron wave function depends strongly on position—it vanishes at the NC surface and is $\pi/2a^3$ at its center, where a is the NC radius—the magnitude of the splitting is very dependent on where the Mn resides in the NC. This is not generally known, and if we, therefore, assume that there is an equal probability that the Mn sits at

any of its possible positions in the NC, then the splitting we obtain is some six times smaller than if it sat at the NC center. The expression for the splitting averaged over these Mn positions is

$$\Delta E_{e,h} = |\alpha_{e,h}| \frac{5}{2} \frac{3\nu_0}{16\pi a^3} = |\alpha_{e,h}| \frac{5}{2} x , \qquad (3)$$

where x is the fractional Mn composition in samples that have, on average, one Mn ion per NC. The splitting of the hole levels has a more complicated form than is shown in Eq. (2) due to the spin-orbit coupling in the valence band, but one sees that it too grows as the inverse cube of the NC radius. In bulk, increasing the Mn concentration leads to pairing of Mn ion spins and a decrease in the magnetic field. Isolation of the Mn in NCs tends to reduce this effect. If we take the values of the exchange integrals for a Mn dopant ion in CdS, α_e = 0.22 eV and α_h = –2.7 eV,[1] one finds an average splitting of the conduction and valence bands in CdS NCs of some 10 to 100 MeV. This is a value of the splitting that would be caused by an external field whose magnitude is on the order of 100 to 1000 Tesla!

Observing the Splitting: Strong evidence for these giant magnetic fields has been found in the measurements of the magneto-circular-dichroism (MCD) signal in Mn-doped CdS NCs.[2] In these experiments, the transmission of right σ^+ and left σ^- circularly polarized light through the CdS sample is measured. The σ^+ (σ^-) polarized light excites the upper (lower) state of the split band edge level, and the magnitude of the splitting can be determined from the MCD signal, $I_{MCD} = (I_+ - I_-)/(I_+ + I_-)$, where I_+ and I_- are the transmitted intensities of the right and left circularly polarized light, respectively. But, this is so only under certain carefully prepared circumstances. Generally, the spins of the dopant ions in the NC sample are randomly oriented. Now, the magnetic field felt by the excited electron is parallel to the dopant ion spin, and unless the Mn spins are aligned parallel to the direction of the incident light, no preferred direction is defined, and spin projection selection rules do not govern the optical absorption. That is, right and left circularly polarized light will each excite both the upper and lower split electron and hole sublevels. Instead of split levels, then, only one broadened level will be observed—even though cleanly split electron and hole spin sublevels exist in the NCs. To observe the splitting, then, we need to establish a physical direction in the sample that is seen by all the NCs. We do this by applying a small external magnetic field, directed along the direction of incident light, that is sufficiently large to align the Mn spins in the sample NCs along the direction of the incident light, but yet does not itself add significantly to the splitting of the sublevels. For a dopant with spin S_I, the sample-averaged spin aligned along the external field B instead of 5/2 is

$$< S_I > = S_I B_S \left(\frac{g\mu_B S_I B}{kT} \right), \qquad (4)$$

where B_S is the Brillouin function, and $B_S(x) = 1$ when $x >> 1$, so all the Mn spins are aligned at large B or low temperature. The *observed* splitting for an NC sample with one Mn per NC is then B and T dependent, while the actual splitting is independent of both!

Measuring the Splitting: In determining the sublevel splitting from the measured MCD signal, it is important to remember that the doping of an ensemble of NCs is a statistical process, and that in an NC sample

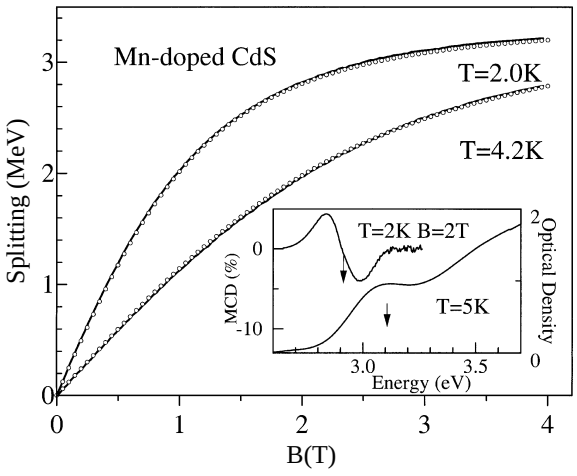

FIGURE 6
The external magnetic field dependence of the band edge splitting obtained from MCD signals at two temperatures (solid lines); the theoretical dependence for a Mn ion concentration of 0.16% (circles). Inset shows an MCD signal together with the absorption band edge of the sample. (From Ref. 2.)

having one Mn per NC on average does not mean that every NC contains exactly one Mn ion. Rather, in such a sample the distribution of Mn ions among the NCs is governed by the binomial distribution function. For a sample of 20 Å radius NCs having an average of 1 Mn per NC, 37% of the NCs are empty, 37% have 1 Mn ion, and 19% have 2 Mn ions (it can be shown that the average magnetic field of a NC with 2 Mn ions is less than that of a NC with only 1 Mn). The net result of having to average over Mn positions in the NC, of all the Mn spins not being aligned along the direction of the incident light, and of a large number of the NCs not containing a Mn ion at all means that the *measured* splitting is bound to be a drastic underestimate of the actual splitting in an NC having an Mn ion at its center.

Figure 6 shows the external magnetic field dependence obtained from the MCD signal at two temperatures for doped CdS samples having, on average, 1 Mn ion per NC.[2] The average size of the NCs contributing to the MCD signal was determined from the absorption band edge to be a = 20 Å. Only a single fitting parameter was required to obtain this excellent agreement—the concentration of dopant ions (16%). A saturation at about 3 MeV is clearly indicated. It can be shown that this value of the observed splitting implies the occurrence of an actual splitting, for an NC with the Mn ion at its center, of 72 MeV.

Summary: We have predicted and it has been demonstrated that giant magnetic fields occur in Mn ion-doped CdS nanocrystals that cause a huge splitting of electron and hole spin sublevels on the order of tens to a hundred MeV.

[Sponsored by ONR]

References

[1] V.G. Abramishvili, S.I. Gubarev, A.V. Komarov, and S.M. Ryabchenko, "Magnetooptic Studies of the Exciton Spectra of the Magnetically Mixed Crystal $Cd_{1-x}Mn_xS$," *Sov. Phys. Solid State* **26**, 666-669 (1984).

[2] D.M. Hoffman, B.K. Meyer, A.I. Ekimov, I.A. Merkulov, A.L. Efros, M. Rosen, G. Couino, T. Gacoin, and J.P. Boilot, "Giant Internal Magnetic Fields in Mn Doped Nanocrystal Quantum Dot," Solid State Commun. **114**, 547 (2000).

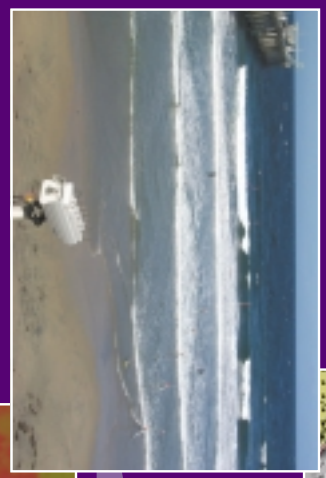

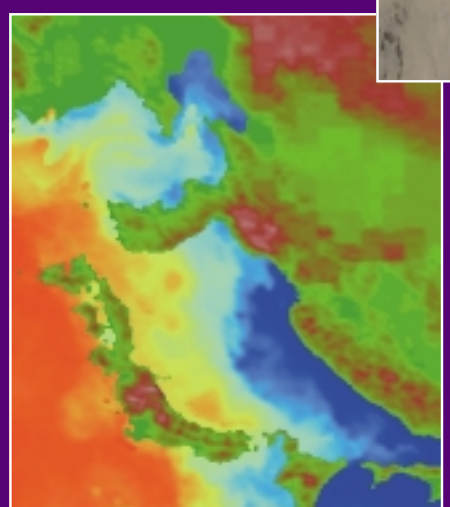

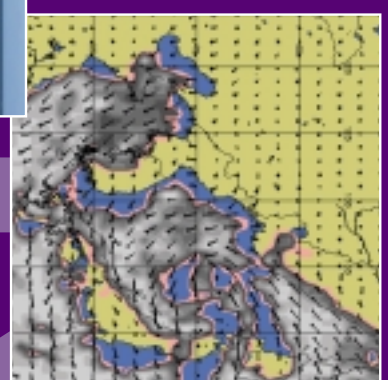

Ocean Science and Technology

Plugging into the Seafloor

S. Fertig
NOVA Research, Inc.

L.M. Tender
Center for Bio/Molecular Science and Engineering

A simple 2-electrode device, consisting of an anode shallowly imbedded in marine sediment and a cathode in seawater, can harvest low-level power from natural, microbe established, voltage gradients at reconstructed ocean floors in laboratory aquaria. Sustained power on the order of milliwatts has been demonstrated thus far from nonoptimized 100 cm^2 sized devices. This sediment-anode/seawater-cathode assembly constitutes a microbial fuel cell, with power resulting from oxidation of sediment organic matter by dissolved seawater oxygen. Considering typical reduced carbon contents of continental margin sediments (< 1000 meters deep), fluxes of additional reduced carbon by sedimentation to the seafloor, and the proven viability of dissolved seawater oxygen as an oxidant by seawater batteries, it is envisioned that optimized power supplies based on this 2-electrode configuration could indefinitely power oceanographic instruments requiring up to 1 watt.

A multitude of sensors are deployed to the seafloor that provide important oceanographic information for the Navy and scientific communities. Many of these sensors make measurements and manipulate and telemeter their data on less than 1 watt continuous average power. Their mission duration, typically less than 1 year, is limited by exhaustion of their battery-based power supplies. Long-term monitoring is impossible without costly and time-intensive retrieval and redeployment of the instrument. We describe here an approach to harvest power directly from the sea floor that may enable uninterrupted long-term sensor operation.

It has been known for some time that a naturally occurring voltage gradient exists just below the seafloor. Here, microbes consume a depth-dependent succession of oxidants as they decompose sediment organic matter that is based on energy of reaction and availability. In the organic-rich sediments of continental margins, oxygen reduction dominates the sediment surface because of its high reaction energy and immediate availability from seawater. Nitrate, manganese, and iron reduction occur within the next few centimeters because of oxygen depletion by microbes closer to the sediment surface. Similarly, sulfate reduction dominates deeper sediment. As each oxidant is successively exhausted and its byproducts generated, sediment pore water becomes more reducing, resulting in a voltage drop as large as 0.8 volts within the top few centimeters of the sediment. This voltage gradient can sustain low-level power for prolonged periods by a simple fuel cell-like device consisting of an electrode shallowly embedded in marine sediment (anode), connected through an external load to a second electrode in seawater (cathode) (Fig. 1). At the anode, oxidation of a microbe-produced oxidation byproduct (represented as $X_{red} \rightarrow X_{ox}$) occurs, regenerating the microbe oxidant and resulting in accelerated oxidation of sediment organic matter. At the cathode, oxygen reduction occurs. The

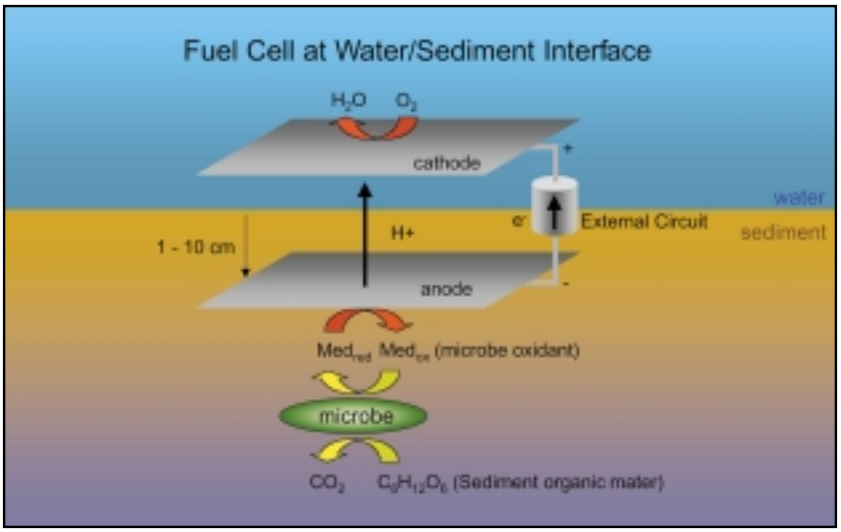

FIGURE 1
Fuel cell at water/sediment interface.

viability of dissolved seawater oxygen as an oxidant for power generation has been established by seawater batteries. Typical sediments on continental margins (< 1000 meters deep) are 2-3% by dry-weight organic carbon, the oxidation of which could liberate 0.01 watt-yr/liter of sediment by this approach. It is conceivable that optimized meter-dimensioned devices based on the device described here could provide abundant power for seafloor sensors.

Acknowledgments: We are grateful to our collaborators: Clare Reimers, College of Oceanic and Atmospheric Sciences, Oregon State University, Corvallis, Oregon, and Wei Wang, Institute of Marine and Coastal Sciences, Rutgers University, New Brunswick, N.J., and to ONR and DARPA for funding.

[Sponsored by ONR and DARPA]

Providing METOC Support for Global 2000

R.A. Allard,[1] R.A. Siquig,[2] and S.J. Lowe[3]
[1]*Oceanography Division*
[2]*Marine Meteorology Division*
[3]*SAIC*

Introduction: The Naval War College (NWC) conducts approximately 50 war games each year to study issues ranging from antisubmarine warfare, unconventional warfare, to global war. Participants in the war games can include junior officers to four-star officers and civilian equivalents. NWC's most recent annual wargame, Global 2000, occurred 14-25 August 2000 and involved more than 800 military and civilian personnel from Newport, Rhode Island, to the U.S. West Coast through distributive gaming efforts. This mission's effort was to experiment with emerging meteorological and oceanographic (METOC) systems, technologies, and concepts that could be used to support (1) the Capstone Concept for Network Centric Operations, which was the underlining theme for Global 2000; and (2) future war games. The Naval Research Laboratory, in association with SAIC, supported Global 2000 by providing a suite of METOC numerical model hindcasts consisting of an 18-day period representative of winter conditions in Southeast Asia. Model results were converted to the World Meteorological Organization standard GRIB format and ingested into the Tactical Environmental Data Server (TEDS). METOC data were used on the "gamefloor" as inputs to effects-based decision aids.

Environmental Scenario Generator: The availability of a turnkey environmental scenario generation process is essential to the success of DoD simulations. The process must be robust, efficient, and repeatable; but they also must be highly customizable and flexible to support the wide range of scenario requirements likely to evolve over the coming years. The Environmental Scenario Generator (ESG) provides an automated capability for the generation of integrated and physically consistent environmental data sets. It meets modeling and simulation customer requirements for an authoritative and realistic representation of atmosphere, oceanic, and/or space natural environment elements for specified regions, time frames, and conditions.

The ESG architecture consists of an intelligent search mechanism to locate desired conditions in reference datasets and a just-in-time production (Fig. 2) capability to provide authoritative representation of the environment when none exist off the shelf. ESG currently exists as a distributed software application providing data mining and database production services. The data mining functionality allows the customer to identify specific environmental events within reference environmental databases. A custom scenario database is then produced based on the actual historical event that provided the desired conditions.

During Global 2000, a specific time frame was selected by NWC based on the availability of auxiliary data sets. Therefore, the data mining portion of ESG was not used for Global 2000. Customized Coupled Ocean Atmosphere Mesoscale Prediction System (COAMPS) model hindcasts for two nested areas at resolutions of 81 and 27 km were generated for Global 2000, using the 1.0° NOGAPS data available from the Master Environmental Library[1] (http://mel.dmso.mil) for the time frame specified by NWC. Figure 3 depicts COAMPS cloud cover and wind vectors over Southeast Asia for 19 December 1999.

Integrated Ocean Prediction System: The Integrated Ocean Prediction System (IOPS) is a suite of wave, tide, and surf models that produce hindcasts/forecasts for essentially any worldwide location. A prototype version of IOPS running on a UNIX workstation was used to support Global 2000 by producing a nested WAM wave model hindcast. A basin-scale WAM model was forced with 1.0° Navy Operational Global Atmospheric Prediction System (NOGAPS) 10-m wind. An inner nest of a regional WAM was forced with 27-km COAMPS wind forc-

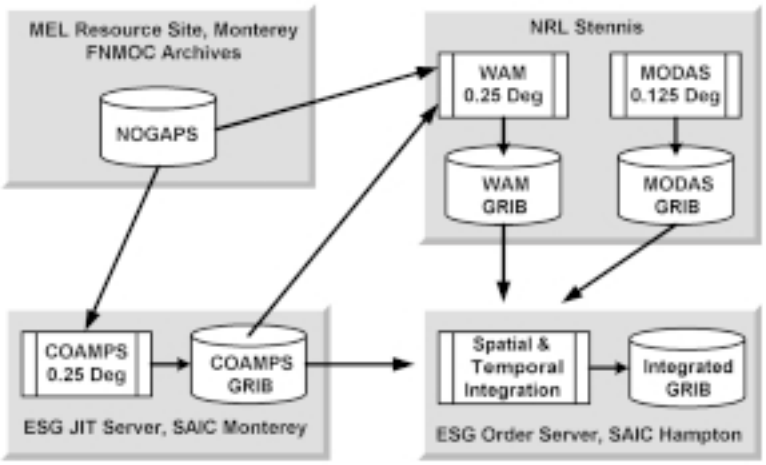

FIGURE 2
ESG just-in-time production capability. COAMPS forcing is converted to GRIB format and sent to NRL Stennis for wave model hindcasts. WAM and MODAS fields are sent to SAIC Hampton for preparation prior to integration into TEDS.

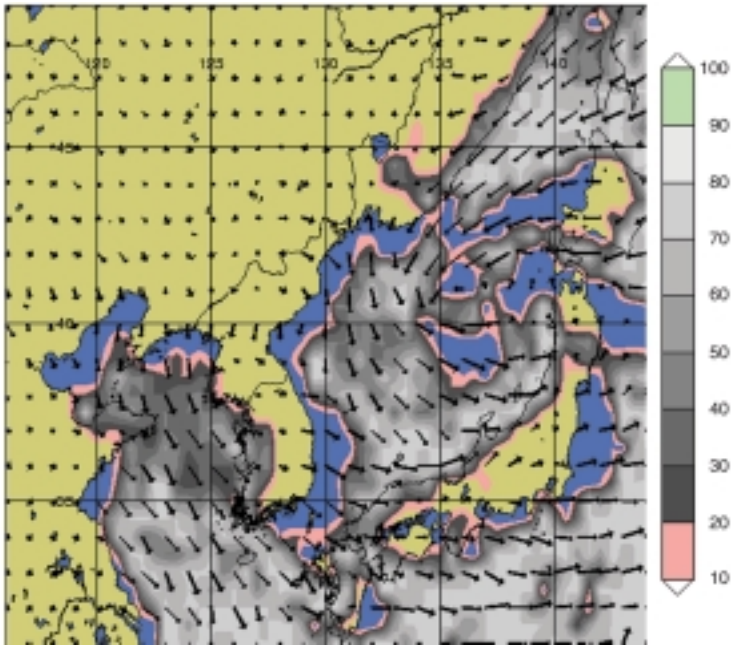

FIGURE 3
COAMPS cloud cover and 10-m winds for 19 December 1999. Wind vectors are proporational to wind magnitude.

ing generated by ESG. Typical WAM outputs include wave heights, wave direction, and wave period.

Modular Ocean Data Assimilation System: The Modular Ocean Data Assimilation System (MODAS), developed by NRL, computes synthetic three-dimensional (3D) fields of temperature and salinity based on gridded sea surface temperature (SST) and sea surface height (SSH) variations. Climatological relationships between subsurface temperature, subsurface salinity, and SST and SSH derived from historic profile observations are used to generate the synthetic fields. Operationally, MODAS can assimilate in situ data such as expendable bathythermographs (XBTs) in addition to remotely sensed data. In support of Global 2000, NRL provided MODAS 3D fields of temperature, salinity, and sound speed for the scenario domain in Southwest Asia for the same

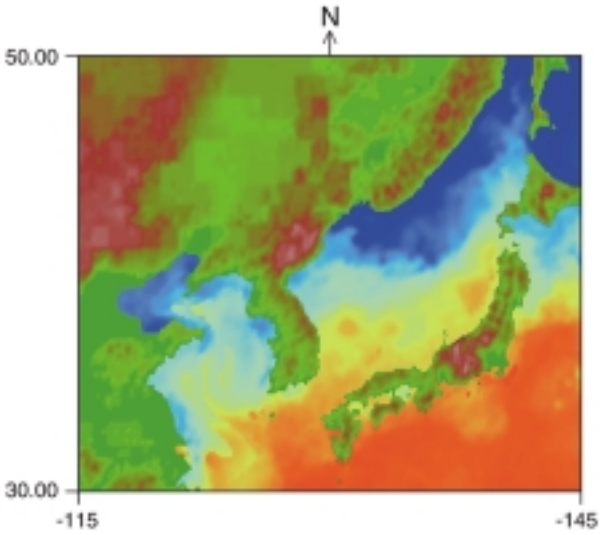

FIGURE 4
MODAS surface temperature for 28 December 1999. Temperatures range from 1 °C (dark blue) to 25 °C (red).

18-day period used for the ESG applications. Figure 4 shows a MODAS surface temperature for 28 December 1999.

Tactical Environmental Data Server: The Tactical Environmental Data Server (TEDS) consists of a set of database, data, and software segments that serve as the primary repository and source of METOC data and products for the Navy Integrated Tactical Environmental Subsystem (NITES). The dynamic data server portion of TEDS is composed of the METOC database and a set of Application Program Interfaces (APIs). These provide storage for and access to dynamic METOC data (e.g., analysis/forecasts of grid field data, observations, and textual observations). In support of Global 2000, COAMPS, WAM, and MODAS hindcast data were converted to GRIB format, timestamped, ingested into TEDS, and made accessible to the NWC "gamefloor."

Summary: State-of-the-art METOC numerical prediction models and analysis systems developed through NRL R&D research programs have been implemented to produce a realistic, custom-designed integrated natural environment for NWC's wargame Global 2000. A goal of this effort was to ensure that the modeling and simulation community could use essentially the same type of METOC information available to the operational fleet today. Future plans will examine the possibility of providing a custom-tailored METOC environment to support Fleet Battle Experiments.

Acknowledgments: The authors thank Mr. Larry Jendro (New Age Systems) who coordinated this METOC effort and LCDR Ben Webb (NWC) who was the catalyst for integrating the METOC environmental data into Global 2000.

[Sponsored by DMSO and SPAWAR]

References

[1] R.A. Siquig, R.A. Allard, and J.H. Spencer, "The Master Environmental Library (MEL)", *1997 NRL Review*, NRL/PU/5230--97-320, 115-117 (1997).

A Real-time 1/16° Global Ocean Nowcast/Forecast System

R.C. Rhodes,[1] H.E. Hurlburt,[1] A.J. Wallcraft,[1] E.J. Metzger,[1] J.F. Shriver,[1] O.M. Smedstad,[2] and A.B. Kara[3]
[1]*Oceanography Division*
[2]*Planning Systems, Inc.*
[3]*Sverdrup Technology, Inc.*

Introduction: The world's first eddy-resolving global ocean prediction system has been developed at NRL. This system uses the NRL Layered Ocean Model (NLOM) with 1/16° (~7.5 km) resolution and is running in real time at the Naval Oceanographic Office (NAVO), which was recently given the Navy lead for operational ocean products. NAVO is scheduled to begin operational testing of the system on 15 December 2000. Pending a successful outcome, it will become an operational product.[1] This system assimilates sea surface temperature (SST) and near real-time satellite altimeter data from TOPEX/POSEIDON and ERS-2 that are available from NAVO's Altimeter Data Fusion Center. The system gives a real-time view of the ocean down to the 50 to 200 km scale of

ocean eddies and the meandering of ocean currents and fronts. It will be used by NAVO for ocean front and eddy analyses and predictions and to provide accurate sea surface height (SSH) for use in computing Modular Ocean Data Assimilation System (MODAS) synthetic temperature and salinity profiles, among other applications. Real-time and archived results from the system can be viewed on the Internet at the NRL Web address: http://www.7300.nrlssc.navy.mil/global_nlom and the NAVO Web address: http://www.navo.navy.mil. To view the results on the NAVO Web page, click on Operational Products, then Keyword Search, and enter NLOM under Topic Search Selection.

Predicting the Ocean vs the Atmosphere: Ocean forecasting is, in principle, similar to atmospheric forecasting, but with two major complications: (a) ocean eddies, at about 100 km across, are typically 20 to 30 times smaller than comparable atmospheric highs and lows. This means that roughly four orders of magnitude more computer time and three orders of magnitude more computer memory are required; and (b) there are relatively few observations below the ocean surface, so data assimilation is effectively confined to using satellite observations of the surface. The duration of forecast skill for the ocean is not restricted to the 10 to 14 day limit for atmospheric highs and lows. We have demonstrated at least 30-day predictive skill for ocean eddies and the meandering of ocean currents and fronts, given sufficient ocean model resolution and satellite altimeter data.

Model Resolution Requirements and Some Impacts of Basic Research: A major component of NRL's ocean modeling program has been a detailed study of the resolution required for ocean prediction. For each prognostic variable, there is strong evidence that NLOM and other popular ocean models need to use grid cells that are at most about 8 km across at mid latitudes.[2,3] Our research has shown that doubling the resolution to 4 km per cell gives substantial improvement, but doubling again to 2 km gives only modest additional improvement. For the NLOM grid, these resolutions translate to 1/16°, 1/32°, and 1/64°, respectively. This is for the global and basin-scale. Limited area coastal models would use the global forecast for boundary conditions and would require much smaller cells.

At 4 km, the optimal resolution is finer than might be expected based on the size of eddies. In relation to ocean eddy size, it is similar to the resolution currently used by the leading weather forecasting models in relation to the size of atmospheric highs and lows. More specifically, our research has shown that fine resolution of the ocean eddy scale is required to obtain coupling between upper ocean currents and seafloor topography via turbulent flow instabilities. This coupling can strongly affect the pathways of upper ocean currents and fronts, including the Gulf Stream in the Atlantic (Fig. 5) and the Kuroshio in the Pacific (Fig. 6).[3,4] The high resolution is also required to obtain sharp fronts that span major ocean basins and associated nonlinear recirculation gyres. Simulation skill for the preceding is crucial for an ocean model to act as an effective dynamical interpolator for satellite altimeter data and for successful forecasting of ocean eddies and the meandering of ocean currents and fronts (Fig. 7).[5]

The Computational Challenge: As far back as 1989, the President's Office of Science and Technology recognized global ocean modeling and prediction as a "Grand Challenge" problem,[6] defined as requiring a computer system capable of sustaining at least one trillion floating point adds or multiplies per second. By taking a multifaceted approach to cost minimization, we are solving the problem on systems capable of only a few percent of this performance. This is the result of a sustained, coordinated 6.1-6.4 NRL effort aimed at developing the first eddy-resolving global ocean prediction system, an effort that has been a leading user of DoD High Performance Computing capabilities. The NLOM computer code is widely portable and has demonstrated very good scalability on up to 1152 Cray T3E processors.[7]

Significance: This first eddy-resolving global ocean prediction system revolutionizes the ability to nowcast and forecast the global ocean circulation down to the scale of oceanic fronts and eddies. The significance of this work has been recognized by the Smithsonian Institution, which solicits case studies each year as one means of developing a history of information technology and its benefits to society. An invited case study on this work, entitled "Eddy-resolving Global Ocean Modeling and Prediction," has been archived in the permanent research collection of the Smithsonian National Museum of American History. It is permanently viewable at http://innovate.Si.edu/cgi-bin/db3/innovate.pl?fid=951423219.36201 8&cgifunction=form.

The system is also a contribution to the Global Ocean Data Assimilation Experiment (GODAE), a multinational effort designed to help justify a permanent global ocean observing system by demonstrating useful real-time operational ocean products. Applications include assimilation and synthesis of global satellite data; ocean prediction; optimum ship track

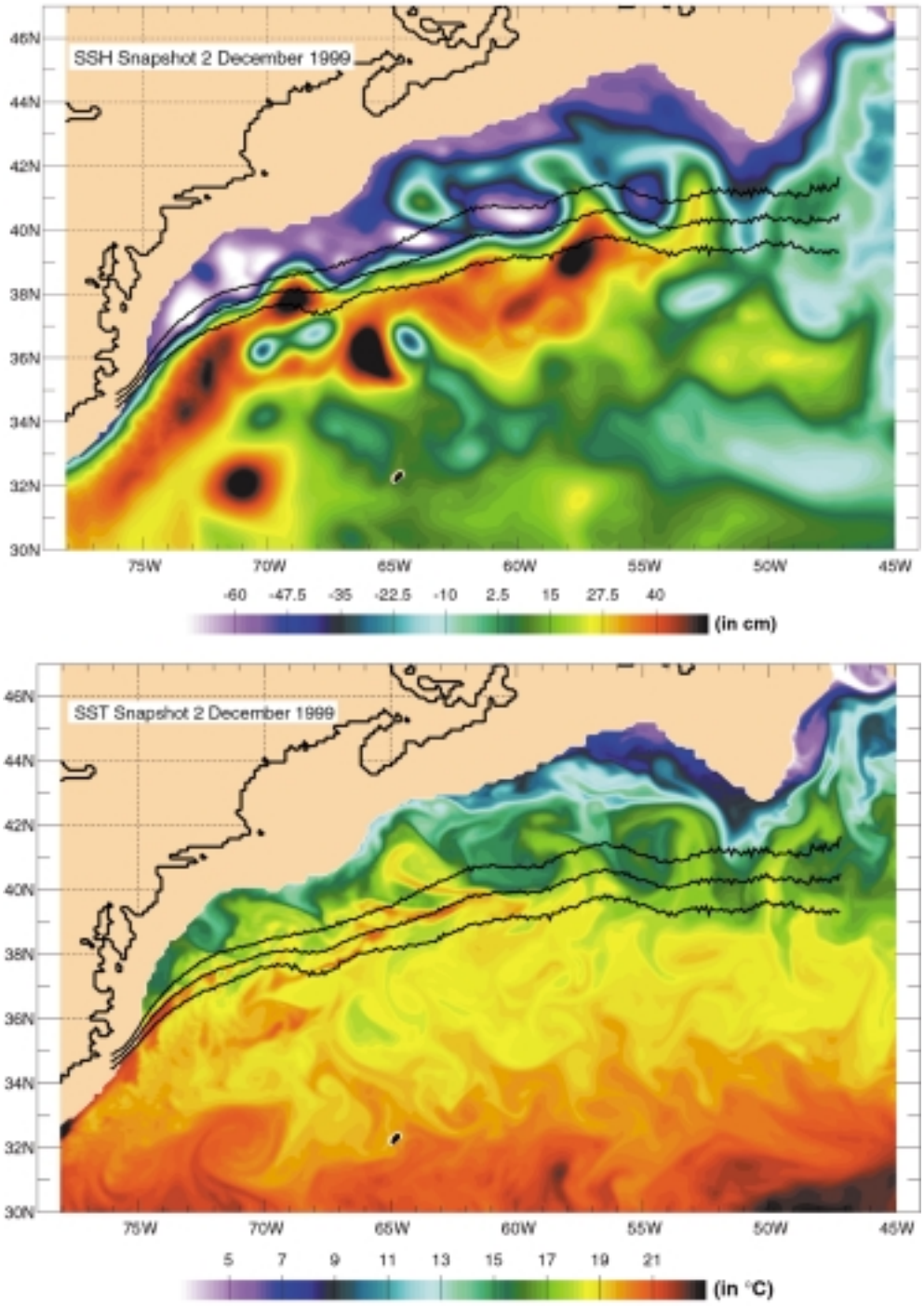

FIGURE 5
Snapshots of SSH and SST zoomed in on the Gulf Stream region. These were simulated by the 1/16° global ocean model with no assimilation of oceanic data. The model was forced by 12 hourly wind stresses and 6 hourly thermal fluxes from Fleet Numerical Meteorology and Oceanography Center. Superimposed is the Gulf Stream IR northwall 1982-96 mean + standard deviation by Z. Sirkes and P. Comillion (personal communication).

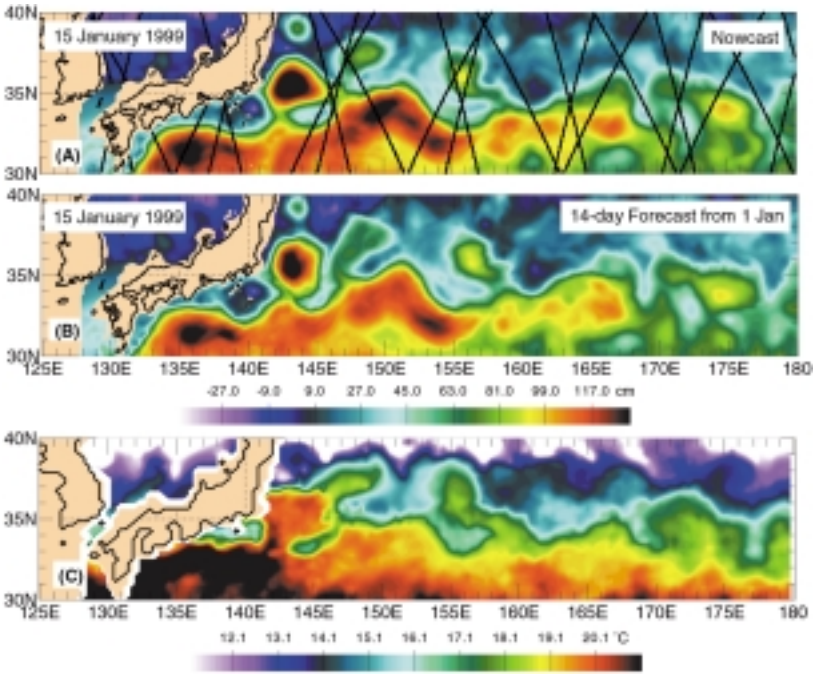

FIGURE 6
Zoom on the Kuroshio south and east of Japan. (a) SSH for 15 January 1999 from the 1/16° global nowcast/forecast system with assimilation of satellite altimeter data from TOPEX/POSEIDON and ERS-2. The altimeter tracks with data available for this update cycle are overlaid. (b) The corresponding SSH snapshot from a 14-day forecast initialized from 1 January 1999. (c) The MODAS 1/8° SST analysis from satellite IR imagery. MODAS is an operational product at NAVO. The SST color bar is designed to highlight the Kuroshio pathway.

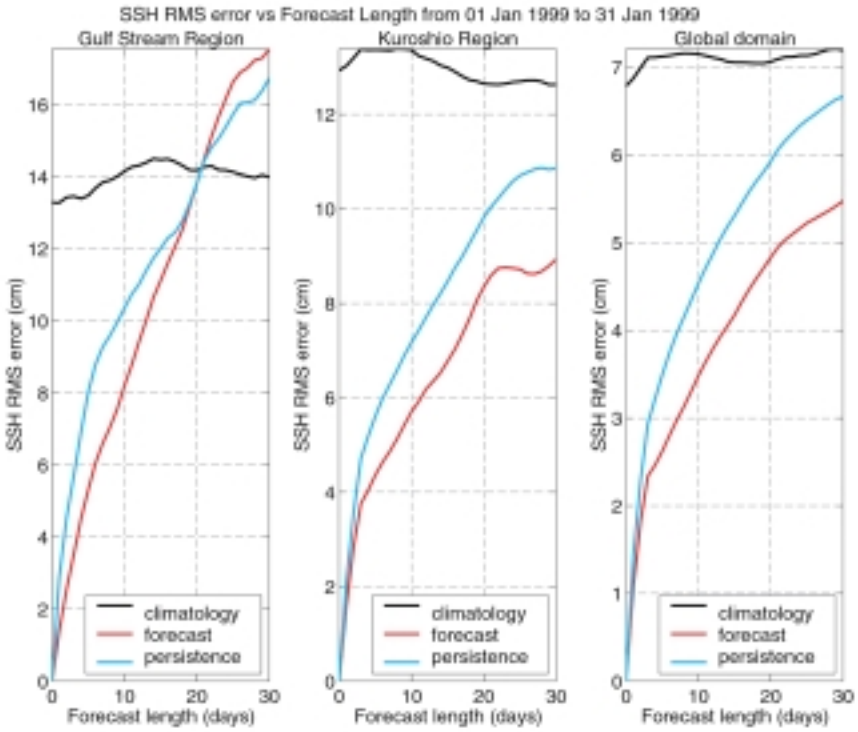

FIGURE 7
The 1/16° global SSH forecast verification against the model with TOPEX and ERS-2 data assimilation.

routing; search and rescue; antisubmarine warfare and surveillance; tactical planning; high-resolution boundary conditions for even higher resolution coastal models; inputs to ice, atmospheric, and bio-physical models and shipboard environmental products; environmental simulation and synthetic environments; observing system simulations; ocean research; pollution and tracer tracking; and inputs to water quality assessment.

[Sponsored by ONR and SPAWAR]

References

[1] S.L. Cross and J. Schmitz, "Navy Layered Ocean Model: The First 100 Days," *NAVO Bull.*, 1, 4-5, Aug. 2000.

[2] E.P. Chassignet, Z.D. Garraffo, R.D. Smith, and H.E. Hurlburt, "High-resolution Gulf Stream Modeling," *Geophy. Res. Lett.* (submitted) (2000).

[3] H.E. Hurlburt and P.J. Hogan, "Impact of 1/8° to 1/64° Resolution on Gulf Stream Model—Data Comparisons in Basin-scale Subtropical Atlantic Ocean Models," *Dyn. Atmos. Ocean.* **32**, 283-329 (2000).

[4] H.E. Hurlburt, A.J. Wallcraft, W.J. Schmitz, Jr., P.J. Hogan, and E.J. Metzger, "Dynamics of the Kuroshio/Oyashio Current System Using Eddy-resolving Models of the North Pacific Ocean," *J. Geophys. Res.* **101**, 941-976 (1996).

[5] H.E. Hurlburt, R.C. Rhodes, C.N. Barron, E.J. Metzger, O.M. Smedstad, and J.-F. Caynla, "A Feasibility Demonstration of Ocean Model Eddy-resolving Nowcast/Forecast Skill Using Satellite Altimeter Data," NRL/MR/7320--00-8235, 23 pp. (2000).

[6] Office of Science and Technology Policy, "Appendix A: Summary of Grand Challenges," in *The Federal High Performance Computing Program*, Executive Office of the President (1989).

[7] A.J. Wallcraft and D.R. Moore, "The NRL Layered Ocean Model," *Parallel Comput.* **23**, 2227-2242 (1997).

Bimodal Directional Distribution of the Second Kind: Resonant Propagation of Wind-Generated Ocean Waves

P.A. Hwang,[1] D.W. Wang,[1] W.E. Rogers,[1]
J.M. Kaihatu,[1] J. Yungel,[2] R.N. Swift,[2]
and W.B. Krabill[3]
[1]*Oceanography Division*
[2]*EG&G*
[3]*NASA*

Introduction: Over the last several decades, it has been accepted that under steady forcing, wind-generated waves travel in the direction of wind. Last year, we presented two-dimensional (2D) spectral analysis of 3D ocean wave topography at equilibrium stage.[1] The results demonstrate unequivocally a robust bimodal directionality in wave components shorter than the dominant wavelength. The generation mechanism of the bimodality is clarified to be nonlinear wave-wave interaction. Continued investigation reveals a second kind of bimodal directional distribution produced by resonant propagation of waves with the forcing wind field. In this situation, the *dominant* waves in a young sea align in oblique angles with the wind direction to maintain propagation resonance for a more efficient air-sea momentum transfer. As a result, two symmetric wave systems straddle the wind vector. The results from these analyses will revise our fundamental understanding of the physics of wind-wave generation and the forcing functions governing the dynamics of ocean waves. The implications of these directional observations on remote sensing (directional characteristics of ocean surface roughness) and air-sea interaction (directional properties of mass, momentum, and energy transfers) are significant.

Airborne Observation and Analysis: Reference 1 reports spatial measurements of ocean waves using an airborne topographic mapper (ATM, an airborne scanning lidar system). The 3D topography provides an excellent directional resolution. Figure 8 shows images of the wave conditions at three different fetches along a flight track in the Gulf of Mexico. The waves are generated by a steady offshore wind following a cold front passing through the region. The top image (Fig. 8(a)) is in the near-shore region, and the coastline is visible in the image. The orientation of the surface undulations is perpendicular to the wind. The next two images (Figs. 8(b)-(c)) are farther downwind. The crosshatched patterns suggest that two wave systems of about equal intensity are crossing each other at a large angle. It is quite obvious that these wave patterns do not fit the conventional unimodal directional distribution function, which has been assumed explicitly or implicitly in the description of surface roughness properties relating to remote sensing and air-sea transfers.

Recent advances in global positioning, laser ranging, and computer technologies provide the capability to acquire high-resolution topography of ocean surface waves for quantitative analysis of their spatial and temporal evolutions. Figure 9(a) shows a sequence of surface wave topography over the 42-km flight track, along which the three photographs shown in Fig. 8 were taken. The corresponding directional wavenumber spectra are shown on the right-hand side of the figure (Fig. 9(b)). The dominant waves of this sequence of spectra are obviously directionally bimodal. At short fetches, the dominant wave direction is crosswind rather than along-wind. As fetch increases, two distinct wave systems propagate obliquely to the wind, forming a crosshatched pattern (Fig. 9(a)). These are characteristics of resonant propa-

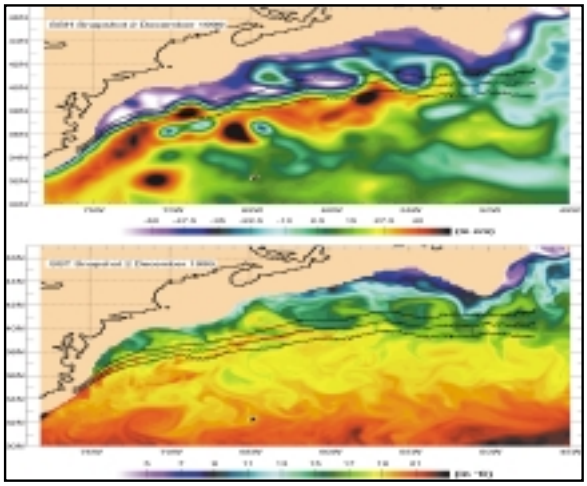

FIGURE 8
Ocean surface waves produced by a steady offshore wind. The fetch (distance from shore) increases from top to bottom.

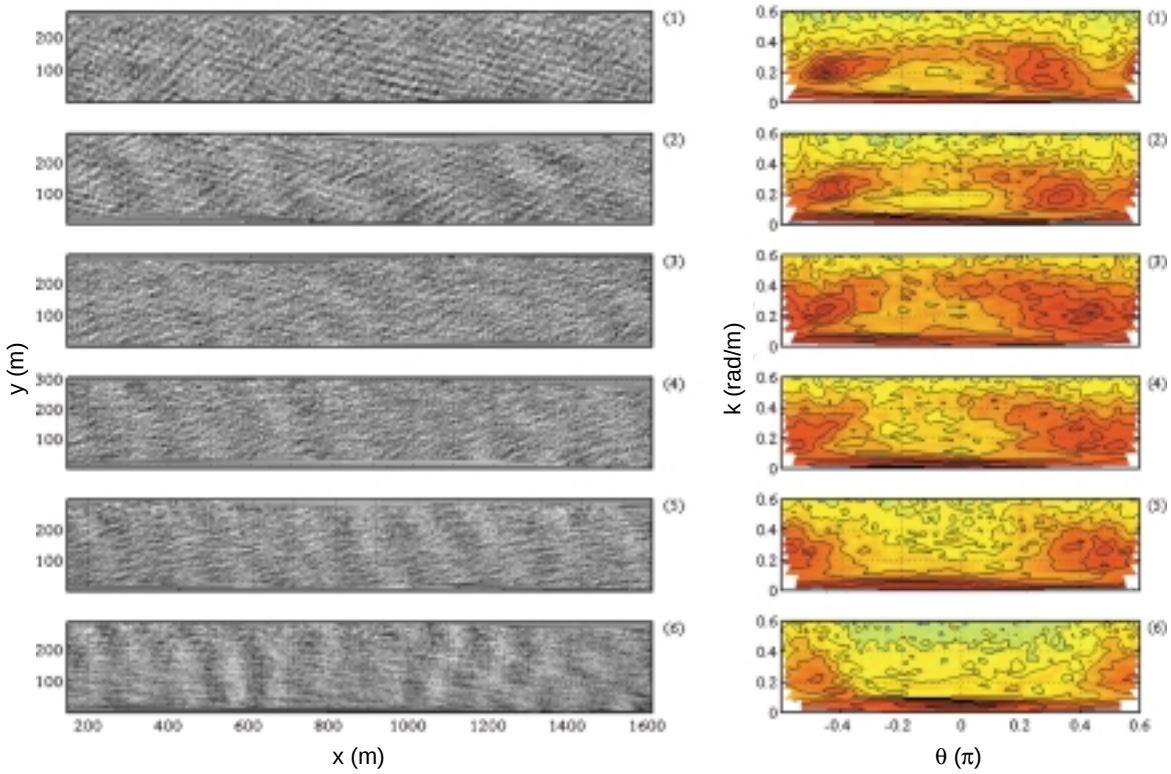

FIGURE 9
(a) 3D surface topography of ocean waves along a flight track at 6 different fetches (38.1, 31.5, 24.8, 18.2, 11.5, and 4.93 km from top to bottom). The wind is blowing from right to left. (b) The corresponding 2D spectra calculated from the surface topographies shown in (a). The wind direction is at θ = 0°.

gation between winds and waves. Under the resonant condition, waves propagate in step with the wind field to receive continuous nourishment from the wind. Because the phase velocity of young waves is much slower than the wind speed, to maintain propagation resonance, they travel at oblique angles from the wind. Reference 2 provides details of the analysis on the spatial and temporal evolution of wind-generated waves.

Summary: It has been held as common knowledge that wind-generated waves propagate in the direction of the wind. This concept has been incorporated into unimodal directional distribution functions in virtually all spectral wave models, as well as in the wind input function in the equation governing the dynamics of ocean surface waves. Recent field measurements of 3D ocean surface topography, however, do not support the assumption. The analysis of 3D wave topography indicates that the directional distribution of ocean surface waves is primarily bimodal. Two different kinds of directional bimodality are confirmed. The first kind, bimodality, occurs at the equilibrium stage and in wave components shorter than the dominant wavelength. The physical mechanism is nonlinear wave-wave interaction that distributes energy from near the spectral peak toward oblique components, forming a resonant quartet. The second kind, bimodality, occurs at the young stage and on dominant waves. The generation mechanism is resonant propagation between winds and waves.

[Sponsored by ONR.]

References

[1] P.A. Hwang, D.W. Wang, E.J. Walsh, W.B. Krabill, W. Wright, and R.N. Swift, "Airborne Measurements of the Directional Wavenumber Spectra of Ocean Surface Waves. Part 2. Directional Distribution," *J. Phys. Oceanogr.* **30**, 2768-2787 (2000).

[2] P.A. Hwang, D.W. Wang, W.E. Rogers, J. Yungel, R.N. Swift, and W.B. Krabill, "Bimodal Directional Propagation of Wind-generated Ocean Waves," *J. Phys. Oceanogr.* (submitted) (2000).

A Video-Based Particle Image Velocimetry (PIV) Technique for Nearshore Flows

J.A. Puleo, K. Holland, and T.N. Kooney
Marine Geosciences Division

Introduction: Natural beaches undergo constant change as they are forced by local physical processes (such as waves and currents) and human-induced processes (such as nourishment or structure development). In addition to scientific and societal interest, beach or nearshore extreme conditions can also be important for military operations relating to amphibious landings and mine burial. While no accurate model exists to predict beach change, it is generally accepted that nearshore (littoral) processes such as beach erosion are largely forced by waves and current variability. Of these two processes, the current field is most difficult, given that flows in this region are typically very complex and nonuniform in space and time. The traditional approach involves in situ instrumentation, but, due to cost and logistics difficulty in placing instruments in the dynamic nearshore, deployments tend to be extremely sparse. An alternate method to standard instrumentation is needed to densely and accurately record nearshore flow phenomena.

Particle Image Velocimetry (PIV): Recently, a video-based remote sensing technique was developed at the Naval Research Laboratory for quantifying nearshore flow fields using particle image velocimetry (PIV).[1] PIV is a nonintrusive technique to extract nearly instantaneous flow fields by correlating sequential images of a passive, tracer-laden flow. Here, we use foam patterns caused by breaking waves and bores as they move across the nearshore region and the subsequent motion of the foam by local currents.

Synthetic Example: Figure 10 shows two synthetic sequential images separated in time by Δt. The offset between Fig. 10(b) and Fig. 10(a) was manually introduced as 7 pixels to the right and 4 pixels down. Up to 15% noise at each pixel location was also introduced to both images. The overlain grid of nodes (blue dots) is where velocity vectors are to be evaluated. For a given grid node, a collection of pixels I is selected from the first image and repeatedly compared using an error correlation function (very similar to cross correlation) to search windows S of the same size as I in the second image. The maximum correlation is then determined such that the spatial offsets Δx and Δy and the time separation yield the horizontal velocity components as $u = \Delta x/\Delta t$ and $v = \Delta y/\Delta t$. The magenta vectors in Fig. 10(b) are those returned from the PIV routine and correspond to the manual offsets introduced to the images. In the field, swash zone foam patterns are captured via video camera, digitized, and then geo-rectified[2] to a real-world coordinate system before PIV application.

Swash Zone Flows: Figure 11 shows two examples of the PIV technique applied to video data

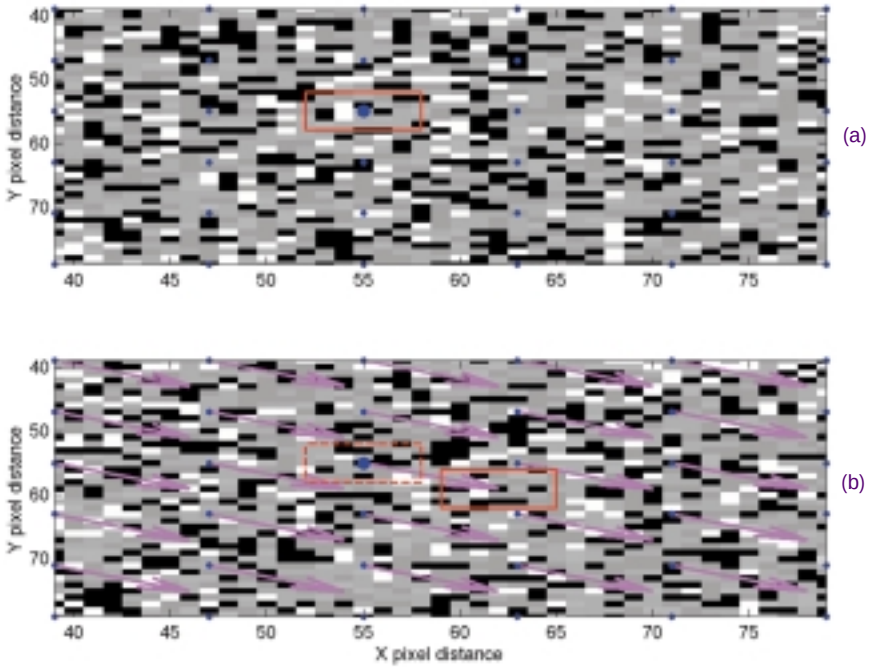

FIGURE 10
Synthetic PIV example. (a) Random placement of image intensities. Blue dots denote location of grid points. (b) The image in Fig. 10(a) manually offset to the right and down. Magenta vectors are returned from the PIV technique and correspond to the manual offsets.

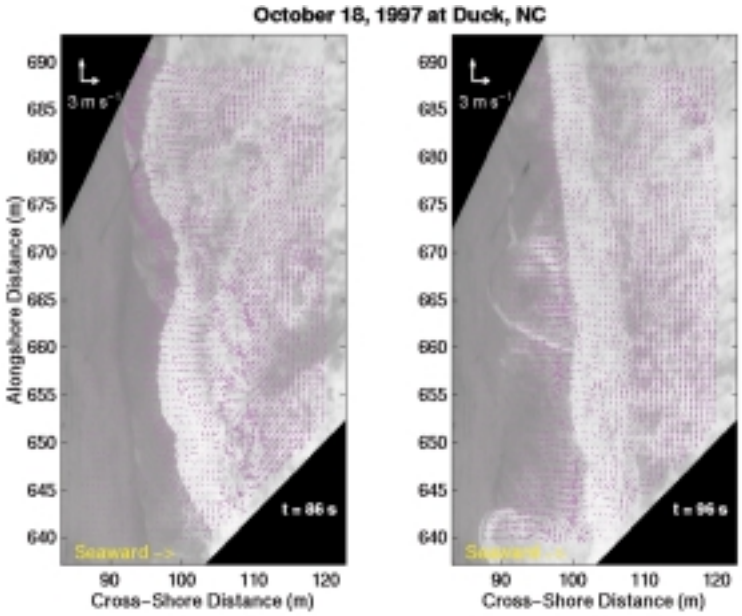

FIGURE 11
Time history of PIV vectors overlain on geo-rectified swash images. Strong onshore flow is seen at t = 86 s (uprush) in the leading edge with a strong alongshore flow further seaward. At t = 96 s, the backwash has collided with the next uprush and alongshore variability in the offshore is evident. The 3 m s^{-1} scale vectors are in upper left-hand corner.

FIGURE 12
Field set up for typical current meter deployment. The instrumentation can be seen as the tripods extending offshore from the right. The camera located in lower center of image is used for PIV.

from the field. The dense estimate of the flow field (over 2700 estimates in a roughly 35 × 55 m area) can be seen in the vector overlay. In both phases of flow, the uprush (left) and the backwash (right), the flow complexity in this region is obvious and emphasizes the importance of spatial coverage when trying to understand the currents and their effect on sediment transport. Also of importance is the fact that swash currents are not restricted to strictly onshore/offshore motion. These particular examples demonstrate how alongshore-directed currents may dominate the nearshore, even close to the shoreline.

To date, the PIV technique was shown to be robust when compared to alternate video methods.[1] Future groundtruth will require direct comparisons with standard instrumentation, such as that seen in Fig. 12. The disadvantages of standard instrumentation are: (1) point measurements in only a handful of locations can realistically be obtained, and (2) each instrument package is quite expensive. But PIV can alleviate both of these problems through its dense spatial sampling and cost effectiveness. For instance, to estimate the velocity at 1000 grid points would yield about a 3000-fold cost savings over standard in situ instrumentation.

Summary: A new video-based remote sensing technique has been developed at the Naval Research Laboratory to quantify nearshore surface flow fields. This cost-effective technique yields thousands of estimates of surface current velocities over a large spatial area as opposed to sparse collection by standard instrumentation. These dense flow field measurements should further our understanding of nearshore flows and lead to a better understanding of sediment transport and its effect on coastal erosion.

[Sponsored by ONR]

References

[1] K.T. Holland, J.A. Puleo, and T.N. Kooney, "Quantification of Swash Flows Using Video-based Particle Image Velocimetry," submitted to *Coastal Eng.*

[2] K.T. Holland, R.A. Holman, T.C. Lippmann, J. Stanley, and N. Plant, "Practical Use of Video Imagery in Nearshore Oceanographic Field Studies," *IEEE J. Ocean. Eng.* **22**, 81-92 (1997).

Arctic Oceanographic Measurements from P-3 Aircraft

V.A. Childers,[1] B. Ekwurzel,[2] and J.M. Brozena[1]
[1]*Marine Geosciences Division*
[2]*University of Arizona*

Do dramatic changes in the Arctic Ocean detected in the 1990s represent: (1) a normal cycle within the cyclical climatic pattern known as the Arctic Oscillation, (2) anthropogenic global warming, or (3) the superposition of these two signals? To date, the logistical difficulties of accessing the Arctic Ocean have interfered with the systematic data collection needed to resolve the debate linking the forcing mechanisms for these changes. In 1999, the Naval Research Laboratory (NRL) tested a method that could provide these answers by extending time series measurements of temperature and salinity over any region within range of an airport. Using a P-3 Orion aircraft in our test, we successfully deployed three out of six expendable conductivity, temperature, depth (CTD) buoys into normal-sized leads in the ice (Fig. 13). Buoys deployed near the North Pole and on the Gakkel Ridge and Siberian Shelf recorded Atlantic water core temperatures that reflect North Atlantic Oscillation forcing.

Climatic Forcing in the Arctic: The North Atlantic Oscillation (NAO) index between 1988 and 1995 attained extreme positive values for winter climatic forcing over the Arctic and the Nordic Seas that are the largest on record over the past century. The NAO and, by extension, the Arctic Oscillation are terms used to describe the oscillation between atmospheric pressure regimes: (1) The Icelandic low with the Azores high (NAO positive index) vs the Icelandic high with Azores low (NAO negative index); and (2) the Icelandic low with a Siberian high vs the reverse pressure fields.[1] In 1996, the NAO again dropped to negative values. Spectral analysis of tree ring records indicates that the NAO index oscillates at periods of 2, 8, 24, and 70 years. The ocean-atmosphere link is demonstrated by the correspondence of the NAO index with oceanographic change in the Arctic and North Atlantic seas.[1]

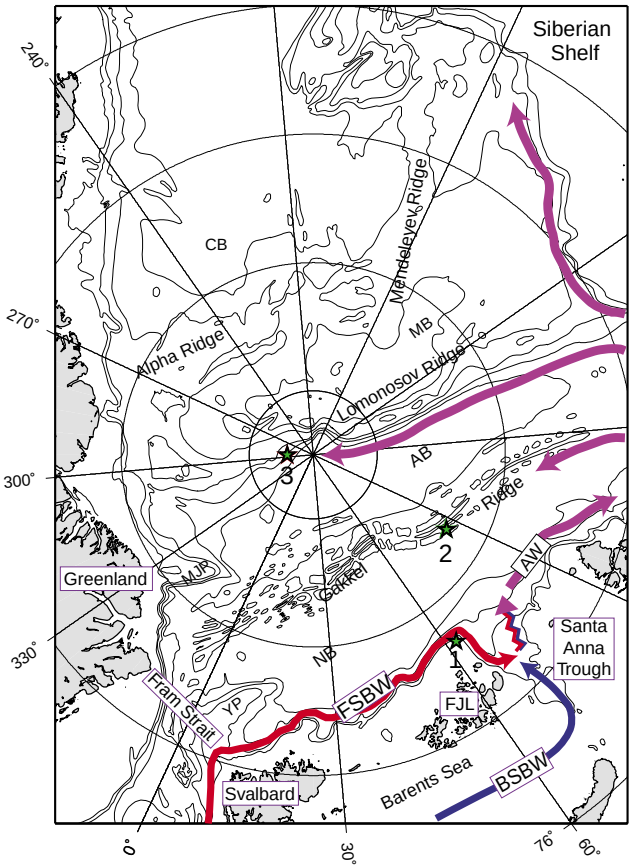

FIGURE 13
Location of the three CTD buoys is indicated by stars. The bathymetric contour interval is 1000 m with the addition of the 500 m contour to delineate the Santa Anna Trough. YP is Yermack Plateau, MJP is Morris Jesup Plateau, NB is Nansen Basin, AB is Amundsen Basin, MB is Makarov Basin, FJL is Franz Josef Land, FSBW is Fram Strait branch water, and BSBW is Barents Sea branch water. Arrows denote the circulation path of the Atlantic water (AW) through the Arctic Ocean.

The Experiment: NRL has recently completed seven field seasons of an aerogeophysical campaign to measure gravity, magnetics, and sea surface topography over the Arctic Ocean. During the 1999 field season, NRL tested the deployment of airborne expendable conductivity-temperature-depth (axCTD) buoys in the ice-covered region of the Arctic Ocean's Eurasian Basin (Fig. 14). These buoys measure temperature and salinity to 1000-m depth.

Six axCTD buoys were deployed in this test during turns and transits of the geophysical survey. Of those six, three were successful in hitting a lead. With practice and without the maneuvering constraints imposed by the primary gravity mission, we expect that the success rate could be substantially improved.

Results: Atlantic water flows northward into the Arctic from the Norwegian-Greenland Sea and separates into two branches. One branch, termed the Fram Strait branch water (FSBW) enters through Fram Strait and travels eastward along the shelf slope. Barents Sea branch water (BSBW) flows onto the Barents Sea Shelf between Norway and Svalbard. The water cools on its transit across the shelf to the Santa Anna Trough, where it again enters the basin and mixes into the FSBW.[2] The merged branch waters continue their cyclonic motion into the Eurasian and Canadian Basin and the core of the Atlantic water progressively cools. The temperature of any Atlantic core water mass is a function of time spent in the Arctic Ocean; its location in the circulation system; and the initial temperature of the inflowing Atlantic water, which corresponds directly to the NAO index.[2,3]

Buoy 1 represents only FSBW, and the Atlantic water core temperature at this station reaches 1.82 °C at ~210 m depth. Buoy 2 is located in the return flow along the Gakkel Ridge where the Atlantic water is a mixture of FSBW and BSBW, with the highest Atlantic water core temperature of the three stations of 2.1 °C located at 260 m depth. Amundsen Basin Buoy 3 is located in the return flow along the Eurasian Basin side of the Lomonosov Ridge and reflects the continued cooling of the Atlantic water, with a core temperature of 1.41 °C at ~275 m depth. The North Pole has been repeatedly occupied by Arctic cruises over the past decade. Historical data collected at the North Pole in 1991 and 1994 (Fig. 15) demonstrate an increase in Atlantic water core temperature over this period. NRL Buoy 3, 90 km

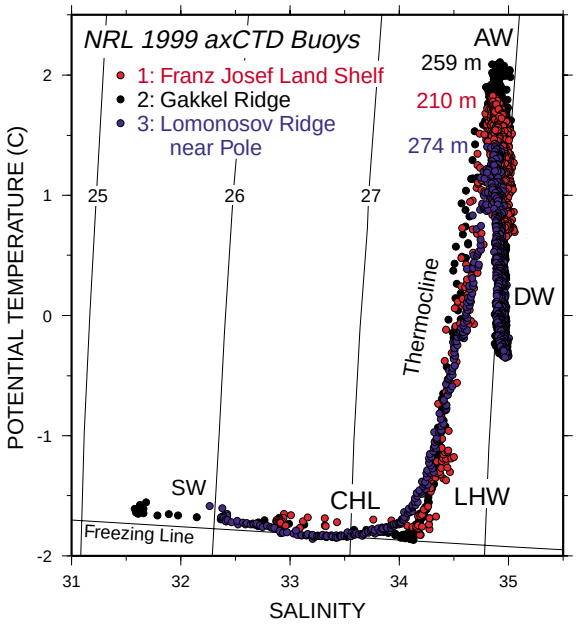

FIGURE 14
The three axCTD stations displayed in potential temperature-salinity space, which helps delineate the various water masses. The potential temperature calculation removes the adiabatic temperature effects from the in situ measurement. SW is surface water, CHL is cold halocline layer, LHW is lower halocline water, AW is Atlantic water, and DW is deep water. The depths of the highest temperatures are noted. The contours denote surfaces of equal density.

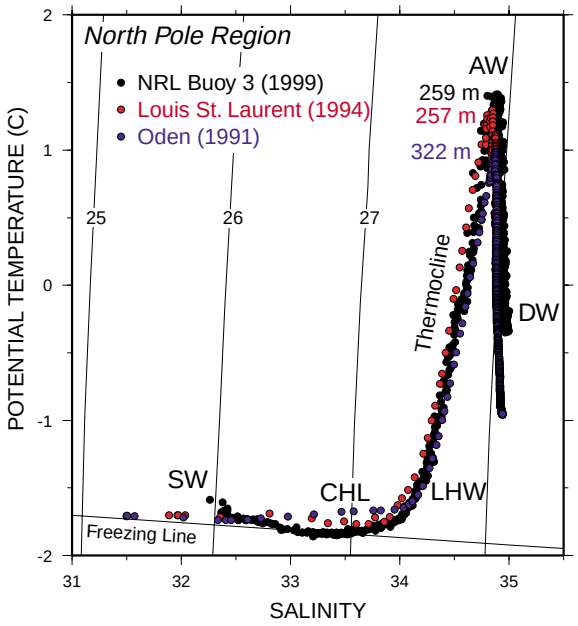

FIGURE 15
Buoy 3 data are compared with historical CTD measurements from the North Pole[4,5] in potential temperature-salinity space. Abbreviations are as in Fig. 14.

from the pole, records a higher temperature yet, suggesting a trend of continuing temperature increase in this water mass, although the warming seems to be slowing. Temperatures warmed by 0.3 °C from 1991 to 1994, and only an additional 0.1° from 1994 to 1999. This trend is consistent with how the NAO values plateau near the end of the extrema.

Discussion and Summary: The Arctic Ocean is experiencing rapid climatic and oceanographic change. The P-3 Orion aircraft as a platform provides a unique opportunity to measure temperature and salinity very quickly over any region within range of an airport for significantly lower cost than required for an icebreaker or a nuclear submarine. In addition, the P-3 can capture temporal change by resurveying its own and other measurements made by the SCICEX submarine program or other ice-breaker cruises. This technique could provide the data sampling needed to identify any global warming signal in the Arctic today.

Acknowledgments: This program was sponsored by the Office of Naval Research through the NRL Core Research Funds Element no. 6153N and 6.1 platform support funding. Knut Aagaard, University of Washington at Seattle, suggested the buoy drop locations.

[Sponsored by ONR]

References

[1] R. Dickson, J. Lazier, J. Meincke, P. Rhines, and J. Swift, "Long-term Coordinated Changes in the Convective Activity of the North Atlantic," *Prog. Oceanog.* **38**, 241-295 (1996).

[2] B. Rudels, E.P. Jones, L.G. Anderson, and G. Kattner, "On the Intermediate Depth Waters of the Arctic Ocean," in *The Polar Oceans and Their Role in Shaping the Global Environment*, edited by O.M. Johannessen, R.D. Muench, and J.E. Overland, (American Geophysical Union, Washington, D.C., 1994) pp. 33-46.

[3] J. Blindheim, V. Borovkov, B. Hansen, S.-A. Malmberg, W.R. Turrell, and S. Østerhus, "Upper Layer Cooling and Freshening in the Norwegian Sea in Relation to Atmospheric Forcing," *Deep-Sea Res. I*, **47**, 655-680 (2000).

[4] L.G. Anderson, G. Björk, O. Holby, E.P. Jones, G. Kattner, K.P. Koltermann, B. Liljeblad, R. Lindegren, B. Rudels, and J. Swift, "Water Masses and Circulation in the Eurasian Basin: Results from the Oden 91 Expedition," *J. Geophys. Res.* **99**(C2), 3273–3283 (1994).

[5] J.H. Swift, E.P. Jones, K. Aagaard, E.C. Carmack, M. Hingston, R.W. Macdonald, F.A. McLaughlin, and R.G. Perkin, "Waters of the Makarov and Canada Basins," *Deep-Sea Res., Part B*, **44**(8), 1503-1529 (1997).

Optical Science

RGB Emission in Organic Light-Emitting Devices

L.C. Picciolo, H. Murata, and Z.H. Kafafi
Optical Sciences Division

Full-color electronic displays have numerous uses in today's ever-expanding technology—from military applications (e.g., helmet-mounted, cockpit, submarine, and map displays) to commercial uses (e.g., high-definition televisions (HDTVs), video monitors, and personal digital assistants (PDAs)). This exciting technology is beginning to emerge with the incorporation of organic light-emitting devices (OLEDs). OLEDs have many highly desirable characteristics, such as self-emission, high brightness, wide viewing angles, lightweight, low-power consumption, and compatibility with flexible substrates (Fig. 1(a)). A display is made up of many tiny individual pixels (picture elements) where an OLED represents one pixel. In a full-color display, each pixel contains one or all of the three color components—red, green, and blue (RGB) (Fig. 1(b)).

The realization of full-color molecular OLED (MOLED)-based displays will depend on several technological advances. These include the development of a streamlined approach to the manufacture of RGB patterned pixels, efficient and stable red emitting materials, and the improvement of the device operational stability at and above room temperature. Our research here at NRL focuses on meeting these challenges through innovative approaches. To this end, a unique and simplified approach has been developed to fabricate RGB pixels through the use of a "universal host" for RGB emitters.[1] Also, a highly fluorescent and stable red emitter was synthesized and used as the dopant in MOLEDs, with excellent color chromaticity coordinates that are ideally suited for display applications.[2] In addition, we have developed thermally and temporally stable MOLEDs using a multilayered structure. This multilayered structure consists of hole injection and transport layers with high glass transitions temperatures, a highly fluorescent guest-host emitter layer, and a thermally stable electron transport layer.[3]

RGB Patterning: There are currently four proposed methods for patterning multicolor OLEDs: (1) RGB emission from a white light source using color filters, (2) conversion of blue light to green and green to red, (3) using a multistack RGB OLED configuration, and (4) patterning discrete RGB components through a mask. The first approach leads to devices with a shortened lifetime. These devices must be operated at high brightness (or current density) to overcome the reduced optical power due to filtering from the white OLED. A reduction in device efficiency is often the case when using the color down-conversion process. The third and fourth methods take advantage of RGB dopants in individual hosts. Doping is an effective approach for achieving color tunability and improving device efficiency and stability. The former requires a complicated fabrication process whereas the latter is challenging since patterning organic materials is quite difficult. A novel approach to patterning that uses a "universal host" for the RGB guest emitters along with a precise shadow mask has been developed at NRL.[1] This technique offers a simple OLED structure and minimizes the number of guest and host materials used. Figure 2(a) shows RGB emission from a MOLED structure based on 6,13-diphenylpentacene (DPP), *N, N′*-diethylquinacridone (DEQ), and 4,4-bis(1-naphthylphenylamino)biphenyl (NPB), respectively, and the RG universal host, 5,5′-bis(dimesitylboryl)-2,2′-bithiophene (BMB-2T). Figure 2(b) shows the Commission Internationale de l'Eclairage (CIE) color gamut with the RGB chromaticity coordinates, which closely match those of typical cathode ray tubes (CRTs) and HDTVs. Our unique approach takes advantage of efficient energy transfer from host to guest combined, in some cases, with direct carrier recombination on the guest molecules to achieve the desired chromaticity. Devices containing the red emitting layer, DPP doped into tris(8-hydroxyquinolinato) (Alq_3), have demonstrated good external electroluminescence (EL) quantum efficiencies (1.3%, close to the theoretical limit) and remarkable stability in device efficiency over a wide range of brightness (current density). This is an important property for passive and active matrix displays.

Thermal and Temporal Stability: OLEDs must be able to maintain optimized device characteristics (device efficiency, color emission) at different operating temperatures. In addition, it is particularly important for full-color displays to maintain good RGB color balance with temperature fluctuations. The combined use of thermally and morphologically stable hole and electron transporters, and doping the emissive layer has been shown to improve device durability and efficiency below, at, and above room temperature.[3] The external EL quantum efficiency of such devices remains constant over a wide operating temperature. Figure 3(a) shows the temperature dependence of the voltage and luminous power efficiency of devices containing a DEQ: Alq_3 emitter layer. The voltage decreases with increasing temperature, which

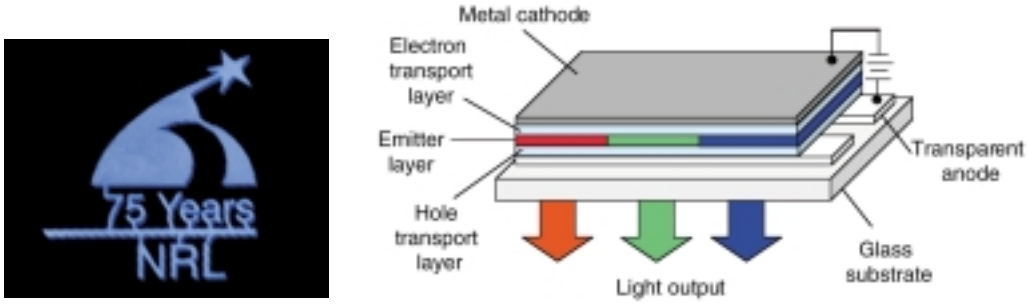

(a) (b)

FIGURE 1
(a) Blue OLED on a flexible plastic substrate (NRL logo celebrating its 75th anniversary). (b) OLED device structure with RGB color components.

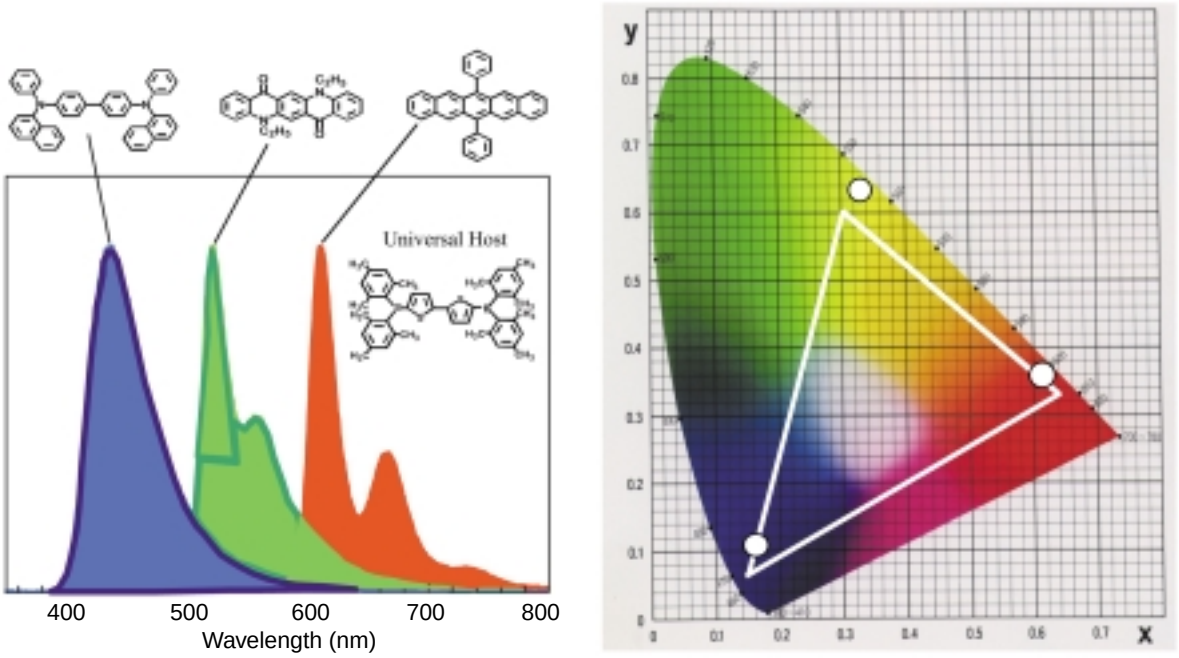

(a) (b)

FIGURE 2
(a) Electroluminescence spectra. (b) CIE color coordinates from devices using an RG universal host.

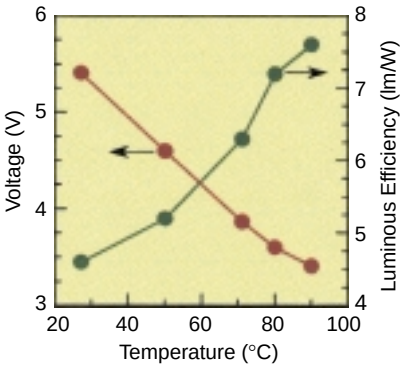

(a)

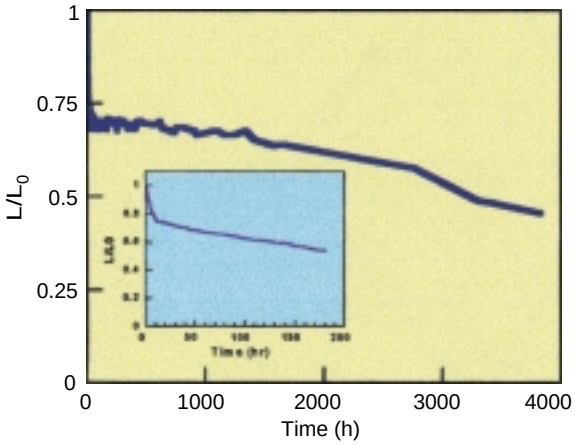

(b)

FIGURE 3
(a) Voltage and luminous power efficiency as a function of temperature. (b) Luminance as a function of time for a device measured at room temperature and at 80 °C (inset).

is probably due to an increase in the electron mobility in the Alq_3 layer. Since the EL quantum efficiency is stable with increasing temperature, the reduction in the operating voltage is directly reflected as an increase in the luminous power efficiency of the devices. An improvement in the lifetime of these devices has also been observed. The lifetime of a device is defined as the time it takes to reach half of the initial luminance (half-life). Figure 3(b) shows the decay in the luminance of two devices as a function of time measured at 80 °C and room temperature (at a constant current of 100 A/m^2). With initial luminances of 850 and 780 cd/m^2, the devices reach their half-life after 200 and 3200 hours, respectively. These same devices are projected to reach a continual operating lifetime of >10,000 hours, with an initial luminance comparable to that typical for CRTs and televisions.

[Sponsored by ONR and DARPA]

References

[1] Z.H. Kafafi, L.C. Picciolo, and H. Murata, "A Universal Host for RG or RGB Emission in Organic Light Emitting Devices," Navy Case No. 82,530 (2000).

[2] L.C. Picciolo, H. Murata, and Z.H. Kafafi, "Pentacene Derivatives as Red Emitters in Organic Light Emitting Devices," Navy Case No. 79, 914 and U.S. Patent Application Serial No. 09/464,090 (1999).

[3] H. Murata, C.D. Merritt, H. Inada, Y. Shirota, and Z.H. Kafafi, "Molecular Organic Light Emitting Diodes with Temperature–Independent Quantum Efficiency and Improved Thermal Durability," *Appl. Phys. Lett.* **75**, 3252 (1999).

WAR HORSE—Wide Area Reconnaissance—Hyperspectral Overhead Real-time Surveillance Experiment

C.M. Stellman and J.V. Michalowicz
Optical Sciences Division

The need for strategic surveillance of critical ground targets is well recognized in the military community. It is generally accepted that future mission planning for scenarios involving ground targets will require real-time surveillance and reconnaissance reports to improve battlefield situational awareness, decrease targeting sensor-to-shooter cycle times, and provide timely battle damage assessments. These reports will have to provide the image analyst with target information in the form of both detection (where is the target?) and recognition (what is the target?). In response to this need, numerous electro-optical imaging sensors that detect reflected and/or thermally emitted radiance have been developed. While these high-resolution panchromatic imaging systems have demonstrated strong target recognition capabilities, they are not without limitations. When covering large search areas, target detection can often become difficult due to the overwhelming quantity of data presented to the image analyst.

In contrast to this, hyperspectral imaging systems, when used in conjunction with appropriate detection algorithms, can cover large search areas while greatly reducing the amount of information relayed to the analyst. The key to hyperspectral detection is exploitation of the inherent spectral differences between targets of interest and background clutter. The trade-off is that data must be collected at low to moderate spatial resolutions, making target recognition difficult. By pairing the target-detection capabilities of hyperspectral imaging with the target-recognition capabilities of high-resolution panchromatic imaging, the best of both worlds can be realized. Furthermore,

by combining these state-of-the-art capabilities with recent technological advances in computing power and algorithm development, the development of real-time target detection and recognition systems can be realized. On this premise, NRL's Dark HORSE program has been working to develop real-time hyperspectral detection, cueing, target location, and target designation capabilities. As a result of these efforts, NRL has recently developed and demonstrated WAR HORSE (Wide Area Reconnaissance—Hyperspectral Overhead Real-Time Surveillance Experiment), the first autonomous real-time hyperspectral target detection system to be flown aboard a Predator unmanned air vehicle (UAV).

WAR HORSE Components: The complete WAR HORSE system is composed of seven components: a visual/near-infrared (VIS-NIR) hyperspectral sensor, a visible high-resolution panchromatic line-scan sensor, a sensor interface computer, a real-time data processing computer, a stand-alone GPS/INS system, a digital line-of-sight data link, and a ground station interface computer. The push-broom hyperspectral sensor records reflected light in many narrow contiguous bands in the wavelength region of the electromagnetic spectrum. The sensor consists of an American Holographic grating spectrometer and a 1024 × 1024 Silicon Mountain Designs custom CCD camera. The sensor operates at a frame rate of 40 Hz and provides 1024 cross-track spatial pixels and 64 wavelength bands (450-900 nm). The panchromatic imaging sensor also operates in the visible wavelength region and offers imagery with resolution six times better than that of the hyperspectral sensor. The sensor consists of a Dalsa 6000-pixel CCD line scanner and a large-format Pentax lens (300 mm); it operates at a frame rate of 240 Hz. The systems signal processor and interface computer are responsible for processing the hyperspectral data and for declaring target detections. Detections consist of objects within the scene that are spectrally anomalous and meet a specific spatial constraint. The processor system consists of two Quad SHARC digital signal processors (DSPs) and a Pentium II processor. The DSPs perform all required calibration and run the subspace RX anomaly detection algorithm in real-time. Custom software provides the image analyst with data output in the form of a 3-band false-color waterfall display of the hyperspectral imagery with overlaid target cue information (relative image location). For each target cue, a high-resolution image chip (collected from the bore-sighted line scanner) is also presented to the analyst. This imagery, along with image chip geo-coordinates, are transmitted to a ground station in real time via a digital RS-170 data link. The link uses a custom board that encodes digital data to a video-compatible analog output with Reed-Solomon forward error correction. A high-frame-rate video frame grabber and custom demodulation software decode the transmitted data and presents it to the image analyst via the ground station interface computer.

WAR HORSE Demonstration: The WAR HORSE system was flown on a Navy Postgraduate School (NPS) Predator UAV (Fig. 4) over the Camp Roberts (California) training facility. Integration and flight support were provided by the NPS Center for Interdisciplinary Remotely Piloted Aircraft Studies (CIRPAS). Typical flight parameters for the Predator were an altitude of 10,000 feet and an airspeed of 70 knots. This provided a hyperspectral ground sampling dimension of approximately 1 meter and a high-resolution line scan ground sampling dimension of approximately 6 inches. During the demonstration, data from the hyperspectral sensor were analyzed by the onboard real-time processor. When a target (namely, a spectral anomaly meeting a specific spatial constraint) was detected, a high-resolution image was collected from the bore-sighted panchromatic visible sensor. A 3-band false-color waterfall display of the hyperspectral data (Fig. 5 - left image) with overlaid target cues (Fig. 5 - red boxes) and the corresponding high-resolution image chips (Fig. 5 - right images) were then transmitted to the ground station in real time and presented to the image analyst. In addition to processing the data in real time, all data (full-up hyperspectral and high-resolution) were stored to disk for additional follow-on postflight analysis. The data are currently being used in the characterization of sensor performance and in the development of new detection algorithms.

FIGURE 4
WAR HORSE hyperspectral target detection system installed aboard the NPS Predator UAV.

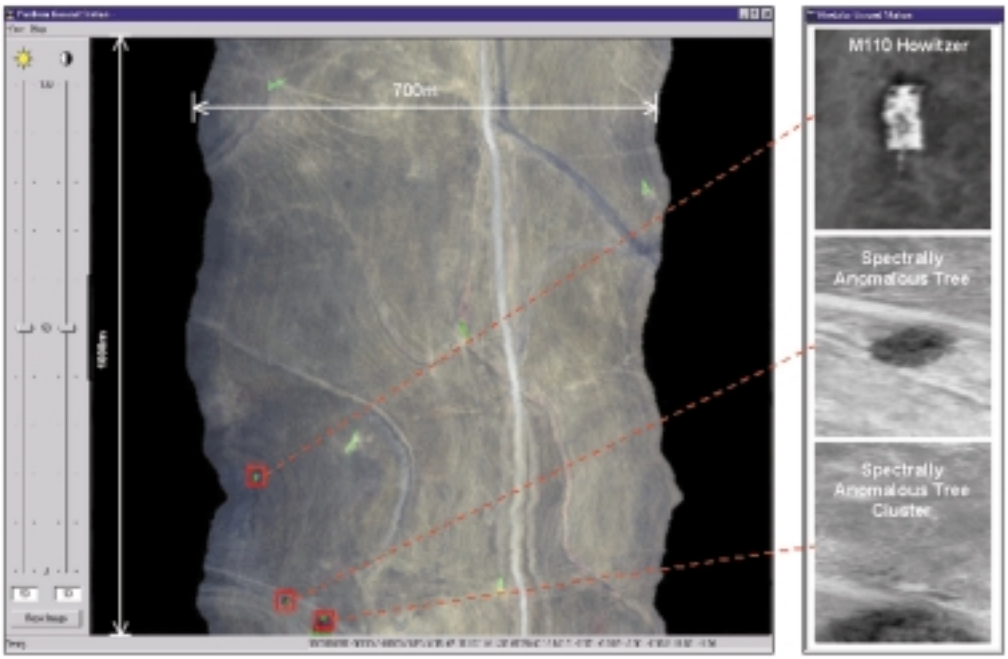

FIGURE 5
WAR HORSE ground station data output.

Future Plans: The demonstrated effectiveness of these approaches to locate and identify anomalous targets of interest has provided the impetus for entering the next stages of development. This includes continued work in the areas of advanced algorithm and processor development. Future hyperspectral algorithms will exploit not only spectral information but also the relationships between a given target's spectral signature and its spatial dimensions. In addition, algorithms will explore the advantages of change detection (the monitoring of changes in spectral/spatial information over time). These efforts will be advanced by the ever-evolving changes in processor technology and architectures. In addition to improving hyperspectral algorithms and processing, NRL has also begun efforts to develop state-of-the-art hyperspectral sensors that extend into other spectral wavelength regimes of interest. One example is the HISTAR (Hyperspectral Imaging for Surveillance and TARgetting) sensor, a long-wave infrared hyperspectral imaging system that will provide a wide-area standoff hyperspectral search capability. A second NRL sensor development effort is the Diamond Head Sensor, a short-wave infrared hyperspectral imaging system that will provide a wide-area standoff search capability complimentary to that of HISTAR.

Summary: NRL has successfully demonstrated the first autonomous real-time hyperspectral target detection system flown aboard a Predator unmanned air vehicle. The WAR HORSE sensor system has demonstrated the utility of hyperspectral target detection and cueing, and will provide an enabling technology for numerous existing and/or future UAVs, uninhabited combat air vehicles (UCAVs), and/or manned reconnaissance platforms.

Acknowledgments: The authors acknowledge the other members of the WAR HORSE team: F. Olchowski and G. Hazel of NRL's Optical Sciences Division and B. Schaff, B. Kendall, A. Stocker, and E. Ensafi of Space Computer Corporation.

[Sponsored by ONR]

2-D Radiation Imaging Using Optically Stimulated Luminescence Glass

A.L. Huston, P.L. Falkenstein, and B.L. Justus
Optical Sciences Division

Introduction: Radiation imaging is an important diagnostic tool that is used in applications ranging from medicine to nondestructive testing. High-energy radiation penetrates through materials that are opaque to visible light, allowing one to visualize

features that are buried within the material. Everybody is familiar with traditional diagnostic x-ray films that are used by physicians to diagnose problems ranging from broken bones to pneumonia. Traditional x-ray film works reasonably well when the features of interest have significantly different densities such as bone and muscle tissue. The problem arises when the features have similar densities. The useful dynamic range for x-ray film is quite low, making it difficult to discern features such as cancerous lesions within normal tissue. A new radiation imaging technology has been developed in the Optical Sciences Division that uses optically stimulated luminescent (OSL) glass materials that are incorporated into flexible plastic sheets. Images are recorded in the sheets in a manner similar to that used for traditional x-ray film. The images are read by scanning a near-infrared laser source over the surface of the film and collecting the optically stimulated luminescence signal. The digital images that are obtained using this technique have a number of advantages over the use of x-ray film. The OSL film has a much wider, linear dynamic range, allowing features that would not be visible using x-ray film to be easily extracted using simple digital image processing techniques. The OSL imaging sheets are waterproof and flexible so that they can be used in environments that would preclude the use of traditional radiation imaging technologies. The imaging sheet can be archived or the image can be erased by exposure to bright incandescent lights, and the sheet can then be reused. Finally, the OSL sheets do not require chemical processing, thereby eliminating problems associated with personnel exposure and hazardous waste disposal.

Optically Stimulated Luminescent Glass: The OSL glass material is prepared by doping fused quartz glass with Cu^{+1} ions. When the glass is illuminated with a source of ionizing radiation such as X rays or gamma rays, electrons from the Cu^{+1} ions are ejected into the glass matrix where they become trapped, leaving behind a Cu^{+2} ion. The trapped electrons will remain trapped for periods of time ranging from days to many months. By exposing the OSL glass to a near-infrared light source, the trapped electrons can be stimulated to recombine with Cu^{+2} ions to produce excited state Cu^{+1} ions. The excited state ions relax to the ground state by the emission of a visible, blue-green luminescence. The intensity of the OSL signal is proportional to the amount of radiation that was absorbed.

Imaging System: The OSL glass was ground into a fine powder and incorporated into a liquid polymer material. Imaging sheets were prepared by coating the glass/polymer mixture onto flexible, clear polyester sheets. Images were recorded by laying various objects on top of the sheets and then exposing them to an x-ray source. The images were read out by scanning the focused spot from a 790-nm diode laser over the surface of the imaging sheet and collecting the blue-green OSL signal with a photomultiplier tube. The signals were recorded into a two-dimensional data array using a personal computer and displayed as an intensity image. Figures 6 through 8 show some examples of images obtained using the OSL imaging system. These figures represent the same image viewed using different contrast and brightness settings. The image consists of a very large gummy bear, a turkey wishbone, an electronic connector, a plastic centrifuge tube, a glass bottle with a plastic cap and a dense glass pellet inside, and a screwdriver with a plastic handle. By changing the brightness control, one can observe different ranges of

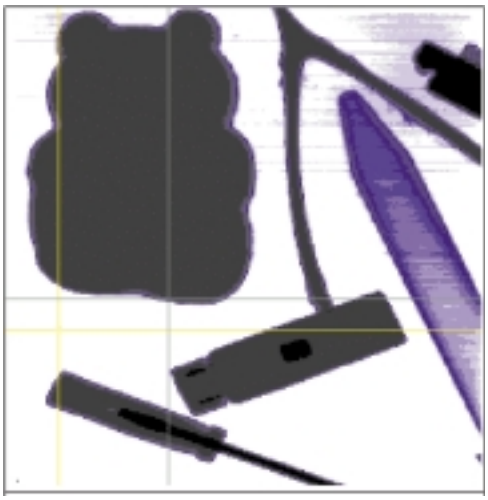

FIGURE 6
X-ray image of miscellaneous objects recorded using OSL glass/polymer composite imaging sheet.

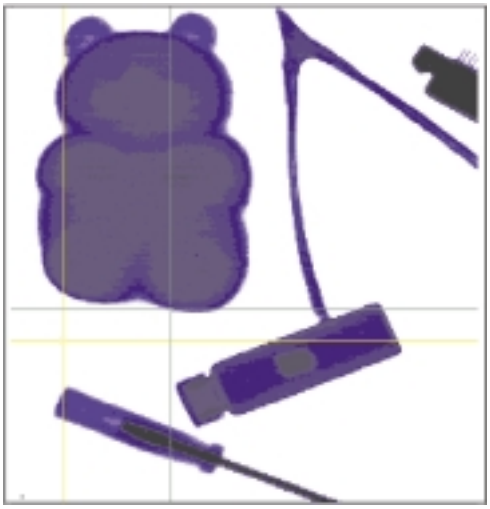

FIGURE 7
The same image as in Fig. 6 using digital image processing to reveal new features.

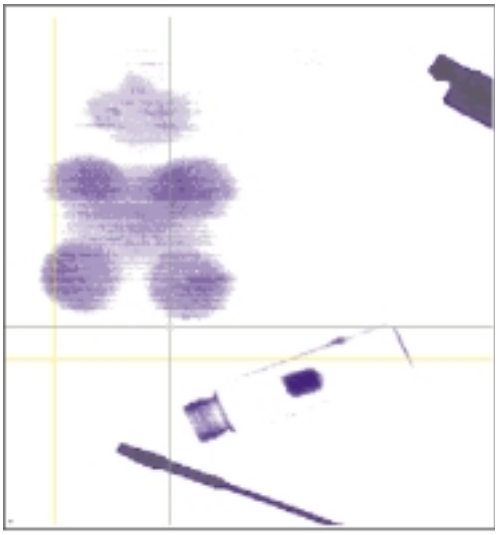

FIGURE 8
Additional image processing reveals the thread structure on the glass bottle.

densities. For example, in Fig. 7, the low-density-plastic centrifuge tube has completely disappeared and areas of different thickness in the gummy bear begin to appear. In Fig. 8, only the thickest portions of the gummy bear are visible; the wishbone has disappeared, the plastic lid on the glass bottle disappears, revealing the thread structure on the bottle; and the plastic handle of the screwdriver is gone. This degree of digital manipulation of an x-ray image is not possible using traditional x-ray film.

Applications: This imaging technology is currently being evaluated in cooperation with researchers at the National Cancer Institute for use in radiotherapy treatment planning applications. The Navy can apply this technology for nondestructive testing of advanced composite materials to examine the internal features of multilayered materials to assure that no air pockets or foreign bodies are present that could compromise the integrity of the structure.

[Sponsored by ONR]

Remote Sensing

Automated Coastal Classification Products Using a Nested Multisensor Approach

C.M. Bachmann, T.F. Donato, and R.A. Fusina
Remote Sensing Division

Overview: Analysis of coastal data derived from remote sensing imagery plays a significant role in many military and civilian applications. The advent of new commercial remote sensing platforms, such as IKONOS and HYMAP, with high spatial and spectral resolution, has brought new opportunities for detailed analysis of coastal environments. We combine automatic classification models using these new imagery sources at a local scale with other remote sensing data, such as Landsat Thematic Mapper imagery (TM) and Radarsat Synthetic Aperture Radar (SAR), that are more appropriate for regional-scale analyses. Our research program addresses the development and large-scale validation of algorithms for automatically producing coastal land-cover and nearshore ocean feature analyses at both regional and local scales. We highlight examples of our nested product approach with automatic models developed for the Virginia Coast Reserve, which includes a system of barrier islands near the mouth of the Chesapeake Bay. A second example of regional-scale analysis is shown in the Delaware Bay.

Automatic Classification Models: Our approach has been to develop a modular software toolbox of both new and extant statistical pattern-recognition algorithms to rigorously evaluate relative performance against ground reference data. One of the significant challenges in model validation is the availability of accurate ground reference data. Depending on the area of interest, many reference data standards for coastal land-cover within the U.S., such as the National Wetlands Inventory (NWI), may contain dated information or may not contain sufficient resolution to be useful for local-scale analyses. Outside of North America, there are many areas where such standards are nonexistent. This means that we must be prepared to develop models either with or without a significant amount of ground truth data. In terms of statistical pattern-recognition algorithms, this motivates the development of models using both "supervised" and "unsupervised" approaches. The term "supervised" implies that previously labeled, representative data are available to develop a model, while "unsupervised" refers to an exploratory data analysis from which natural clusters or groupings of the data emerge, but for which there is no a priori knowledge of category information. In the latter case, cluster identities must be determined later by some other means, such as a field survey at selected locations or comparison against known spectral libraries.

Coastal Products: Figure 1 shows a subset of one of our regional scale products for the Delaware Bay region. This figure compares the output of one of our automatically generated composite models, which combines both unsupervised and supervised approaches.[1,2] The automatically generated product is compared with a reference mask developed in an intensive, interactive analysis by an expert interpreter using multidate Landsat TM imagery and multiple ancillary data sources. Our automatic product was developed using a single Landsat TM image and a co-registered Radarsat SAR image as input, and a small portion of the reference mask. For 80% of the data, our analysis showed that, rather than having to perform the labor-intensive analysis across the entire scene, it would be sufficient to develop a detailed mask on a very small subset of the entire scene, using the automatic model to complete the task.

A second example (Fig. 2) depicts an unsupervised approach to categorization on a local scale. Figure 2(a) shows a HYMAP scene of Smith Island, Virginia, and the lower portion of Myrtle Island, Virginia, acquired on May 8, 2000, with 128 spectral channels covering the 440 to 2500 nmi range at a spatial resolution of 4.5 m. The final data product delivered by Analytical Imaging and Geophysics, LLC, contained 126 channels that were atmospherically corrected using the ATREM/EFFORT model. Unfortunately, the most recent survey data available for this area were completed in 1975. Because barrier islands such as Smith Island are in a constant state of flux due to the action of wind, waves, and sudden storm surge events, this necessitated the use of an unsupervised approach. Figure 2(b) shows the HYMAP data after filtering by a projection pursuit (PP) algorithm, which was used to identify potential clusters in significant low-dimensional views of the 126-dimensional HYMAP spectral data distribution; three projections are portrayed in an RGB representation. These projections and two others were partitioned into distinct clusters using the ISODATA algorithm, leading to 34 distinct categories (Fig. 2(c)).

In Situ Validation and Utility: To validate our product, we have been visiting specific sites to identify the clusters found in Fig. 2(c). Figures 2(d) and 2(e) show examples of two automatically derived categories: a dense Myrica thicket and dune line/beach grass, that have been verified on a limited basis using a GPS and in situ field observations. Figures 3(a) and 3(b) show

Inputs:

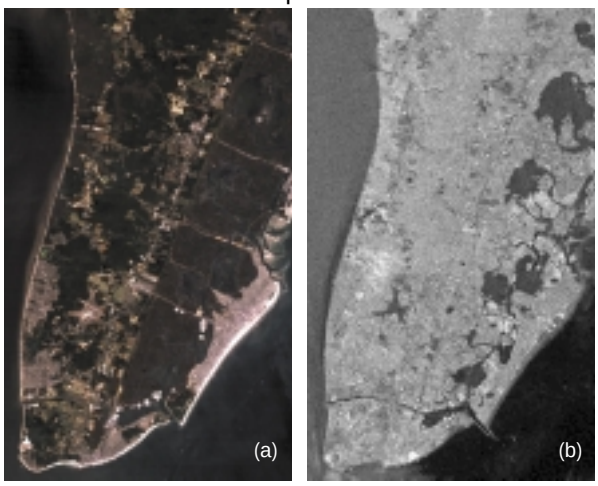

LANDSAT TM
Test Region 15

RADARSAT SAR
Test Region 15

Output:

Reference:

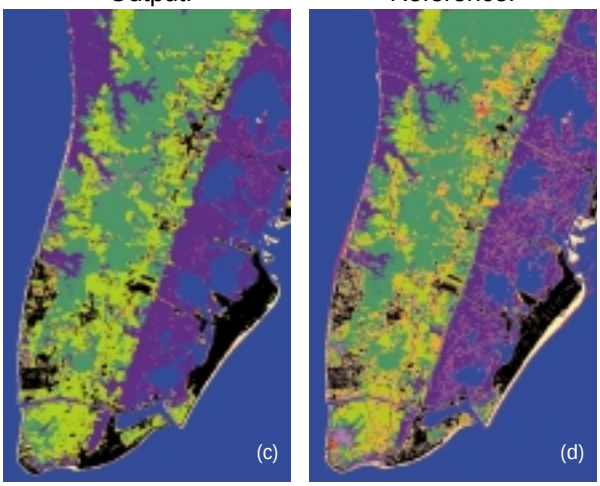

PURSUIT Automatic
Classification Output

NWI-Based Reference Data

FIGURE 1
Regional scale automatic classification in the Delaware Bay for a sequestered test region: (a) RGB composite of Landsat TM channels 1, 2, and 3; (b) co-registered Radarsat SAR also used as input; (c) automatic classification product; (d) human interpreted reference database on multidate Landsat TM, NWI, and other ancillary data sources.

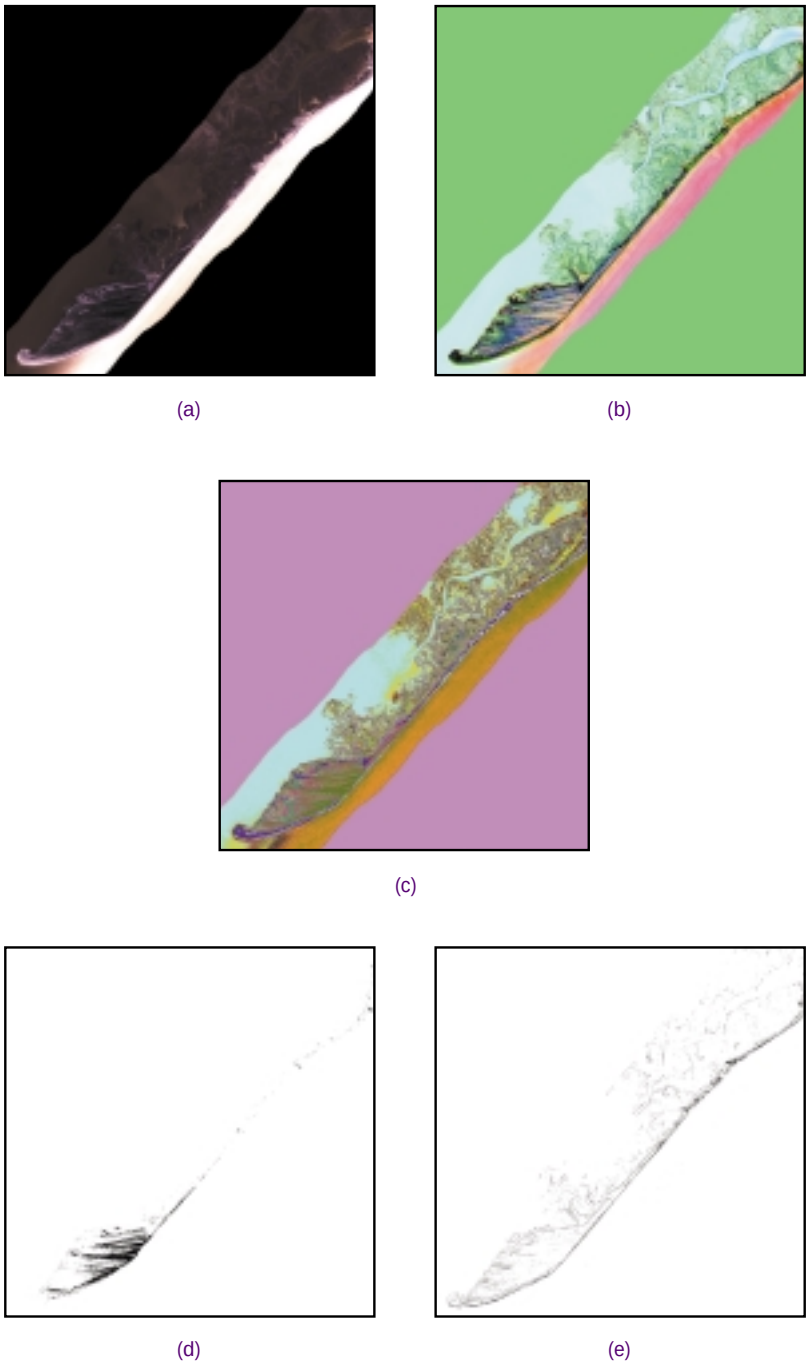

FIGURE 2
(a) RGB composite of channels 4, 8, and 14 from HYMAP scene of Smith Island and a portion of Myrtle Island in the Virginia Coast Reserve acquired on May 8, 2000; (b) the HYMAP scene projected by three projection pursuit (PP) filters and displayed as an RGB composite image; (c) automatic classification product: unlabeled clusters found by ISODATA in a five-dimensional PP projection of the HYMAP scene, including the three PP projections shown in (b); (d) Myrica thicket category derived from (c); (e) dune line / beach grass category derived from (c).

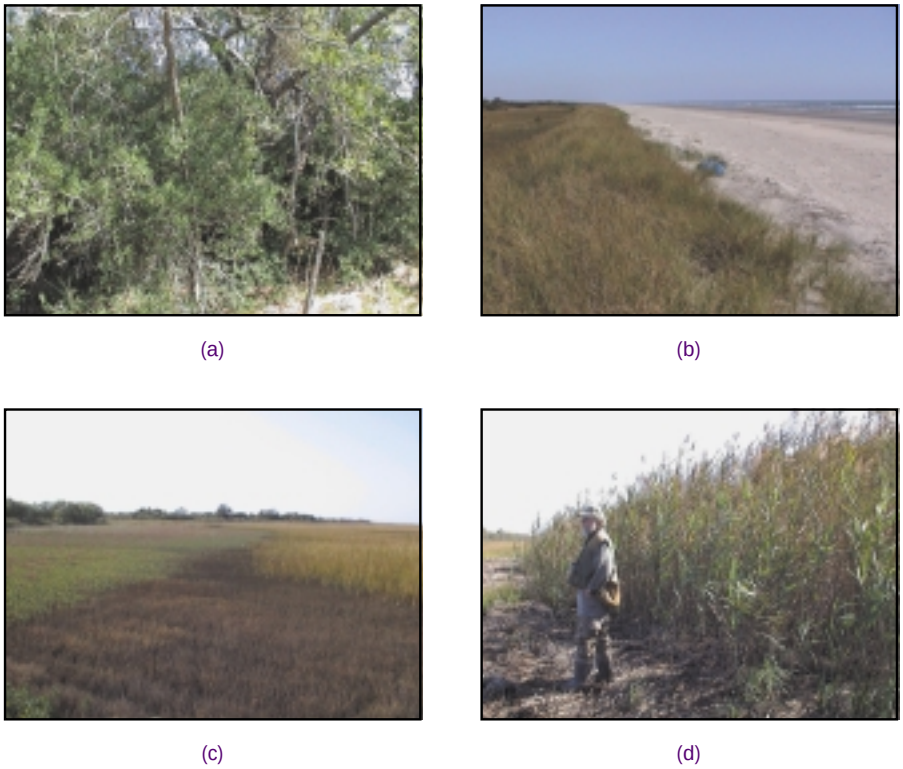

(a) (b) (c) (d)

FIGURE 3
(a) Dense Myrica thicket at georeferenced way-point for validation of this automatic classification category; (b) dune-line / beach grass at way-point for this category; (c) rapid change in land-cover due to degree of elevation, soil moisture, and salinity: (right) spartina alterniflora, (center) salicornia and distichlis spicata, (left) borrichia frutescens, (far left and background) thicket boundary; (d) invasive plant species phragmites australis.

digital photographs acquired at georeferenced waypoints for these two categories. Comparison of the automatic classification product with the historical reference data from 1975 reveals that the predicted extent of the Myrica thicket (Fig. 2(d)) is larger today than it was 25 years ago. In a mission-planning exercise, this would be an important consideration because, on foot, these regions are extremely difficult to traverse due to the density of the vegetation and the extensive presence of briars. Our in situ observations on the island have revealed a great diversity of vegetation (Fig. 3(c)), some of which can be discriminated using new sensors such as HYMAP. Automatic classification products can aid military and civilian land-use managers as well as ecologists, for instance, in identifying the presence of invasive plant species (Fig. 3(d)).

Summary: New commercial sensors such as HYMAP have allowed us to develop automatic classification products at a local scale for integration with regional-scale analyses from sensors such as Landsat TM and Radarsat SAR. We have demonstrated both regional and local automatic classification products using these imagery sources. The resulting products have potential utility in both DoD and civilian applications.

Acknowledgments: We thank Professor John Porter and Randy Carlson of the University of Virginia for historical land-cover data of Smith Island and assistance during field work at Smith Island, and Barry Truitt of The Nature Conservancy for access to the island. We thank Oliver Weatherbee for the Delaware Bay reference data.

{Sponsored by ONR]

References

[1] C.M. Bachmann and T.F. Donato, "An Information Theoretic Comparison of Projection Pursuit and Principal Component Features for Classification of Landsat TM Imagery of Central Colorado," *Int. J. Remote Sens.* **21**(15), 2927-2935 (2000).

[2] C.M. Bachmann and T. F. Donato, "Mixtures of Projection Pursuit Models: An Automated Approach to Land-Cover Classification in Landsat Thematic Mapper Imagery," in *Proceedings of the International Geoscience and Remote Sensing Symposium* (IGARSS99'), Hamburg, Germany, June 28-July 2, 1999, pp. 339-341.

Dragon Eye: Airborne Sensor System for USMC Small Units

R.J. Foch and J.P. Dahlburg
Tactical Electronic Warfare Division

Introduction: The Naval Research Laboratory (NRL), in collaboration with the Marine Corps Warfighting Laboratory (MCWL), is developing an affordably expendable airborne sensor platform system, Dragon Eye. This Office of Naval Research (ONR)/MCWL-sponsored system is demonstrating small unit reconnaissance and threat detection capabilities. Dragon Eye consists of a man-portable, 2 kg, hand-launched autonomous air vehicle, and a wearable ground control station (GCS) to provide control of, and receive intelligence information from, the air vehicle. Using electric propulsion, an endurance of 60 min can be achieved at airspeeds of 65 km/hr with an operating radius of 10 km. Vehicle characteristics also enable an operational capability in adverse weather conditions. Interchangeable payloads for Dragon Eye include daylight, low light, and infrared cameras with a robust communication link. Figure 4(a) shows the prototype Dragon Eye unmanned air vehicle (UAV) in flight. For GCS development, the Dragon Eye project is enhancing the MCWL/ONR-sponsored end user terminal (EUT+) effort currently being executed at NRL. The existing EUT+ is a ruggedized, wearable computer configured on a modular lightweight load-carrying equipment vest; Fig. 4(b) shows a Marine Corps officer wearing an EUT+. Figure 4(c) shows the form factor of the Dragon Eye stored in its backpack container.

The Dragon Eye effort is an experiment that is in direct response to the Secretary of the Navy's Small Unmanned Air Vehicle Initiative to demonstrate a rapid transition from advanced technology research to a mission-ready system. The goals are to develop and deliver a close-in reconnaissance airborne sensor platform to the warfighter, as embodied in the Marine Corps' Interim Small Unit Remote Scouting System (ISURSS) requirement, and to position that system for limited production—all within a three-year timeframe. This effort, which uses commercial off-the-shelf components wherever possible, is capitalizing on the Navy S&T investment toward miniaturization of mission payloads, autonomous flight enabling technologies, and affordably expendable air vehicles.

Timeline: The Dragon Eye project started in March 2000. Flight testing of a hand-built concept demonstrator began in early May 2000. These flight tests verified the estimated performance characteristics and formed an empirical baseline for developing the definitive airframe design. Tooling for the fabrication of advanced composite airframes was ready during June 2000, and flight testing with the first prototype fabricated from tooling began in July 2000. The autonomous-enabling avionics, mission payloads,

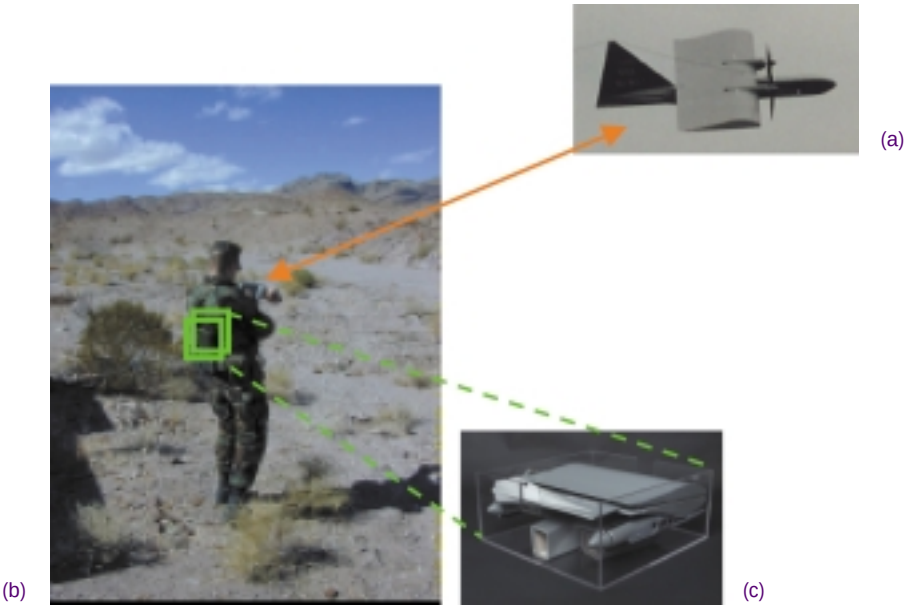

FIGURE 4
(a) Dragon Eye in flight. (b) EUT+ wearable GCS. (c) Storage pack—15 × 15 × 7 in.

communications link, and the wearable ground control station are also undergoing rapid development in parallel with that of the air vehicle. Developmental goals include a 70% mission capability with daylight imager payloads and semi-autonomous operation by January 2001; 90% mission capability with IR imagery and fully autonomous operation by January 2002; and delivery of full capability residual units for warfighter experimentation throughout FY02.

Throughout the development of Dragon Eye prototypes, MCWL is conducting test experimentation and functional demonstrations. In early November 2000, Dragon Eye participated in Project Metropolis, a Marine Corps urban warfare exercise. Imagery transmitted from the Dragon Eye provided increased situational awareness to the warfighter (Fig. 5), which enhanced his ability to deploy and maneuver in a hostile urban environment.

Upgrades: As technology evolves, the inherent flexibility of the modular payload interfaces on Dragon Eye readily allows continual upgrades to mission capabilities. The Dragon Eye system provides a framework from which to develop affordably expendable small UAVs as tools for an unprecedented range of capabilities. These include: decoying/spoofing; battle damage assessment; close-in communication/radar jamming for suppression of enemy air defenses; electro-optical communication links; meteorological measurements; scientific exploration of terrestrial phenomena; and search and rescue operations in natural disaster situations.

Dragon Eye supports the highest priority mission for small UAVs: over-the-hill reconnaissance, surveillance, and target acquisition (OTH RSTA) by small units (company sized and below). It is to be an organic asset that will allow the user to establish mission priority. By providing payload data directly to the small unit, an unprecedented level of situational awareness will be achieved. It is planned that Dragon Eye will earn its wings as a warfighter UAV. Dragon Eye is to provide the airborne eyes to the small unit commander when and where they are needed, without adding an accompanying cumbersome support package that would detract from overall mission capability.

FIGURE 5
U.S. Marine with Dragon Eye and developmental GCS.

Acknowledgments: The authors acknowledge the support of CNR, VCNR, and Dr. John Montgomery, for enabling this project, and note the superlative efforts of personnel from NRL Codes 5712, 5703, 5707, 6440, 6410, 5523, 5520, 5551, and ITT – the Dragon Eye development team.

[Sponsored by ONR and MCWL]

Large Aperture Multiple Quantum Well Retromodulator for Free-Space Optical Data Transfer

G.C. Gilbreath
Remote Sensing Division

W.S. Rabinovich
Optical Sciences Division

Introduction: Free-space optical communications has emerged in recent years as an attractive alternative to the conventional radio frequency (RF) approach. This evolution has been due to the increasing maturity of lasers and compact optical systems, which enable exploitation of the inherent advantages of the much shorter wavelengths characteristic of optical and near-infrared carriers. These advantages include: large bandwidth, low probability of intercept, immunity from interference or jamming, frequency allocation relief, and in many cases, smaller, lighter payloads that, in turn, enable more compact, covert communications systems. For a conventional optical link, a good-to-high quality telescope that provides relatively accurate pointing and tracking capability is needed. Also needed is a robust laser with sufficient power, temperature stabilization, and requisite electronics, in addition to the usual modulating and demodulation and control and acquisition instrumentation and software. There are many applications, however, where reducing the parasitic payload requirements for the onboard communications system would be advantageous.

One such approach makes use of a simple optical corner cube coupled with a fast shutter to enable compact covert communications by reducing the payload's power, space, and weight requirements to nominal levels. Until relatively recently, however, no material existed that could support data rates on the order of a megabit per second and higher with efficiency and compactness. The Naval Research Laboratory has been developing a semiconductor electroabsorptive shutter for this purpose using multiple quantum well (MQW) technology.[1] This paper describes this device, including recent demonstrations of an infrared data link between a small rotary-wing unmanned airborne vehicle and a ground-based laser interrogator.

Wide Aperture Multiple Quantum Well Modulators: Semiconductor multiple quantum well (MQW) technology is the basis for commercially available laser diodes. When used as a shutter, MQW technology offers many advantages. It is robust and all-solid state. In addition, it operates at low voltages (less than 20 volts) and low power (less than 1 watt). Most importantly, it is capable of very high switching speeds (Fig. 6). MQW modulators have been run at data rates in the gigabits per second regime in fiber applications. The MQW modulators used in this program were grown at NRL by molecular-beam epitaxy (MBE) and have been shown to support a bit error rate of at least 10^{-6} at data rates of 10 megabits per second and higher.[2] The details of the growth and some optimizations used to improve the material quality are discussed in Ref. 3.

Briefly, the modulators consist of about 100 very thin (~10 nanometers) layers of several semiconductor materials, such as GaAs, AlGaAs, and InGaAs, epitaxially deposited on a large (3-inch diameter) semiconductor wafer. Electrically, they take the form of a P-I-N diode. Optically, the thin layers induce a sharp absorption feature at a wavelength that is determined by the constituent materials and the exact structure that is grown. The devices developed for this program operate between 850 nanometers and 1.06 microns.

When a moderate voltage (~15 volts) is placed across the shutter in reverse bias, the absorption feature changes, shifting to longer wavelengths and dropping in magnitude. Thus, the transmission of the device near this absorption feature changes dramatically. Figure 7 shows absorbance data for an InGaAs MQW modulator designed and grown at NRL for use in a modulating retroreflector system. The figure illustrates how the application of a moderate voltage shifts the transmittance. Hence, a signal can be encoded in an on-off-keying format onto the carrier interrogation beam.

The challenge presented by this application is that because the device is essentially a semiconductor, its speed is driven by the resistance-capacitance product in the time response. Capacitance is driven by area, but the area must be large to close a given link over useful ranges (typically on the order of a kilometer or more). NRL has successfully experimented with segmentation of the device, which both increases speed and increases yield while maintaining low-power draws.

Field Tests: Successful implementation of a modulating retroreflector link requires the integration of the device onto a platform as well as the ability to close a link while in flight. As a first step in developing an operational modulating retroreflector communications link, NRL has conducted two field tests to date, with follow-on tests planned. The aim of these tests was to demonstrate a short-range link to a platform that carried no active pointing system and indeed had relatively low platform stability. The tests were conducted in the fall of 1999 and in the winter

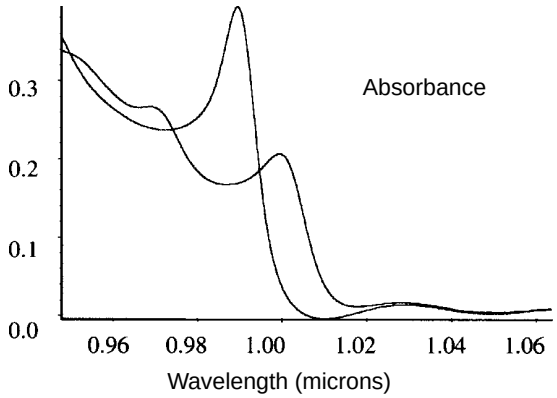

FIGURE 6
Absorbance vs frequency. In its quiescent state, the MQW shutter blocks the transmission of incident light. When a moderate voltage is applied, the absorbance shifts and light is transmitted through to the retroreflector.

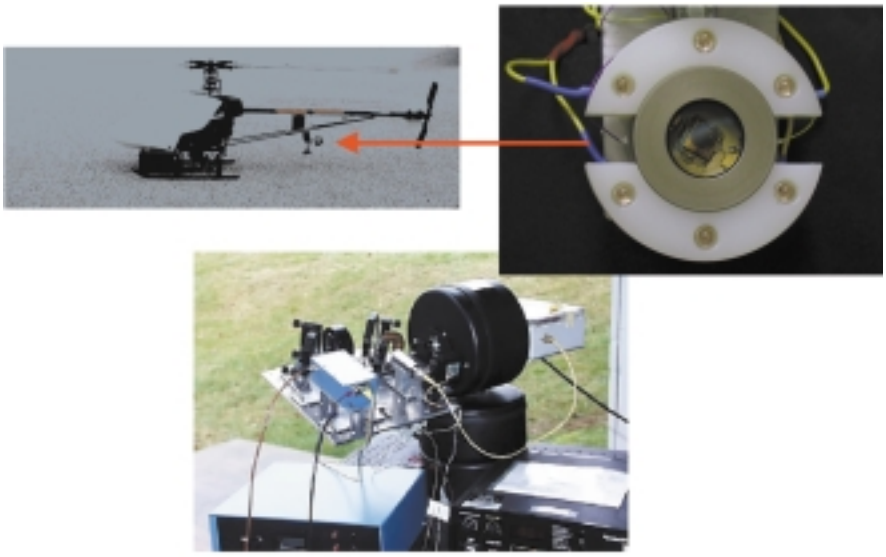

FIGURE 7
UAV, payload, and interrogator for NRL in-flight modulating retroreflector field test. The helicopter is about 1-1/2 meters long; the payload consists of a modulating retroreflector ringed by LEDs to aid in daytime acquisition and tracking; the interrogator consists of a laser diode and optics, with an avalanche photodiode configured in a Naysmith-mounted design on a small gimbal.

of 2000 at the NRL Chesapeake Bay Detachment facility in Maryland.

A 0.5-cm diameter InGaAs transmissive MQW modulating retroreflector was mounted on a small rotary-wing unmanned airborne vehicle (UAV), which was about 1-1/2 meters long. The retromodulator assembly was ringed by infrared LEDs that were used to provide a beacon for acquisition and tracking of the UAV. In future tests, these will be replaced with a ring of retromodulators to test self-acquisition and jitter-resistant tracking.

The modulating retroreflector was placed on the tail of the UAV pointing down. The UAV was flown at an altitude of about 35 meters and a range of 35 to 65 meters from the transmit/receive laser. The conditions for the test were somewhat adverse, with a light rain, fog, and low visibility. The second test was conducted with snow cover and in icy outdoor conditions. The UAV, payload, and interrogator are shown in Fig. 7.

Figure 8 shows a typical return from the field tests. In the two tests conducted, the modulation rates received in flight were 400 and 910 kilobits per second. However, the modulator and detector bandwidth and the returned signal level were sufficient to support a 2 Mbps link at low bit error rates, and in fact,

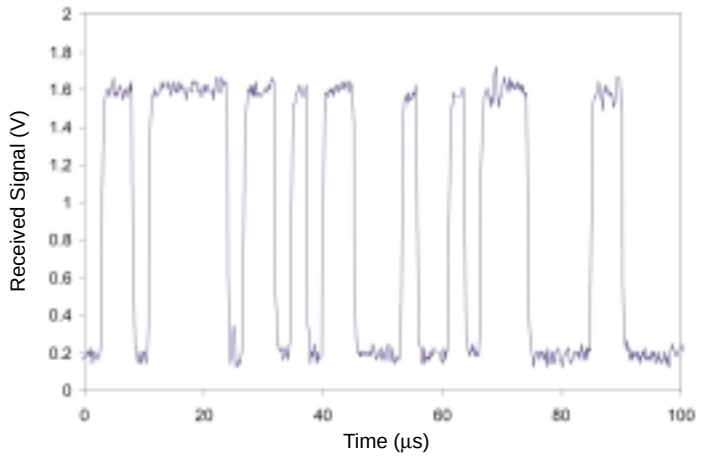

FIGURE 8
A sample of the return from data captured in flight using the NRL MQW retroreflector. As long as the link was maintained through accurate pointing and tracking, signal amplitudes were high enough to maintain a robust communications link.

captured uncompressed black and white video in preflight ground tests. The modulator consumed 40 mW of electrical power at this modulation rate.

Summary: We have shown that a multiple quantum well-based modulating retroreflector can enable a very small platform to passively close an optical data link. The use of such modulators can allow much higher bandwidth communications over longer ranges than is typical of such platforms using radio frequencies. In addition, the link is covert, very difficult to jam, and immune from the frequency congestion problems to which RF communications are susceptible.

[Sponsored by ONR]

References

[1] G.C. Gilbreath, S. Bowman, W. Rabinovich, C. Merk, and H.E. Senasak, "Modulating Retroreflector for Free Space Optical Data Transfer using Multiple Quantum Well Technology," U.S. patent no. 6154-299, granted November 28, 2000.

[2] G.C. Gilbreath, W.S. Rabinovich, T.J. Meehan, M.J. Vilcheck, R. Mahon, R. Burris, M. Ferraro, I. Sokolsky, J.A. Vasquez, C.S. Bovais, K. Cochrell, K.C. Goins, R. Barbehenn, D.S. Katzer, K. Ikossi-Anastasiou, and M.J. Montes, "Compact, Lightweight Payload for Covert Data Link using a Multiple Quantum Well Modulating Retroreflector on a Small Rotary-Wing Unmanned Airborne Vehicle," *SPIE Proc.* **4127**, July 2000, in press.

[3] D.S. Katzer, W.S. Rabinovich, K. Ikossi-Anastasiou, and G.C. Gilbreath, "Optimization of Buffer Layers for InGaAs/AlGaAs PIN Optical Modulators Grown on GaAs Substrates by Molecular Beam Epitaxy," *J. Vac. Sci. Technol.* **B 18**, 1609-1613 (2000).

Discriminating Interceptor Technology Program Ground Testing at the KHILS Facility

K.A. Clark,[1] A. Bosse,[2] J.R. Waterman,[3]
T.J. Meehan,[1] H.C. Merk,[2] R.A. Thompson,[4]
and W.J. Krawczyk[5]
[1]*Space Systems Development Department*
[2]*Spacecraft Engineering Department*
[3]*Optical Sciences Division*
[4]*U.S. Air Force Research Laboratory*
[5]*SAIC*

Introduction: The Discriminating Interceptor Technology Program (DITP) is a BMDO-sponsored program whose purpose is to develop and demonstrate new technologies for next-generation interceptors. The technologies to be demonstrated are: a three-dimensional imaging LADAR, a passive sensor subsystem (PSS), and a fusion processor (FP) running detection, tracking, and discrimination algorithms. The Naval Research Laboratory is the test bed integrator (TBI). The TBI is responsible for integrating these three technologies and executing a test and demonstration program meaningful to the National Missile Defense (NMD) community. The technologies are provided by the U.S. Army Space and Missile Defense Command (USASMDC) and the Air Force Research Laboratory (AFRL). The Kinetic Kill Vehicle Hardware in the Loop Simulator (KHILS) is managed by the Air Force Research Laboratory Munitions Directorate (AFRL/MNG) at Eglin AFB, Florida. It provides a comprehensive, hardware-in-the-loop ground test capability for BMDO interceptor concepts.

The DITP Test and Demonstration Program has two primary objectives: to demonstrate successful operation in a meaningful exo-atmospheric mission and to verify the capability of the DITP technologies against future NMD threats. A combined flight and ground test program is necessary to meet these objectives. The proposed flight demonstration will consist of an NMD-like encounter between two sounding rockets. One sounding rocket is dubbed the seeker. It contains the integrated DITP technologies. The other sounding rocket will launch NMD-like targets. The flight test will allow the DITP technologies to demonstrate functionality against the targets.

The purpose of the DITP ground test program is twofold: risk reduction for the flight demonstration and performance assessment against simulated NMD targets. The ground test program is composed of a series of subsystem tests followed by systems-level tests. The KHILS systems-level tests provide risk reduction for the proposed flight demonstration as well as a system performance assessment against an advanced threat.

Test Overview: The KHILS tests consist of a series of tests that begin with basic functionality and progressively increase in complexity up to assessing performance in the flight test for risk reduction. The sequence of the risk reduction tests is as follows: signal injection, signal projection, flight demonstration rehearsal, and off-nominal excursions. These tests are followed by a performance assessment test against an advanced NMD threat. Figure 9 is a block diagram of the simulation configuration for the risk-reduction tests. The items hosted at the KHILS facility are in the blue rectangle. The red rectangle depicts the DITP hardware and software.

Nominal operation is as follows: the scenario definition is initiated. This drives the system models to provide the in-flight target update (IFTU) to the seeker. The fusion processor uses the IFTU, coupled with the seeker's position and attitude information (from the GPS and inertial measurement unit (IMU)

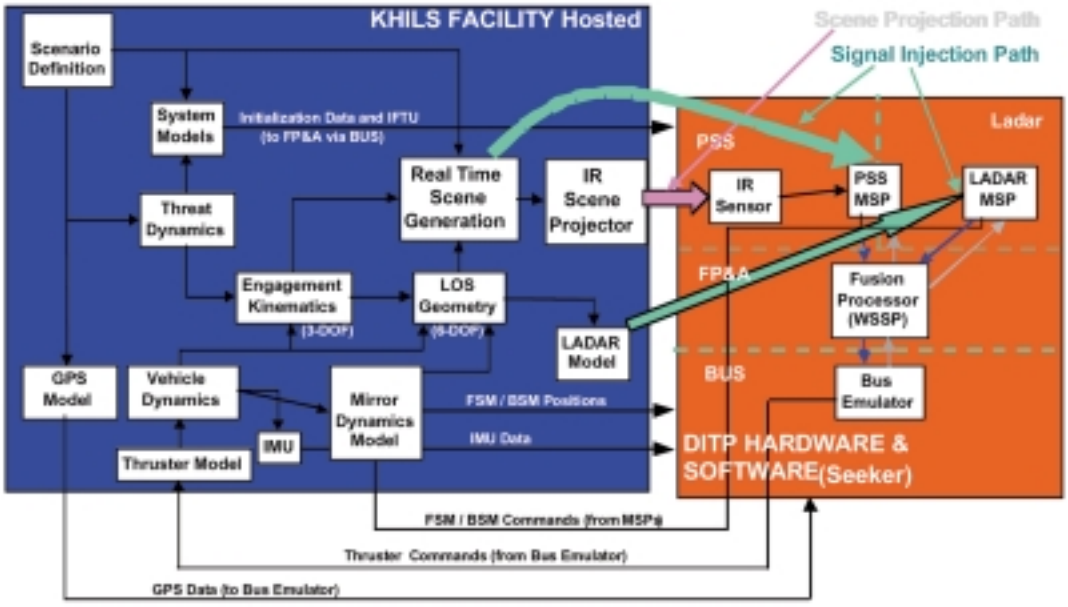

FIGURE 9
Hardware-in-the-loop configuration.

modules) and sends an attitude command to the bus emulator. The bus emulator translates this to a thruster command, which is sent to the KHILS thruster model. The KHILS modules respond together by updating the PSS image in the real-time scene generation module. This image is passed digitally to the PSS MSP in the signal injection test and drives the WISP array in the projection mode. Once target acquisition has occurred, the fusion processor initializes target constellation tracking.

Once a credible track file has been created on a single target cluster, the simulated LADAR begins acquisition and track. The KHILS LADAR model provides LADAR data to the fusion processor via the LADAR MSP. In this dual mode, the fusion processor attempts to track with both the PSS and LADAR detections. This IR and LADAR tracking continues until the simulation run is terminated. In later test entries, discrimination algorithms will be included on the fusion processor. During the test, the fusion processor continually refreshes attitude and mirror commands. The KHILS modules close the control loop in real time, updating the outputs to the PSS and LADAR.

Signal Injection Results: The first DITP signal injection test was run at KHILS in February/March 2000. The main objective was to check the functionality of the system. The derived goal was to successfully run through the flight demonstration with all control loops closed. To reach this goal, the test sequence was broken down into eleven steps that started with all control loops open and progressed to the full closed-loop test. Upon completion, proper interface operation and functionality was demonstrated and the attitude control system (ACS) software was validated.[1] Figure 10 shows an attitude control system phase plane plot for the pitch axis tracking error. The initial system state is shown in the lower right hand corner; the steady state is represented by the limit cycle shown around the (0,0) point.

Signal Projection Results: The first signal projection tests occurred in June-July 2000. The main objectives of the tests were to validate the signal projection test and insert the DITP infrared sensor into the hardware loop. These objectives were met. Additionally, improvements in software were proven out. Figure 11 shows a sequence of images from the IR sensor, showing the evolution of the tracks of six target objects from near deployment (far left) to near endgame (far right). Although the objects are unresolved point sources throughout the engagement, oversampling of the optical system blur spot results in the illumination of multiple pixels by each object.

Conclusion: The KHILS facility has and will continue to play a key role in the DITP Test and Demonstration Program. The signal injection and projection tests made several important accomplishments. Future HWIL tests will demonstrate additional functionality.

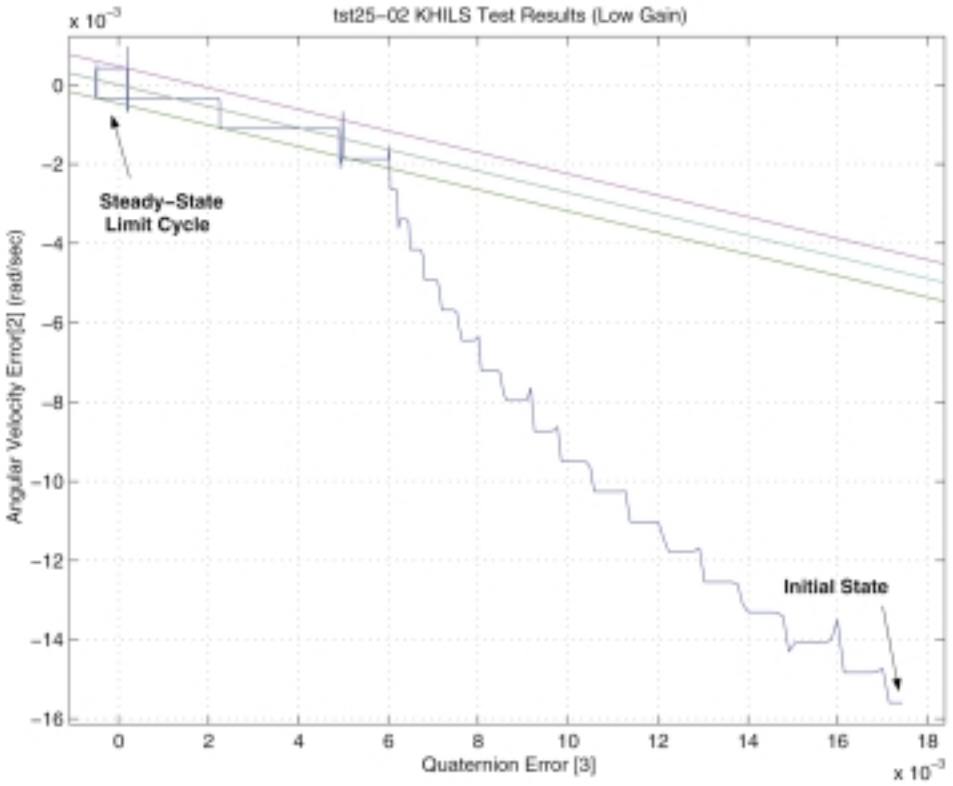

FIGURE 10
Attitude control system phase plane error plots.

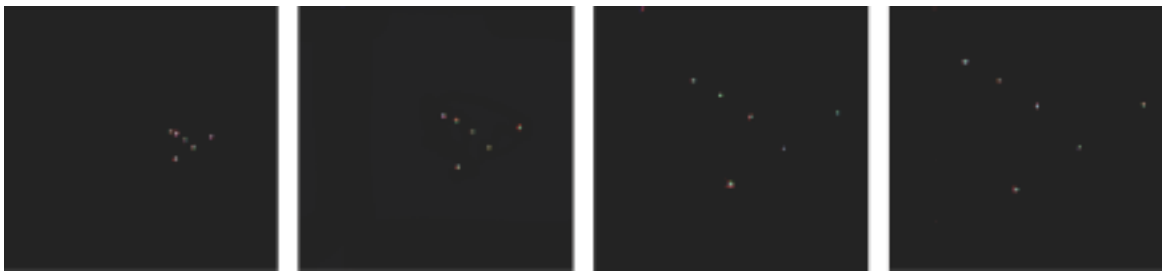

FIGURE 11
Images as seen by infrared sensor as engagement progresses.

Acknowledgments: The authors gratefully acknowledge all participants in the NRL TBI team and the DITP/KHILS team. It was the long hours and dedication of the team that made the accomplishments presented in this paper possible. We also thank the past DITP BMDO program managers, LCDR Chip Buckley, USN, and MAJ Michael Gregg, USAF, for their support.

[Sponsored by BMDO]

Reference

[1] A. Bosse, T. Carter, and C. Hill, "Guidance Navigation and Control Subsystem Post-Test Analysis for DITP KHILS Test Sequence #1," internal report to DITP team, May 5, 2000.

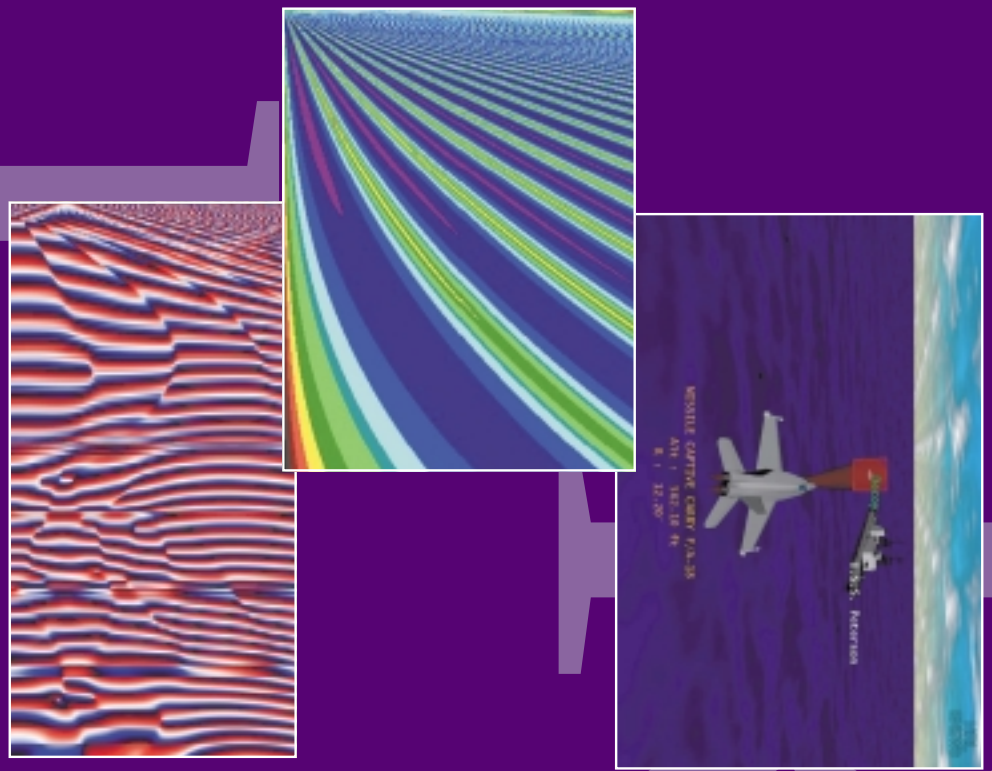

Simulation, Computing, and Modeling

High-Accuracy Radio Frequency Propagation Simulation

L. Schuette,[1] T. Troyer,[2] and F. Ryan[3]
[1]*Tactical Electronic Warfare Division*
[2]*STI*
[3]*SPAWAR Systems Center*

Introduction: The design of high fidelity electronic support measures (ESM) hardware requires highly accurate models of the radio frequency (RF) propagation environment during development and testing. Under sponsorship of the Office of Naval Research, the authors have developed such a simulation environment. Next-generation surface ships will be equipped with the Advanced Integrated Electronic Warfare System (AIEWS) with an ESM capability that proposes to have significantly better angle resolution and accuracy than current systems. The interferometer will develop angle-of-arrival (AOA) estimates by measuring the relative signal phase between multiple spatially separated antennas in the array. Our efforts have focused on using the Variable Terrain Radiowave Parabolic Equation (VTRPE) RF propagation model to faithfully represent the complex electric field emanated from a low-flying antiship cruise missile that would impinge on the array. Results from the simulation can be used to determine if the ESM signal processing accurately predicts the AOA in a variety of at-sea conditions

The Need for Simulation: The AN/SLY-2 Advanced Integrated Electronic Warfare System is the U.S. Navy's newest shipboard ESM receiver, with vastly greater performance than existing systems. To ensure that performance is as expected, extensive field testing is being performed. Because of the expense of field testing, simulation is often used prior to field-testing to mimic the environment in which the system is expected to operate. Additionally, for safety reasons, there may be tests that cannot be accomplished in the field but are feasible in a simulation.

The AIEWS is a crucial element in the self-defense capabilities of the surface Navy. The emerging threat of low-RCS, sea-skimming antiship cruise missiles (ASCM) against surface ships has driven the requirement for better target tracking and localization. Because of the short reaction times required to successfully counter the ASCM threat and the large number of air targets that must be considered to sort the threats from the nonthreats in littoral environments, high-precision angle measurements are required. These high-precision measurements support track correlation for other combat systems sensors (i.e., radar), provide a valuable discriminant for de-interleaving closely spaced emitters that are waveform and frequency agile, and cue combat system fire control and multifunction radars.

To provide the accuracy required, the AIEWS is designed around a sensitive two-dimensional (2D) cross-shaped multichannel phase interferometer. The interferometer develops AOA estimates by measuring the relative signal phase between multiple spatially separated antennas in the array.

Description of Simulation: To test this type of interferometer in the laboratory, scientists at the Naval Research Laboratory (NRL) and SPAWAR Systems Center San Diego (SSC-SD) have developed a simulation tool that provides an exceptionally high-resolution propagation environment within which the ESM processing algorithms and hardware can be tested. For shipboard electronic support (ES) sensors operating against low elevation angle emitters, the littoral environment can produce anomalous propagation paths between the sensor and emitter including: surface multipath (Lloyd's mirror), multiple forward-scattering arrivals due to ducting, and pulse distortion and time spread due to channel dispersion. All these environmentally induced effects can significantly distort the signal field at the ES antenna/array (interferometer) and prevent accurate AOA estimation.

For a single plane wave signal incident on the vertical interferometer array, the measured phase difference $\Delta\phi$ between sensor pairs is directly related to the signal arrival angle (with respect to horizontal) Θ via

$$\Theta = 2\pi/\lambda\, d \sin(\Delta\phi),$$

where d is the baseline separation between the sensors, and λ is the wavelength.

When the signal wave front is planar, this technique can yield very accurate AOA estimates. This allows processing of time-difference-of-arrival (TDOA) data, relative phase, or spatial beamforming (via time delays or phase shifters) to deduce the target elevation and bearing. However, in real-world scenarios, the incident signal field is not always a simple plane-wave, due to propagation anomalies that significantly distort it. This leads to multiple arrivals (multipath) and spreads in time and angle. These effects are caused by atmospheric refraction and ducting, terrain diffraction, and surface scattering. This in turn, leads to degradation in the sensor's signal processing gain due to an inability to coherently recombine all the available target signal energy.

As an example of the potential difficulties faced by threat location in complex littoral environments, consider the problem of tracking and localization of a sea-skimmer cruise missile by the AIEWS interferometer array. The interferometer array will develop a target direction by measuring the incident signal's phase difference between vertically separated receivers. The accuracy and resolution of this angle measurement is directly related to the planar nature of the incident signal field.

To simulate this, a full-wave (amplitude and phase) electromagnetic propagation model based on the parabolic wave equation (PWE) is used to compute the expected signal field incident on the AIEWS interferometer array in varying environmental conditions. The VTRPE code used in this study allows for high-fidelity simulations of the complex electromagnetic field in littoral environments for both smooth and rough sea surfaces. In addition, the VTRPE model allows for a spectral plane wave decomposition of the electric field to study signal arrival angle structure at the AIEWS interferometer array.

Using the Simulation: Typical output from a VTRPE simulation is a two-dimensional plot (coverage diagram) of pattern propagation factor (PF) in decibels vs altitude and range. Propagation factor is related to signal strength, with $PF = 0$ corresponding to free-space levels.

Figure 1 is an example of VTRPE coverage diagram for an X-band target located at an altitude of 5 m. The propagation environment is over a smooth ocean surface in a standard atmosphere refractivity profile (i.e., constant positive refractivity gradient).

The Lloyd's mirror interference lobes are clearly visible in the plot, and result from constructive/destructive interference between signal energy propagating along direct and surface-reflected paths between the target ($z = 5$ m) and the AIEWS array ($z = 15$ m). At sufficient range separation, the radar horizon is crossed, and signal energy is via weak diffractive paths.

The coverage diagram illustrates the relative field strength at a particular point in space arriving from the missile seeker. The AIEWS interferometer is then introduced at some point downrange from the missile. An estimate of the vertical AOA is developed by performing a plane wave spectral decomposition of the incident VTRPE signal field at the aperture plane of the interferometer. This spectral decomposition is done via a Bartlett-type beamformer applied to a virtual aperture (~200λ) located at the interferometer phase center.

Such a calculation is shown in Fig. 2 for a 5-m (msl) missile target in standard atmosphere propagation over a smooth sea surface. The vertical axis is the plane wave arrival angle at the AIEWS interferometer array located at 15 m (msl) with positive angles corresponding to an incident signal field that is traveling upward; negative angles correspond to downward traveling signals. The plot displays the AOA power spectrum at each target range normalized to the peak. Since the AIEWS array is higher than the missile, a conventional ray analysis would predict two upgoing arrivals at the interferometer: a direct arrival and a surface-reflected arrival at steeper angle. As the missile moves downrange, these two arrivals should merge and asymptote to zero. The AOA spectrum in Fig. 2 shows this to be the case, although the long-range AOA asymptotes to a small positive angle instead of zero.

Effectively, the simulation provides the ability to place the AIEWS array at any location in the world,

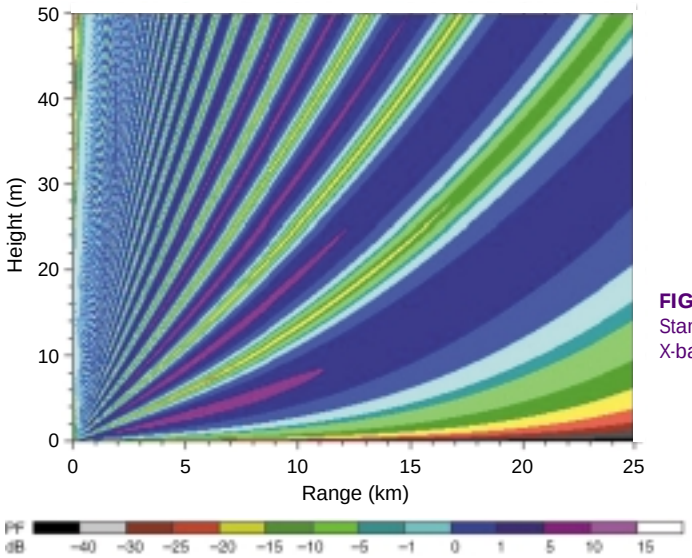

FIGURE 1
Standard atmosphere, 5-m target, X-band, 0-kt wind.

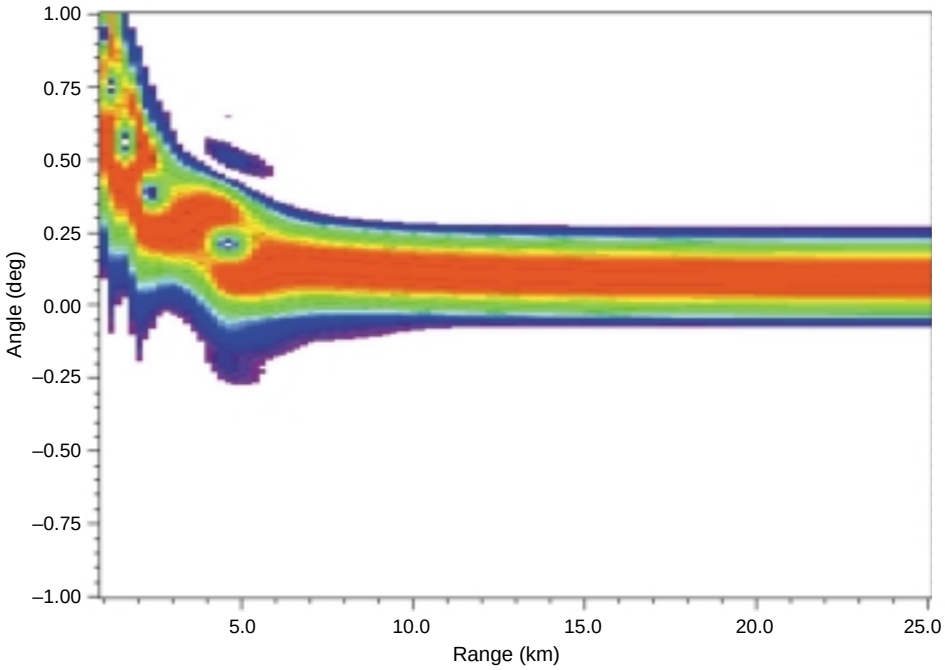

FIGURE 2
AOA spectrum: X-band, standard atmosphere, 5-m target.

with any sea state, and in any atmospheric conditions. Because the propagation path distorts the signal received by the interferometer, it is important to ensure that the AIEWS system works, regardless of the propagation environment.

Wallops Island Example: A more realistic example is shown in Fig. 3, which corresponds to X-band propagation in littoral conditions measured at Wallops Island, Virginia, during April 1998. The target is a missile seeker at a nominal height of 10 m (msl) , and the sea is smooth. The coverage diagram shows a convoluted vertical pattern arising from ducted propagation of energy near the ocean surface caused by near-surface atmospheric refractivity ducts.

Figure 4 is the incident signal phase diagram; it illustrates rapid phase changes near the multipath

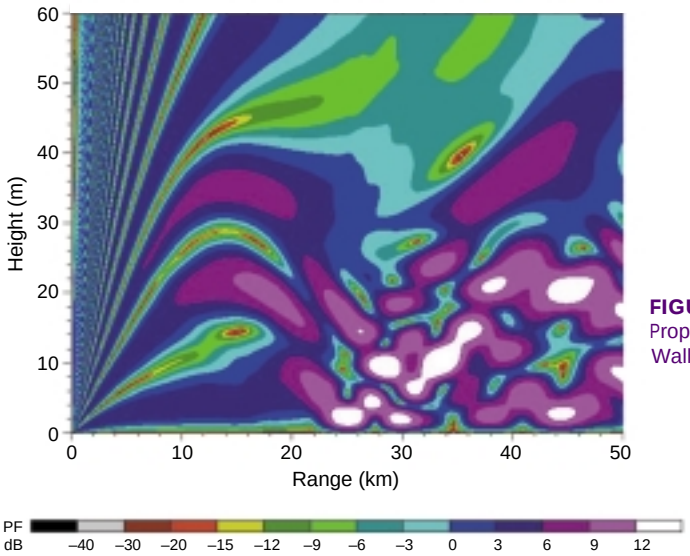

FIGURE 3
Propagation factor coverage diagram: Wallops Island, X-band, wind = 0 kt.

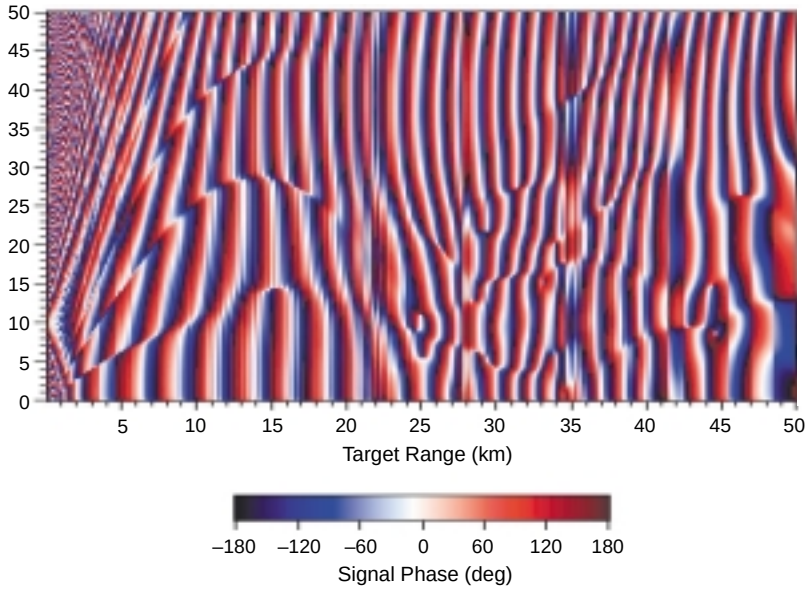

FIGURE 4
Signal phase: Wallops Island, X-band, wind = 0 kt.

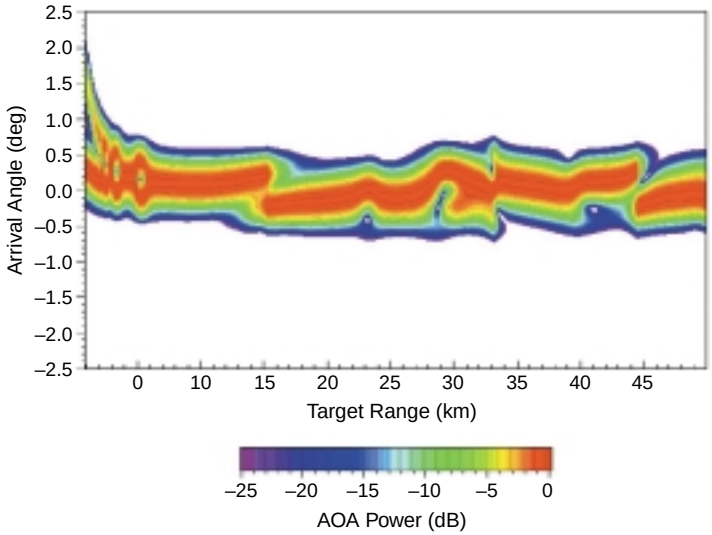

FIGURE 5
AOA spectrum: Wallops Island, X-band, wind = 0 kt.

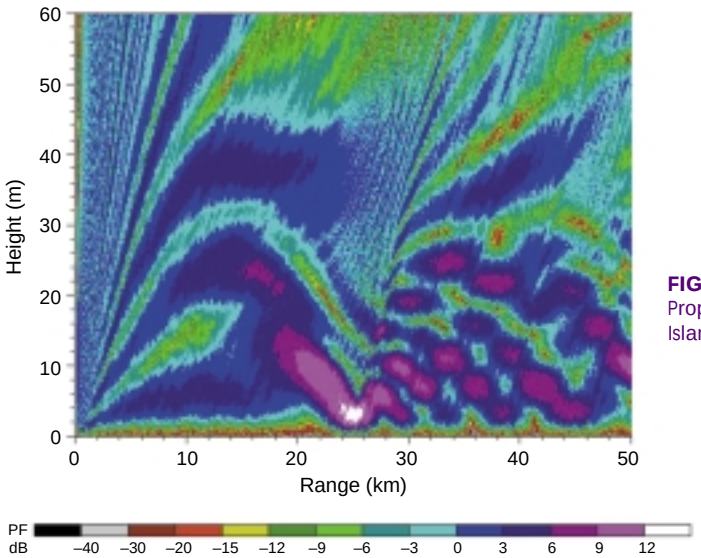

FIGURE 6
Propagation factor coverage: Wallops Island, X-band, wind = 20 kt.

nulls and the anthrodromic points (quasi-circular regions of low signal).

Figure 5 shows the AOA spectrum and displays a more complex structure than the standard atmosphere example. A careful examination of Fig. 5 illustrates that for some target ranges (e.g., 15 to 20 km) the incident signal field is coming from *above* (negative angles), even though the interferometer array is located higher than the missile.

An even more complex scenario results when propagation over a rough sea surface is modeled. Figure 6 depicts propagation for a moderate 20-kt wind in the previous Wallops Island example. The rough sea surface has significantly modified the coverage diagram. Figure 7 shows the corresponding phase diagram, and Figure 8 shows the AOA spectrum.

[Sponsored by ONR]

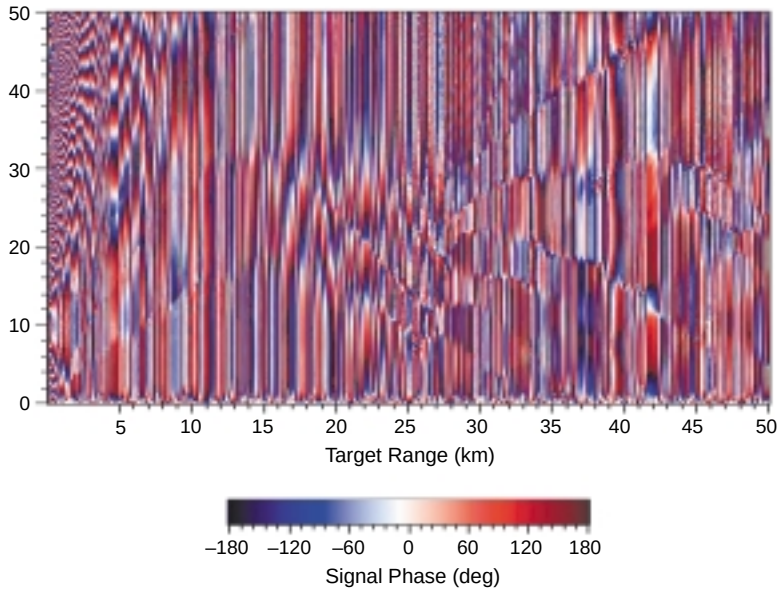

FIGURE 7
Signal phase: Wallops Island, X-band, wind = 20 kt.

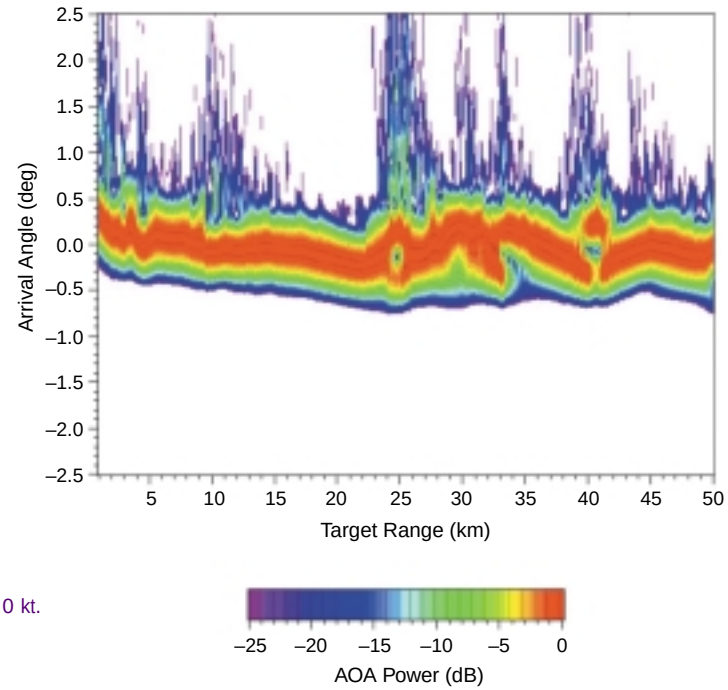

FIGURE 8
AOA spectrum: Wallops Island, X-band, wind = 20 kt.

Visualization and Analysis of Nulka Operational Evaluation

J.Q. Binford, W.A. Doughty, and S.A. Wolford
Tactical Electronic Warfare Division

Introduction: The Nulka ship decoy, designed to counter RF antiship threat missiles, recently underwent operational evaluation (OPEVAL) testing aboard the destroyer USS *Peterson* (DD-969). During the testing, Nulka decoys were fired in response to captive carry antiship cruise missiles (ASCM) from the NRL NP-3D aircraft and two F/A-18s. A total of eight operationally simulated ASCM test engagements were conducted. When the data were analyzed, Operational Test and Evaluation Force (OPTEVFOR) determined that the data had inconsistencies between platforms and that, consequently, additional tests might have to be performed before OPTEVFOR could recommend Fleet introduction. This initial determination and subsequent recommended actions would have delayed the Nulka production decision at great cost to the Nulka program and would have delayed introduction of this very capable system to the Fleet. The Program Executive Office for Theater Air Defense/Surface Combatants PEO(TSC), the Nulka acquisition sponsor, tasked NRL to perform an analysis of the data and report the results to a "blue ribbon panel" that would make an independent assessment and brief the Milestone Decision Authority on their conclusions.

SIMDIS: NRL's Tactical Electronic Warfare Division (Code 5707) applied modeling and simulation tools, specifically the SIMDIS analysis and visualization toolset, sponsored by the ONR/NRL Base Electronic Warfare Applied Research Program (Figs. 9 and 10). NRL worked closely with engineers from Naval Surface Weapons Center (NSWC) Dahlgren Division, NSWC Aircraft Division, and NSWC Weapons Division in gathering and understanding the various data collections from the test. NRL developed software tools for processing the time-space position information (TSPI) and missile telemetry data into a consistent time and coordinate reference frame. NRL processed the various data collections and integrated the data into the SIMDIS toolset. Using SIMDIS, analysis of the collected Nulka test data allowed actual flight sequences to be meticulously analyzed through two- and three-dimensional visualizations. The data were re-evaluated with confidence and demonstrated that the system performed significantly better than conclusions drawn from OPTEVFOR's initial findings. OPTEVFOR agreed with the analysis. A positive Milestone III decision was made, and Nulka is proceeding with installation starting on three Aegis cruisers. The more precise findings prevented any negative impact on the Nulka program.

Key to comprehensive understanding of the available data was the SIMDIS analysis tool that provided a powerful three-dimensional (3D) display. SIMDIS takes advantage of specific advances in new highly accurate Global Positioning System/Inertial Positioning System (GPS/INS)-based positioning systems as well as improved digital data collection capabilities. It provides a high-fidelity 3D visual reconstruction of test assets and sensor systems. SIMDIS operates in either a live or postprocessed display mode. As government off-the-shelf (OTS) software, SIMDIS has been developed into a formal software product and distributed to several Navy ranges and systems centers. It is currently operational across several platforms including PC, Silicon Graphics, and Sun workstations that provide OpenGL hardware accelerated 3D graphics. SIMDIS provides a view of normal TSPI and orientation data of all the test players, as well as the "unseen" data such as interactions of sensor systems with targets, countermeasures, and the environment. SIMDIS provides tools for interactively analyzing data using custom tools for displaying equipment modes, spatial grids, ranges, angles, and antenna patterns.

Conclusions: By using reconstructed and simulated data sets with interactive playbacks, SIMDIS also allows various, often-confusing, aspects of the operational testing to be readily visualized and comprehended.

The Nulka OPEVAL data reconstruction and analysis effort showed that:

- A need exists for improved data standards among the ranges, laboratories, and warfare centers (in terms of consistent well-documented formats). Significant efforts were required to correctly interpret the data and integrate it into a consistent time and coordinate reference frame.
- Visual analysis tools for analyzing test data can greatly improve the understanding of test results and provide a powerful means to communicate results to others, and
- Future electronic warfare tests should make maximum use of advanced visualization tools such as SIMDIS.

The application of advanced graphical analysis tools for creating a coherent, integrated, high-fidelity display of the Nulka test data proved invaluable.

[Sponsored by ONR]

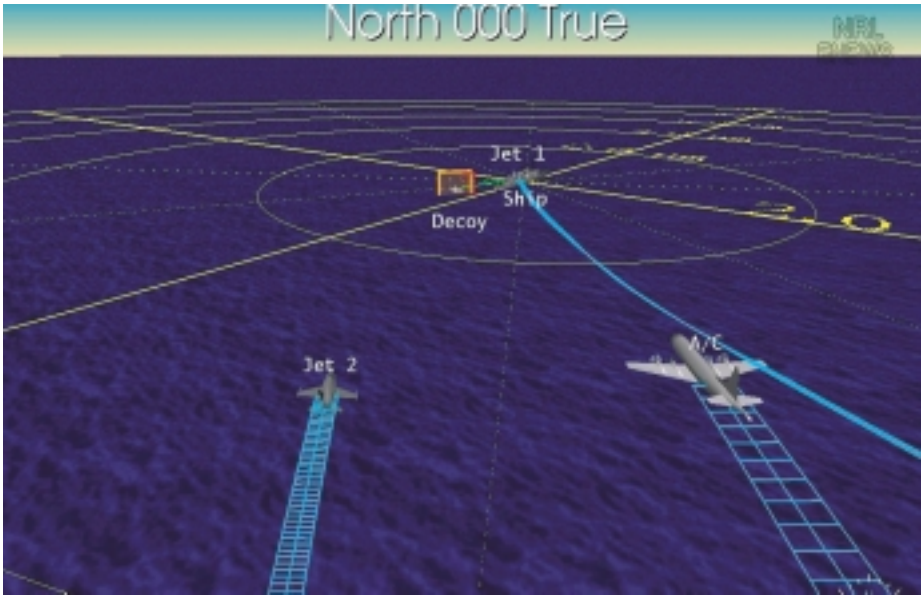

FIGURE 9
Visualization of Nulka operational evaluation using SIMDIS.

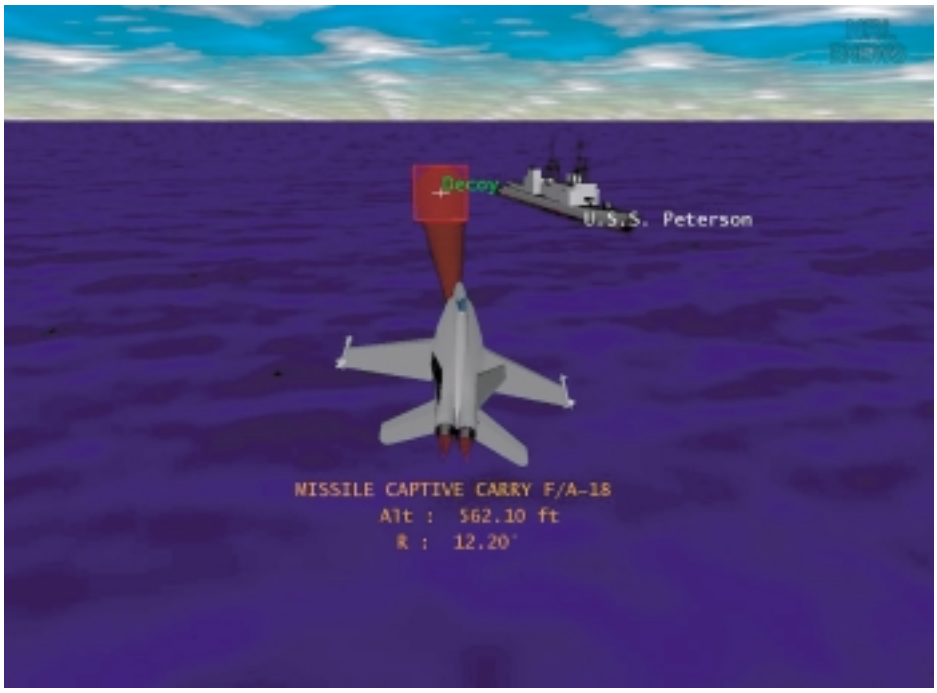

FIGURE 10
SIMDIS display of F/A-18 captive carry missile seeker track.

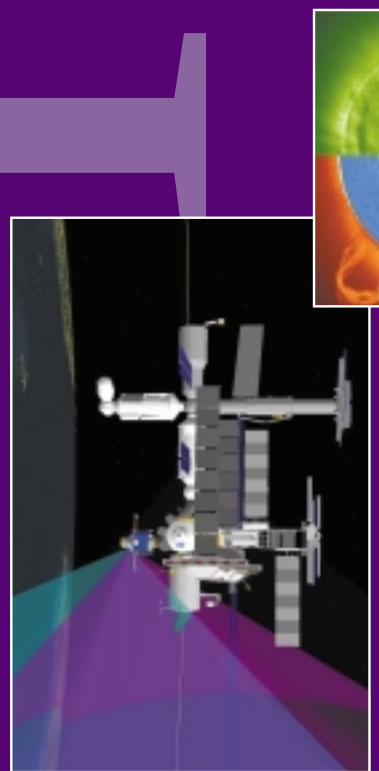

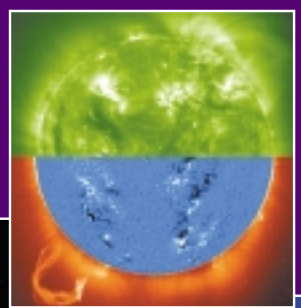

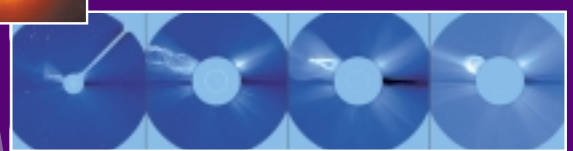

Space Research and Satellite Technology

Sun Earth Connection Coronal and Heliospheric Investigation (SECCHI)

R.A. Howard, J.D. Moses, D.G. Socker,
and K.P. Dere
Space Science Division

The STEREO Mission: NASA recently developed a mission concept to place two identically instrumented spacecraft into an orbit about the Sun—one trailing Earth and the other leading Earth. The primary objective of this mission, called STEREO, is to understand the physics of coronal mass ejections (CMEs). By having two spacecraft, CMEs can be observed from two vantage points, and thus three-dimensional information can be gained. The basic physics that expels these plasma clouds into the heliosphere is still not well understood. The role of the magnetic field development in the photosphere and corona and its coupling to the propagation and acceleration processes is crucial to a fuller understanding of these potentially geoeffective events. The STEREO mission combines remote sensing and in situ observations from two distinct views. It is well suited to the exploration of all manifestations of CMEs, both at their initiation and during their propagation to 1 astronomical unit (AU). Major advances in understanding the connection between solar events and their terrestrial response have come when interdisciplinary studies are able to combine data from solar observations with those from the inner heliosphere and from terrestrial observation. In addition to the observations, numerical and analytical modeling analyses will be necessary to connect the observations from the disparate regions.

Why STEREO?: By placing two spacecraft into orbit around the Sun, the STEREO mission removes two difficulties encountered in previous missions that have observed CMEs. A white light coronagraph best observes CMEs that are on the limb; it cannot observe the CME material that would eventually impact Earth. Since each STEREO spacecraft will drift away from the Earth at the rate of 22°/year, CMEs headed toward Earth will be clearly imaged. The second difficulty is that our perception of the corona has been obtained from two-dimensional images. The third dimension has been inferred. Identical instrumentation will be on the two STEREO spacecraft, which will enable simultaneous stereoscopic viewing of quiescent coronal structures as well as dynamic phenomena such as CMEs.

CMEs: Discovered in 1971 by an NRL experiment on-board a NASA satellite, CMEs have become extremely important in understanding the effect of solar emissions on Earth. The NRL Large Angle Spectrometric Coronagraph (LASCO) experiment[1] on the European Space Agency (ESA) and NASA Solar and Heliospheric Observatory (SOHO) has been observing CMEs in unprecedented clarity. Real-time images from LASCO are available on the Web at http://lasco-www.nrl.navv.mil. Figure 1 shows the development of a CME moving through the solar corona on June 2, 1998. This event shows the prototypical three-part structure of a CME—the bright leading material, followed by a dim region, and then complex, twisted bright material. The twisted structure is a solar prominence erupting, carrying magnetic field and ionized material.

SECCHI: In December 1999, NRL was selected by NASA to develop an instrument called the Sun Earth Connection Coronal and Heliospheric Investigation (SECCHI) for the STEREO mission. SECCHI is also the name of an Italian astronomer, Angelo Secchi (1818-1878), who pioneered the use of the new medium of photography to solar physics and is considered by some to be the father of astrophysics. SECCHI is designed to explore various manifestations of the CME process with three types of tele-

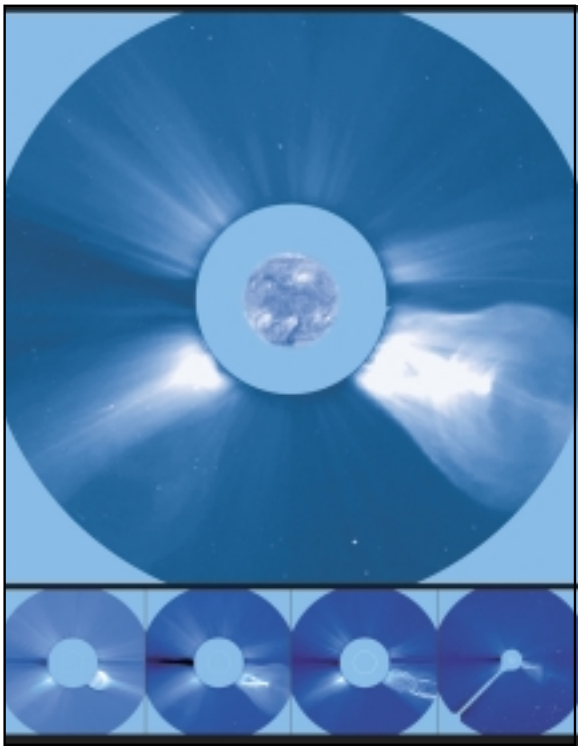

FIGURE 1
Development of a coronal mass ejection moving through the solar corona.

scopes. The first is an extreme ultraviolet (EUV) imager (EUVI) that will image the chromosphere and low corona in four emission lines. The second type, a white light coronagraph, actually is two coronagraphs to explore the inner corona and the outer corona (COR1 and COR2). This function was split into two telescopes because of the large radial gradient in coronal brightness. The third type is a wide field heliospheric imager (HI) to image the inner heliosphere between the Sun and Earth. This region was also split into two telescopes, HI-1 and HI-2, to optimize the stray light requirements.

Scientific Objectives: Figure 2 illustrates the scientific objectives and the approach of SECCHI. These objectives are: What configurations of the corona lead to a CME? What initiates a CME? What accelerates CMEs? and How does a CME interact with the heliosphere? How do CMEs cause space weather disturbances? The EUV, COR1, and COR2 telescopes will address the first two questions. The COR1, COR2, and HI-1 will address the third and fourth questions, and the HI-1 and HI-2 will address the fourth and fifth questions. The final telescope (HI-2) will observe the CME as it impinges on the Earth's atmosphere. The suite of SECCHI telescopes will observe the structures (in stereo) involved in the eruption and will then follow the eruption as it travels through the corona, providing a unique perspective into the physics of CMEs.

Acknowledgments: SECCHI is an international collaboration between the United States (NRL, NASA/Goddard Space Flight Center, the Lockheed Martin Solar and Astrophysics Laboratory, Boston College, Jet Propulsion Laboratory, Smithsonian Astrophysical Observatory, Space Applications International Corporation, Southwest Research Institute, Stanford University), Belgium (Royal Observatory, Centre Spatiale de Liege), France (Institut d'Optique, Institut d'Astrophysique Spatiale, Observatoire de Paris, Laboratoire d'Astronmie Spatiale, University d'Orleans), Germany (Max-Planck-Institut für Aeronomie, Universität Kiel), and the United Kingdom (University of Birmingham, Rutherford Appleton Laboratory, Mullard Space Science Laboratory). In the U.S., the primary sponsor is NASA, but the USAF Space Test Program is supporting the SECCHI integration and test efforts.

[Sponsored by NASA and USAF/STP]

Reference

[1] G.E. Brueckner, R.A. Howard, K.P. Dere, *et al.*, "The Large Angle Spectroscopic Coronagraph (LASCO)," *Solar Phys.* **162,** 357-402 [1995].

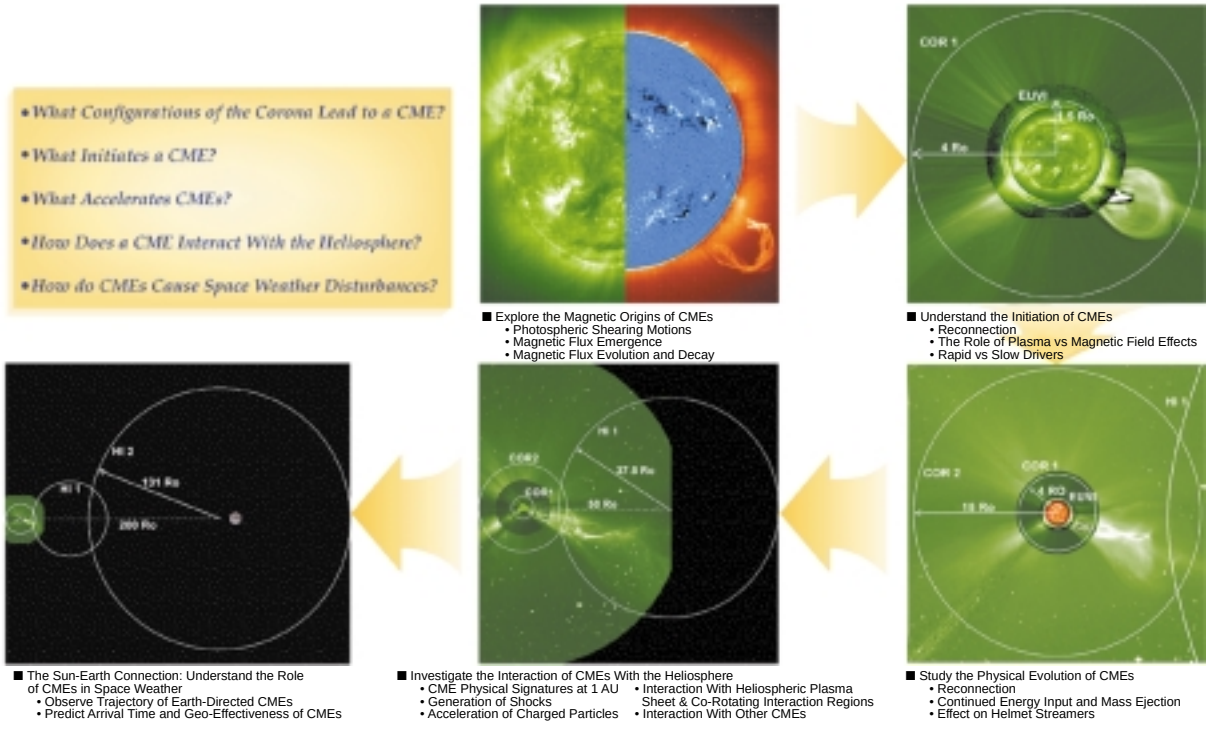

FIGURE 2
SECCHI exploration of CMEs and the heliosphere on STEREO.

FAME Radiometric Data Requirements and Processing

A.S. Hope
Space Systems Development Department

Introduction: The Full-sky Astrometric Mapping Explorer (FAME) spacecraft is being integrated by the Naval Center for Space Technology (NCST) for launch in 2004. FAME is a NASA Medium-Class Explorers mission. Its Principal Investigator is located at the U.S. Naval Observatory. The goal of the FAME mission is to create new star catalogs of unprecedented accuracy. A significant challenge to meeting this goal is to determine the velocity of the satellite to within 1 centimeter per second with a minimum of tracking data. (Collection of tracking data can impact the return of science data.) The Astrodynamics and Space Applications Office (ASAO), Code 8103, is providing support for mission planning, operations, and science data reduction. In preparation for flight operations, Code 8103 analyzed the FAME orbit and determined the amount of tracking data required from NRL's Blossom Point (Maryland) Tracking Facility to meet the velocity knowledge requirement. This process demonstrates an important capability within NRL and NCST to design, analyze, track, and compute satellite orbits.

The Orbit: The FAME operational orbit is a geosynchronous orbit at 105 degrees west longitude, inclined to the Earth equator at 28.7 degrees. The ground station for mission operations is located near NRL in southern Maryland at Blossom Point. Figure 3 shows the ground track for the FAME spacecraft as well as the location of the Blossom Point ground station. The pink line shows the field of view for the ground station to satellites at geosynchronous altitude. The selected orbit provides for continuous coverage to the ground station. This orbit is stable and will remain within a few degrees of its original longitude over the lifetime of FAME.

Code 8103 in NCST is providing the definitive orbital ephemeris for FAME. The ephemeris contains the position and velocity of the spacecraft with respect to the center of the Earth over time. The FAME science team has allocated a portion of the error budget for FAME science data reduction to the spacecraft velocity knowledge. This knowledge is important for reduction of the data in that it allows the science team to correct for the abberation in the FAME measurements due to spacecraft motion. The allocation for velocity error is 1 cm/s. Code 8103 has determined the minimum amount and types of tracking data that meet this requirement. Minimizing the amount of tracking data for FAME is valuable because the collection of active ranging measurements interrupts the downlink of science data.

FIGURE 3
Graphical representation of nominal FAME ground track, tracking station, and tracking station field of view.

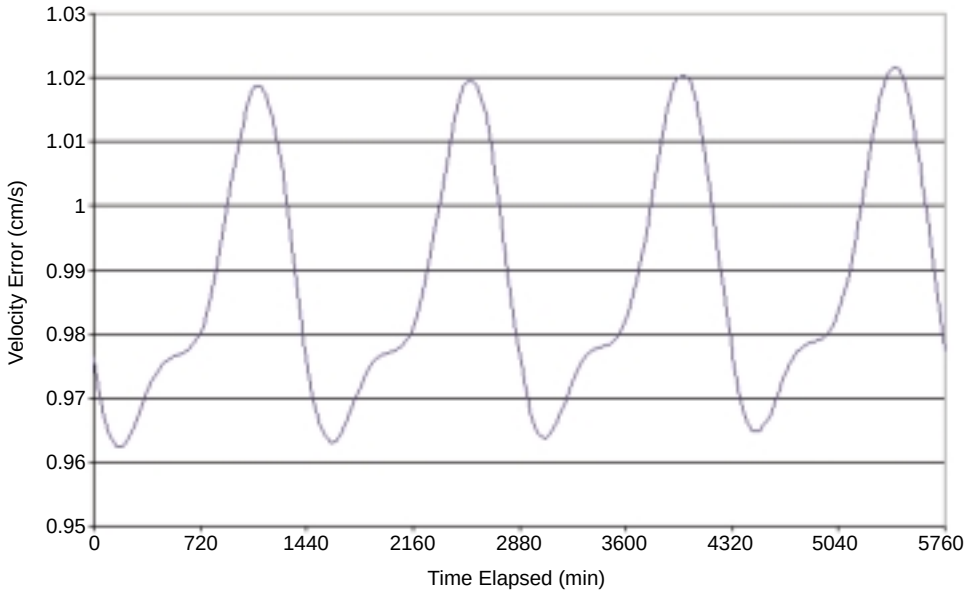

FIGURE 4
Plot of estimated FAME velocity error vs time over 4 days.

Analysis: Covariance analysis was used to determine the system tracking requirements. The covariance analysis tool models the system, the measurements, and the errors according to user-defined parameters. An iterative process was performed in which various satellite orbits, ground stations, measurement types, measurement duration, and measurement intervals were modeled to determine the most likely operations scenario for FAME. Various measurement errors were modeled to determine the sensitivity of the orbit determination (OD) solution to the error levels. The results of the analysis show that with FAME in a 105-degree west longitude geosynchronous orbit inclined at 28.7 degrees, and a single ground station located at Blossom Point, Maryland, the FAME velocity knowledge requirements can be met. The covariance analysis was then verified using a Monte-Carlo simulation using a similar system and tracking scheme. The measurement data used to determine the FAME orbit are one hour of Doppler range rate data three times per day and ten minutes of active range data three times per day. Figure 4 is a plot of the expected velocity errors. Although the figure shows that the expected velocity will exceed the 1 cm/s velocity requirement over a portion of the orbit, this was deemed acceptable by the science team because the covariance analysis uses 3-s measurement and model errors.

Summary: The next step in the orbit determination validation process will be to process simulated range and range rate data generated by the covariance analysis tool using the OD software. Simulated measurements will be processed using NRL's OCEAN software (Orbit Covariance and Estimation Analysis). OCEAN is a state-of-the-art, sub-meter-level, multi-satellite orbit determination, ephemeris propagation, and timing calibration software tool. After FAME is launched, OCEAN will produce the definitive orbits used by the science team to correct the astrometric measurements. The level of ephemeris accuracy will allow the abberation due to spacecraft motion to be removed.

[Sponsored by NASA]

Interim Control Module Night Sky Attitude Determination Test

R.S. McClelland and T.W. Lim
Spacecraft Engineering Department

The Interim Control Module (ICM) was designed to provide attitude determination and control (ADAC) and reboost capabilities for the International Space Station (ISS). An end-to-end attitude determination test was conducted to verify the attitude determination requirements and prove out the electrical and software interfaces to the ADAC sensors.

Figure 5 shows the ICM attached to the ISS. The cones depict the bright-object keep-out zone for each of the two star tracker cameras (STC). The ICM flight

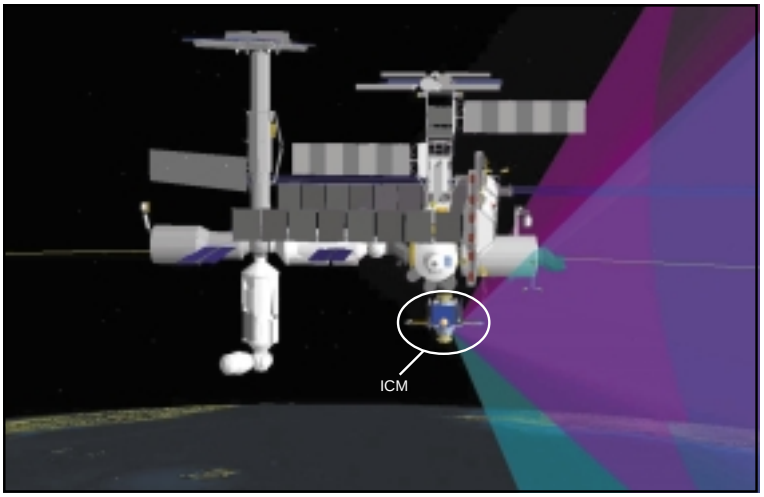

FIGURE 5
ICM attached to International Space Station.

computer processes images from the STCs to determine the ISS orientation (attitude) based on the observed star pattern. The ADAC Kalman filter software blends the STC attitude solutions with Inertial Measurement Unit (IMU) gyroscope readings. The gyroscope angular rate measurements are used to propagate the attitude estimate between STC updates. The Kalman filter uses the STC updates to compute gyroscope bias estimates. The biases are subtracted out to minimize loss of attitude estimate precision during STC outage periods caused by Earth or Sun intrusion. The gyroscope measurements are further used by the ADAC software to provide rate damping for convergent, stable closed-loop control of the ISS attitude.

Test Description: The main goal of the test was to verify attitude knowledge accuracy requirements. The mature state of development of the ICM also provided an opportunity to verify the electrical and software interfaces to the flight sensors and processing electronics as well as the attitude determination Kalman filter processing.

The STCs were mounted to a test platform outside the NCST Payload Checkout Facility;[1] the assembled ICM structure, electronics deck, and IMUs remained inside. To arrive at the "truth" attitude against which the attitude solution accuracy would be judged, the STC mounting platform was leveled with respect to the local gravitational force vector. It was precisely aligned in azimuth using Polaris as a reference and making use of the STC optical alignment cube. Figure 6 shows the test setup. With the STCs in a known orientation with respect to the local reference frame, the predicted inertial attitude was computed by factoring in the latitude and longitude

(a) STCs on mounting platform

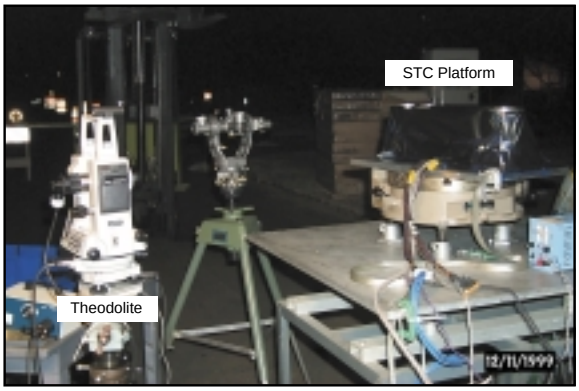

(b) Alignment configuration

FIGURE 6
Night sky test setup.

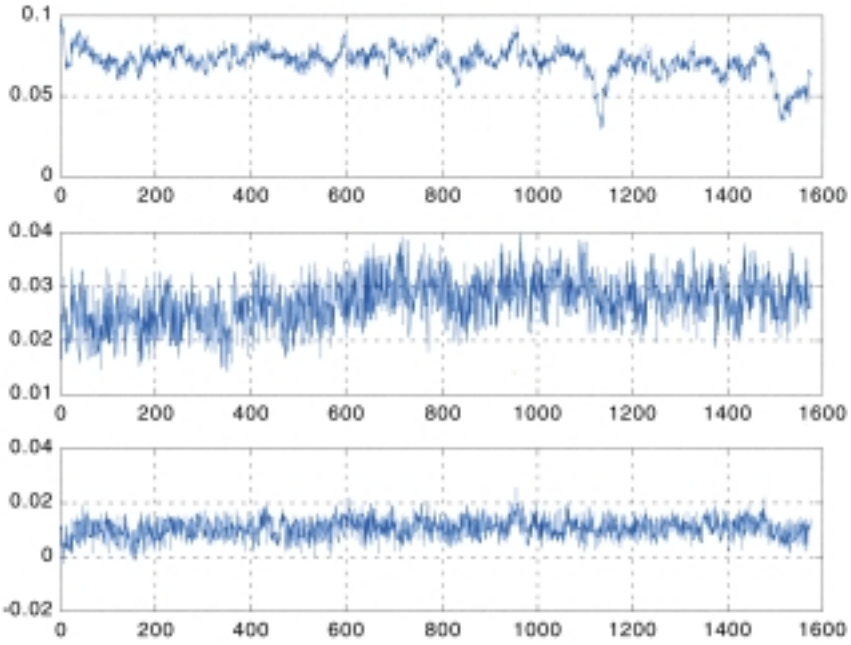

(a) Attitude error with respect to predicted attitude

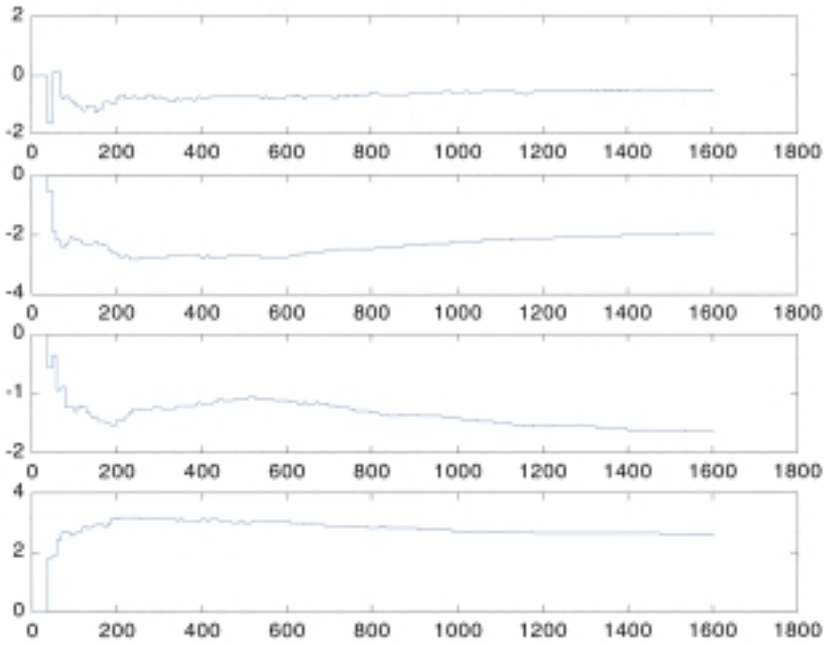

(b) Gyro bias estimates

FIGURE 7
Kalman filter performance.

of the test site and the time of the STC image collection. The attitude of the ICM structure was estimated using several minutes of data collected from the IMU. The components of Earth rate sensed in each of three orthogonally mounted gyroscopes uniquely identified its orientation with respect to the local reference frame. This information was then used in the attitude determination Kalman filter so that the sensor measurements from the STCs and the IMUs were provided to the filter in a consistent reference frame.

Results: The test verified the required accuracy of better than 0.1 degrees per axis (Fig. 7(a)).[2] The validity of the alignment correction terms relating the camera CCD frame to the optical alignment cube were also verified. The attitude determination Kalman filter processing results (Fig. 7(b)) verified correct polarity, convergence, and propagation behavior.

Acknowledgments: The authors acknowledge the concerted efforts of Mike Pilecki, Brian Davis, Ray Caperoon, Ron Zellar, Dave Dawson, and John Gambert in making this test a success.

[Sponsored by NASA]

References

[1] "ICM ACS Integrated Attitude Determination Night Sky Test Procedure, SSD-TD-IM058," NRL, Naval Center for Space Technology, 9 December 1998.

[2] "ICM ACS Integrated Attitude Determination Night Sky Test Report, SSD-TR-IM116," NRL, Naval Center for Space Technology, 22 May 2000.


Special Awards
and Recognition

SPECIAL AWARDS AND RECOGNITION

NRL is proud of its many distinguished scientists, engineers, and support staff. Here we feature some who have received awards from prestigious institutions, the Department of the Navy, and NRL.

OFFICE OF NAVAL RESEARCH'S CAPTAIN ROBERT DEXTER CONRAD AWARD FOR SCIENTIFIC ACHIEVEMENT

Dr. Timothy Coffey — Director of Research

This award is named in honor of CAPT Robert Dexter Conrad, who was a primary architect of the Navy's basic research program and the head of the Planning Division of the Office of Naval Research at the time of its establishment. It is designed to recognize and award outstanding technical and scientific achievement in research and development for the Department of the Navy. As NRL's Director of Research, Dr. Coffey oversees research and development expenditures of approximately $800 million per year. This award recognizes Dr. Coffey for "his exceptional ability to promote an innovative environment at, and foster the scientific breakthroughs of, the Department of Defense's premier laboratory, the U.S. Naval Research Laboratory. As a world-class technical manager, Dr. Coffey's contributions to defense and naval technology policy and his ability to continually enable world-leading science and technology developments have gained sustained recognition from the Defense Department, the Federal Government, academia, industry, and the international defense and scientific communities."

2000 SIGMA XI PURE SCIENCE AWARD

Dr. David Singh — Materials Science and Technology Division

Dr. Singh was recognized for having "made contributions developing and applying first principles methods to the study of materials. He is a world-leading expert on methodology and has applied the methods to diverse physical problems. He has authored 170 scientific publications and is cited more than 3,700 times." According to the award nomination, Dr. Singh has focused his research on the development of first principles methods and their application to materials. He has originated important advances in techniques for such calculations. He is recognized as an expert in the Linearized Augmented Plane Wave method. This is a state-of-the-art method for highly precise density functional calculations on general materials.

2000 SIGMA XI APPLIED SCIENCE AWARD

Dr. Douglas Chrisey — Materials Science and Technology Division

Dr. Chrisey was recognized "for novel laser-based processing of advanced thin films and coatings." According to the award nomination, "Throughout Dr. Chrisey's career, he has been able to connect his fundamental materials science research to Navy, DoD, and national needs. He has taken fundamental research results and run with them to have significant impact on NRL superconducting space experiments, ferrite circulators on GaAs, tunable microwave electronics for SPAWAR and DARPA, polymer thin-films for chemoselective SAW sensors, and a potentially revolutionary direct-write technique for microwave circuit fabrication."

2000 SIGMA XI YOUNG INVESTIGATOR AWARD

Dr. Greg Collins — Chemistry Division

Dr. Collins was recognized "for the development of new materials for application in sensing transducers." According to the nomination, there is a "continuing need for chemical sensor development due to the challenges in chemical warfare/terrorism, long-term habitability in enclosed spaces (submarine, spacecraft), ever-changing national and international environmental laws and regulations, and special operation forces. Dr. Collins has responded to this challenge with an exemplary balance of innovative, noteworthy pure and applied research. He is not only contributing impressive science, but also transitioning the resultant understanding into technology."

INSTITUTE OF ELECTRICAL AND ELECTRONICS ENGINEERS (IEEE) DENNIS J. PICARD MEDAL FOR RADAR TECHNOLOGIES AND APPLICATIONS

Dr. Merrill Skolnik — Radar Division (retired)

The IEEE Picard Medal is sponsored by the Raytheon Company, and is named for the chairman and chief executive officer of the Raytheon Company, Mr. Dennis J. Picard. Dr. Skolnik is the first recipient of the Picard Medal. The citation recognized Dr. Skolnik "for outstanding leadership of Navy radar research, authorship of widely used books on radar, and personal contributions to the advancement of radar technologies and systems."

2000 PRESIDENTIAL RANK OF MERITORIOUS EXECUTIVE AWARD

Dr. Gerald Borsuk — Electronics Science and Technology Division

The Presidential Rank Award is among the highest honors a public employee may receive. The citation reads, "It is recognition of your sustained, outstanding achievements which have brought great credit, not only upon yourself, but the entire Department of the Navy. Your accomplishments have contributed in large measure to our ability to provide for the national security in the most efficient and effective manner. For this, the Department is truly grateful."

INSTITUTE OF ELECTRICAL AND ELECTRONICS ENGINEERS (IEEE-USA) FREDERIK PHILIPS AWARD

The Frederik Philips Award is presented annually to recognize outstanding accomplishments in the management of research and development resulting in effective innovation in the electrical and electronics industry. Dr. Borsuk was recognized for his "managerial and technical leadership in directing the creation and transition of new materials and devices into electronic systems." He is responsible for the in-house execution of a multidisciplinary program of basic and applied research into electronic materials and structures, solid state devices, vacuum electronics, and circuits. He is also responsible for the coordination of the Electronics Science and Technology Program at NRL.

INSTITUTE OF ELECTRICAL AND ELECTRONICS ENGINEERS (IEEE-USA) HARRY DIAMOND MEMORIAL AWARD

The Harry Diamond Memorial Award is presented annually to honor individuals for distinguished technical contributions in the field of electrotechnology while in U.S. government service. Dr. Borsuk was recognized for "his outstanding technical leadership and innovative management skills demonstrated during his many years of service at NRL and in advisory roles to the Department of Defense and other U.S. Government agencies."

INSTITUTE OF ELECTRICAL AND ELECTRONICS ENGINEERS (IEEE-USA) THIRD MILLENNIUM MEDAL

The Millennium Medal is awarded to those individuals whose outstanding contributions made a difference to the engineering profession and to the world in general. Individuals are also being recognized for their contributions to the development of management infrastructure having a significant impact on industry now or in the next millennium. Dr. Borsuk was recognized as "such an individual worthy of this recognition."

INSTITUTE OF ELECTRICAL AND ELECTRONICS ENGINEERS (IEEE) YOUNG RADAR ENGINEER OF THE YEAR AWARD

Dr. Michael Steiner — Radar Division

The IEEE Young Radar Engineer of the Year Award grants international recognition for outstanding contributions to the radar art by IEEE/Aerospace and Electronic Systems Society (AESS) members under the age of forty. This award was established by the IEEE/AESS in honor of the late Fred Nathanson to encourage individual effort and to foster increased professional participation by developing radar engineers. The award nomination stated, "Dr. Steiner is an active contributor in the conception, direction, and development of both theoretical techniques and practical systems aimed at improving the detection capability of radars." According to the nomination, Dr. Steiner is a member of a core planning group responsible for developing advanced Navy radars.

Mr. Jim Gogorik (ONR 334), Jeffrey Benson (NSWCCD, retired), Mr. Lee Gause (NRL – MS&CTD), Brian Kiviat (NSWCCD), Kevin Wilson (NSWCCD), Ms. Arthur E. Bisson, Patrick Porter (NSWCCD), Tammy Campbell (NSWCDL), Douglas Loup (NSWCCD), Robert Cross (formerly NSWCCD), and Bruce Bandos (not pictured)

DR. ARTHUR E. BISSON PRIZE FOR NAVAL TECHNOLOGY ACHIEVEMENT

The Arthur E. Bission Prize recognizes a person or persons who have successfully translated research findings into substantive fleet programs that meet critical Navy requirements. The award was presented to the Advanced Enclosed Mast/Sensor (AEM/S) System Advanced Technology Demonstration (ATD) Team for leadership, dedication, effort, and exceptional S&T development and transition of the AEM/S System ATD project during fiscal years 1995-1997. The AEM/S System ATD, which successfully demonstrated composite, signature, and electromagnetic engineering technology in an integrated mast concept demonstration on the USS *Arthur W. Radford* (DD-968), has made possible radical improvements in the topside design of all future Navy surface ships.

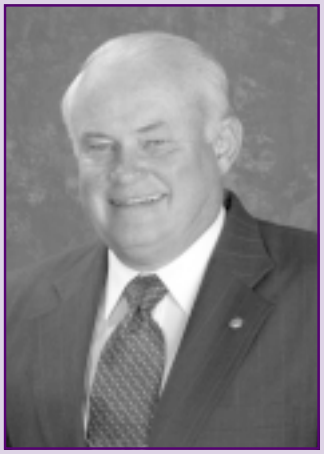

NATIONAL RECONNAISSANCE OFFICE (NRO) GOLD MEDAL

Mr. James O'Connor — Space Systems Development Department (retired)

Mr. O'Connor was cited "for exceptional service as a radio frequency and space systems engineer for the Low Earth Orbit Special Program Office. His long and dedicated service in the research, development, design, and operation of several major satellite systems resulted in a space-based reconnaissance architecture that continues to respond to the dynamically changing and extremely challenging national and tactical threat environment. Additionally, his engineering mastery and unwavering support of legacy systems resulted in his selection as a pivotal member on the concept, design, and evaluation team for the follow-on system architecture. Mr. O'Connor's keen technical abilities, unique insights, and managerial acumen have guaranteed a follow-on architecture that will serve the needs of the nation well into the 21st century. As a consummate engineer, innovator, and team player, Mr. O'Connor contributed greatly to the defense of the United States. The distinctive accomplishments of Mr. O'Connor reflect great credit upon himself, the Naval Research Laboratory, and the National Reconnaissance Office."

INSTITUTE FOR THE DYNAMICS OF ENERGETIC AND REACTIVE SYSTEMS (IDERS) A.K. OPPENHEIM PRIZE

Dr. Elaine Oran — Laboratory for Computational Physics and Fluid Dynamics

This award is given biannually by the Institute for the Dynamics of Energetic and Reactive Systems for outstanding contributions to the theory of the dynamics of explosions and reactive systems. Dr. Oran received the award for her "pioneering contributions to the understanding of the dynamics of reactive flows through the application of numerical modeling and simulation." The Oppenheim Prize is named for and was presented by Professor Emeritus Antoni K. Oppenheim of the University of California, Berkeley. Dr. Oran's current research focuses on the development and application of the methods of fluid dynamics, particle dynamics, and parallel computing to problems in complex flow systems, combustion and propulsion, turbulence, parallel computing, astrophysics, and multiphase flows.

THE COMBUSTION INSTITUTE'S YA. B. ZELDOVICH GOLD MEDAL

The Ya. B. Zeldovich Gold Medal, which was prepared by the Russian Academy of Sciences, is given biennually by the Combustion Institute for outstanding contributions to the theory of combustion and detonations. Dr. Oran received the award for her "pioneering applications of numerical simulation for solving problems in fluid dynamics and reacting flows." She has made pivotal contributions to a wide range of problems in combustion and propulsion, atmospheric physics, and solar physics and astrophysics. Her work has contributed to both basic science and to advanced engineering applications.

NATIONAL INSTITUTE OF SCIENCE (NIS) OUTSTANDING SCIENTIST AWARD

Dr. George Carruthers — Space Science Division

Dr. Carruthers is the first recipient of this award. This award was presented to Dr. Carruthers "in recognition of his distinguished career to space research and for exemplary services to teaching students." The mission of the National Institute of Science is to provide a roadway for the exchange of scientific information and the presentation of scholarly research papers by science students and faculty members primarily from Historically Black Colleges and Universities, and for establishing a science network consisting of students, educators, and research professionals. According to NIS, Dr. Carruthers' career "illustrates the positive outcomes of hard work and commitment to the advancement of science."

VICE ADMIRAL HAROLD G. BOWEN AWARD FOR PATENTED INVENTIONS

Dr. Robert Brady — Chemistry Division

The Bowen award, named in honor of VADM Harold Gardiner Bowen, the first Chief of Naval Research, recognizes inventions of great benefit to the Navy patented by current or former, civilian or military Navy personnel. The winning invention must have a significant impact upon the operation of the Navy as measured by the extent of its use, cost savings, increased military capability, or increased quality of life. This year's winning invention "Nonskid Coating Formulations" covers a range of epoxipolyamide coatings that provide traction and directional control to personnel and machinery operating on decks of ships.

AMERICAN ASTRONAUTICAL SOCIETY'S (AAS) 1999 DIRK BROUWER AWARD

Dr. Shannon Coffey — Spacecraft Engineering Department

Dr. Coffey was awarded for his "significant contribution in solving critical astrodynamics problems using parallel processing." The two significant contributions that won him the Dirk Brouwer Award were his "application of parallel processing to maintaining the space object catalog using special perturbations and the determination of near-miss conjunctions of space objects" and "advancing the state-of-the-art tether satellite dynamics by determining the orbital and attitude dynamics of the TiPS satellite." For the past few years, Dr. Coffey has been researching the use of parallel processing for improving computationally intensive astrodynamics problems.

NAVY SUPERIOR CIVILIAN SERVICE AWARD

Dr. Frances Ligler — Center for Bio/Molecular Science and Engineering

Dr. Ligler was cited for "superior leadership and technical contributions in serving the Navy, Department of Defense, and the Nation as head of the Laboratory for Biosensors and Biomaterials in the Center for Bio/Molecular Science and Engineering at NRL. She has led the laboratory since its inception. Because of her strong leadership and technical contributions, both the laboratory she leads and the Center in which she works are now recognized as the premier research and development group in the DoD for biosensor research…The capability to undertake research, develop the technology, and transition the technology for military and civilian use has placed the Navy at the state-of-the-art in the development of early warning systems for biological warfare attacks. Dr. Ligler's leadership, professionalism, and total dedication to duty reflect great credit upon herself, the Office of Naval Research, and NRL, and are in keeping with the highest traditions of the United States Navy."

NAVY SUPERIOR CIVILIAN SERVICE AWARD

Mr. Paul Hughes II — Radar Division

According to the nomination, Mr. Hughes was recognized "for his superior achievements in serving the Navy, Department of Defense, and the Nation as an employee of the Naval Research Laboratory. From 1988 to 1995, Mr. Hughes adeptly managed two projects associated with the detection of low-observable targets. His outstanding personal contributions and leadership applied to the problem of detecting and tracking the low-observable, low-altitude sea skimming missile demonstrated to the Navy that these targets could be detected using low-cost, pulse-Doppler radar systems. This had a major impact in that it convinced the Navy that stealth targets could be detected at an affordable cost and this led to transitions of counter low-observable systems into the Fleet. Mr. Hughes' leadership, professionalism, and total dedication to duty, reflect great credit upon himself, the Office of Naval Research, and NRL, and are in keeping with the highest tradition of the United States Navy."

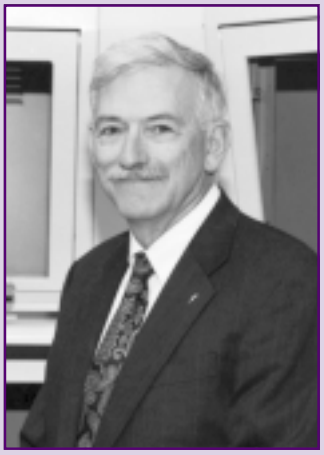

NAVY SUPERIOR CIVILIAN SERVICE AWARD

Dr. Frederick Williams — Chemistry Division

According to the award citation, Dr. Williams was noted "for his superior innovative leadership in serving the Navy, the Department of Defense, and the Nation as Director of Navy Technology Center for Safety and Survivability from June 1994 to March 1999. Dr. Williams developed experimental resources for fire research and development (R&D) that are unquestionably the finest in the Department of Defense; they have substantially improved the capabilities for protecting life and property from the ravages of fire. He created the Navy's damage control research ship, ex-USS *Shadwell* (LSD-15). Under his tireless guidance, this platform has evolved into a world unique research facility. His fleet-installed hardware innovations include new light-weight, low smoke electrical cable installation, a water mist suppression system that compensates for loss of halon firefighting agents, smoke ejection hardware, and fire resistant submarine hull insulation. Dr. Williams' leadership, professionalism, and total dedication to duty, reflect great credit upon himself, the Office of Naval Research, and NRL, and are in keeping with the highest traditions of the United States Navy."

THE TECHNICAL COOPERATION PROGRAM (TTCP) 1998 ACHIEVEMENT AWARD

Dr. Susan Numrich — Information Technology Division

The Technical Cooperation Program is an international consortium dedicated to fostering collaborative research efforts in defense science. The award was presented to Dr. Numrich by the Subcommittee on Non-Atomic Military Research and Development for her contributions toward TTCP collaboration in military distributed modeling and simulation. She was cited for her work on the Modeling and Simulation Technical Panel of the Joint Systems Analysis Group, specifically for making "a significant contribution to conducting international distributed simulation experiments and in developing a User Guide in Setting Up ModSAF International Links." By providing the information to set up cost-effective international links, this work enables the TTCP partners to utilize networked simulations in support of TTCP objectives."

Mr. Dom Panciarelli, Ms. Janice Schultz, Ms. Denise Stewart, Ms. Jennifer Burke, Ms. Donna McKinney, and Mr. Richard Thompson — NRL Public Affairs Office

1999 CHIEF INFORMATION (CHINFO) MERIT AWARD

NRL's *Labstracts* won 2nd place in the 1999 CHINFO Merit Awards Contest under the print media category as a military-funded newspaper. The congratulatory letter from RADM Thomas J. Jurkowsky, USN, Chief of Information, read, "The CHINFO Merit Award program honors excellence in Navy print and broadcast journalism. An aggressive internal relations program keeps our personnel and their families fully informed about the many issues, events, and policies that influence and affect their lives and careers. The superb quality, ingenuity, and originality of *Labstracts* and the attentiveness to your audience's needs were most praiseworthy. Your diligent, creative, and industrious craftmanship make your efforts a prominent part of your command's internal information program. Your winning entry reflects the highest standards of professional journalism excellence."

1999 FEDERAL LIBRARY TECHNICIAN OF THE YEAR

Ms. Rosette Risell — Technical Information Division

Ms. Risell was recognized for "routinely performing beyond the call of duty to maximize her contributions to the mission of the Naval Research Laboratory. Her contributions have significantly enhanced the library's ability to manage its entire procurement process. In 1999, she also assumed the duties of the vacant library management assistant position and participated in two special projects: to prepare an on-line catalog database for authority control processing and to identify and remove duplicate entries to ensure library users an accurate and concise database of library holdings."

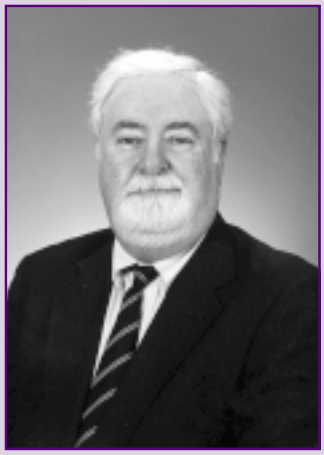

1999 E.O. HULBURT SCIENCE AWARD

Dr. Jack Davis — Plasma Physics Division

The E.O. Hulburt Science Award is the highest civilian honor awarded for scientific achievement by the Naval Research Laboratory. Dr. Davis was commended for "his significant contributions to the theoretical and numerical simulation studies of a wide range of phenomena related to Z-pinch plasmas, laser produced plasmas, radiation transport, and non-LTE emissivity models as well as theories and models applicable to problems involving fundamental atomic processes in dense plasmas. His contributions to these areas have resulted in profound changes in our understanding of laboratory and astrophysical plasmas."

NAVY MERITORIOUS CIVILIAN SERVICE AWARD

Dr. Bruce Gaber — Center for Bio/Molecular Science and Engineering

Dr. Gaber was recognized for achievements in both science and education. The citation read: "Dr. Bruce Gaber, through his extraordinary talent for creative scientific innovation, has contributed significantly to the worldwide recognition of NRL as a center of outstanding biomolecular science. Recognized in particular are his contributions in developing liposome encapsulated hemoglobin, the flow immunoassay, tools for bioinformatics, controlled release from mineral microstructures, and template-directed molecular imprinting. Dr. Gaber's commitment to education and the goals of equal opportunity is exemplified by the pioneering summer research internship program for promising minority college students. The reputation of NRL has been vitally enhanced in an increasingly important part of the world by Dr. Gaber's long-term research and liaison activities in India and the countries of the Pacific Rim."

NAVY MERITORIOUS CIVILIAN SERVICE AWARD

Dr. Graham Hubler — Materials Science and Technology Division

Dr. Hubler was recognized for "major contributions to the general area of ion beam interactions with matter, including the fields of low-energy nuclear physics, ion implantation metallurgy, ion-beam-assisted deposition of thin films, pulsed-laser deposition of thin films, and trace element accelerator mass spectrometry." Recognized for his 25-year career at NRL, Dr. Hubler has made many exceptional contributions. He is considered to be one of the world's experts on ion implantation metallurgy. The most recent application of his skills as an expert in ion beam technology is in the development of the accelerator mass spectrometer (AMS) capability at NRL.

NAVY MERITORIOUS CIVILIAN SERVICE AWARD

Dr. John Lee — Optical Sciences Division

Dr. Lee was cited "for his work on the U.S. Navy's Tactical Airborne Reconnaissance Pod-Completely Digital (TARPS-CD), the first all-digital reconnaissance system to be demonstrated by the Navy, which has highlighted the new capabilities, as well as the challenges of bringing into the Navy new digital technologies. He has successfully led the on-time development, and he worked with the Fleet to bring about as-sea demonstrations to ensure the technology would perform in real-world scenarios. Dr. Lee's work has resulted in a major new thrust area for the Optical Sciences Division and the Department of Defense."

NAVY MERITORIOUS CIVILIAN SERVICE AWARD

Mr. Dale Linne von Berg — Optical Sciences Division

Mr. Linne von Berg received the award "in recognition of his contributions in the development and Fleet insertion of the Navy Input Station (NAVIS) Real-time Imagery Display and Manipulation System." The award specifically cites Mr. Linne von Berg for his leadership role within the Navy in researching and addressing compression and ground station issues for tactical reconnaissance applications. His efforts in developing the NAVIS system have greatly enhanced the Navy's capability to rapidly receive, screen, and disseminate digital airborne reconnaissance imagery for exploitation and targeting applications. His work has been instrumental in defining the architecture and Concept of Operations (CONOPS) for Navy shipboard digital imagery reception and dissemination.

NAVY MERITORIOUS CIVILIAN SERVICE AWARD

Dr. James S. Murday — Chemistry Division

Dr. Murday received the award for "his leadership role as one of the most energetic, dedicated division superintendents" and for "his exceptional performance as a research physicist and technical manager." According to the citation, "he has provided dedicated leadership to the Chemistry Division, NRL, Navy, DoD, and national/international science organizations." The nomination also credits Dr. Murday for his contributions as chairperson of the NRL Library committee and accelerating "the conversion to a digital library making information available to many researchers at any location and any time of the day." He is internationally recognized for his involvement in the area of nanometer-scale science and technology.

NAVY MERITORIOUS CIVILIAN SERVICE AWARD

Dr. Dimitri Papaconstantopoulos — Materials Science and Technology Division

Dr. Papaconstantopoulos was acknowledged for "exceptional leadership and research accomplishments in the areas of electronic structure theory, including superconductivity, magnetism, X-ray spectroscopy, and parameterized computational methods. His leadership has contributed greatly to the high scientific prestige of the NRL Center for Computational Materials Science, which is regarded as one of the best computational materials science groups in the world. His personal research encompasses metals, semiconductors, and insulators. He is a pioneer in the development of tight binding Hamiltonians and has made breakthroughs in the areas that now form the basis for calculations of complex materials properties."

NAVY MERITORIOUS CIVILIAN SERVICE AWARD

Dr. Ranganathan Shashidhar — Center for Bio/Molecular Science and Engineering

Dr. Shashidhar was recognized for "his contributions to the fundamental understanding of advanced materials and the subsequent application of that understanding to the development of advanced displays and sensors for use by the Navy, DoD, and the Nation. In particular, his development of plastic-based liquid crystal (LC) displays, advanced alignment techniques for large-scale LC displays, and his recent work on the development of room temperature pyroelectric sensors have and will continue to make a difference to the Navy, DoD, and U.S. technological community." Advanced liquid crystal materials and displays are a major technology thrust area for the Navy and DoD because of their applications in hand-held displays, readable outdoor displays, and electronic maps and navigation.

LEGION OF MERIT AWARD

CAPT George Brown — Former Chief Staff Officer

CAPT Brown was presented with the Legion of Merit award for exceptionally meritorious conduct in the performance of outstanding service as Chief Staff Officer of NRL. CAPT Brown retired from the U.S. Navy on March 31, 2000 after 24 years of service. CAPT John P. Horsman, Jr., USN, is CAPT Brown's relief.

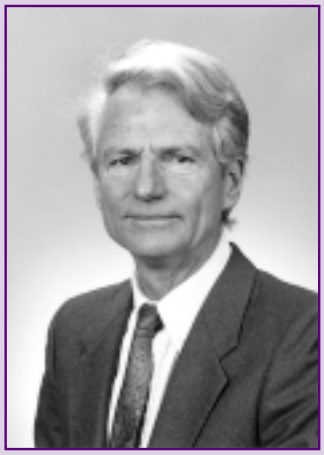

1999 COMMANDING OFFICER'S AWARD FOR ACHIEVEMENT IN THE FIELD OF EQUAL EMPLOYMENT OPPORTUNITY (EEO)

Dr. Edward Stone — Optical Sciences Division

Dr. Stone was recognized for "his outstanding contributions to the EEO Program through the excellence in his leadership skills, imagination, and accomplishments and his service to NRL's community outreach program as a partner school coordinator." In 1985, Dr. Stone became a science volunteer at Patricia Roberts Harris Educational Center, formerly Friendship Educational Center, one of NRL's partner schools in the District of Columbia. In his capacity, he has provided the school with support in the Young astronauts Club, the Library Computer Club, and the Future Engineers of the World. At the request of educators, Dr. Stone has led science and math activities during regular classes at Harris School. In addition, he served as a science judge, provided tours of NRL laboratories for school children, assisted the school faculty by providing materials and activities in science and math, and guided the delivery and set-up of NRL surplus computers.

COMMANDING OFFICER'S AWARD FOR EXCELLENCE IN SECRETARIAL SUPPORT

Ms. Carol Cline — Space Science Division

Ms. Cline was cited for "her outstanding performance and exceptional support of the Solar Terrestrial Branch. Her high level of professionalism and expertise have played a significant role in the success of the Branch's programs. Her considerable accomplishments are well known in the NRL community and in laboratories throughout the world that have collaborative programs with the Solar Terrestrial Relationships Branch." Branch Head Dr. George Doschek noted, "The uniform high quality of her work is consistently outstanding regardless of deadlines or the heavy amount of work." Ms. Cline's advanced computer knowledge frequently results in scientists in the Branch consulting with her as a knowledgeable and reliable source of computer information. Ms. Cline's support for numerous branch programs and activities, which involve outside sponsors, meetings, demonstrations, and travel have earned her the enthusiastic support of the scientists in the branch.

NRL AWARD FOR EXCELLENCE IN MISSION SUPPORT

Ms. Brenda L. Russell — Chemistry Division (retired)

This award is the highest NRL award for staff contributions to the accomplishment of NRL's mission. Ms. Russell was noted for her leadership, work ethic, and personality. The award citation reads, "For your exemplary service to the Department of the Navy, NRL, Chemistry Division, from January 1983 to September 1999. Your outstanding contributions to office automation led to 25% reduction in administrative office staff, an accomplishment made the more impressive by accommodating 25% growth in the division during 1997. Further, you have been an administrative cohesive force, training the ever-changing branch and division heads to be competent business managers, as well as mentoring the division secretaries. Your leadership, work ethic, and consummate cheerfulness have been a cornerstone upon which the Chemistry Division has built its accomplishments. Your dedicated efforts reflect great credit upon yourself, NRL, and the United States Navy."

NRL AWARD FOR EXCELLENCE IN MISSION SUPPORT

Mr. James Headley — Research and Development Services Division

This award is the highest NRL award for staff contributions to the accomplishment of NRL's mission. Mr. Headley was primarily cited for his outstanding service and unmatched dedication and commitment. The award citation states, "For your exemplary service to the Department of the Navy, Naval Research Laboratory (NRL), from October 1, 1992, to the present. Your outstanding contributions in the areas of utility and building operations, service call response, laboratory renovation projects, and customer satisfaction have allowed NRL to continue uninterrupted research operations and missions. Your efforts during utility failures, trouble alarms, and snow removal operations were completed largely during evenings, weekends, and non-working hours, as these are the times such emergencies regularly occur. You have without fail dedicated yourself to the Laboratory, its infrastructure, and its people. Your dedication efforts reflect great credit upon yourself, NRL, and the United States Navy."

THE *2000 NRL REVIEW* ARTICLE AWARDS

Awards for *NRL Review* articles recognize authors who submit outstanding research articles for this scientific publication. The articles are judged on the relevance of the work to the Navy and DoD, readability to the college-graduate level, clearness and conciseness of writing, and the effective use of graphics that are interesting and informative. The following awards were presented for articles that appeared in the *2000 NRL Review*.

FEATURED RESEARCH ARTICLE
"*Advanced Multifunction RF Systems*," Mr. Paul K. Hughes II, Mr. Joon Y. Choe, Mr. James B. Evins, Mr. James J. Alter, Dr. Joseph P. Lawrence III, Dr. David C. Wu, Mr. Gregory P. Hrin, Mr. William Habicht II, and Dr. Paul J. Matthews (Radar Division)

DIRECTORATE AWARDS FOR SCIENTIFIC ARTICLES
Systems Directorate: "*Fleet Demonstration of a Completely Digital Reconnaissance System, TARPS-CD*," Dr. John N. Lee, Dr. Melvin R. Kruer, and Mr. Dale C. Linne von Berg (Optical Sciences Division)

Materials Science and Component Technology Directorate: "*Computational Design of Molecular Magnets*," Mr. Mark R. Pederson (Materials Science and Technology Division)

Ocean and Atmospheric Science and Technology Directorate: "*An Aerophysical Study of the Eurasia Basin*," Mr. John M. Brozena (Marine Geosciences Division)

Naval Center for Space Technology: "*Windsat Antenna Development*," Ms. Wendy L. Lippincott and Dr. Peter Gaiser (Space Systems Development Department)

Ms. Wendy Lippincott, Mr. Paul Hughes II, Mr. Joon Choe, Mr. William Habicht II, Mr. Gregory Hrin, Dr. Paul Matthews, Dr. Timothy Coffey, Mr. James Evins, Mr. James Alter, Dr. Joseph Lawrence III, Mr. Mark Pederson, CAPT Douglas Rau, Dr. David Wu, and Dr. Peter Gaiser

ALAN BERMAN RESEARCH PUBLICATION AND EDISON PATENT AWARDS

The Annual Research Publication Awards Program was established in 1968 to recognize the authors of the best NRL publications each year. These awards not only honor individuals for superior scientific accomplishments in the field of naval research but also seek to promote continued excellence in research and in its documentation. In 1982, the name of this award was changed to the Alan Berman Research Publication Award in honor of its founder.

There were 344 separate publications submitted by the divisions in 2000 to be considered for recognition. Of those considered, 37 were selected. These selected publications represent 166 authors, each of whom received a publication awards certificate, a bronze paperweight, and a booklet listing the publications that were chosen for special recognition. In addition, NRL authors share in their respective division's monetary award.

The winning papers and their respective authors are listed below by their research units. Non-Laboratory coauthors are indicated by an asterisk.

NRL also recognizes patents as part of its annual publication awards program. The NRL Edison Patent Award was established in January 1991 to recognize NRL employees for outstanding patents issued to NRL by the U.S. Patent and Trademark Office during the preceding calendar year. The award recognizes significant NRL contributions to science and engineering as demonstrated by the patent process that are perceived to have the greatest potential benefit to the country. Of the 80 patents considered for 2000, 3 were selected, representing 8 inventors. They are listed under the NRL Edison Patent Awards.

Systems Directorate

Photonic Band Gap Structure and Transmissivity of Frequency-Dependent Metallic-Dielectric Systems
Michael J. Keskinen, Peter Loschialpo, Donald Forester, and John Schelleng

Radar Division

Design of a 5:1 Bandwidth Stripline Notch Array from FDTD Analysis
Mark Kragalott, William R. Pickles, and Michael Kluskens

Fast Converging Adaptive Detection of Doppler-Shifted Range Distributed Targets
Karl Gerlach and Michael Steiner

Information Technology Division

Asimovian Adaptive Agents
Diana F. Gordon

Algorithms for Bandwidth-Limited Energy-Efficient Wireless Broadcasting and Multicasting
Jeffrey E. Wieselthier, Gam D. Nguyen, and Anthony Ephremides

Optical Sciences Division

Real-Time Hyperspectral Detection and Cueing
Christopher M. Stellman, Geoffrey G. Hazel, Joseph V. Michalowicz, Frank Bucholtz, Alan Stocker, and William Schaaf

Single-Mode Operation of a Coiled Multimode Fiber Amplifier
Jeffrey P. Koplow, Lewis Goldberg, and Dahv A.V. Kliner

Tactical Electronic Warfare Division

Robust Tracking of Unknown PRI Sequences Using Kalman Filters Volume 1: Background and Theory
Melinda Hock, Edward N. Khoury, and Steven Peters

High Power Microwave Modeling Effort Using the Finite-Difference Time-Domain Method
Hung C. Ly

Materials Science and Component Technology Directorate

Hepta- and Octanitrocubanes
Richard Gilardi, Mao-Xi Zhang, and Phillip E. Eaton

Chemistry Division

Electronic Connection to the Interior of a Mesoporous Insulator with Nanowires of Crystalline RuO_2
Joseph V. Ryan, Alan Berry, Debra R. Rolison, Michele L.Anderson, Jeffrey W. Long, Veronica M. Cepak, Rhonda M. Stroud, Valerie M. Browning, and Celia I. Merzbacher

Multi-Criteria Fire Detection Systems Using a Probabilistic Neural Network
Susan L. Rose-Pehrsson, Ronald E. Shaffer, Frederick W. Williams, Sean J. Hart, Daniel T. Gottuk, Brooke D. Strehlen, and Scott A. Hill

Materials Science and Technology Division

Robust Electrical Spin Injection into a Semiconductor Heterostructure
Berend T. Jonker, Brian R. Bennett, Yun D. Park, Hai-Du Cheong, George Kioseoglou, and Athos Petrou

Calculation of Polarization Using a Density Functional Method with Localized Charge
Larry L. Boyer, Michael J. Mehl, and Harold T. Stokes

Laboratory for Computational Physics and Fluid Dynamics

Review of Propulsion Applications of Detonation Waves
Kazhikathra Kailasanath

Plasma Physics Division

Self-Pinched Transport of an Intense Proton Beam
Paul F. Ottinger, Stavros John Stephanakis, Jesse M. Neri, Bruce V. Weber, Matthew C. Myers, David D. Hinshelwood, David Mosher, Frank C. Young, David V. Rose, Craig L. Olson, and Dale R. Welch

Model of Enhanced Energy Deposition in a Z-Pinch Plasma
Alexander L. Velikovich, Jack Davis, J. Ward Thornhill, John L. Giuliani, Jr., Leonid I. Rudakov, and Chris Deeney

Electronics Science and Technology Division

Möbius Dual-Model Resonators and Bandpass Filters
Jeffrey M. Pond

Photoionization Spectroscopy of Traps in GaN Metal-Semiconductor Field-Effect Transistors
Paul B. Klein, Steven C. Binari, Jaime A. Freitas, Jr., and Alma E. Wickenden

Center for Bio/Molecular Science and Engineering

Catalytic Silica Particles via Template-Directed Molecular Imprinting
Michael A. Markowitz, Paul E. Schoen, Bruce P. Gaber, Paul R. Kust, Gang Deng, Jonathan S. Dordick, and Douglas S. Clark

Acetylcholine Stimulates Cortical Precursor Cell Proliferation in Vitro via Muscarinic Receptor Activation and MAP Kinase Phosphorylation
Wu Ma, Joanne D. Andreadis, Joseph J. Pancrazio, David A. Stenger, Dragan Maric, Bing-Sheng Li, Qian Hu, Lei Zhang, Qi-Ying Liu, Yoong H. Chang, Harish C. Pant, Jeffery L. Barker, Kara M. Shaffer, and Geraldine M. Grant

Acoustics Division

Collective Oscillations of Fresh and Salt Water Bubble Plumes
Gregory J. Orris and Michael Nicholas

A Time Domain Rough Surface Scattering Model Based on Wedge Diffraction: Application to Low-Frequency Backscattering from Two-Dimensional Sea Surfaces
Richard S. Keiffer and Jorge C. Novarini

Remote Sensing Division

The First Stellar Abundance Measurement in the Galactic Center: the M Supergiant IRS 7
John S. Carr, Kristen Sellgren, and Suchitra C. Balachandran

POAM III Measurements of Dehydration in the Antarctic Lower Stratosphere
Gerald E. Nedoluha, Richard M. Bevilacqua, Karl W. Hoppel, Mark Daehler, Eric P. Shettle, John S. Hornstein, Michael D. Fromm, Jerry D. Lumpe, and Joan E. Rosenfield

Oceanography Division

Impact of 1/8° to 1/64° Resolution on Gulf Stream Model-Data Comparisons in Basin-Scale Subtropical Atlantic Ocean Models
Harley E. Hurlburt and Patrick J. Hogan

Airborne Measurements of the Wavenumber Spectra of Ocean Surface Waves. Part I: Spectral Slope and Dimensionless Spectral Coefficient and Part II: Directional Distribution
Paul H. Hwang, David W. Wang, Edward J. Walsh, William B. Krabill, and Robert N. Swift

Marine Geosciences Division

The Role of Biologically Enhanced Pore Water Transport in Early Diagenesis: An Example from Carbonate Sediments in the Vicinity of North Key Harbor, Dry Tortugas National Park, Florida
Yoko Furukawa, Dawn L. Lavoie, Samuel J. Bentley, Alan M. Shiller, and Philippe Van Cappellen

Acoustic Imagery Evidence for Methane Hydrates in the Ulleung Basin
Joan M. Gardner, Woo-Yeol Jung, and Alexander N. Shor

Marine Meteorology Division

NAVDAS Source Book 2000 NRL Atmospheric Variational Data Assimilation System
Edward H. Barker and Roger Daley

Observation and Background Adjoint Sensitivity in the Adaptive Observation-Targeting Problem
Nancy L. Baker and Roger Daley

Space Science Division

USA Experiment and RXTE Observations of a Variable Low-Frequency Quasi-Periodic Oscillation in XTE J1118+480
Kent S. Wood, Paul S. Ray, Michael T. Wolff, Gilbert Fritz, Michael P. Kowalski, Michael N. Lovellette, Daryl Yentis, Reba M. Bandyopadhyay, Paul Hertz, Jeffrey Scargle, Edward D. Bloom, Berrie Giebels, Gary Godfrey, Kaice Reilly, Pablo Saz-Parkinson, and Gayane Shabad

O^+, and O_2 Densities Derived from Measurements Made by the High Resolution Airglow/Aurora Spectrograph (HIRAAS) Sounding Rocket Experiment
Kenneth F. Dymond, Stefan E. Thonnard, Scott A. Budzien, Robert P. McCoy, Terrence N. Bullett, Ronald J. Thomas, and Eric J. Bucsela

Space Systems Development Department

Design and Test of an Algorithm for Satellite-to-Satellite Time Transfer
Dolan E. Highsmith, Patrick W. Binning, and Penina Axelrad

Orbit Determination Using Space to Ground Differential GPS in NRL's OCEAN Package
Patrick W. Binning, Mark T. Soyka, and Jay W. Middour

Spacecraft Engineering Department

The Main Problem in Satellite Theory Revisited
Liam M. Healy

Modal Filters and Neutral Networks for Adaptive Vibration Control
Albert B. Bosse, Tae W. Lim, and Stuart Shelley

NRL Edison (Patent) Awards

Fiber Optic Sensor Array System with Forward Coupled Topology
Alan D. Kersey, Anthony Dandridge, and Charles J. Stockstill

Modulating Retroreflector Using Multiple Quantum Well Technology
G. Charmaine Gilbreath, Steven R. Bowman,William S. Rabinovich, Charles Merk, H. Edward Senasack, and Amy L. Ressing

MMIC Receiver
Leo W. Lemley and Edward F. Miles

NLR Programs for Professional Development

PROGRAMS FOR NRL EMPLOYEES

The Human Resources Office, Personnel Operations Branch, continues to support and provide traditional and alternative methods of training for employees. During 2000, NRL employees were encouraged to develop their skills by attending training to enhance their job performance in order to continue to meet the future needs of NRL as well as their own goals for growth.

One common study procedure is for employees to work full time at the Laboratory while taking job-related scientific courses at universities and schools in the Washington area. The training ranges from a single course to full graduate and postgraduate programs. Tuition for training is paid by NRL. The formal programs offered by NRL are described here.

GRADUATE PROGRAMS

• The **Advanced Graduate Research Program** (formerly the Sabbatical Study Program, which began in 1964) enables selected professional employees to devote full time to research or pursue work in their own or a related field for 1 year at an institution or research facility of their choice without the loss of regular salary, leave, or fringe benefits. NRL pays all educational costs, travel, and moving expenses for the employee and dependents. Criteria for eligibility include professional stature consistent with the applicant's opportunities and experience, a satisfactory program of study, and acceptance by the facility selected by the applicant. The program is open to paraprofessional employees (and above) who have completed 6 years of Federal Service, 4 of which have been at NRL.

• The **Edison Memorial Graduate Training Program** enables employees to pursue advanced studies in their fields at local universities. Participants in this program work 24 hours each workweek and pursue their studies during the other 16 hours. The criteria for eligibility include a minimum of 1 year of service at NRL, a bachelor's or master's degree in an appropriate field, and professional standing in keeping with the candidate's opportunities and experience.

• To be eligible for the **Select Graduate Training Program**, employees must have a college degree in an appropriate field and must have demonstrated ability and aptitude for advanced training. Students accepted into this program devote a full academic year to graduate study. While attending school, they receive one-half of their salary, and NRL pays for tuition and laboratory expenses.

• The **Naval Postgraduate School** (NPS), located in Monterey, California, provides graduate programs to enhance the technical preparation of Naval officers and civilian employees who serve the Navy in the fields of science, engineering, operations analysis, and management. It awards a master of arts degree in national security affairs and a master of science degree in many technical disciplines.

NRL employees desiring to pursue graduate studies at NPS may apply for a maximum of six quarters away from NRL, with thesis work accomplished at NRL. Specific programs are described in the NPS catalog. Participants will continue to receive full pay and benefits during the period of study.

• In addition to NRL and university offerings, application may be made to a number of noteworthy programs and fellowships. Examples of such opportunities are the **Capitol Hill Workshops**, the **Legislative Fellowship (LEGIS) program**, the **Federal**

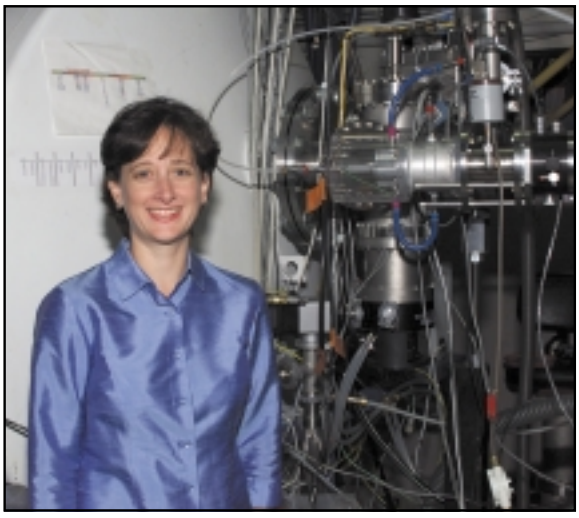

Ms. Sarah McDonald, of the Space Science Division, participated in the Edison Memorial Graduate Training Program at George Mason University in Fairfax, Virginia.

Executive Institute (FEI), the **Fellowship in Congressional Operations**, and the **Women's Executive Leadership Program**. These and other programs are announced from time to time, as schedules are published.

• Research conducted at NRL may be used as **thesis material for an advanced degree**. This original research is supervised by a qualified employee of NRL who is approved by the graduate school. The candidate should have completed the required course work and should have satisfied the language, residence, and other requirements of the graduate school from which the degree is sought. NRL provides space, research facilities, and supervision but leaves decisions on academic policy to the cooperating schools.

CONTINUING EDUCATION

• Local colleges and universities offer **undergraduate and graduate courses** at NRL for employees interested in improving their skills and keeping abreast of current developments in their fields. These courses are also available at many other DoD installations in the Washington, D.C. area.

• The Staffing, Classification, and Training Branch at NRL offers **short courses** to all employees in a number of fields of interest including technical subjects, computer operation, supervisory and management techniques, and clerical/secretarial skills. Laboratory employees may attend these courses at nongovernment facilities as well. Interagency courses in management, personnel, finance, supervisory development, and clerical skills are also available.

For further information on any of the above programs, contact the Staffing, Classification, and Training Branch (Code 1810) at (202) 767-8313.

• The **Scientist-to-Sea Program** (STSP) provides increased opportunities for Navy R&D laboratory/center personnel to go to sea to gain firsthand insight into operational factors affecting system design, performance, and operations on a variety of ships. NRL is a participant of this NSAP-ONR program.

For further information on these and other Technology Base Programs, including BMD, SBIR, and critical technology, contact Dr. Stephen Sacks, Code 5006, at (202) 767-3666.

PROFESSIONAL DEVELOPMENT

NRL has several programs, professional society chapters, and informal clubs that enhance the professional growth of employees. Some of these are listed below.

Dr. James Yesinowski, of the Chemistry Division, participated in the Advanced Graduate Research Program at the National Institutes of Health (NIH) in Bethesda, Maryland.

• **The Counseling Referral Service** (C/RS) helps employees to achieve optimal job performance through counseling and resolution of problems such as family, stress and anxiety, behavioral, emotional, and alcohol- or drug-related problems that may adversely impact job performance.

C/RS provides confidential assessments and short-term counseling, training workshops, and referrals to additional resources in the community. (Contact Dr. Ralph Surette at (202) 767-6857.)

• A chartered chapter of **Women in Science and Engineering** (WISE) was established at NRL in 1983. In 1997, the NRL WISE Chapter and the NRL Women in Science and Technology Network merged to form the NRL WISE Network. The goals of the organization are to encourage and promote the professional growth of women in science and engineering. Informal luncheons and seminars are scheduled to discuss scientific research areas, career opportunities, and career-building strategies, and to brainstorm solutions to problems encountered by women in science and engineering. WISE also sponsors a colloquium series that features outstanding women scientists. (Contact Dr. Joan E. Yater at (202) 404-4494, Dr. Azar Nazeri at (202) 404-6803, or Dr. Kristl Hathaway at (202) 767-4289.)

• **Sigma Xi**, the scientific research society, encourages and acknowledges original investigation in pure and applied science. As an honor society for research scientists, individuals who have demonstrated the ability to perform original research are elected to

membership in local chapters. The NRL Edison Chapter, comprising approximately 400 members, recognizes original research by presenting awards annually in pure and applied science to outstanding NRL staff members. The chapter also sponsors lectures at NRL on a wide range of scientific topics for the entire NRL community. These lectures are delivered by scientists from all over the nation and the world. The highlight of the Sigma Xi lecture series is the Edison Memorial Lecture, traditionally featuring a distinguished scientist. (Contact Dr. J. Selinger at (202) 404-6040 or Dr. M. Pederson at (202) 767-6577.)

• The **NRL Mentor Program** was established to provide an innovative approach to professional and career training and an environment for personal and professional growth. It is open to permanent NRL employees in all job series and at all sites. Mentorees are matched with successful, experienced colleagues with more technical and/or managerial experience who can provide them with the knowledge and skills needed to maximize their contribution to the success of their immediate organization, to NRL, to the Navy, and to their chosen career fields. The ultimate goal of the program is to increase job productivity, creativity, and satisfaction through better communication, understanding, and training. NRL Instruction 12400.1 established the NRL Mentor Program, and it provides the policy and procedures for the program. (Contact Ms. Dawn Brown at (202) 767-2957.)

• The Charlotte Moore-Sitterly Chapter of **Federally Employed Women, Inc.** (FEW) was chartered at NRL in 1993. FEW is an international organization of federally employed women and men whose purpose is to eliminate sex discrimination and sexual harassment and enhance career opportunities for women in government. FEW works closely with other Federal agencies and organizations, including the Office of Personnel Management, Equal Employment Opportunity Commission, and Federal Women's Program subcommittees. (Contact Dr. Virginia Degiorgi at (202) 767-9027.)

• Employees interested in developing effective self-expression, listening, thinking, and leadership potential are invited to join either of two NRL chapters of **Toastmasters International**. Members of these clubs, who possess diverse career backgrounds and talents, meet two to four times a month in an effort to learn to communicate not by rules but by practice in an atmosphere of understanding and helpful fellowship. NRL's Commanding Officer and Director of Research endorse Toastmasters as an official training medium at NRL. (Contact Kathleen Parrish at (202) 767-2782 for more information.)

EQUAL EMPLOYMENT OPPORTUNITY (EEO) PROGRAMS

Equal employment opportunity is a fundamental NRL policy for all employees regardless of race, color, national origin, sex, religion, age, or physical/mental handicap. The NRL EEO Office is a service organization whose major functions include counseling employees in an effort to resolve employee/management conflicts, processing formal discrimination complaints, providing EEO training, and recruiting for affirmative employment candidates. The NRL EEO Office is also responsible for sponsoring special-emphasis programs to promote awareness and increase sensitivity and appreciation of the issues or the history relating to: females; individuals with disabilities; Hispanic Americans; African Americans; and individuals of American Indian/Alaskan-Native and Asian-American/Pacific Islander descent. (Contact the NRL Deputy EEO Officer at (202) 767-5264 for additional information on any of our programs or services.)

OTHER ACTIVITIES

• The **Community Outreach Program** traditionally has used its extensive resources to foster programs that provide benefits to students and other community citizens. Volunteer employees assist with and judge science fairs, give lectures, tutor, mentor, coach, and serve as classroom resource teachers. The program also sponsors African American History Month art and essay contests for local schools, student tours of NRL, a student Toastmasters Youth Leadership Program, an annual holiday party for neighborhood children, and other programs that support the local community. Also through this program, NRL has active partnerships with four District of Columbia, three Aberdeen, Maryland, and three Calvert County, Maryland, public schools. (Contact Mr. Dom Panciarelli at (202) 767-2541.)

• Other programs that enhance the development of NRL employees include four computer user groups (**IBM PC**, **Mac**, **NeXT**, and **Sun**) and the **Amateur Radio Club**. The **Recreation Club** encourages wide interest in sports for employees with its many facilities and programs, such as a heated indoor pool; basketball and volleyball court; weight room; table tennis; hot tub and sauna; five martial arts disciplines; aerobics classes; swimming lessons; water walking and exercise; and softball and basketball leagues. Sportswear, NRL paraphernalia, discount tickets to

The Lisby-Hillsdale students take a break for a photo opportunity in front of NRL's Interim Control Module (ICM).

amusement parks, and film-developing services are available at the Rec Club office. The **Showboaters** (25 years, 1999) is a nonprofit drama group that presents live theater for the enjoyment of NRL and the community. Traditionally, the NRL Showboaters perform two major productions each year in addition to occasional performances at Laboratory functions and benefits for local charities. Although based at NRL, membership is not limited to NRL employees. Because of auditorium renovations, performances have been temporarily suspended. (Contact Ms. Barbarajo Cox at (202) 404-4998.)

PROGRAMS FOR NON-NRL EMPLOYEES

Several programs have been established for non-NRL professionals. These programs encourage and support the participation of visiting scientists and engineers in research of interest to the Laboratory. Some of the programs may serve as stepping-stones to federal careers in science and technology. Their objective is to enhance the quality of the Laboratory's research activities through working associations and interchanges with highly capable scientists and engineers and to provide opportunities for outside scientists and engineers to work in the Navy laboratory environment. Along with enhancing the Laboratory's research, these programs acquaint participants with Navy capabilities and concerns.

RECENT PH.D., FACULTY MEMBER, AND COLLEGE GRADUATE PROGRAMS

• The **National Research Council (NRC) Cooperative Research Associateship Program** selects associates who conduct research at NRL in their chosen fields in collaboration with NRL scientists and engineers. The tenure period is 2 years (renewable for a possible third year).

• The **Office of Naval Research (ONR) Postdoctoral Fellowship Program**, administered by the American Society for Engineering Education (ASEE), aims to increase the involvement of highly trained scientists and engineers in disciplines necessary to meet the evolving needs of naval technology. Appointments are for 1 year (renewable for a second and possible third year).

• The **Consortium for Oceanographic Research Education (CORE) Postdoctoral Fellowship Program** is administered in much the same manner as the above two programs. However, this program is focused on selecting associates with advanced degrees in the oceanic and atmospheric environmental sciences. The purpose of this program is to recruit scientists and engineers in these specialized areas.

• The American Society for Engineering Education also administers the **Navy/ASEE Summer Faculty Research and Sabbatical Leave Program** for university faculty members to work for 10 weeks (or longer, for those eligible for sabbatical leave) with professional peers in participating Navy laboratories on research of mutual interest.

• The **NRL/United States Naval Academy (USNA) Cooperative Program for Scientific Interchange** allows faculty members of the U.S. Naval Academy to participate in NRL research. This collaboration benefits the Academy by providing the opportunity for USNA faculty members to work on research of a more practical or applied nature. In turn, NRL's research program is strengthened by the available scientific and engineering expertise of the USNA faculty.

• The **National Defense Science and Engineering Graduate Fellowship Program** helps U.S. citizens obtain advanced training in disciplines of science and engineering critical to the U.S. Navy. The 3-year program awards fellowships to recent outstanding graduates to support their study and research leading to doctoral degrees in specified disciplines such as electrical engineering, computer sciences, material sciences, applied physics, and ocean engineering. Award recipients are encouraged to continue their study and research in a Navy laboratory during the summer.

For further information about the above six programs, contact Ms. Lesley Renfro at (202) 404-7450.

PROFESSIONAL APPOINTMENTS

• **Faculty Member Appointments** use the special skills and abilities of faculty members for short periods to fill positions of a scientific, engineering, professional, or analytical nature.

• **Consultants and experts** are employed because they are outstanding in their fields of specialization or because they possess ability of a rare nature and could not normally be employed as regular civil servants.

• **Intergovernmental Personnel Act Appointments** temporarily assign personnel from state or local governments or educational institutions to

the Federal Government (or vice versa) to improve public services rendered by all levels of government.

STUDENT PROGRAMS

The student programs are tailored to the undergraduate and graduate students to provide employment opportunities and work experience in naval research. These programs are designed to attract applicants for student and full professional employment in fields such as engineering, physics, mathematics, and computer sciences. The student employment programs are designed to help students and educational institutions gain a better understanding of NRL's research, its challenges, and its opportunities. Employment programs for college students include the following:

• The **Student Career Experience Program** (formerly known as Cooperative Education Program) employs students in study-related occupations. The program is conducted in accordance with a planned schedule and a working agreement among NRL, the educational institution, and the student. Primary focus is on the pursuit of bachelors degrees in engineering, computer science, or the physical sciences.

• The **Student Temporary Employment Program (STEP)** enables students to earn a salary while continuing their studies and offers them valuable work experience.

• The **Summer Employment Program** employs students for the summer in paraprofessional and technician positions in engineering, physical sciences, computer sciences, and mathematics.

• The **Student Volunteer Program** helps students gain valuable experience by allowing them to voluntarily perform educationally related work at NRL.

For additional information on these undergraduate and graduate college student programs, contact Code 1810 at (202) 767-8313.

HIGH SCHOOL PROGRAMS

• **The DoD Science & Engineering Apprentice Program (SEAP)** employs high school juniors, seniors, and college students to serve for 8 weeks as junior research associates. The college students must have participated in SEAP during high school. Under the direction of a mentor, students gain a better understanding of research, its challenges, and its opportunities through participation in scientific programs. Criteria for eligibility are based on science and mathematics courses completed and grades achieved; scientific motivation, curiosity, and capacity for sustained hard work; a desire for a technical career; teacher recommendations; and achievement test scores. The NRL Program is the lead program and the largest in DoD.

For additional information, contact Dawn Brown (Code 1850) at (202) 767-2957.

NRL

General Information

TECHNICAL OUTPUT

The Navy continues to be a pioneer in initiating new developments and a leader in applying these advancements to military requirements. The primary method of informing the scientific and engineering community of the advances made at NRL is through the Laboratory's technical output—reports, articles in scientific journals, contributions to books, papers presented to scientific societies and topical conferences, patents, and inventions.

The figures for calendar year 2000 presented below represent the output of NRL facilities in Washington, D.C.; Bay St. Louis, Mississippi; and Monterey, California.

In addition to the output listed, NRL scientists made more than 1257 oral presentations during 2000.

Type of Contribution	Unclassified	Classified	Total
Articles in periodicals, chapters in books, and papers in published proceedings	1014	9	1023
NRL Formal Reports	20	10	30
NRL Memorandum Reports	94	7	101
Books	0	0	0
Patents granted			80
Statutory Invention Registrations (SIRs)			3

*This is a provisional total based on information available to the Ruth H. Hooker Research Library and Technical Information Center on January 25, 2001. Additional publications carrying a 2000 publication date are anticipated.

TECHNOLOGY TRANSFER AT NRL

NRL is committed to transitioning the technologies it develops into products or services for military or civilian use. Many of NRL's technologies have commercial applications in addition to the defense-oriented objectives for which they were originally developed. NRL developments in areas such as radar, radio, satellite navigation, fiber optics, chemical and biological sensors, and a wide variety of materials and coatings have made significant contributions to the safety and welfare of the military and civilian communities.

An example of an important NRL technology transfer to the operational Navy is the nonskid coating formulations developed by Dr. Robert Brady and Mr. Larry Kraft of NRL's Chemistry Division. The patent covering these formulations was awarded the 1999 Vice Admiral Harold G. Bowen Award. This award is given annually to a patented invention that has been of the greatest benefit to the Navy. The NRL nonskid coatings have improved safety for the sailors aboard Navy ships and have reduced maintenance costs.

The transitioning of NRL's dual-use technologies to the private sector is facilitated by NRL's Technology Transfer Office. This office implements the Technology Transfer Act by which Congress authorized Federal Laboratories such as NRL to participate in Cooperative Research and Development Agreements (CRADAs) and patent licensing agreements. NRL has entered into more than 250 CRADAs with industry, universities, nonprofit organizations, and other government organizations. In addition, NRL has executed more than 40 licenses to its inventions.

Entering into a CRADA is an excellent way for U.S. companies to gain access to commercially important NRL research and development capabilities. As the Navy's corporate laboratory, NRL draws on the powerful resources of an interdisciplinary combination of scientific expertise and modern facilities. NRL's technical staff is recruited from all disciplines of engineering and the physical sciences and is available to work with private companies to solve technical problems in any area of research that is consistent with NRL's mission.

During FY 00, NRL signed CRADAs with small and large companies as well as with universities. In some cases, NRL is working under a CRADA to transition technology that has been licensed to the CRADA partner or is under negotiation for license. In other cases, NRL is contributing expertise in the development of new technology for commercial use or to benefit the civilian community.

For example, the Materials Science and Technology Division is collaborating under a CRADA with Nanosphere, Inc., to adapt NRL's surface acoustic wave sensors for application in monitoring patients for compliance with prescription drug dosage instructions. These sensors, incorporated into a breath analysis device, use chemoselective polymers to detect specific pharmaceuticals or odorant taggants.

Under the scope of another CRADA, Cessna Aircraft Company is working with NRL on a project directed at the design of quieter aircraft interiors. NRL is using its near acoustic holography method to develop a structural acoustic model of a Cessna aircraft interior. The design guidance enabled with this NRL tool is aimed at a next generation of quieter business jets.

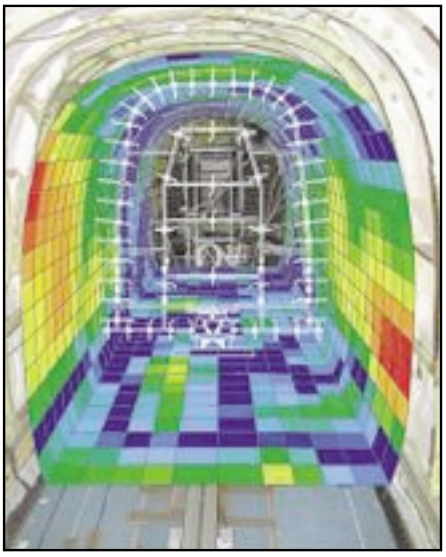

Under a CRADA with Cessna Aircraft Company, nearfield acoustical holography has been combined with boundary element methods to model airplane fuselage vibration. In this reconstruction, highest vibration levels are observed on the wall in front of the propellers and on the floor in front of the wing support.

NRL supports an active licensing program and has more than 500 patents available for licensing in fields as diverse as advanced materials, chemistry, biotechnology, optics, ocean and atmospheric sciences, electronics, radar, and satellite technology. A license to a Navy invention authorizes the licensee to manufacture and sell a product based on NRL's technology in exchange for royalty payments that are shared by the Laboratory and the inventors. In FY 00 NRL licensed phthalonitrile resin compositions for use in composite structures in the aerospace, marine, and transportation industries; an optical fiber amplifier for optical communications, test, and measurement instrumentation and lasers; and routing software for use in wireless communication networks.

For additional information, contact NRL's Technology Transfer Office, Code 1004, 4555 Overlook Avenue, S.W., Washington, D.C. 20375-5320, or call (202)767-7230; e-mail: techtransfer@nrl.navy.mil; URL: http://labwide14/techtransfer.

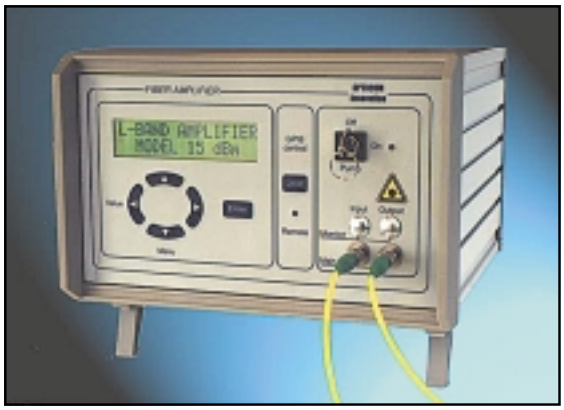

The high-power erbium-doped fiber amplifier shown here is manufactured and sold worldwide by OptoCom Innovation under license from NRL.

KEY PERSONNEL

Area Code (202) unless otherwise listed
Personnel Locator - 767-3200
DSN-297 or 754

Code	Office		Phone Number
	EXECUTIVE DIRECTORATE		
1000	Commanding Officer	CAPT D.H. Rau, USN	767-3403
1000.1	Inspector General	CAPT J.P. Horsman, Jr., USN	767-3621
1001	Director of Research	Dr. T. Coffey	767-3301
1001.1	Executive Assistant	Mr. D. DeYoung	767-2445
1002	Chief Staff Officer	CAPT J.P. Horsman, Jr., USN	767-3621
1004	Head, Technology Transfer	Dr. C. Cotell	404-8411
1006	Head, Office of Program Administration and Policy Development	Ms. L. McDonald	767-3091
1008	Office of Counsel	Mr. J. McCutcheon	767-2244
1030	Public Affairs Officer	Mr. R. Thompson (Acting)	767-2541
1200	Head, Command Support Division	CAPT J.P. Horsman, USN	767-3621
1220	Head, Security	Dr. J.T. Miller	767-0793
1240	Head, Safety Branch	Mr. J.S. Burns	767-2232
1400	Head, Military Support Division	CDR R.B. Grimm, USN	767-2272
1600	Officer-in-Charge, Flight Support Detachment	CDR T.M. Munns, USN	301-342-3751
1800	Director, Human Resources Office	Ms. B.A. Duffield	767-3421
1830	Deputy EEO Officer	Ms. D. Erwin	767-5264
3204	Deputy for Small Business	Ms. M. Nicholl	767-6263
	BUSINESS OPERATIONS DIRECTORATE		
3000	Associate Director of Research	Mr. D. Therning	767-2371
3200	Head, Contracting Division	Mr. J.C. Ely	767-5227
3300	Comptroller, Financial Management Division	Mr. S.A. Birk	767-3405
3400	Supply Officer	Ms. C. Hartman	767-3446
3500	Director, Research and Development Services Division	Mr. S. Harrison	767-3697
	SYSTEMS DIRECTORATE		
5000	Associate Director of Research	Dr. R.A. LeFande	767-3324
5200	Head, Technical Information Division	Mr. J. Lucas (Acting)	767-2187
5300	Superintendent, Radar Division	Dr. P.K. Hughes II (Acting)	404-2700
5500	Superintendent, Information Technology Division	Dr. R.P. Shumaker	767-2903
5600	Superintendent, Optical Sciences Division	Dr. T.G. Giallorenzi	767-3171
5700	Superintendent, Tactical Electronic Warfare Division	Dr. J.A. Montgomery	767-6278
	MATERIALS SCIENCE AND COMPONENT TECHNOLOGY DIRECTORATE		
6000	Associate Director of Research	Dr. B.B. Rath	767-3566
6030	Head, Laboratory for Structure of Matter	Dr. J. Karle	767-2665
6100	Superintendent, Chemistry Division	Dr. J.S. Murday	767-3026
6300	Superintendent, Materials Science & Technology Division	Dr. D.U. Gubser	767-2926
6400	Director, Lab. for Computational Physics and Fluid Dynamics	Dr. J.P. Boris	767-3055
6700	Superintendent, Plasma Physics Division	Dr. S. Ossakow	767-2723
6800	Superintendent, Electronics Science & Technology Division	Dr. G.M. Borsuk	767-3525
6900	Director, Center for Bio/Molecular Science and Engineering	Dr. J.M. Schnur	404-6000
	OCEAN AND ATMOSPHERIC SCIENCE AND TECHNOLOGY DIRECTORATE		
7000	Associate Director of Research	Dr. E.O. Hartwig	404-8690
7100	Superintendent, Acoustics Division	Dr. E.R. Franchi	767-3482
7200	Superintendent, Remote Sensing Division	Dr. P. Schwartz	767-3391
7300	Superintendent, Oceanography Division	Dr. W.J. Jobst	228-688-4670
7400	Superintendent, Marine Geosciences Division	Dr. H.C. Eppert, Jr.	228-688-4650
7500	Superintendent, Marine Meteorology Division	Dr. P.E. Merilees	831-656-4721
7600	Superintendent, Space Science Division	Dr. H. Gursky	767-6343
	NAVAL CENTER FOR SPACE TECHNOLOGY		
8000	Director	Mr. P.G. Wilhelm	767-6547
8100	Superintendent, Space Systems Development Department	Mr. R.E. Eisenhauer	767-0410
8200	Superintendent, Spacecraft Engineering Department	Mr. H.E. Senasack, Jr.	767-6411

EMPLOYMENT OPPORTUNITIES FOR ENTRY-LEVEL AND EXPERIENCED PERSONNEL

The *NRL Review* illustrates some of the exciting science and engineering carried out at the Naval Research Laboratory, as well as the potential for new personnel. In this regard, NRL offers a wide variety of challenging positions that involve the full range of work, from basic and applied research to equipment development. The nature of the research and development conducted at NRL requires professionals with experience. Typically there is a continuing need for electronics, mechanical, aerospace, ceramic and materials engineers, metallurgists, computer scientists, and oceanographers with bachelor's and/or advanced degrees and physical and computer scientists with Ph.D. degrees. Opportunities exist in the areas described below:

Ceramic Engineers and Materials Scientists/ Engineers. These employees are recruited to work on materials, microstructure characterization, electronic ceramics, solid-state physics, fiber optics, electro-optics, microelectronics, fracture mechanics, vacuum science, laser physics technology, and radio frequency/microwave/millimeter wave/infrared technology.

Electronics Engineers and Computer Scientists. These employees may work in the areas of communications systems, electromagnetic scattering, electronics instrumentation, electronic warfare systems, radio frequency/microwave/millimeter wave/ infrared technology, radar systems, laser physics technology, radio-wave propagation, electron device technology, spacecraft design, artificial intelligence, information processing, signal processing, plasma physics, vacuum science, microelectronics, electro-optics, fiber optics, solid state, software engineering, computer design/architecture, ocean acoustics, stress analysis, and expert systems.

Mechanical Engineers. These employees may be assigned to spacecraft design, remote sensing, propulsion, experimental fluid mechanics, experimental structural mechanics, solid mechanics, elastic/plastic fracture mechanics, materials, finite-element methods, nondestructive evaluation, characterization of fracture resistance of structural alloys, combustion, and CAD/CAM.

Chemists. Chemists are recruited to work in the areas of combustion, polymer science, bioengineering and molecular engineering, surface science, materials, fiber optics, electro-optics, microelectronics, electron-device technology, and laser physics.

Physicists. Physics graduates may concentrate on such fields as materials, solid-state physics, fiber optics, electro-optics, microelectronics, vacuum science, plasma physics, fluid mechanics, signal processing, ocean acoustics, information processing, artificial intelligence, electron-device technology, radio-wave propagation, laser physics, ultraviolet/X-ray/gamma-ray technology, electronic warfare, electromagnetic interaction, communications systems, radio frequency/microwave/millimeter wave/infrared technology, and computa-tional physics.

Oceanographers, Meteorologists, and Marine Geophysicists. These employees work in the areas of ocean dynamics, air-sea interaction, upper-ocean dynamics, oceanographic bio-optical modeling, oceanic and atmospheric numerical modeling and prediction, artificial intelligence applications for satellite analyses, benthic processes, aerogeophysics, marine sedimentary processes, and advanced mapping techniques. Oceanographers and marine geophysicists are located in Washington, D.C., and the Stennis Space Center, Bay St. Louis, Mississippi. Meteorologists are located in Washington, D.C., and Monterey, California.

APPLICATION AND INFORMATION

Interested applicants should submit an Application for Federal Employment (SF-171), an Optional Application for Federal Employment (OF-612), or a resume. The OF-612 and SF-171 can be obtained from local Office of Personnel Management and Human Resource Offices of federal agencies.

Direct inquiries to:

Naval Research Laboratory
Human Resources Office, Code 1810 RV
Washington, DC 20375-5324
(202) 767-3030

LOCATION OF NRL IN THE CAPITAL AREA

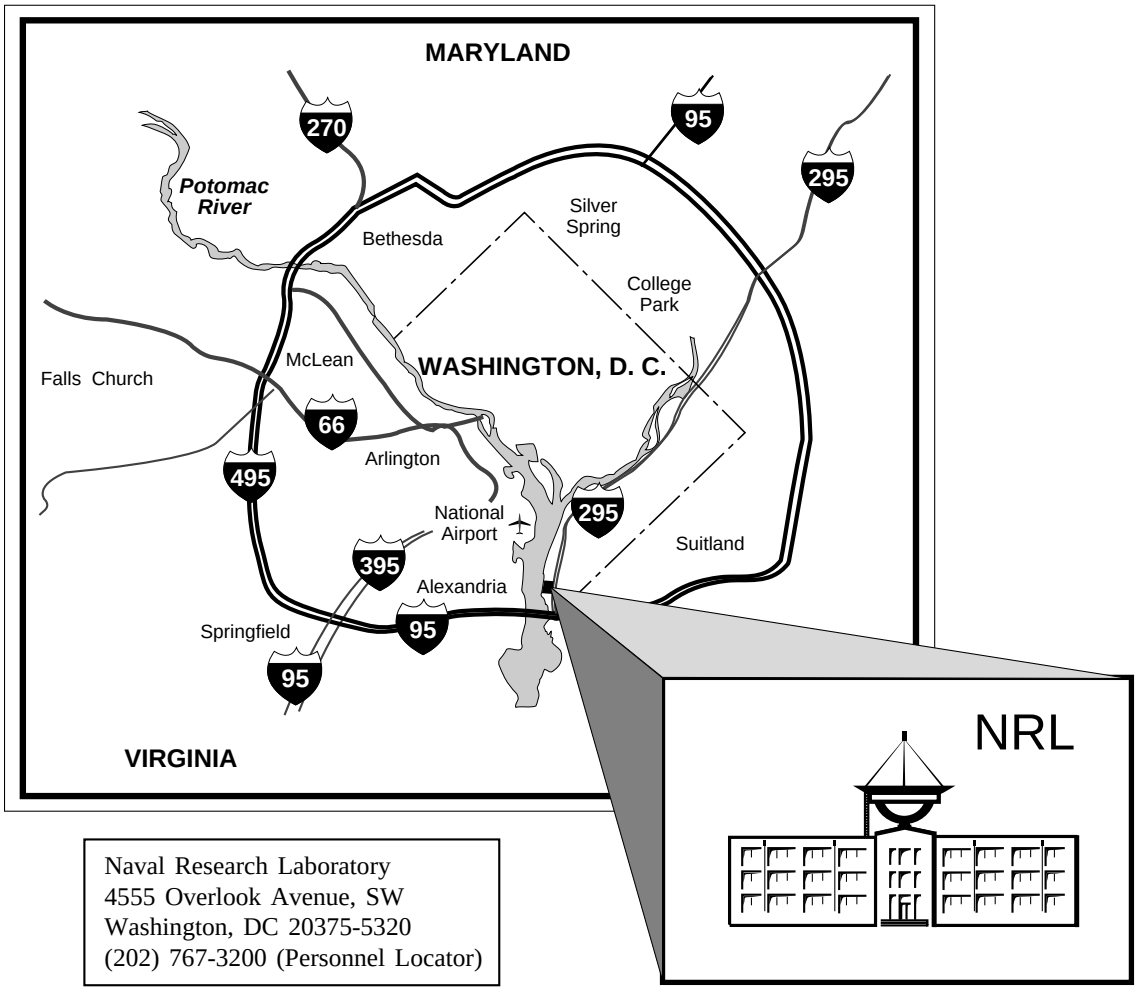

Naval Research Laboratory
4555 Overlook Avenue, SW
Washington, DC 20375-5320
(202) 767-3200 (Personnel Locator)

CONTRIBUTIONS BY DIVISIONS, LABORATORIES, AND DEPARTMENTS

Materials Science and Technology Division

Laboratory for Computational Physics and Fluid Dynamics

Plasma Physics Division

Electronics Science and Technology Division

Center for Bio/Molecular Science and Engineering

Acoustics Division

SUBJECT INDEX

AUTHOR INDEX

General information on the research described in this *NRL Review* can be obtained from the Public Affairs Office, Code 1030, (202) 767-2541. Information concerning Technology Transfer is available from Dr. Catherine Cotell, head of the Technology Transfer Office, Code 1004, (202) 767-7230. Sources of information on the various educational programs at NRL are listed in the chapter entitled "Programs for Professional Development."

For additional information about NRL, the *Fact Book* lists the organization, key personnel, and major facilities for each division. It contains information about Laboratory funding, programs, and field sites. The *Fact Book* can be obtained from the Technical Information Division, Publications Services Section, Code 5211, (202) 767-2782.

Quick Reference Telephone Numbers

	NRL Washington	NRL-SSC	NRL-Monterey	NRL CBD
Hotline	(202) 767-6543	(228) 688-5001	(831) 656-4721	(202) 767-6543
Personnel Locator	(202) 767-3200	(228) 688-3390	(831) 656-4731	(410) 257-4000
DSN	297- or 754-	485	878	—
Direct-in-Dialing	767- or 404-	688	656	257
Public Affairs	(202) 767-2541	(228) 688-5328	(831) 656-4708	—

Additional telephone numbers are listed on page 244.

REVIEWED AND APPROVED
NRL/PU/5211-01-431
April 2001

Douglas H. Rau, Captain, USN
Commanding Officer

Naval Research Laboratory
4555 Overlook Ave., SW
Washington, DC 20375-5320
Public Affairs Office, Code 1030
(202) 767-2541

2001 NRL REVIEW